Optimization of UiO-67 type Metal-Organic Frameworks for Catalysis

Dissertation for the Degree of

Philosophiae Doctor

Gurpreet Kaur

Department of Chemistry

Faculty of Mathematics and Natural Sciences

University of Oslo

February 2020

Series of dissertations submitted to the
Faculty of Mathematics and Natural Sciences, University of Oslo
No. 2257

ISSN 1501-7710

Cover: Hanne Baadsgaard Utigard.
Print production: Reprosentralen, University of Oslo.

Preface

This work constitutes the results from a three year PhD programme (Feb, 2017 to Jan, 2020) in the CONFINE project. The work has been funded by the Norwegian Research Council and mainly performed at the Department of Chemistry, University of Oslo.

Prof. Karl Petter Lillerud has been my principal supervisor who is greatly acknowledged for his support throughout. I am thankful to him for giving this precious opportunity and allowing me to work freely and pursue scientific questions of interest to me. I am extremely thankful to Dr. Sigurd Øien-Ødegaard for mentoring me as co-supervisor and for his continuous determined participation in my work. This thesis would not have been possible without his support. He was not only always ready to listen to my thoughts and queries about my scientific projects, but also helped to make my stay at UiO and in Norway as smooth as possible despite the several nearly hopeless situations that arose.

Prof. Unni Olsbye, the CONFINE project leader, is acknowledged for her guidance, excellent feedback and endless patience. I absolutely admire her way of working, keeping things on track, and following up on project details and results closely. Moreover, I will always cherish and appreciate the invitations from her and Prof. Lillerud during my first Christmas in Norway.

These acknowledgements would not be complete without thanking all the lovely catalysis research group members. I thank them for being affable, encouraging and providing a wonderful environment. Moreover, it was great to share office with Sigurd, Chris and Erlend, before Sigurd decided to leave us to share the office with more mature scientists. Many thanks for always being ready for scientific suggestions and discussions as well as fun gossip sessions. I specially thank Erlend and Grieg C. Shearer for their valuable feedback on this thesis.

I would like to thank Andrea, Olesia and Giuseppe for making my social life so much fun, they are amazing and have been my first and best friends in Norway. I would also like to express my special thanks to Rohit for motivating and supporting me throughout with endless love and patience.

Finally, I am eternally grateful to my family, who have loved and encouraged me from the day when I decided to move abroad until today and ever after. Each day, they give me strength to be stronger and make right decisions. I would not have been where I am today without their support.

Table of Contents

List of papers presented in this thesis

Paper I: *Controlling the Synthesis of Metal-Organic Framework UiO-67 by Tuning Its Kinetic Driving Force,* G. Kaur; S. Øien-Ødegaard; A. Lazzarini; S. M. Chavan; S. Bordiga; K. P. Lillerud; U. Olsbye. Crystal Growth & Design **2019**, *19 (8),* 4246-4251.

Paper II: *Water a structure and defect controlling agent in the synthesis of UiO-67,* G. Kaur; S. Øien-Ødegaard; K. P. Lillerud. *Preliminary manuscript.*

Paper III: *Post-synthetic construction of a tetradentate Schiff-base catalytic site in Zr-based metal-organic frameworks,* G. Kaur; S. Øien-Ødegaard; S. Gadolini; K. T. Hylland; A. Lazzarini; S. Bordiga; M. Tilset; K. P. Lillerud. *Preliminary manuscript.*

Author's contribution

Paper I: Synthesis of all samples. Performed all PXRD, TGA-DSC, ^{1}H NMR, nitrogen adsorption and SEM. Analysis and interpretation of the experimental data was made with assistance of Sigurd Øien-Ødegaard, Karl Petter Lillerud and Unni Olsbye. Participated in the interpretation of IR data with Andrea Lazzarini and Silvia Bordiga. Preparation of manuscript and figures and revision.

Paper II: Synthesis of all samples. Performed PXRD, TGA-DSC, ^{1}H NMR, nitrogen adsorption and SEM. Preparation of manuscript and figures.

Paper III: Synthesis of all MOF bases samples and synthesis of single crystal of isolated Pd complex. Performed all PXRD, TGA-DSC, ^{1}H NMR, nitrogen adsorption and SEM-EDX. Participated in the catalytic testing. Analysis and interpretation of all the experimental data. Preparation of manuscript and figures.

Papers not included in this thesis

Paper I: *Hydrogenation of CO_2 to Methanol by Pt Nanoparticles Encapsulated in UiO-67: Deciphering the Role of the MOF,* E. S. Gutterød; A. Lazzarini; T. Fjermestad; G. Kaur; Maela Manzoli; S. Bordiga; S. Svelle; K. P. Lillerud; E. Skulason; S. Øien-Ødegaard; A. Nova; U. Olsbye. J. Am. Chem. Soc. **2020**, *142*, *2*, 999-1009.

Paper II: *Co-catalyst free ethene dimerization over Zr-based metal-organic framework (UiO-67) functionalized with Ni and bipyridine,* M. Kømurcu; A. Lazzarini; G. Kaur; E. Borfecchia; S. Øien-Ødegaard; D. Gianolio; S. Bordiga; K. P. Lillerud; U. Olsbye. Catalysis Today, **2020**.

Paper III: *Strongly Visible Light-Absorbing Metal-Organic Frameworks Functionalized by Cyclometalated Ruthenium(II) Complexes,* E. M. Thoresen; S. Øien-Ødegaard; G. Kaur; M. Tilset; K. P. Lillerud; M. Amedjkouh. RSC Adv., **2020**, *10*, 9052-9062.

Paper IV: *Operando study of palladium nanoparticles inside UiO-67 MOF for catalytic hydrogenation of hydrocarbons,* A. L. Bugaev; A. A. Guda; K. A. Lomachenko, E. G. Kamyshova; M. A. Soldatov; G. Kaur; S. Øien-Ødegaard; L. Braglia; A. Lazzarini; M. Manzoli; S. Bordiga; U. Olsbye; K. P. Lillerud; A. V. Solatov; C. Lamberti. Faraday Discussions **2018**, *208 (0),* 287-306.

Paper V: *Influence of Defects and H_2O co-feed on the Hydrogenation of CO_2 to Methanol over Pt Nanoparticles in UiO-67 Metal-Organic Framework,* E. S. Gutterød; G. Kaur; A. Lazzarini; U. Olsbye. *Manuscript in preparation.*

Paper VI: *Qualitative Phase Estimation of UiO-67 by Serial Rotation Electron Diffraction*, L. Samperisi; G. Kaur; K. P. Lillerud; Z. Huang; X. Zou. *Manuscript in preparation.*

Scope

This work was a part of the CONFINE project where the main goal was "Unravelling the potential of confinement effects in catalysts and adsorbents". The main objective of my work as part of this project was primarily to synthesize metal-organic framework (MOF) materials with specific catalytically active sites, and to utilize the flexibility of MOFs to modify the immediate surrounding of these sites. As basis of the study, the Zr-biphenyl MOF UiO-67 was chosen, due to its demonstrated abilities to harbor a wide range of catalytic sites and its high stability at the reaction conditions of interest in this project.

The scope is also motivated by previous work in the group focusing on fundamental understanding of materials and their properties, which includes detailed investigations into the structure and properties of UiO-66. However, the related UiO-67 has not been as thoroughly studied despite its prominence in the literature. There are many reports describing the synthesis of UiO-67 and its use in various applications, but large deviations in the presented characterization data points to severe reproducibility issues and lack of deep understanding of the effect of the synthesis parameters. In order to have a stable and reliable development of a catalyst, it is important to refine, understand the synthesis and its effects, and thus be able to obtain the desired material properties.

Therefore, this work focusses on the following key points:

1) Optimization of the synthesis of UiO-67 by single-variable studies of synthesis parameters.
2) Using state of the art methodology to understand the defectivity of the MOF and how that is determined by the synthesis.
3) Synthesis of UiO-67-type and UiO-67-mixed linker MOFs using the optimized protocol.
4) Post-synthetic modification of the MOFs to create new coordination metal sites for catalysis.

The optimized protocols were used to synthesize MOF catalysts for kinetic studies performed by other members of the CONFINE project (such as CO_2 hydrogenation, ethene oligomerization and cyclopropanation). Some of the major contributions have been listed in the *Papers not included in this thesis* section. Thus, this thesis is presented in four chapters: 1) Introduction gives the background of MOFs, and in particular UiO-67, 2) Experimental section

detailing the motivation behind various experiments and how they were performed, 3) Results and Discussion presenting the data and supporting evidence for proposed hypotheses and 4) Conclusions, where key points from the work are summarized.

1. Introduction

Metal-Organic Frameworks

1.1. Definition

A Metal-Organic Framework (MOF) is a coordination network with organic ligands containing potential voids, according to IUPAC.[1] A coordination network can be defined as a solid compound extended through repeating molecules, composed of a central metal atom and a group of atoms (called ligand) in two or three dimensions.[1]

1.2. Background

MOFs are emerging as a potent class of material as heterogeneous catalysts, adsorbents and sensors due to their structural diversity, tunable porosity and potential to host a wide range of active sites.[2] Importantly, such active sites can be incorporated into the structures of MOFs in well-controlled and verifiable ways. To simplify the definition, it can be said that MOFs are porous compounds where metal containing nodes known as secondary building units (SBUs) are linked by multidentate organic ligands (linkers) by strong chemical bonds.[3] Nevertheless, before the concept of SBUs came many open frameworks like Werner complexes, ß-M(4-Methylpyridyl)$_4$(NCS)$_2$ (M=Ni^{2+} or Co^{2+}) and Prussian blue compounds, $Fe_4[Fe(CN)_6]_3.xH_2O$ (x=14-16), existed. These compounds were typically built of individual metal ions linked with multiple neutral, mono-dentate ligands like cyanide or pyridine (Figure 1). These inorganic compounds had the ability to sorb small molecules but lacked rigidity, hence to introduce rigidity and build a framework, organic species like bis- and tris-bidentate carboxylate linkers were employed. This concept was later developed into what we now know as MOFs.[4]

Omar M. Yaghi and coworkers published some of the early examples of MOFs, the series MOF-n (n=1 to 5) where some of them were discovered before the existence of naming terminology for MOFs. For example Zn(bdc)·(DMF)(H_2O) (bdc= 1,4- benzenedicarboxylate and DMF=*N*,*N*-dimethylformamide),[5] reported in 1998 was later named as MOF-2.[4] The major concerns with MOF type structures were their lack of stability and porosity after the removal of solvents. MOF-5 ($Zn_4O(bdc)_3$)[6-7] was the benchmark discovery as it is highly stable, porous

and showed the ability of reversible adsorption/desorption. During the evolution of MOFs, a standard was also marked by the development of HKUST-1 ($Cu_3(btc)_2$, btc= 1,3,5,-benzenetricarboxylate),[8] MIL-101 ($Cr_3O(OH, F, H_2O)_3(1,4\text{-bdc})_3$),[9] and MOF-74 ($Zn_2$(dhbdc), dhbdc = 2,5-dihydroxy-1,4-benzenedicarboxylate)[10]. Figure 1 summarizes these developments with respect to time.

MOFs can be regarded as connected metal clusters, many of which are known and studied in the field of inorganic chemistry. For example, the structure of MOF-5 emanates from the zinc acetate structure where the acetates are replaced by terephthalic acid.[3] Similarly, in 2008 UiO (Universitetet i Oslo) MOFs were established which were based on $Zr_6O_4(OH)_4(bdc)_6$.[11] The structure of UiO Zr-MOF can be seen to emanate from isolated $Zr_6O_4(OH)_4(CO_2)_{12}$ cluster bridged by bidentate terephthalate ligands.[12]

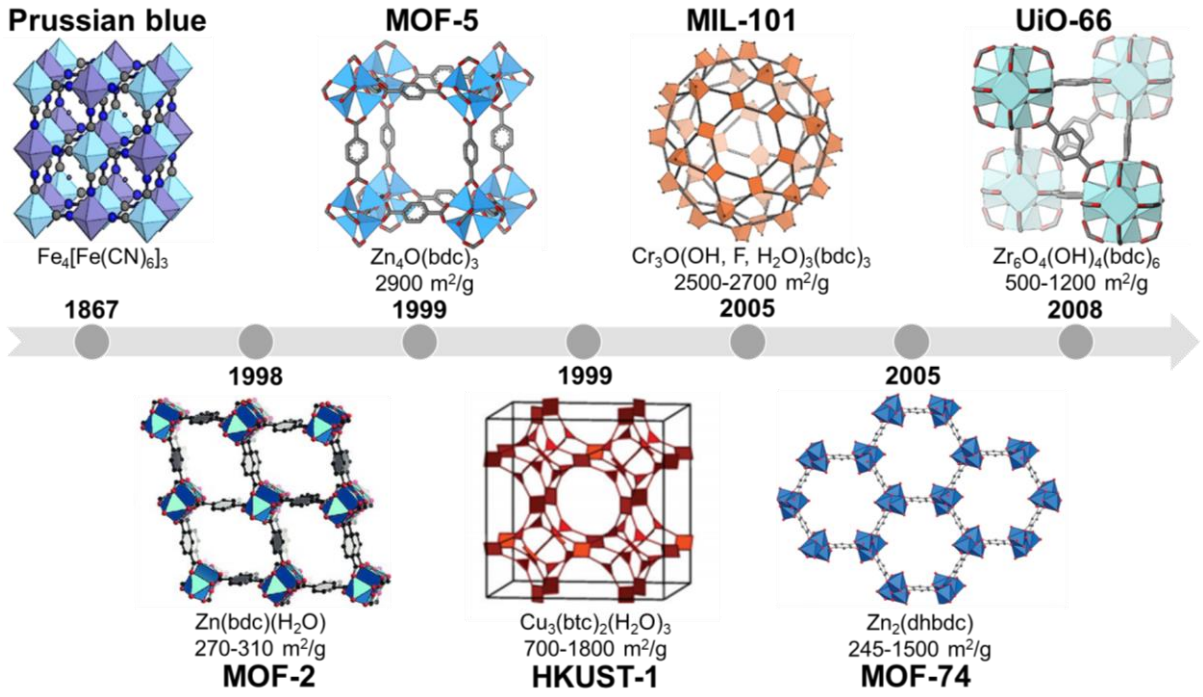

Figure 1. Illustration of the development on some of the porous metal-organic network structures with time. Each structure highlights its structural formula and surface area where bdc is 1,4-benzenedicarboxylate, btc is 1,3,5,-benzenetricarboxylate and dhbdc is 2,5-dihydroxy-1,4-benzenedicarboxylate.

Moreover, the possibility for the formation of different MOF structures is enormous. By altering the SBUs and/or linkers, a myriad of different structures can be obtained.[13-14] The networks formed by the connectivity of the SBUs can be described by their topology and MOFs with identical network topology are called isoreticular MOFs. Hence, if a linker of two MOFs is different but has same cluster and connectivity number are called isoreticular MOFs. An

example of isoreticular MOFs are the UiO Zr-MOF series with UiO-66, UiO-67 and UiO-68. They are all based on 12 connected Zr6O8 clusters with linear ditopic linkers, 1,4-benzene-dicarboxylate (BDC), 4,4′ biphenyl-dicarboxylate (bpdc) and terphenyl dicarboxylate (TPDC) linkers, forming a fcu network topology.[11]

1.3. Potential applications

MOFs depicts characteristics of organic as well as inorganic species and therefore provide structural richness along with high thermal and chemical stability. Additionally, they have large pores, high surface area and tunable functionality, contrary to other classes of porous materials such as zeolites. Zeolites are strictly made up of inorganic components (silicon, aluminum and oxygen) forming a 3-D network with cavities and channels. Besides sharing the crystallinity and textural properties common to zeolites, MOFs are highly versatile materials as it is possible to determine the size, shape and chemical functionality of their cavity by choosing the appropriate organic ligands.[15] These intrinsic properties of MOFs makes them a potential candidate for a variety of applications and some of the most important ones are gas storage, adsorption and separation, sensing and catalysis.[16-20]

1.3.1. Storage and adsorption

MOFs with their high surface area, adjustable pore sizes and acceptable thermal stability make them suitable as adsorbents.[21-22] Gas adsorptive separation by a porous material is usually achieved by one of the following mechanism, 1) selective adsorption or separation due to restrictive entry of the molecules due to size and/or shape of the accessible pore, 2) due to preferential different adsorbate surface or different adsorbate packing interaction and 3) due to different diffusion rates.[19] MOF have the capability of storing and separating useful gases such as potential transportation fuels like hydrogen, methane or greenhouse gases like carbon dioxide and even toxic gases.[14, 23-24] MOFs are used as adsorbents in storing toxic gases such as arsine, phosphine and boron trifluoride to apply as dopants in the manufacture of electronics. This gas storage and delivery system was built into a cylinder, which was commercialized as ION-X where the gases were stored under one atmosphere of pressure.[25] This is a significant application of MOF, which allows the storage of toxic gases at such low pressure by providing a large surface area, reducing safety risks in case of leakage. Moreover, MOFs are used for the storage of 1-methylcyclopropene (1-MCP) which is released in air when in contact with water.

This concept is used in the commercialization of the product called TruPick, which is used to lengthen the shelf life of fruits and vegetables as the released 1-MCP blocks the effect of ethylene which is released during the natural ripening of fruits and vegetables.[25]

1.3.2. Catalysis

The parent MOF itself and its modified version (mixed linker, mixed metal or post synthetically modified MOF) are seen to be a promising catalyst.[26-27] The term "parent MOFs" refer to the classic MOFs that are composed of only one type of linker and secondary building unit. The uncoordinated metal sites in the clusters of the MOFs provide Lewis acidity. These sites create a more open material which has demonstrated unexpected catalytic activities.[28] Moreover, these sites can be post-synthetically modified and used to remove water or introduce other moieties to serve as a catalyst.[29-30] In addition, the MOFs can also be modified by altering their basic structure at the organic linker and/or metal centers, where the resultant MOF will have two or more type of linker and/or metals in the frameworks (also discussed in section 1.9).[31-32] These transformed MOFs have given a range of catalyst in the field.[33-34] By altering the basic MOF structure, functionalities are introduced to the MOFs, hence MOF can also be seen as a support for the active site for catalysis.[35] Another advantage of MOF as a catalyst is that it is used as a heterogeneous catalyst and gives the opportunity to be reused to multiple times, under right regeneration conditions.[36-37]

1.4. Challenges

Even though MOFs are gaining a lot of popularity, there are still challenges associated with MOFs. These challenges are a barrier for MOFs to be used on a large scale. Apart from the synthetic challenges (like proper reaction condition for targeted structure, activation of MOF, nucleation and growth of MOF), issues such as cost, upscaling and reproducibility and stability are still problematic.

1.4.1. Stability

There are 75,600 MOF structures registered in the *Cambridge Data Centre (CSD)* in 2019,[38] but many of them have limited interest due to poor thermal, mechanical or chemical stability.[39] Many of the known MOFs are sensitive towards moisture/humid aid and if they can handle such exposure, they might degrade upon contact with water. The presence of water can

hydrolyze M-O bonds, lead to the formation of oxides or dissolve MOF constituents, leading to collapse of framework. However, the study of stability of MOFs is an active research topic. Recently, an introduction of hemilabile 'sacrificial' bonds in the MOF is seen to increase the hydrolytic stability. By deliberate incorporation of such species in HKUST-1, the MOF retains its structure for over 1 year in contact of water, unlike the non-modified MOF.[40] Moreover, thermal stability of MOFs are of great importance for applications like catalysis. But usually the thermal stability of MOFs is limited to 250-350 °C.[41-43] In this regard, the thermal stability of UiO-67 has been investigated in this thesis. Furthermore, for processing or main application it will be beneficial that MOFs can resist mechanical strain.[44-45] The stability of most MOFs towards mechanical strain is limited and often results in partial pore collapse or amorphization.[46-49] Mechanical strength of MOFs is calculated by determining its Young's modulus, shear modulus, bulk modulus, Poisson's ratio and linear compressibility. These factors helps in determining the elements for practical post-synthetic processes such as extrustion or pellet making. MOF-5 exhibits amorphization by the destruction of its carboxylate group at the pressure of 3.5 MPa and ambient temperature.[50] This is 100 times lower pressure than required for the amorphization of other solid materials at that temperature. The sample of MOF-5 was placed in a cylindrical sample holder and compressed for 30 min by pressurizing a punch rod into the sample. This will considerably affect the sheer and young's modulus of the material. The study of such changes at ambient temperature and pressure is interesting as these changes strongly affect the properties of the material. It is worth mentioning that UiO Zr-MOFs are among the top performers when it comes to thermal, chemical and mechanical stability.

1.4.2. Cost

MOFs contain both organic and inorganic species, as discussed in the previous sections. The cost of MOF manufacturing primarily depends on the cost of the starting materials such as the metal source, linkers, solvents and additives. The organic linker is generally the most expensive part of a MOF (especially the tailored linkers) followed by the solvent (usually N,N'-dimethylformamide) and metal source. Many research groups are trying to use alternative cheaper starting materials to reduce cost without compromising on the quality. This is necessary in order to enable the scaling up of MOFs, potentially to an industrial scale. Nevertheless, MOFs are already much cheaper than they were 10 years ago. In order to decrease the price of the overall MOF:

i) Ideally, the MOF should be synthesized in water, which is not only a green solvent but also lowers the risk of handling when upscaling MOFs.[51] Failing that, then simply reducing the amount of solvent without compromising with the quality of MOF would help reduce waste and cost (this strategy was employed in the work reported herein).
ii) Use commonly available linker such as terephthalate: Terephthalate is widely used in the PET (polyethylene terephthalate) plastic materials which a huge industry and hence the price of terephthalate is much lower because of supply and demand. MOFs synthesized by linkers made in multiple steps using expensive or uncommon starting materials will hardly be able to find an industrial use, in the author's opinion.

1.5. Zirconium (IV)-based MOFs

The class of zirconium(IV)-based metal organic frameworks (Zr-MOFs) are recognized for their exceptional chemical and thermal stability and thus gain significant attention in the field. In cluster chemistry, many isolated Zr clusters have been reported containing Zr_3, Zr_4, Zr_5, Zr_6, Zr_8, $Zr_{10,}$ Zr_{12} and Zr_{18} units, however the majority of Zr-based MOFs are observed to have Zr_6O_8 clusters).[52] This 12-connected node, $[Zr_6O_4(OH)_4]^{12+}$ has the triangular face of the Zr_6-octahedron alternatively capped by μ_3-O and μ_3-OH groups. Therefore, the 12 points of connection, which binds with the linkers makes a MOF framework (Figure 2). This also determines the topology of the MOF, depending on the occupancy of the point of connections. If all the 12 point are linked with ditopic linear linker like BDC (terephthalate), it forms UiO-66 (**fcu**) and this is the most stable Zr-MOF because of saturated connectivity of the cluster. Zr-MOFs are also possible with 10 or 8 connections where linkers like TDC (2,5-thiophenedicarboxylate) or TBAPy (1,3,6,8-tetrakis(p-benzoate)pyrene) are utilized yielding DUT-69 (**bct**)[53] and NU-1000 (**csq**)[54], respectively. Furthermore, 6-connected framework is obtained with tritopic linkers BTC (benzene-1,3,5-tricarboxylate) to obtain MOF-808 (**spn).**[21]

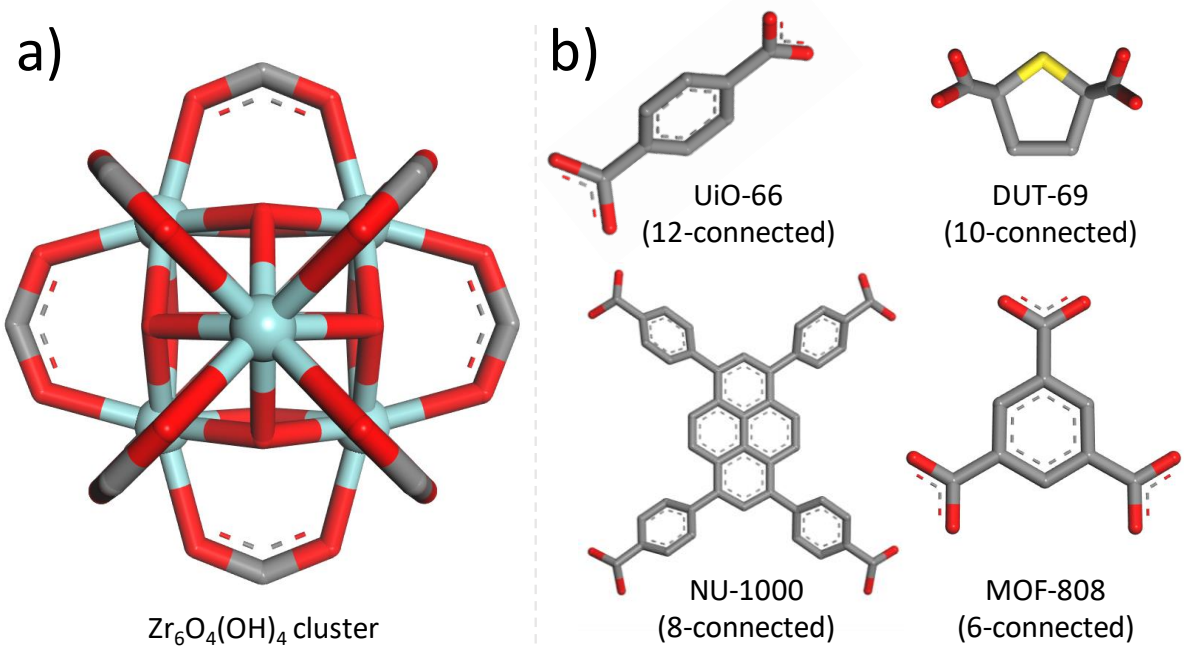

Figure 2. Illustration of the a) Zr_6-cluster common to a majority of Zr(IV)-based MOFs, which together with b) different sets of linkers form different MOFs with varying degree of connectivity.

Another interesting feature of these inorganic building units is that they can undergo structural dehydration under the heat treatment at about 250-300 °C.[11, 55] During this process cluster loses two water molecules and changes from the "hydroxylated" form $Zr_6(\mu_3\text{-}O)_4(\mu_3\text{-}OH)_4$ to the distorted "dehydroxylated" form $Zr_6(\mu_3\text{-}O)_6$.[52] It is worth mentioning that this behavior is completely reversible and the clusters return to their original hydroxylated form when the MOF is exposed to water vapor.

1.6. UiO-67

Among the prime MOF candidates for heterogeneous catalysis are the Zr-UiO MOFs. The parent UiO-66 (with terephthalate linkers) has been extensively studied.[56-58] The methods of synthesis and post-synthetic modifications exist to obtain UiO-66 with desired material properties (e.g. Lewis acidity, stability, porosity) and types and concentration of defects available in UiO-66 are well understood.[59-62] However, UiO-67 (isoreticular to UiO-66) is an interesting MOF as it maintains most of the advantages of UiO-66 with an additional benefit of larger pore size and surface area.[63] UiO-67 is highly thermally and chemically stable, and may incorporate a wide range of catalytically active ligands as part of its structure.[64-66] For example, by replacing a fraction of its biphenyl linkers with 2,2'-bipyridine-5,5'-dicarboxylate (or similar), it can chelate ligands for coordination complexes on its linkers. UiO-67 or its

functionalized versions are therefore viewed as a promising candidate for many applications, mainly sensing and catalysis.[67-76]

1.6.1. Structure

As discussed before, UiO-67 is a Zr-MOF composed of $Zr_6O_4(OH)_4$ inorganic clusters and H_2bpdc linkers (4,4′-biphenyl-dicarboxylate) (Figure 3).The core of the cluster comprises of six Zr^{4+} atoms arranged in an octahedron whose 8 faces are alternatively capped by oxide and hydroxide. Each Zr atom is 8-coordinated with square anti-prismatic geometry.[11] An additional 12 carboxylate groups (from H_2bpdc linkers) complete the cluster to form $Zr_6O_4(OH)_4(COO)_{12}$ or MOF composition as $Zr_6O_4(OH)_4(bpdc)_6$.

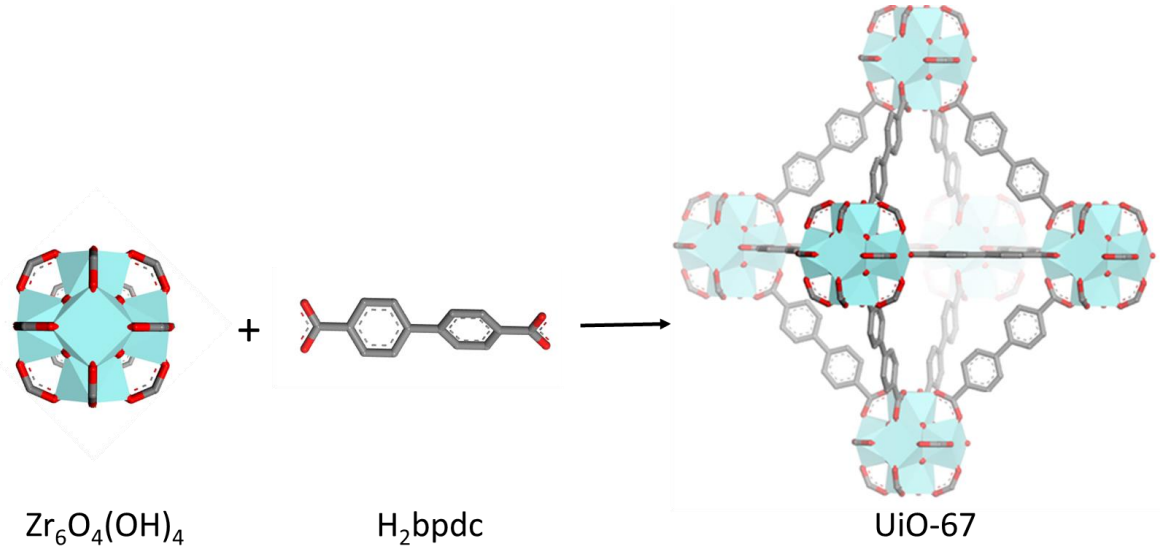

Figure 3. Construction of UiO-67. Carbon, oxygen and zirconium atoms are shown in grey, red and cyan, respectively. Hydrogen atoms are omitted for clarity.

UiO-67 have two kinds of pore windows of tetrahedral and octahedral cages of 12 and 16 Å, which is slightly bigger than that of UiO-66 (8 and 11 Å), shown in Figure 4. The tetrahedral cages share their faces with octahedral cages and the octahedral cages share their face with one another. Therefore, octahedral and tetrahedral cages are in a 1:2 ratio. The langmuir surface area of an reported for UiO-67 structure in first report is 3000 m^2/g in contrast with UiO-66, which has 1187 m^2/g.[11] As discussed above, the structural dehydration takes place in UiO-67 as well. The hydroxylated form of UiO-67; $Zr_6O_4(OH)_4(bpdc)_6$ loses two water molecules to give the dehydroxylated form; $Zr_6O_6(bpdc)_6$. This is evidently seen in TGA-DSC curves of UiO-67 by a slight weight loss between 200 to 400 °C (in the subsequent sections).

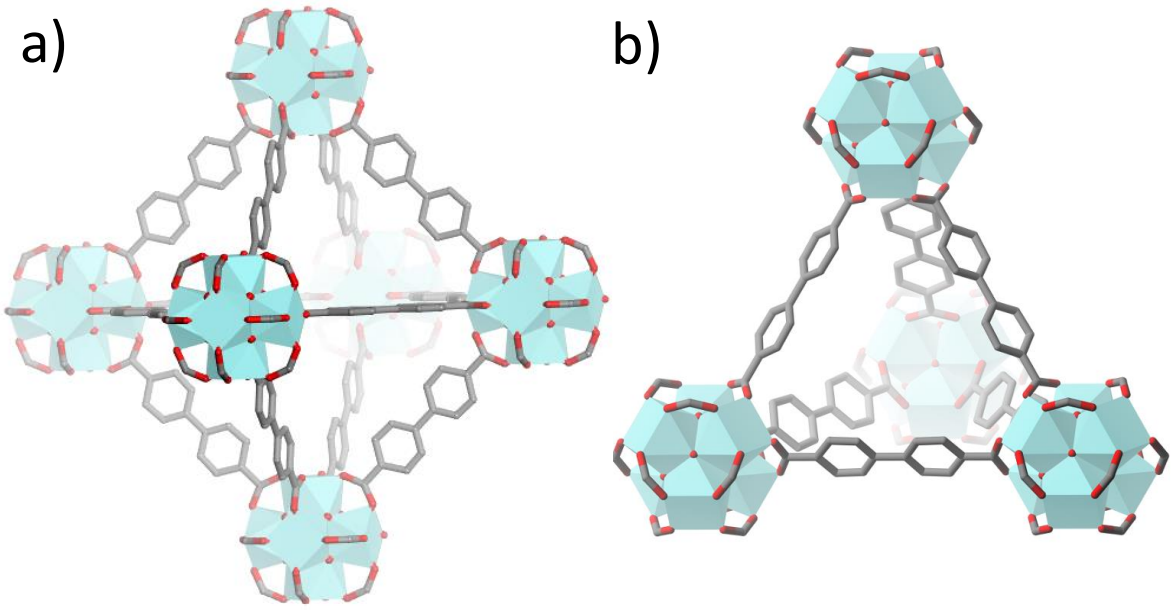

Figure 4. The a) octahedral and b) tetrahedral pores of UiO-67. Carbon, oxygen and zirconium atoms are shown in grey, red and cyan, respectively. Hydrogen atoms are omitted for clarity.

1.6.2. Synthetic conditions and reagents

Most UiO Zr-MOFs are obtained by the reaction of a Zr source with its respective linker (in acid form) at elevated temperatures (80 °C to 220 °C), using DMF as solvent.[77-78] The following subsection will briefly discuss the role of these reagents.

1.6.2.1. Zr(IV) source and linkers

The ideal Zr (IV) source should be non-corrosive, easy to handle and soluble in the crystalizing solvent to yield a good quality material. UiO-67 is mostly seen to be synthesized using zirconium tetrachloride ($ZrCl_4$). $ZrCl_4$ has a polymeric structure of edge-sharing $ZrCl_6$ octahedra which is solvated in the presence of DMF and water. Also, $ZrCl_4$ hydrolyzes in the presence of water to give $ZrOCl_2$ and corrosive HCl. Other problems associated with $ZrCl_4$ is that it is highly hygroscopic, corrosive and generates halogenated waste. Alternatively, other zirconium (IV) salts used in the literature for the synthesis of UiO-67 are zirconium oxychloride octahydrate ($ZrOCl_2 \cdot 8H_2O$),[21, 79] zirconium methacrylate oxoclusters $Zr_6O_4(OH)_4(OMc)_{12}$, (OMc = CH_2=CH(CH_3)COO)[80]. Other sources like zirconium tetrabromide ($ZrBr_4$),[81] zirconium isopropoxide ($Zr(OC_3H_7)_4$)[81-82] and zirconium oxynitrate ($ZrO(NO_3)_2 \cdot xH_2O$),[83] have been used for the synthesis UiO-66 but have not been observed for UiO-67.

Furthermore, MOF linkers/ligands are generally organic soluble compounds which has two or more points of connections to bind with metal source to result into a three-dimensional

continuous structure. Some of the common examples are ditopic 2-methylimidazole and 1,4-benzenedicarboxylic acid (H_2bpdc) and tritopic 1,3,5-benzenetricarboxylic acid. Hence, biphenyl linkers are suitable for the synthesis of UiO-67 in a equimolar ratio with respect to Zr. Similarly, functionalized biphenyl linkers can be used for the formation of MOF to provide functionalization in the structure (discussed in section 2.5).

1.6.2.2. Modulators

Synthesis of UiO-67 and other Zr-MOFs is often reported with the use of a monocarboxylic acid as a growth modulating agent (modulator) in order to obtain larger and individual crystals, and higher degree of crystallinity or as a tool to control defectivity.[84] A modulator can be any monocarboxylic acid, which either deprotonates the linker or competes with the linker to form bonds with the metal node, eventually slowing down the rate of nucleation and crystal growth. Independent of the specific mechanism, modulation often improves the reproducibility of the MOF synthesis and the crystallinity of the product and may be used to control crystal size and morphology.[85] Kitagawa and coworkers were the first to use monocarboxylic acid as modulators in 2009 and later in 2011, Behrens and coworkers published the first report of their use in the formation of UiO-67.[86] Some of the commonly used modulators are formic acid, acetic acid, benzoic acid and related compounds like triflouroacetic acid, 4-nitrobenzoic acid, 2-phenylacetic acid etc. It was demonstrated that controlling the ratio between Zr and modulator enhances the particle size, morphology and the reproducibility of the synthesis.[84] On the other hand, if the linker fails to replace the modulator in the final product, the result is a defective MOF where the modulator occupies the coordination site. This type of defect, when a linker site is vacant or occupied by another entity, is known as a linker vacancy defect or "missing-linker" defect (discussed in section 1.8).

1.6.2.3. Aqueous additives

Furthermore, besides modulators the addition of water or aqueous hydrochloric acid ($HCl_{(aq)}$) is seen in the synthesis of UiO-67.[79, 87-88] The addition of water or $HCl_{(aq)}$ is referred to as aqueous additives in this work. Although modulators facilitate the crystal formation by slowing down the rate of formation of particles, additives like strong acids have the tendency to protonate the linker which acts as a barrier in particle formation.[89] Farha and coworkers observes and increase in the rate of formation of product whereas Shafir and coworkers observes decrease in porosity, with the use of HCl in the formation of UiO-67.[79, 88] The effect of HCl versus water is of particular interest since it seems to be in disagreement in several

reports and hence, its factual effect of these additives is uncertain.[79, 84, 88, 90] It has recently been demonstrated that the amount of water also plays a major role in the synthesis of UiO-type MOFs. Behrens and coworkers observed that the rate of reaction is strongly correlated with increasing water content in the DMF-based modulated synthesis of UiO-66-fumarate.[85] It is worth highlighting that DMF is a highly hygroscopic solvent, and thus the amount of water may vary significantly for different MOF syntheses. Therefore, a detailed study is performed to see the effect of the varying amount of water in the synthesis, discussed later in this work.

1.6.2.4. DMF

Dimethylformamide is a polar aprotic solvent with high boiling point, and is by far the most common solvent used in MOF synthesis. Apart from providing a medium to dissolve all the MOF components, solvents coordinate or solvate the ions in the MOF synthesis solution to ease the assembly of the building units of the MOF. However, at higher temperatures in the presence of water and an acid catalyst, DMF hydrolyses into formate and dimethylamine. The hydrolysis can also occur in presence of stoichiometric amounts of aqueous base.

$$(CH_3)_2NCHO + H_2O \leftrightarrow HCO_2H + (CH_3)NH$$

Hence, this side reaction can also affect the synthesis of UiO Zr-MOFs. Moreover, since the first report of UiO-66, the Zr:DMF molar ratio in reported methods deviates, from 1:1500 in the original report,[11] to the more generally reported 1:300-600.[66, 79, 91-94] Previous work in our group suggested that the linker must be dissolved completely if large crystal growth is desired (to avoid MOF crystal nucleation on linker particles). H_2bpdc has a solubility of around 1:150-200 in DMF at the boiling point. Hence, it is interesting to verify the large range of amount of DMF and investigate its effect (studied in this work).

1.7. Stability

The stability of a complex is based on the metal to ligand bond strength and Zr(IV) in UiO MOFs is in high oxidation state. Due to its high charge density and bond polarization, Zr (IV) has a high affinity towards the O atoms on the carboxylate ligand. This explains why Zr(IV) MOF structures such as UiO-67 are highly stable. However in the presence of a basic aqueous solution, Zr (IV) has higher affinity for OH^- and therefore the framework tends to collapse.[52] Such collapse also happens in the presence of water. Interestingly, it occurs during the

evacuation of water from the MOF which indicated that hydrolysis of Zr-O bond may not be the primary pathway of collapse. It has also been observed that the framework collapse due to the capillary forces acting on the framework during water removal. Therefore, the structure remains intact if the MOF is dried after solvent exchange with less polar solvents (with weaker intermolecular interactions).[95-96] Moreover, the framework collapse in the presence of aqueous base solutions is used for the sample preparation for recording ^{1}H NMR spectra, as the MOF dissolves in the base solution.

Furthermore, UiO-67 is thermally stable up to 450 °C with a ramp rate of 5 °C/min under air. However, the true thermal stability of the MOF is addressed when the material is held static at elevated temperature for prolonged times (Section 3.1.4). Interestingly, analogue materials such as UiO-67-(bpdc-Me) and UiO-67-bndc based on 3,3′-dimethylbiphenyl and 1,1′-binaphthyl linkers respectively, have shown higher stability towards water as compared to UiO-67.[65] UiO-67-bndc is discussed in detail, later in this thesis (section 1.9).

1.8. Defects in MOFs

An ideal arrangement of atoms and molecules forming a unit cell in a continuous fashion is viewed as a perfect crystal. These unit cells should assemble in a three-dimension with no distortion. However, crystalline materials tend to deviate from this ideal behavior by having imperfections. There may be atoms or molecules misplaced in the crystal which disturbs the uniformity, hence known as crystal defects. The defects in a solid-state materials are well studied and known. As there is nothing as a defect-free crystalline solid, this also applies to MOFs. There are many types of defects observed by different research groups on numerous MOFs, summarized in Figure 5.[97]

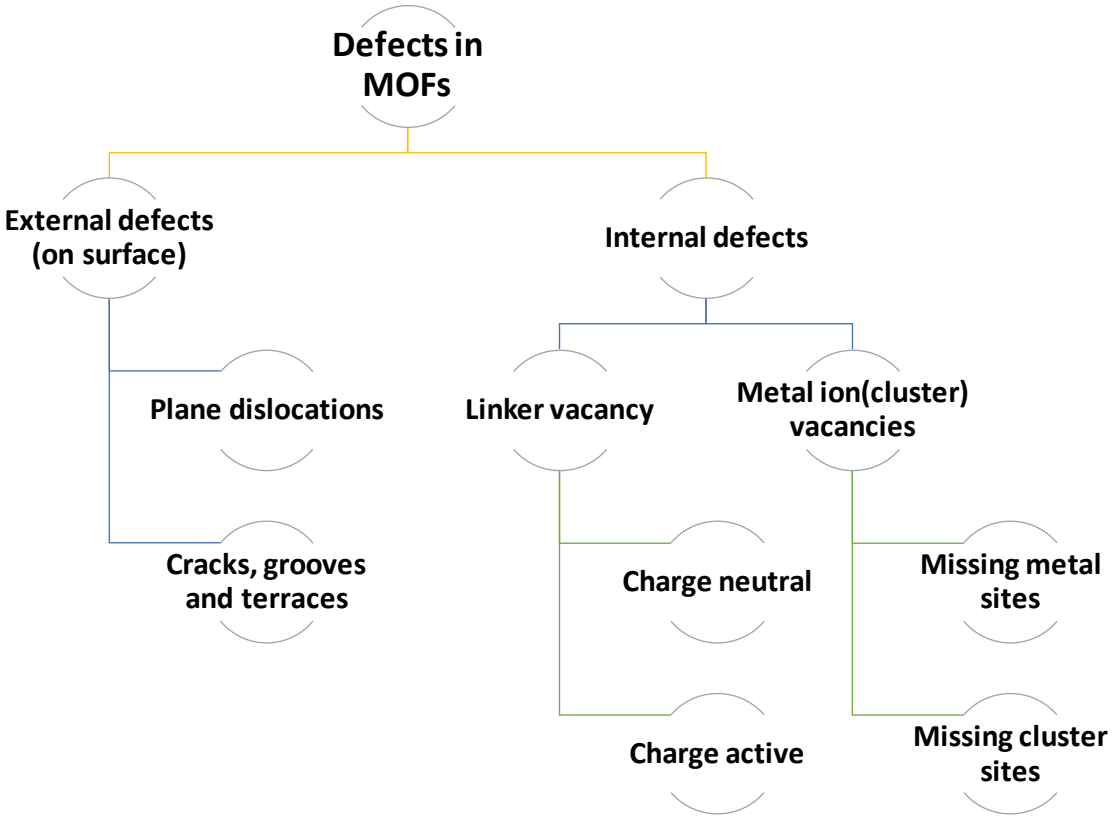

Figure 5. Some of the common types of defects in MOFs.

Internal defects are prevalent in MOFs and occurs when either the metal center/metal cluster of the MOF is missing (metal cluster defect) or the linkers of the MOF is missing (missing-linkers defect). Nevertheless, the absence of these species does not affect the integrity of the MOF framework, as they are typically found in low concentration. Although, metal cluster defects are observed in high concentrations in UiO-66 but there is no literature report for UiO-67.[56, 98] The presence of missing cluster defects in UiO-66 is observed by the existence of a very broad peak in 2θ range of 2°-7° in the PXRD pattern.[56] The stoichiometry of the non-defective (ideal) UiO-67 MOF dictates a 1:1 molar ratio between Zr and the linker. However, the typical linker occupancy coefficient is observed to be less than 1 (determined by TGA-DSC) in our previously reported works.[65, 99] The predominant type of UiO-67 defects that is reported in the literature is linker vacancies (often referred to as missing-linker defects).[79] To preserve the charge neutrality of the compounds, simultaneous removal or insertion of oppositely charged ions at the new lattice position takes place in-situ during the synthesis or post-synthetically. These vacant sites are occupied by modulators, additives, products of solvent hydrolysis, inorganic anions (from the Zr precursor) or water/hydroxide pairs (from water).[58, 100]

On the other hand, the charge compensation can also be performed by deliberately adding similar molecules which also gives a chance to modify the compound after its synthesis; post-synthetic modification (PSM). The defective MOF is saturated with the dopant in order to compensate the charge by new bond formation. These dopants can be the parent linker or any other similar linker. This is observed by Shafir and coworkers where they synthesis UiO-67 with a minimum of missing-linkers defects, where the defective MOF was "healed" post-synthetically by infusing it with a solution of bpdc.[79] Moreover, these defects can occur naturally in a MOF crystal or they can be introduced intentionally. The term used for naturally occurring defects is inherent defects and the term for deliberately introduced of such defects is engineered defects. It is widely seen that defective MOFs are preferred over non-defective MOFs because they provide functionalization and irregularities which could be helpful for catalysis and adsorption. It is important to detect and quantify defects in order to better understanding of the system one is working with, so that it can be employed in the right application. The defects can be detected using many different techniques. The external defects are often observed by SEM, AFM and confocal florescence microscopy.[101-102] It is tricky to observe internal defects and combination of techniques are required to observe them, mostly by TGA-DSC, TGA-MS, NMR, FTIR, PXRD, gas adsorption (Figure 6).

Technique	Advantage	Disadvantage
TGA	Quantify the amount of defect	No direct structural evidence; fail to distinguish cluster and linker missing defects; accuracy is debatable
Acid-base titration	More accurate: give more details on terminal species attached to defect sites	fail to distinguish cluster and linker missing defects
Nitrogen adsorption	Roughly provide the evidence of the existence of defects	No linear relation between BET surface area and amount of defects
XRD	Characterize the crystallinity of defective UiO-66; PXRD is able to characterize cluster missing defects	Difficult to quantify defect occupancy; insensitive to organic linkers; single crystals is only applicable to large crystals (5-100 μm)
FTIR and Raman spectra	Offer information of proton transfer and local defect structures	Difficult or quantify the defect occupancy and distinguish cluster missing defect
NMR	Provide chemical state of modulator species and linkers and information on local defect structures	Difficult to quantify the defect and distinguish cluster missing defect from linker missing defect
Water sorption	Characterize Lewis acid sites and atomic level	Difficult to quantify the defect
HRTEM	Direct observation of defects at atomic level	Difficult to quantify the defect

Figure 6. Various characterization techniques employed to detect and quantify defects in UiO Zr-MOFs, and their advantages and disadvantages. Reused with permission.[103]

UiO Zr-MOFs often contains free or bonded i) water molecules, ii) benzoic acid, iii) formic acid and/or iv) DMF. If these are in free state, most of them should be removed during the work-up unless trapped in the pores. If they are still present in the MOF material after work-up, then it is likely that they are present as the capping sites at the vacancy created by missing-linkers. If the amounts of all these species is calculated, they can help to determine the true composition of a given MOF. As discussed before, defects in MOFs is a major topic of research. To have a deep understanding of the material, it is important to know the true composition of

the MOF and therefore recognize them. The defects in UiO-67 are primarily missing-linker defects, leaving charged species. The charge compensation often occurs by the capping of these vacancies by other charges species like benzoate, formate, and hydroxide present in the reaction mixture. Therefore, if we quantify the presence of these capping agents, we can estimate the approximate missing-linker defects in UiO-67.

1.9. UiO-67 type mixed linker MOFs and metal incorporation

UiO-67-bndc is synthesized using [1,1'-binaphthalene]-4,4'-dicarboxylic acid (H_2bndc) linker under similar synthesis condition as UiO-67, instead of H_2bpdc. It can be regarded as a UiO-67-type MOF as its crystal structure is identical as that of UiO-67 (Figure 7). The important aspects for using H_2bndc as a linker is that it gives higher stability towards water and it has reduced pore size. Previous research in the group has shown that UiO-67-bndc depicts exceptional stability to aqueous solutions over a wide pH range and to water vapor in repeated adsorption/desorption cycles.[65] It retains its structure after being dried from water, unlike UiO-67 as the H_2bndc linker partially shields the strongest adsorption sites, as seen by single crystal structural determination. The advantage of a material which has the properties of UiO-67 but reduced pore size is a great candidate for studying the confinement effect.

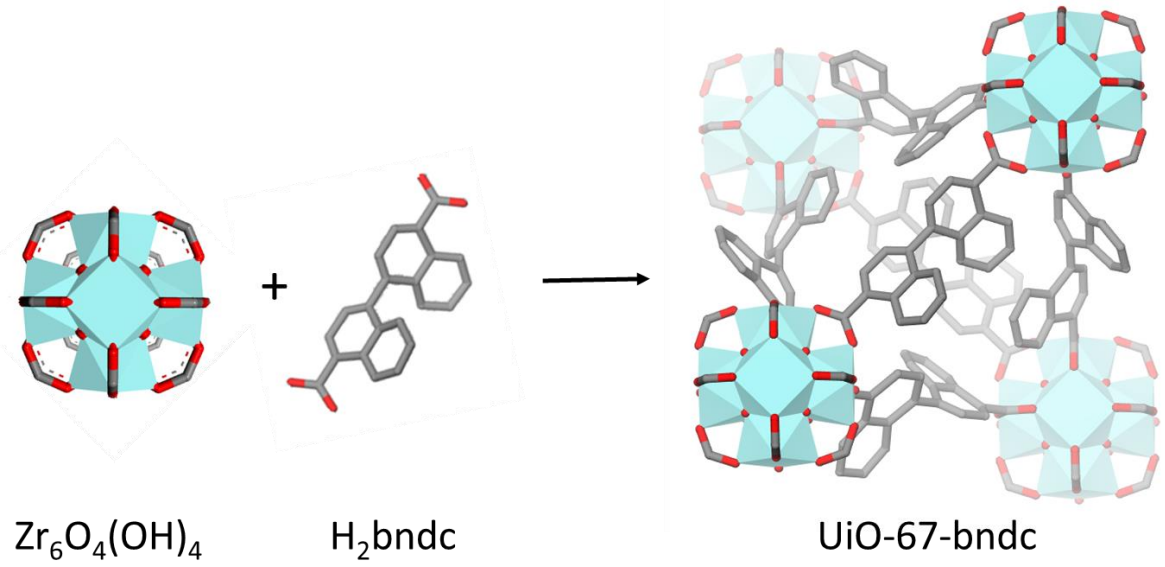

Figure 7. Illustration showing the formation of UiO-67-bndc which is composed of $Zr_6O_4(OH)_4$ clusters and H_2bndc linker and is isostructural to UiO-67.

Generally, a MOF catalyst is synthesized using a mixture of inert and functionalized ligands to obtain a density of sites in the framework that provides balance between activity and catalyst

stability, colloquially called a "mixed-linker MOF". Mixed-linker MOFs are synthesized with the combination of two or more linkers. Some percentage of the linker of a MOF is substituted with another suitable linker (called functionalized linker) by ensuring that the node of the MOF remains unaffected.[75] It is a common way for providing functionalization to an established MOF, opening added possibilities of applications.[104-106] Mixed-linker MOFs can also offer an anchoring site for the introduction of an active metal center in the pores of MOFs. This binding site helps to stabilize the metal in the pores of the MOFs. The biphenyl moiety of UiO-67 provides a more versatile anchoring point for functional groups than the single phenyl ring of UiO-66.[69, 107] Its higher porosity also allows reactants and products of a catalyzed reaction to diffuse more freely, with less steric limitations. There are many factors, which are necessary for selecting the linkers which can be used for making mixed linker MOFs:

a) The length of the linker: The length of the functionalized linker is advisable to be similar to that of the original linker of the MOF unless the intent is to introduce changes to the crystal structure of the MOF. Hence, for example benzene-1,4-dicarboxylate linkers can be partially substituted by 2-aminobenzene-1,4-dicarboxylate. This was done for well-established MOF-5 where the added NH_2 group was beneficial for Pd immobalisation.[108] Moreover, UiO-67 is seen to be often functionalized by partial substitution of the H_2bpdc linker by [2,2'-bipyridine]-5,5'-dicarboxylic acid (H_2bpydc). H_2bpydc thus provides two nitrogen atoms, which are used for binding metal centers as a bidentate ligand in the pores of the MOF. Literature shows the incorporation of metals like Pt, Cu, Fe, Pd, Co, Ce in the bpydc-bpdc UiO-67 system.[66, 74, 99, 109-114]

b) Size of the linker: The size of the functionalized linker has a great impact in the formation of MOFs. The steric hindrance of large linkers/complexes may obstruct the crystallization of the MOF.[72] Therefore, introduction of bulky complexes in the framework of the MOF by direct synthesis is difficult. Cohen and coworkers functionalize UiO-67 with (bis(2,2'-bipyridine)(5,5'-dicarboxy-2,2'-bipyridine)ruthenium(II)) by three different strategies, a) direct synthesis, b) post-synthetic exchange (PSE) and c) post-synthetic modification (PSM).[75] With the direct synthesis, the Ru loading was very low. Therefore, for larger molecules it is advisable to use PSM as it gave evidently 10 % loading, in this case.

c) Solubility of the linker: It is important to know the relative solubility of the linkers in the reaction conditions. This will ensure the incorporation of both linkers homogeneously. In case,

one linker has lower solubility, it is advisable to add the linkers in the sequence of low to high solubility to allow them to dissolve and distribute evenly in the solution.

d) Percentage of mixed linker: Low amounts (up to 20-30 %) of functionalized linkers in the framework of the MOFs maintains the crystal structure and does not shows large deviation in stability of the MOF. It also helps to bind sufficient amount of metal for catalytic testing. Alterations in the MOF by mixed-linker synthesis often decreases its thermal stability as the percentage of mixed-linkers is increased (50 % and above).[105, 108]

e) Effect of reaction conditions: The reaction conditions should be suitable for maintaining the stability of mixed-linker. For instance UiO-67 is crystallized in an acidic reaction mixture as HCl is produced by the reaction of DMF and H_2bpdc. We tried to introduce 10 % of 3,3'-diethoxy-[1,1'-biphenyl]-4,4'-dicarboxylic acid (H_2bpdc-$(OMe)_2$) in UiO-67 by direct synthesis but this functionalized linker showed decomposition in acidic conditions.[115] H_2bpdc-$(OMe)_2$ cleaved under acidic condition to yield 3,3'-dihydroxy-[1,1'-biphenyl]-4,4'-dicarboxylic acid (H_2bpdc-$(OH)_2$) which inhibited the introduction of this linker in the MOF. The decomposition of the linker was confirmed by performing reaction directly on H_2bpdc-$(OMe)_2$ linker (Figure 8). This highlights the importance to know the effect of reaction condition to the functionalized linker, prior to the synthesis of mixed-linker MOF.

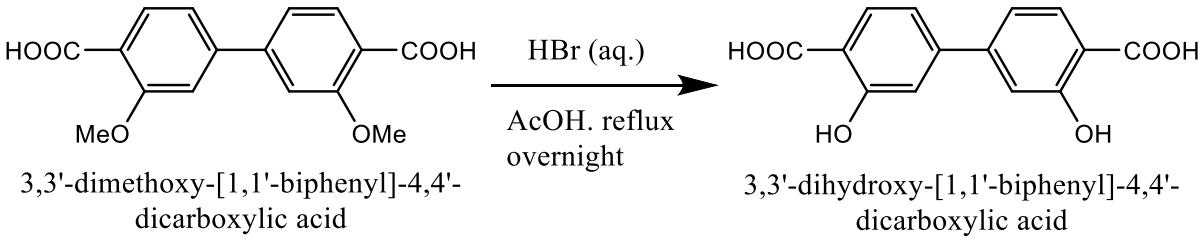

Figure 8. Reaction of H_2bpdc-$(OMe)_2$ to H_2bpdc-$(OH)_2$ as an effect of reaction condition in the synthesis of UiO-67.

The amount of functionalized linker in the final mixed-linker MOF is lower than the intended amount in most of the cases, as observed during the work of this thesis. For example, an incorporation of 10 % of the functionalized linker in the MOF framework was intended but the NMR reveals that the functionalized linker is between 5-8 % with respect to H_2bpdc in case of UiO-67 type mixed linker MOF. There can be many reasons for the low incorporation such as, i) low selective binding of the functionalized linker towards Zr, ii) low solubility of the functionalized linker than H_2bpdc or iii) synthesis approach as the author has used only direct synthesis approach for the synthesis of mixed linker MOFs in this work. Therefore, it is challenging to state the true reason for the lower incorporation.

Furthermore, these mixed linker MOFs were used for the metal incorporation. Introduction of chemically active metal sites in the MOF pores is of great interest for catalysis as discussed above. The choice of the metal depends on the reaction of interest. Ni grafted MFU-4l MOF was seen to be used as a catalyst for selective dimerization of ethene to 1-butene. MFU-4l is a Zn-based MOF; $Zn_5Cl_4(BTDD)_3$ where BTDD is bis(1*H*-1,2,3-triazolo[4,5-*b*][4′,5′-*i*])dibenzo[1,4]dioxin). Ni grafted MFU-4l has shown exceptionally high selectivity of more than 90 % towards 1-butene.[116] Moreover, Ni grafted H_2bpydc linker was introduced on the free Zr-OH sites in the NU-1000 and seen to be catalytically active.[117] NU-1000 is based on $Zr_6(\mu_3\text{-}O)_4(\mu_3\text{-}OH)_4(H_2O)_4(OH)_4$ nodes and tetratopic 1,3,6,8-(p-benzoate)pyrene ($TBAPy^{4-}$) linkers. On similar grounds, in our group UiO-67 with 10 % of H_2bpydc was synthesized and Ni was grafted to the free nitrogen sites of the H_2bpydc linker and tested for ethene dimerisation.[118] This catalyst yielded up to 6 % conversion with 99 % selectivity to linear 1- and 2-butenes without the use of co-catalyst, unlike other common catalysts.

Moreover, such metal incorporation also makes the MOF catalyst interesting towards redox chemistry. For example, incorporation of Pt in the mixed linker H_2bpydc UiO-67 MOF would exhibit Pt site which has various stable oxidation state (0, II and IV). Furthermore, for an active catalyst, it is interesting to investigate the local environment of the metal site in order to draw estimations about the state of metal. This is a challenging tasks and requires combination of various techniques using synchrotron facilities. The structural and oxidation state of the metal site can be determined using extended X-ray spectroscopy fine structure (EXAFS) and X-ray absorption near edge structure (XANES). These techniques can also help in the estimation of counter ions attached to the active metal sites which helps to understand its local coordination. In case of Pt incorporated H_2bpydc UiO-67 MOF, the counter ions were seen to be chloride molecules.[66] The removal of Cl ions was observed using operando TPR-EXAFS experiments, leaving the Pt atom to be coordinative unsaturated open site possible for catalytic application.

The synthesis of similar metal incorporated various mixed-linker MOFs of this work is discussed in detail in section 2.5. These MOF catalysts were used tested for various reaction.

2. Experimental methods

2.1. Characterisation techniques and their use in the thesis

There were many characterization techniques employed for the investigation of the synthesized MOFs in this thesis. Five characterization techniques (PXRD, nitrogen sorption, TGA-DSC, SEM-EDX and 1H NMR) are central and are performed for mostly all of the synthesized material. Other than these techniques, important information was inferred by extended techniques like fourier-transform infrared spectroscopy (FTIR), ultraviolet–visible spectroscopy (UV-Vis), x-ray Absorption Spectroscopy (XAS), single crystal X-ray diffraction (SC-XRD). These techniques were employed only on selected samples and were performed with extended help and collaboration.

2.1.1. Powder X-ray diffraction (PXRD)

PXRD was used as a major tool to characterize all the synthesized materials. It was utilized to determine, i) crystallinity of MOF (as-synthesized, after modification and stability tests), ii) presence of forbidden reflections and iii) the correct phase of the product. Samples were prepared using ∼20 mg of the sample on a glass plate XRD sample holder by spreading it evenly and covering with transparent plastic film. The plastic film gives a small signal in the PXRD patterns observed at 2θ = ∼22 ° and 34 ° as broad peaks. PXRD patterns (Cu Kα radiation, λ = 1.5418 Å, 2θ range = 2-50 °, time scale = 1, resulting in a d-spacing to 1.82 Å) were collected in reflectance Bragg-Brentano geometry with a Bruker D8 Discovery diffractometer equipped with a focusing Ge-monochromator and a Bruker LYNXEYE detector. The crystallite size was estimated by refining the diffraction pattern by “Rietveld” refinement using the software TOPAS against an ideal UiO-67 structure (Table A1 and Figure A1). The Rietveld method was used in a very restricted mode, where only the crystallite size parameter and sample displacement were allowed to refine freely, and all atomic positions and occupancies were restrained. This method was used because it takes the peak intensities into account, which would have provided the opportunity to explore e.g. difference maps. For the purpose of crystallite size determination, however, a Pawley refinement might as well have been used.

2.1.2. Thermogravimetric analysis-Differential scanning calorimetry (TGA-DSC)

The TGA-DSC technique gives a temperature profile where a sample is heated under a controlled atmosphere with a specified temperature program. Therefore, weight loss can be seen as a function of temperature. For UiO-67, weight losses are observed with the i) loss of water or solvent frim the MOF pores, ii) dihydroxylation of cornerstones, iii) removal of modulator molecules and iv) MOF framework breakdown via combustion of MOF linkers. Moreover, DSC measures the amount of heat released or required during the heating of the sample. A positive peak in the DSC is indicative of exothermic process whereas a negative peak shows endothermic process. For UiO-67, mostly endothermic peaks were observed due to removal or breakdown of framework. TGA-DSC was performed to know the thermal stability of all the samples and it was also employed in the static thermal stability tests. Also, TGA plays an important role for the calculation of defects as it is possible to calculate the mass of organics in the MOF sample using TGA analysis (Section 2.3.2). TGA-DSC analysis was performed on a Netzsch STA 449 F3-Jupiter instrument, by flowing a mixture of 5 mL/min O_2 and 20 mL/min of N_2 and using a ramp rate of 5 °C/min. ~20 mg of the sample was weighed and transferred into an Al_2O_3 sample holder and the data was collected for the temperature range of 30 °C to 800 °C.

2.1.3. ^{1}H NMR spectroscopy

^{1}H NMR is basically the dissolution NMR where MOF is digested in a deuterated base solution. By treating the MOF with base solution, the organic part of the MOF (linker, modulator, solvent etc) dissolves in the solution and this solution is analyzed to quantify the composition of the MOF. This is an indirect way to perform solution NMR on MOFs and estimate the organic components as it does not confirm the true bond in the MOF (as it is estimated after the MOF framework is destroyed). These results are combined with the TGA results to get a quantified individual organic components to find out the amount of capping agents and therefore discuss the extent of defects in UiO-67 samples (Section 2.3.2). Samples were prepared by weighing 20 mg of the dry sample in a centrifuging tube and adding 1 mL of 1M NaOH (in D_2O). The tubes were shaked properly to get a homogeneous suspension and kept overnight for digestion. After centrifuging the digested suspension for 15 min, 600 µL solution was pipetted to an NMR tube. This hydroxide-based procedure dissolves only the organic portion of the MOF (linker, modulator, solvent etc.), while the inorganic content is converted into mixed oxides/hydroxides

of Zr that settle at the bottom of the NMR tube and do not influence the spectra. Liquid ^{1}H NMR spectra were obtained with a Bruker AVII 400 NMR Spectrometer (400 MHz). The relaxation delay (d1) was set to 20 seconds with 64 scans.

2.1.4. Scanning Electron Microscopy (SEM) and Energy Dispersive X-ray Spectroscopy (EDS)

SEM was used to analyse the morphology and size of the crystals in various UIO-67 samples. The metal to Zr ratio was calculated using EDS for the samples for the metal incorporated samples. SEM and EDS were taken on a Hitachi SU8230 Field Emission Scanning Electron Microscope (FE-SEM). EDS was performed using an XFlash 6|10 EDX detector.

2.1.5. Nitrogen sorption measurements at 77 K

Nitrogen sorption is employed for measuring the volume of nitrogen adsorbed by the sample as a function of pressure. It is used for assessing the porosity of all the MOF samples and calculate surface area and pore volume from it. Nitrogen sorption were performed with a BelSorp mini II instrument. In each measurement, ~ 40 mg of the sample was weighed into a 9.001 cm^3 glass cell and pretreated at 80 °C for 30 min and 200 °C for 60 minutes, under vacuum.

2.2. General approach to synthesize UiO-67 and UiO-67-type MOFs

UiO-67 was synthesized via a simple one-pot reaction in DMF at 130 °C, using benzoic acid as modulator and water as aqueous additive (section 1.6.2). $ZrCl_4$ was added to the solution of water and DMF at room temperature on a stirring plate. This solution was heated and benzoic acid was added, waited until completely dissolved and then added the linker/s. The solution was transferred to a round bottom flask, fitted with the water condenser and stirred overnight at 130 °C. The product was filtered and washed with hot DMF (around 100-120 °C) and acetone (room temperature), followed by drying at 150 °C overnight. Details about the precise amounts can be found in the following sections, depending on the kind of synthesis.

2.3. UiO-67

In recent years, UiO-66 has been studied thoroughly in many aspects, such as optimization of the regular synthesis procedure to a scalable, reproducible and low-cost protocol aiming for high quality material with enhanced properties.[84, 88-89, 119-120] The relationship between synthesis parameters and MOF properties has not been investigated to the same degree for UiO-67 as for UiO-66, and reported methods show poor reproducibility in terms of the porosity and stability of the product MOF.[84, 91-92] Conventional UiO-67 synthesis is carried out by reaction of $ZrCl_4$:H_2bpdc:DMF in a molar ratio (equiv) of 1:1:300-500 and crystallizing at 120 °C. The significance of molar equivalent (denoted by "equiv") is to highlight the interdependent ratio between various reagents used for the synthesis. In other words, in conventional UiO-67 synthesis, for every mole of $ZrCl_4$, one mole of H_2bpdc is used to react in the presence of 300 to 500 moles of DMF. Under these conditions, the reagents dissolve completely, and upon MOF formation, the concentration of reagents in solution, drops. The linker can exist in its solid form, dissolved in the mother liquor or as part of the MOF structure (equation 1):

$$\mathbf{H_2bpdc_{(s)}} \leftrightarrow \mathbf{H_2bpdc_{(sol)}} \leftrightarrow \boldsymbol{H^+_{(sol)}} + \mathbf{Hbpdc^-_{(sol)}} \leftrightarrow \mathbf{2H^+_{(sol)}} + \mathbf{bpdc^{2-}_{(sol)}} \leftrightarrow \boldsymbol{2H^+_{(sol)}} + \mathbf{bpdc^{2-}_{(sol,\ MOF)}} \quad (\mathbf{1})$$

Addition of a modulator helps forming well-defined crystals of UiO-67. Due to the common ion effect (in this case H^+), modulator addition further decreases the already limited solubility of the H_2bpdc linker (Figure 9). Solvent hydrolysis represents a further complication; like the modulator, it adds to the H^+ content of solution, and the deprotonated formic acid competes with the linker for interaction with Zr^{4+} sites (Figure 9).

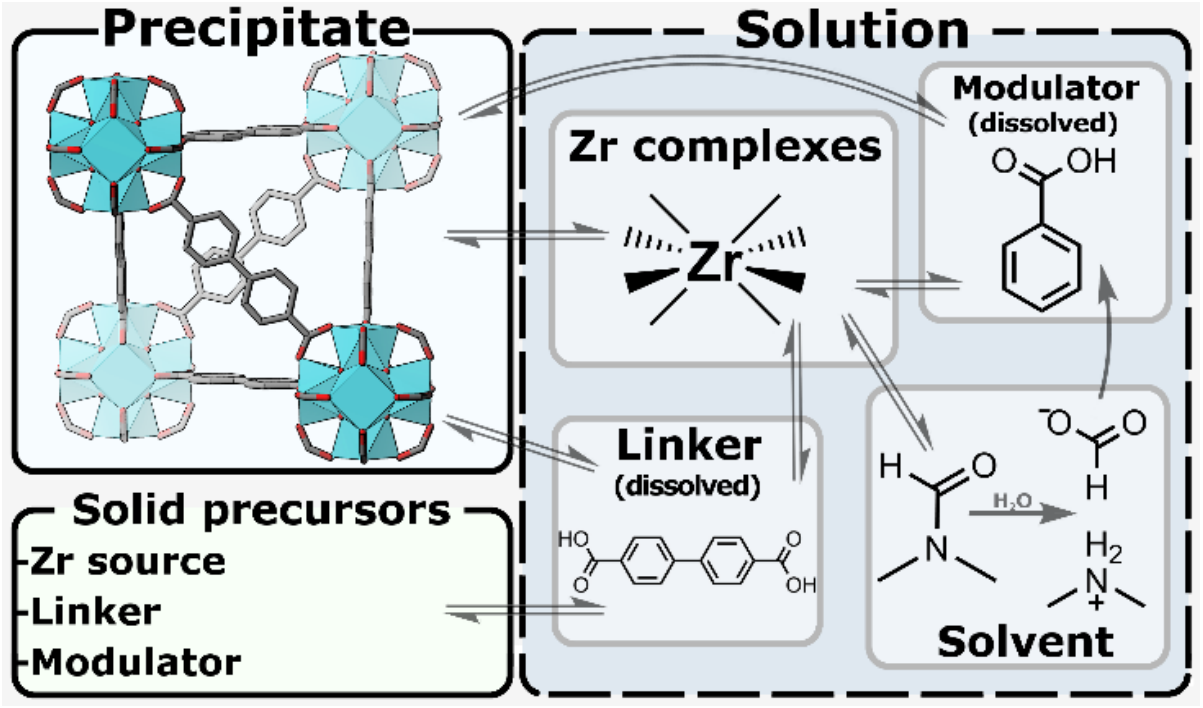

Figure 9. Reversible interactions (simplified) occurring during the formation of UiO-67.

Therefore, the effect of interdependence of reagents in the synthesis of UiO-67 and its consequences on the defectivity of the MOF is discussed in detail in this thesis (section 2.3). Further, the best conditions obtained for the synthesis of UiO-67 are tested by employing it to other UiO-67-type MOFs like UiO-67-bndc, where the linker is [1,1'-binaphthalene]-4,4'-dicarboxylic acid (H_2bndc) instead of H_2bpdc (section 2.3.5). The results from UiO-67 and UiO-67-bndc were further used to make mixed-linker MOFs based on replacing certain fraction of linkers (H_2bndc and H_2bpdc) and substituting it with functionalized biphenyl linkers (section 2.5). Furthermore, these MOFs are post-synthetically modified and incorporated with metals to test their catalytic activity, discussed in section 2.5.2.

2.3.1. Screening the reaction conditions

UiO-67 is synthesized using $ZrCl_4$, H_2bpdc linker, modulator and additive in DMF at elevated temperature. Therefore, it is necessary to understand the effect of various crystallization environment and determine the factors to control their degree and correlation to the quality of the material.

2.3.1.1. Preliminary high-throughput synthesis

An initial high-throughput screening of several parameters of UiO-67 synthesis was performed to confirm the effects of the already explored variables in the literature:

i) effect of additives

ii) effect of modulator

iii) reaction temperature

iv) amount of modulator

The precise details are summarized in Table 1. The synthesis of the MOF was performed with a Zr:DMF as a ratio of 1:300 (equiv). The thermal stability of the samples were later investigated by heating them at 450 °C for 2 hours in air.

Table 1. Synthesis parameters for the initial high-throughput screen of UiO-67 syntheses.

Synthesis parameter	Parameter value
Solvent amount (DMF:Zr) (molar equiv w.r.t. to Zr moles)	300, 100, 50, 35, 20
Modulator type	Benzoic acid (BA), acetic acid (Ac)
Modulator amount (molar equiv w.r.t.to Zr moles)	0, 3, 6, 9, 12, 15, 18
Additives	HCl (35 %), H_2O
Temperature (°C)	120, 130, 140

503 µL of water (0.0280 mol/ 3.00 equiv) was added to a beaker containing 216 mL of DMF (2.79 mol/ 300 equiv) and a magnet. 2.17 g of $ZrCl_4$ (0.00930 mol/ 1.00 equiv) was added at room temperature and the solution was heated to 110 °C, under stirring. The solution was transferred to twelve beakers (18 mL each) labelled 0 Ac, 3 Ac, 6 Ac, 9 Ac, 12 Ac, 15 Ac, 0 BA, 3 BA, 6 BA, 9 BA, 12 BA and 15 BA, where Ac and BA stands for acetic acid and benzoic acid, respectively (Figure 10).

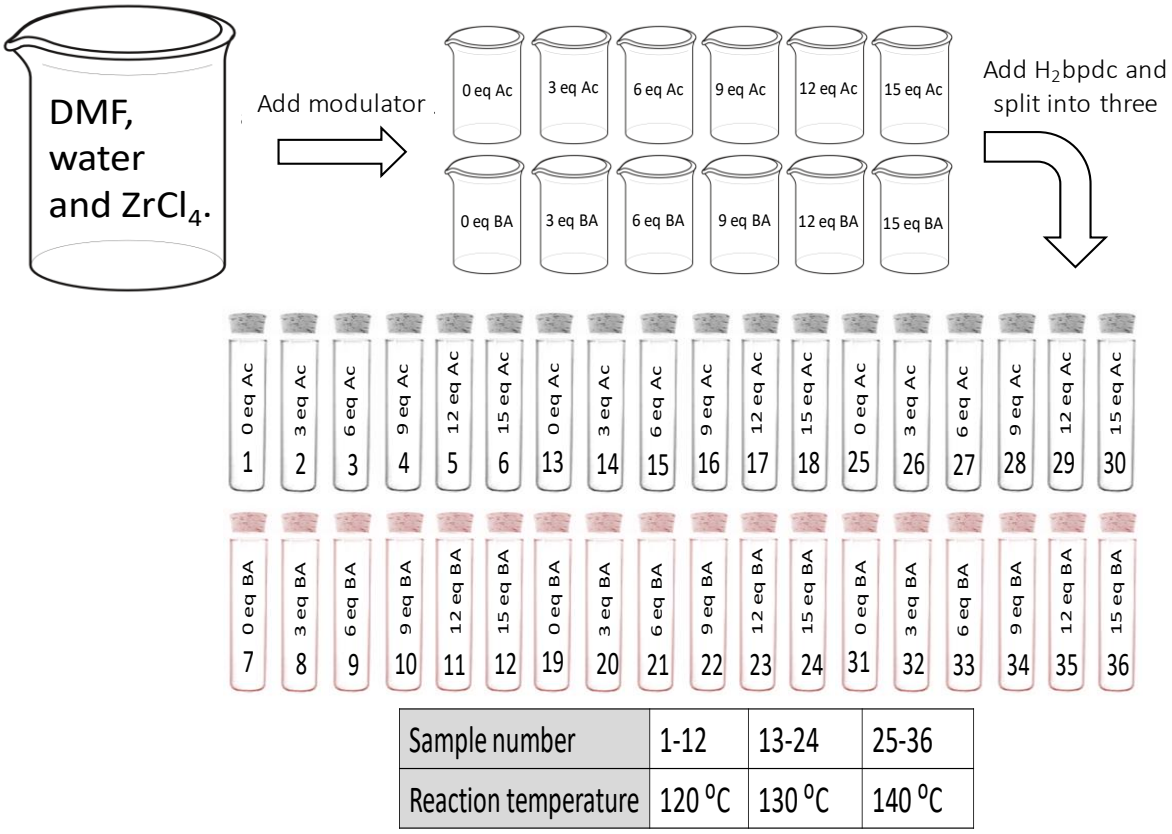

Figure 10. Schematic representation of the formation of 36 samples of set W. Similarly, set H was made by adding $HCl_{(aq)}$ instead of water giving rise to another 36 samples.

Ac and BA was added to the 12 beakers according to Table 2, followed by 0.188 g of H_2bpdc linker (0.00930 mol/ 1 equiv). The solution of each beaker was divided into three test tubes (6.00 mL each) and closed loosely with a Teflon cap. Thus obtained three group of twelve test tubes called set W (as it has water), kept at 120 °C, 130 °C and 140 °C overnight (Figure 10). The white solid was collected by centrifugation and washed with acetone (5.00 mL*1) and dried overnight at 150 °C. The above procedure was repeated to obtain Set H (three sets of twelve samples each) by adding 658 µL of hydrochloric acid (3 equiv) instead of water. The PXRD of all the samples (72 samples) were recorded. Set W and set H were heated for 2 hours at 450 °C and recorded the PXRD to check their thermal stability.

Table 2. Amount of modulator used to make set W and set H, for preliminary optimization of UiO-67.

Entry	Modulator	Amount of modulator to be added					
		0 equiv (0 mol)	3 equiv (0.030 mol)	6 equiv (0.060 mol)	9 equiv (0.080 mol)	12 equiv (0.120 mol)	15 equiv (0.140 mol)
1	Ac (µL)	-	133	266	399	532	665
2	BA (g)	-	0.284	0.568	0.862	1.14	1.42

2.3.1.2. Screening the amount of solvent for UiO-67 synthesis

This sub-section focuses on the Zr:DMF ratio and attempting to establish the interdependence of the amount of solvent and modulator (Zr:DMF:BA). The main goal of this study was to optimize the synthesis condition of the UiO-67, obtain a high quality, stable UiO-67 with high porosity and high yield by pushing the use of the solvent to the lower limits. A set of five reactions were prepared where amount of DMF was screened with 20 equiv (0.170 mol), 35 equiv (0.300 mol), 50 equiv (0.430 mol), 100 equiv (0.860 mol) and 300 equiv (2.57 mol) and other parameters as constant. Zr = 1 equiv (0.00860 mol), H_2bpdc = 1 equiv (0.00860 mol), BA = 9.00 equiv (9.430 mol); H_2O = 3.00 equiv (0.0260 mol); DMF = vary, at 130 °C. UiO-67 was synthesized using the procedure described in section 2.2 and washed with hot DMF (30 mL*3) and acetone (30 mL*3).

Table 3. Amount of reagents used in the screening of Zr:DMF for UiO-67 synthesis.

Entry	DMF (equiv)	DMF (mL)
1	20	13.3
2	35	23.3
3	50	33.3
4	100	66.5
5	150	200
2.00 g of $ZrCl_4$, 2.08 g of H_2bpdc, 9.40 g of BA and 0.460 mL of H_2O		

2.3.1.3. Screening the amount of modulator for UiO-67 synthesis

The core results of the study were obtained by two syntheses series in which the Zr:modulator ratio was systematically varied with solvent concentration to be 50 equiv or 300 equiv. These series of UiO-67 are labeled C-x_{BA} and Dx_{BA}, signifying “concentrated” and “dilute”, respectively, in which $ZrCl_4$:H_2bpdc:H_2O:DMF molar ratios of 1:1:3:50 and 1:1:3:300. In the respective concentrations, up to 18 molar equiv of BA with respect to reagents were used, and each material is labeled with this number (see Table 4). Thus, sample C-3_{BA} refers to UiO-67 made in a concentrated synthesis with 3 molar equiv of BA, the ratios of $ZrCl_4$:H_2bpdc:BA:H_2O:DMF as 1:1:3:3:50 (see Table 5). Characterization data is discussed in section 3.1.1.3.

Table 4. Moles of benzoic acid used for the synthesis of C-x_{BA} and Dx_{BA} series.

Entry	C-x_{BA} series	D-x_{BA} series	BA (molar equiv)	BA (mol)
1	C-0_{BA}	D-0_{BA}	0	0
2	C-3_{BA}	D-3_{BA}	3	0.0260
3	C-6_{BA}	D-6_{BA}	6	0.0520
4	C-9_{BA}	D-9_{BA}	9	0.0770
5	C-12_{BA}	D-12_{BA}	12	0.103
6	C-15_{BA}	D-15_{BA}	15	0.129
7	-	D-18_{BA}	18	0.154

Concentrated synthesis (C-x_{BA}): A set of 6 reactions were performed using the procedure described in section 2.2 where benzoic acid was screened using 0 equiv, 3 equiv, 6 equiv, 9 equiv, 12 equiv and 15 equiv with other parameters as constant. Zr = 1 equiv (0.009 mol), H_2bpdc = 1 equiv (0.009 mol), BA:vary; H_2O = 3 equiv (0.0260 mol); DMF = 50 equiv (0.430 mol), at 130 °C. They were labelled as C-x_{BA} where x ranges from 0 to 15 equiv depending on amount of benzoic acid used in the preparation of the sample and C stands for concentrated synthesis.

Table 5. Amount of reagents used in the screening of amount of BA for 50 equiv DMF (concentrated synthesis) for UiO-67.

Entry	Label	BA (g)
1	C-0_{BA}	0
2	C-3_{BA}	3.14
3	C-6_{BA}	6.29
4	C-9_{BA}	9.43
5	C-12_{BA}	12.08
6	C-15_{BA}	15.72
2.00 g $ZrCl_4$, 2.08 g H_2bpdc, 0.460 mL H_2O and 33.3 mL DMF		

Dilute synthesis (D-x_{BA}): A set of 7 experiments was prepared for the screening of benzoic acid for dilute synthesis using the procedure described in section 2.2 where BA was screened using 0 equiv, 3 equiv, 6 equiv, 9 equiv, 12 equiv, 15 equiv and 18 equiv with other parameters as constant. Zr = 1 equiv, H_2bpdc = 1 equiv, BA = vary; H_2O = 3 equiv; DMF = 300 equiv at 130 °C. They were labelled as D-x_{BA} where x ranges from 0 to 18 equiv depending on amount of benzoic acid used in the preparation of the sample and D stands for dilute synthesis.

Table 6. Amount of reagents used in the screening of amount of BA for 300 equiv DMF (diluted synthesis).

Entry	Label	BA (g)
1	D-0_{BA}	0
2	D-3_{BA}	3.14
3	D-6_{BA}	6.29
4	D-9_{BA}	9.43
5	D-12_{BA}	12.08
6	D-15_{BA}	15.72
7	D-18_{BA}	18.87
2.00 g $ZrCl_4$, 2.08 g H_2bpdc, 0.460 mL H_2O and 33.3 mL DMF		

2.3.2. Calculation of missing-linker defects

The main organic constituents in UiO-67 are deprotonated analogues of linker ($bpdc^{2-}$), modulator (benzoate) and hydrolyzed solvent (formic acid (FA); an *in situ* product of the hydrolysis of DMF).[58, 100] Their presence (after extensive washing) shows that the organic constituents are bonded to the framework. Their relative ratio gives an estimate of the true composition of the as-synthesized material. The combination of TGA-DSC and 1H NMR data gives an estimate of the relative amount of organic constituent in the MOF samples. This has been used to calculate missing-linker defects in the samples of UiO-67, based on the previously published report for UiO-66.[59]

Assumptions associated with these methods:

i. The amount of cluster vacancy defects is negligible (checked for signs of forbidden low-angle reflections in the PXRD)
ii. There is no mesoporosity associated with such defects (checked by adsorption isotherms).
iii. The residual species at 800 °C is pure ZrO_2 (checked by PXRD).

TGA-DSC analysis gives a MOF decomposition profile with respect to temperature. 20 mg of the sample was weighed in an Al_2O_3 sample holder and heated up to 800 °C in synthetic air. Thus obtained data reveals the removal of water and organics in the MOF by showing weight loss by increase in temperature, before the MOF framework collapse (at about 450 °C). With the temperature profile of 30 to 800 °C, UiO-67 shows transition from hydroxylated ($Zr_6O_4(OH)_4(bpdc)_6$) form of UiO-67 to dehydroxylated form ($Zr_6O_6(bpdc)_6$) and at higher temperature to zirconium oxide (ZrO_2).

$$Zr_6O_4(OH)_4(bpdc)_6 \rightarrow Zr_6O_6(bpdc)_6 \rightarrow 6ZrO_2$$

Therefore, we can calculate the molar mass of an ideal UiO-67 material.

Molar mass of dehydroxylated UiO-67 ($Zr_6O_6(bpdc)_6$) $= 2084.57\ g/mol$

Molar mass of hydroxylated UiO-67 ($Zr_6O_4(OH)_4(bpdc)_6$) $= 2120.59\ g/mol$

Molar mass of 6 formula units of ZrO_2 $= 739.308\ g/mol$

This implies that in case of dehydroxylated UiO-67, $2084.57\ g/mol$ is higher than 6 moles of ZrO_2 with the factor of 2.819. So, the ideal TGA-DSC plateau should be at 281.9 % $= \sim 282$ %.

On the other hand, in case of hydroxylated UiO-67, $2120.59\ g/mol$ is higher than 6 moles of ZrO_2 with the factor of 2.868. Therefore, the ideal TGA-DSC plateau should be at 286.8 %.

The difference between the ideal plateau of hydroxylated UiO-67 and dehydroxylated UiO-67 can thus be calculated by subtracting both the values i.e. 4.8 %, assuming that only two water molecules per cluster are lost and no BA or $bpdc^{2-}$ linkers are affected.

Hence, if the MOF material is perfectly coordinated to 6 bpdc linkers, its TGA-DSC plateau should be at 282 % and 286.8 %. At about 375 °C, the plateau of the material should be at 286.8 % (called theoretical dehydroxylated ideal mass) of relative molar ratio percent. Indeed, the material may deviate from ideality where two cases arises where the plateau is i) above or ii) below the theoretical mass loss, depending on the actual mass of the synthesized MOF. The excess mass in the TGA would indicate the presence of excess mass corresponding to the chemical species in the pores whereas the mass deficient MOF will indicate the missing chemical species. Together with results from PXRD and nitrogen adsorption indicates the absence of missing clusters defects which implies that the samples in this work should mainly contain missing-linker defects.

The ideal composition of UiO-67 after the dehydration of the cluster is $Zr_6O_6(bpdc)_6$, but in the presence of missing-linkers it is $Zr_6O_6(bpdc)_{6-x}$ where x is the amount of missing-linkers. Assuming all benzoate and formate is decomposed.

$$n_{linker} = \frac{\frac{Wt._{200\ ^\circ C} * Mm_{6ZrO_2}}{100} - Mm_{Zr_6O_6(OH)_4}}{Mm_{linker}}$$

Where n_{linker} gives the estimate of the number of total linkers in the MOF sample coordinated to Zr_6 cluster, which is six in case of ideal UiO-67.

The major drawback of calculation of defects based on only TGA-DSC is that it does not give the estimate of detailed composition of the MOF to support the claims of the number of linkers associated per cluster. The decomposition of the organics of the MOF is also affected by the increase in internal temperature of the material due to combustion of other organic species. This may delay the decomposition of a particular species, hence giving no distinct peaks in the data. Therefore, to quantify the amount of organics more precisely, the results from TGA-DSC are combined with ^{1}H NMR which gives deeper understanding and quantifiable results. 20 mg of the sample is heated in air at 200 °C for 24 hours to remove residual solvent, digested in NaOD and the organic components are quantified with ^{1}H NMR. The composition (a mixture of $bpdc^{2-}$, benzoate and formate) is then scaled to the relative ratio of the organic constituents of the MOF using the mass value of the sample at 200 °C from TGA-DSC measurements.

The ideal composition of UiO-67 at 200 °C is $Zr_6O_4(OH)_4(bpdc)_6$, but in the presence of missing-linkers it is $Zr_6O_4(OH)_4(bpdc)_x(BA)_y(FA)_z$, where $x + y + z = 6$. The ratios of x:y:z is determined by ^{1}H NMR , and thus the average molar mass of the organic components ($Mm_{organics}$) can be found. The total amount of organic species will be the sum of molar masses of linker, BA and FA in the MOF sample and can be calculated using equation (2):

$$Total\ Mm_{organics} = Mm_{x\ linker} + Mm_{y\ linker} + Mm_{BA} + Mm_{FA} \quad (2)$$

Each of the molar mass can be calculated by using the integrals from the NMR,

$$Mm_{x\ linker} = \frac{Relative\ amount\ of\ x\ linker}{Relative\ amount\ of\ (x\ linker + y\ linker + BA + FA)} * Mm_{bpdc}$$

Similarly, other values for equation (2) can be calculated.

To calculate the total amount of organics per Zr cluster, the $Total\ Mm_{organics}$ should be divided by the mass of the cluster of the synthesized sample. This mass of the cluster can be found from the TGA-DSC curve, and the data point at 200 °C will be used to find the mass of the hydroxylated cluster.

Hence, total organic per Zr_6 cluster,

$$\frac{n_{total\ organics}}{Zr_6\ cluster} = \frac{Mass\ of\ cluster\ using\ Wt_{200\,°C}}{Total\ Mm_{organics}(from\ eq\ (1))}$$

And to find out number of individual constituents per Zr_6 cluster,

$$\frac{n_{x\ linker}}{Zr_6\ cluster} = \frac{Relative\ amount\ of\ x\ linker}{Relative\ amount\ of\ (x\ linker + y\ linker + BA + FA)} * \frac{n_{total\ organics}}{Zr_6\ cluster}$$

Similarly for y linker, BA and FA. These are the values used in results and discussion chapter which gives the number of individual organic constituents and therefore an estimation of composition of the MOF samples (for example Figure 25).

2.3.3. Time course synthesis

The insights to the mechanism of the synthesis of MOFs are still regarded as a challenge. Most of the synthesis of such materials are seen to be performed with 24 hours. It is interesting to see the formation of the particles with respect to time. Therefore, to monitor the synthesis of UiO-67 and follow it with respect to time, a time course study was performed. A reaction for the synthesis of UiO-67 was set up using the dilute synthesis protocol and samples were extracted at various intervals. These samples were characterized with ^{1}H NMR, TGA-DSC and SEM.

Synthesis of D-9_{BA} was repeated by using 2.00 g of $ZrCl_4$ (0.009 mol/ 1 equiv), 0.460 mL water (0.0260 mol/ 3 equiv), 200 mL of DMF (2.56 mol/ 300 equiv), 9.43 g of benzoic acid (0.077 mol/ 9 equiv) and 2.08 g of H_2bpdc linker (0.009 mol/ 1 equiv), using the procedure described in section 2.2. After the addition of linker (considered time zero), 20 mL of the reaction mixture was drawn out using a pipette at intervals of 4 h after the onset of precipitation i.e. at 0.5 h. Thus the samples were collected at 0.5 h, 4.5 h, 8.5 h, 12.5 h, 16.5 h, 20.5 h and after the end of reaction at 24 h. Three identical reactions were carried out to obtain sample for 0.5 h from reaction 1; 4.5 h, 8.5 h and 12.5 h from reaction 2 and 16.5 h and 20.5 h from reaction 3. These samples were filtered and washed with hot DMF (10 mL*3) and acetone (10 mL*3), followed by drying at 150 °C overnight. The samples were characterized by SEM, ^{1}H NMR and TGA-DSC and the results are discussed in section 3.1.2.

Synthesis of C-3_{BA} was repeated 2.00 g of $ZrCl_4$ (0.009 mol/ 1 equiv), 0.460 mL water (0.0260 mol/ 3 equiv), 33.3 mL of DMF (0.429 mol/ 50 equiv), 3.14 g of benzoic acid (0.0260 mol/ 3 equiv) and 2.08 g of H_2bpdc linker (0.009 mol/ 1 equiv). After the addition of linker (considered

0 minute), 3 mL of the reaction mixtures were collected at an interval of 4 hours after 0.5 h (as our previous experiments shows that precipitation starts after 0.5 h). Thus the samples were collected at 0.5 h, 4.5 h, 8.5 h, 12.5 h, 16.5 h, 20.5 h and after the end of reaction at 24 h. These samples were filtered and washed with hot DMF (2 mL*3) and acetone (2 mL*3), followed by drying at 150 °C overnight. Three identical reactions were carried out to obtain sample for 0.5 h from reaction 1; 4.5 h, 8.5 h and 12.5 h from reaction 2 and 16.5 h and 20.5 h from reaction 3. The samples were characterized by SEM and PXRD and the results are discussed in section 3.1.2.

2.3.4. Screening the amount of water for UiO-67

Upon some preliminary observations of unknown additional peaks in the X-ray diffraction pattern of some of the batches of UiO-67, the amount of water in the synthesis was examined. To our surprise the water addition both alters the zirconium cluster and the incorporation of benzoic acid into the MOF crystals. The benzoic acid act as “capping” ligands to compensate for the charge created from missing ligand defect in the MOF.

Therefore, a systematic series of samples were prepared to see the effect of water as an additive in the synthesis of UiO-67 MOF. For this partially substituted UiO-67 was used where the MOF is composed of 0.1 equiv of H_2bpydc linker ([2,2'-bipyridine]-5,5'-dicarboxylic acid) and 90 equiv of H_2bpdc ([1,1'-biphenyl]-4,4'-dicarboxylic acid), denoted as UiO-67-bpydc$_{(0.1)}$. The effect of varying amount of water in the synthesis of UiO-67-bpydc$_{(0.1)}$ was then studied by five samples, synthesized using 3, 4, 5, 6 and 9 molar equiv of water.

A set of six reactions was prepared using the procedure described in section 2.2, where amount of water was varied with 0.3 equiv (0.0026 mol), 3 equiv (0.0260 mol), 4 equiv (0.034 mol), 5 equiv (0.043 mol), 6 equiv (0.050 mol) and 9 equiv (0.077 mol) for the synthesis of UiO-67-bpydc$_{0.1}$ and other parameters as constant. Zr = 1 equiv, linker (H_2bpdc (0.9 equiv) + H_2bpydc (0.1 equiv)) = 1 equiv, BA = 3 equiv; H_2O = vary; DMF = 50 equiv, at 130 °C.

Table 7. Amount of water screened for the synthesis of UiO-67-bpydc$_{0.1}$.

Entry	Label	H_2O (equiv)	H_2O (mL)
1	UiO-67-bpydc$_{0.1}$-0.3$_{H_2O}$	0.3	0.046
2	UiO-67-bpydc$_{0.1}$-3$_{H_2O}$	3	0.46
3	UiO-67-bpydc$_{0.1}$-4$_{H_2O}$	4	0.62
4	UiO-67-bpydc$_{0.1}$-5$_{H_2O}$	5	0.77
5	UiO-67-bpydc$_{0.1}$-6$_{H_2O}$	6	0.93
6	UiO-67-bpydc$_{0.1}$-9$_{H_2O}$	9	1.39
2.00 g $ZrCl_4$, 1.87 g H_2bpdc, 0.209 g H_2bpydc, 3.14 g BA and 33.3 mL DMF			

Furthermore, Grey and coworkers show that different phases can be obtained for the Hafnium (Hf) analogue of UiO-67 by changing the concentration of water.[121] By carefully adjusting the amount of modulator (formic acid in this case) and the amount of water, the formation of **fcu**, **hcp** and **hexagonal nanosheets** (hns) phases are observed.[121] The amount of formic acid (19 to 152 equiv) and water (0 to 38 equiv) was screened. In the presence of 90 equiv of formic acid and 10 equiv or 38 equiv of water, phase-pure hcp or hexagonal nanosheets were observed, respectively. Other reaction conditions were kept constant such that $HfCl_4$ (1 equiv), H_2bpdc (1 equiv) and DMF (175 equiv) in an autoclave at 150 °C for 24 hours. The **hcp** phase of Zr-bpdc is very interesting as it has double cluster type inorganic nodes, $Zr_{12}O_8(\mu_3\text{-}OH)_8(\mu_2\text{-}OH)_6(CO_2)_{18}$ (condensation of 12-coordinate $Zr_6O_4(OH)_4(CO_2)_{12}$), Figure 11. The μ_3-OH and μ_2-OH sites are interesting for functionalization so that the MOF can be used as a metal-based catalyst.[122]

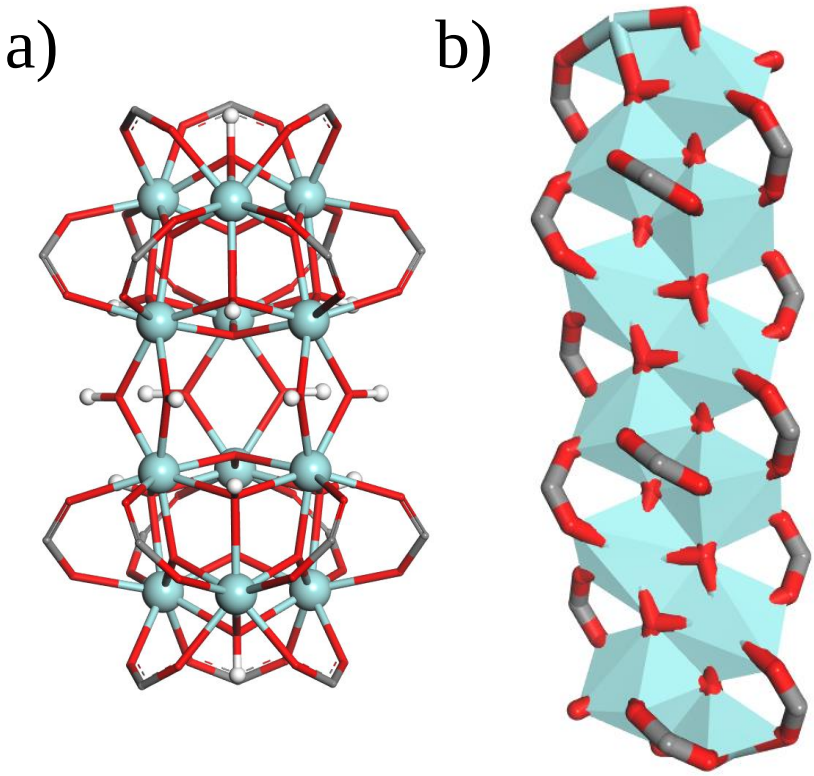

Figure 11. Illustration of the a) $Zr_{12}O_8(\mu_3\text{-}OH)_8$ $(\mu_2\text{-}OH)_6(CO_2)_{18}$ cluster of hcp phase of Zr-bpdc and b) $ZrO[O_2C\text{-}C_{12}H_8\text{-}CO_2]$ cluster of MIL-160C (right).

Synthesis of **hcp** and **hexagonal nanosheets** phase: 0.100 g of $ZrCl_4$ (0.00043 mol/ 1 equiv) and 0.104 g of H_2bpdc linker (0.00043 mol/ 1 equiv) was added to a 10 mL teflon liner of an autoclave, followed by the addition of 5.814 mL DMF (0.075 mol/ 175 equiv), 0.077 mL of water (0.0043 mol/ 10 equiv) and 1.457 mL of formic acid (FA, 0.039 mol/ 90 equiv), at room temperature. The mixture was sonicated for 15 min and autoclave was sealed, kept at 150 °C for 24 h. The white product was filtered and washed with hot DMF (5 mL*3) and acetone (5 mL*3) and dried at 150 °C overnight. For the synthesis of **hexagonal nanosheets** phase, instead of 10 equiv of water, 38 equiv of water was used. Therefore, 0.294 mL of water (0.016 mol/ 38 equiv) was added, keeping all the other things same.

Table 8. Amount of reagents used for the synthesis of hcp and hexagonal nanosheets phase using H_2bpdc linker.

Entry	Label	H_2O (equiv)	H_2O (mL)
1	hcp phase	10	0.077
2	hexagonal nanosheets phase	38	0.294
0.100 g $ZrCl_4$, 0.104 g H_2bpdc, 1.46 mL FA and 5.81 mL DMF			

2.3.5. Thermal stability

UiO MOFs are well known for their exceptional stability. Section 1.7 discusses the stability of UiO-67 with respect to temperature, time and pH. In order to evaluate the true thermal stability of UiO-67 synthesized by concentrated synthesis protocol, C-3_{BA} was calcined at various temperatures at 300 °C, 350 °C, 375 °C and 400 °C. The calcination was performed for 24 hours in air and the samples were labelled as C-3_{BA}@300 °C, C-3_{BA}@350 °C, C-3_{BA}@375 °C and C-3_{BA}@400 °C, respectively. After calcination and characterized with XRD and nitrogen adsorption isotherm to compare their stability with the parent C-3_{BA}. Furthermore, C-3_{BA} was calcined in-situ in the TGA-DSC instrument to obtain the static heat treatment with time results. Program with following steps was prepared (under a mixture of 5 mL/min O_2 and 20 mL/min of N_2):

i) Dynamic heating from 30 to 300 °C at 5 °C/ min
ii) Static heating for 12 hours at 300 °C
iii) Dynamic cooling from 300 to 30 °C at 20 °C/min
iv) Dynamic heating from 30 to 800 °C with the at 5°C/min

Repeated the procedure for obtaining the samples at 350 °C, 375 °C and 400 °C and the results are shown in Figure 40.

2.4. UiO-67-bndc (bndc = [1,1'-binaphthalene]-4,4'-dicarboxylate)

As discussed in the introduction, UiO-67-bndc is an important UiO-67-type MOF (section 1.9). Hence, a deeper insight on the synthesis parameters is necessary such that these results can be used for the synthesis of UiO-67-bndc based catalyst. Therefore, the screening of various parameters for the synthesis of UiO-67-bndc was performed, similarly as for UiO-67. The results from the best synthetic conditions for the synthesis of UiO-67 was used for the optimization of UiO-67-bndc.

2.4.1. Screening the reaction conditions

2.4.1.1. Preliminary screening

A preliminary screening of synthesis of UiO-67-bndc was performed to confirm the effects of variables used in the synthesis. Mainly, the effect of varying amount of benzoic acid was studied

ranging from 0 to 15 molar equiv (Table 9). The synthesis of UiO-67-bndc was performed at Zr:DMF as 1:150 molar equiv as the solubility of H_2bndc linker is much higher than of H_2bpdc linker.

Table 9. Synthesis parameters for the initial high-throughput synthesis.

Synthesis parameter	Parameter value
Solvent amount (DMF:Zr) (molar equiv w.r.t.to Zr moles)	150
Modulator type	Benzoic acid (BA)
Modulator amount (molar equiv w.r.t.to Zr moles)	0, 3, 6, 9, 12, 15
Additives	H_2O
Temperature (°C)	120/ 130/ 140

503 µL of water (0.028 mol/ 3 equiv) was added to a beaker containing 108 mL of DMF (1.40 mol/ 150 equiv) and a magnet. 2.17 g of $ZrCl_4$ (0.009 mol/ 1 equiv) was added at room temperature and the solution was heated to 110 °C, under stirring. This solution was split to six beakers (18 mL each) labelled 0 equiv BA, 3 equiv BA, 6 equiv BA, 9 equiv BA, 12 equiv BA and 15 equiv BA, where BA is benzoic acid. BA was added to the 6 beakers according to Table 10, followed by 0.527 g of H_2bndc linker (0.009 mol/ 1 equiv) to each beaker. This solution of each beaker was split into three glass vials (6 mL each) and closed loosely with a Teflon cap. Thus, obtained three sets of six vials were kept at 120 °C, 130 °C and 140 °C overnight (Figure 12). The white solid was collected by centrifugation and washed with acetone and dried at 150 °C overnight.

Table 10. Amount of modulator used for optimization of UiO-67-bndc.

Entry	Modulator	Amount of modulator to be added					
		0 equiv (0 mol)	3 equiv (0.028 mol)	6 equiv (0.056 mol)	9 equiv (0.084 mol)	12 equiv (0.112 mol)	15 equiv (0.140 mol)
1	BA (g)	-	0.570	1.140	1.703	2.271	2.840

Sample	1-6	7-12	13-18
Reaction T (° C)	120	130	140

Figure 12. Schematic representation of the formation of 18 reactions for the optimization of UiO-67-bndc.

These samples were exposed to inspect their stability towards temperature and water. The thermal stability tests were performed by heating all the samples at 400 °C for 2 h in air. The water stability test, 50 mg of each sample was immersed in 2 mL water for 24 hours. The samples were centrifuged and water was removed. PXRD of dried samples were recorded (section 3.2.1.1).

2.4.1.2. Screening the amount of solvent for UiO-67-bndc

With the results from the preliminary screening of UiO-67-bndc, it was interesting to see the synthesis of this material with the use of different amount of DMF, like UiO-67. Hence, the amount of DMF was screened using no modulator at 130 °C. This was performed by preparing a set of three experiments using the general procedure described in section 2.2, where the amount of DMF was screened with 50 equiv (concentrated "C"), 150 equiv (dilute "D") and 300 equiv (very dilute "VD") and other parameters as constant; Zr = 0.009 mol/ 1 equiv, H_2bndc = 0.009 mol/ 1 equiv, water = 0.0260 mol/ 3 equiv, benzoic acid = 0 equiv at 130 °C (Table 11). The resultant product was labelled as C-0_{BA}-bndc, D-0_{BA}-bndc and VD-0_{BA}-bndc for 50 equiv, 150 equiv and 300 equiv of DMF, respectively. These samples were washed with hot DMF (30 mL*3) and acetone (30 mL*3) and dried overnight at 150 °C.

Table 11. Amount of reagents used in the screening of Zr = DMF for UiO-67-bndc.

Entry	Sample	DMF (mol)	DMF (mL)
1	C-0_{BA}-bndc	0.429	13.3
2	D-0_{BA}-bndc	1.287	23.3
3	VD-0_{BA}-bndc	2.575	33.3
2.00 g of $ZrCl_4$, 2.96 g of H_2bndc, no BA and 0.460 mL of H_2O			

2.4.1.3. Screening the amount of modulator for UiO-67-bndc

The previous section of the UiO-67 screening reveals the interdependence of amount of solvent and modulator. Hence, for the final protocol modification for the synthesis of UiO-67-bndc will be completed by adjusting the amount of BA with respect to 50 equiv of DMF. By previous experiments it is known that the 3 equiv gives good quality UiO-67 in the presence of 50 equiv of DMF. Therefore, UiO-67-bndc is synthesized with 3 equiv BA using the concentrated synthesis. Moreover, C-0_{BA}-bndc is already presented in section 3.2.1.2, so this section shows the data for C-3_{BA}-bndc, only. This was performed in order to see the effect of modulator for the concentrated synthesis of UiO-67-bndc. Except the benzoic acid concentration, other parameters were kept constant, Zr = 1 equiv, H_2bndc = 1 equiv, water = 3 equiv, BA = 3 equiv, DMF = 50 equiv at 130 °C (Table 12).

Table 12. Amount of reagents used in the screening of benzoic acid for UiO-67-bndc.

Entry	Sample	BA (mol)	BA (g)
1	C-3_{BA}-bndc	3	3.14
2.00 g of $ZrCl_4$, 2.96 g of H_2bndc, 3.14 g BA, 0.460 mL of H_2O and 33.3 mL DMF			

2.4.1.4. Screening the amount of water for UiO-67-bndc

0.100 g of $ZrCl_4$ (0.00043 mol/ 1 equiv) and 0.147 g of H_2bndc linker (0.00043 mol/ 1 equiv) was added to a 10 mL Teflon liner of an autoclave, followed by the addition of 5.814 mL DMF (0.075 mol/ 175 equiv) and varying amount of water (3 equiv (0.001 mol), 10 equiv (0.004 mol) , 40 equiv (0.017 mol) and 80 equiv (0.034 mol)), at room temperature. The mixture was sonicated for 15 min, the autoclave was sealed and kept at 150 °C for 24 h. The white product was filtered and washed with hot DMF (5 mL*3) and acetone (5 mL*3) and dried at 150 °C overnight.

Table 13. Reaction conditions for water screening for UiO-67-bndc.

Entry	Label	H_2O (equivl)	H_2O (mL)
1	UiO-67-bndc-3_{H_2O}	3	0.023
2	UiO-67-bndc-10_{H_2O}	10	0.077
3	UiO-67-bndc-40_{H_2O}	40	0.309
4	UiO-67-bndc-80_{H_2O}	80	0.618
0.100 g $ZrCl_4$, 0.147 g H_2bndc and 5.82 mL DMF			

2.5. Mixed linker UiO-67 MOFs

The previous section has shown how the synthesis procedure for UiO-67 and UiO-67-bndc were tuned to assess and their effects on the quality of the final product. By making the right choice of synthesis conditions, one can obtain a desired material in terms of phase and defectivity. Some of the important approaches for using UiO-67 type MOFs in catalysis are:

i) immobilization of the active catalytic species such as metal nanoparticles in the pores of the material,
ii) catalysis at coordinatively unsaturated metal centers of the framework, and
iii) incorporation of catalytically active functional groups/ metals at the organic linker molecules.

The main focus to synthesis UiO-67 type catalyst was to incorporate metals in a mixed linker MOF where the framework is composed of H_2bpdc or H_2bndc together with functionalized biphenyl linkers. The following section outlines the synthesis of these mixed linker MOFs and how they were modified to host a metal to obtain metal active UiO-67 catalysts.

2.5.1. Synthesis of mixed linker UiO-67

Mixed linker MOFs can be synthesized by standard one-pot synthesis or post-synthetic exchange (PSE). In the former method all of the linkers are added while the MOF is synthesized and in the latter the linkers of the as-synthesized MOF are exchanged with the functionalized biphenyl linker to yield mixed linker MOFs. In this work, mixed linker MOFs are synthesized using the one-pot synthesis method using 10 % of functionalized biphenyl linker (0.1 equiv). Mixed linker MOFs, labelled "UiO-67-x-$linker_{0.9}$-y-$linker_{0.1}$" was synthesized in DMF at 130 °C, using benzoic acid as modulator and water as additive. Here, x-linker is the major linker (0.9 equiv which in most of the cases is H_2bpdc and in one case H_2bndc linker) and y-linker is

the minor linker (0.1 equiv- H_2bpydc, H_2bpdc-$(NH_2)_2$, H_2bpdc-(NH_2), H_2bpdc-$(OH)_2$), shown in Figure 13. UiO-67-bpdc$_{0.9}$-y-linker$_{0.1}$ was written as UiO-67-y-linker$_{0.1}$ for simplicity. The overall molar ration of Zr:linker is maintained as 1:1. Hence, five mixed linker MOFs are synthesized UiO-67-bpydc$_{0.1}$, UiO-67-(bpdc-$(NH_2)_2)_{0.1}$, UiO-67-(bpdc-(NH_2))$_{0.1}$ and UiO-67-(bpdc-$(OH)_2)_{0.1}$ and UiO-67-bndc$_{0.9}$-bpydc$_{0.1}$, explained in Table 14. The product was filtered and washed with hot DMF (30 mL*3) and acetone (30 mL*3), followed by drying at 150 °C.

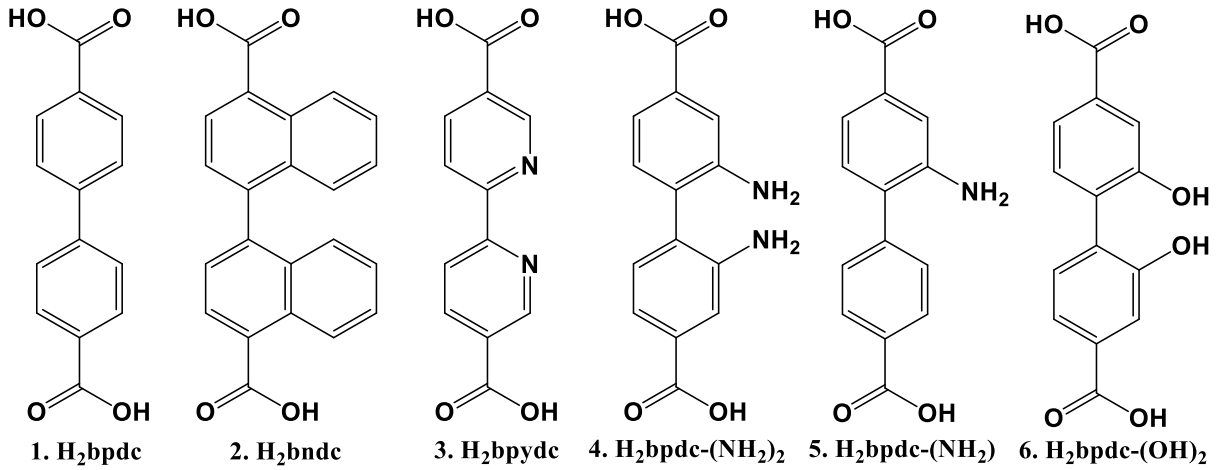

Figure 13. Structures of all the linkers used in this work; 1. [1,1'-biphenyl]-4,4'-dicarboxylic acid (H_2bpdc), 2. [1,1'-binaphthalene]-4,4'-dicarboxylic acid (H_2bndc), 3. [2,2'-bipyridine]-5,5'-dicarboxylic acid (H_2bpydc), 4. 2,2'-diamino-[1,1'-biphenyl]-4,4'-dicarboxylic acid (H_2bpdc-$(NH_2)_2$), 5. 2-amino-[1,1'-biphenyl]-4,4'-dicarboxylic acid (H_2bpdc-(NH_2)) and 6. 2,2'-dihydroxy-[1,1'-biphenyl]-4,4'-dicarboxylic acid (H_2bpdc-$(OH)_2$).

Mixed linker MOFs were synthesized by the concentrated synthesis using the method described in section 2.2. 2.00 g of $ZrCl_4$ (0.009 mol/ 1 equiv) was added to the mixture of 0.460 mL distilled water (0.0260 mol/ 3 equiv) and 33.2 mL DMF (0.429 mol/ 50 equiv) at room temperature on a stirring plate. This solution was heated and 3.14 g of benzoic acid (0.0260 mol/ 3 equiv) was added, waited until completely dissolved. This solution was transferred to a round bottom flask containing weighed amounts of linkers and a magnet, fitted with a water condenser and heated at 130 °C overnight. The product was filtered and washed with hot DMF (30 mL*3) and acetone (30 mL*3), followed by drying at 150 °C overnight. All the mixed-linker UiO-67 type MOFs were thoroughly characterized using PXRD, TGA-DSC, SEM, ^{1}H NMR and nitrogen adsorption. The results are presented in section 3.3.1.

Table 14. Names and amounts of linkers used in the synthesis of mixed-linker MOFs.

Entry	MOF name	x-linker (90 %)	y-linker (10 %)	x-linker (g)	y-linker (g)
1	UiO-67-bpydc$_{0.1}$	H_2bpdc	H_2bpydc	1.87	0.209
2	UiO-67-(bpdc(NH_2)$_2$)$_{0.1}$	H_2bpdc	H_2bpdc-(NH_2)$_2$	1.87	0.233
3	UiO-67-(bpdc(NH_2))$_{0.1}$	H_2bpdc	H_2bpdc-(NH_2)	1.87	0.221
4	UiO-67-(bpdc(OH)$_2$)$_{0.1}$	H_2bpdc	H_2bpdc-(OH)$_2$	1.87	0.236
5	UiO-67-bndc$_{0.9}$-bpydc$_{0.1}$	H_2bndc	H_2bpydc	2.64	0.209

2.5.2. Metal incorporation in UiO-67 type MOFs

The functional groups present on organic linkers of the mixed linker MOFs serve as anchoring sites to bind metals. Therefore, metals can be grafted at -N (in H_2bpydc linker), -NH_2 (in H_2bpdc-NH_2) and H_2bpdc-(NH_2)$_2$ linker) or -OH (in H_2bpdc-(OH)$_2$ linker). The most common procedure for metal incorporation in MOFs is by wet impregnation. Using this method, the MOF is dispersed in a solvent and a metal solution is added before the mixture is heated at elevated temperatures overnight. The following day the material is extensively washed to remove the excess metal source before drying. Mixed linker MOFs are advantageous as they provide anchoring sites for immobilization of metal in the pores of established MOFs while maintaining similar stability to the parent framework. Therefore, the metal incorporation can be performed directly on the as-synthesized mixed linker MOF or the mixed linker MOF can be modified and then grafted with the metal on the new obtained coordination site.[110, 123-125] The choice of metal depends on the available coordination site and the targeted catalytic reaction.

One of the examples of a MOF catalyst obtained by direct metal incorporation is UiO-67-bpydc$_{0.1}$. It was used to graft Pt metal which has been extensively studied in our group. It is an interesting catalyst as Pt can be reduced to form nanoparticles under flow of H_2 gas in the 600-700 K range and it is as stable as the parent UiO-67 MOF.[66] It has been used for CO_2 hydrogenation and a correlation between the degree of Pt reduction and CO_2 conversion was observed. CO was seen as a primary product with CH_4 as the secondary product where the catalyst was stable during 60 h of testing.[99] Hence, UiO-67-bpydc$_{0.1}$ was synthesized using the concentrated synthesis method developed in this work and was grafted with Pt to study mechanistic aspects in the hydrogenation of CO_2 to methanol.[126] The author has significantly contributed to the synthesis of all the samples for this manuscript (listed in the *Papers not included in the thesis*). Moreover, UiO-67-bpydc$_{0.1}$ was also used to graft Ni and Pd and further

studied in detail for ethene oligomerisation and CO_2 hydrogenation, respectively. (*Manuscript in preparation or submitted*).

Interestingly, another way of metal incorporation in the MOFs is by modifying the as-synthesized mixed-linker MOF. Thus, sterically separated from the groups that are involved in the framework-forming bonds, and instead be directed into the cavities of the MOF. To demonstrate such metal based MOF catalyst, UiO-67-bpdc-$(NH_2)_2)_{0.1}$ is used (denoted by **MOF**).

The H_2bpdc-$(NH_2)_2$ linker offers two $–NH_2$ functional group in the MOFs which can be condensed with salicylaldehyde to yield H_2bpdc-$(NH_2)_2$-salicylaldehyde (denoted as **MOF-sal),** which with its phenol groups and imine bonds forms a tetradentate pocket suitable for metal coordination. MOF-sal was treated with metal satls of Pd (bis(acetonitrile)dichloropalladium(II)), Cu (copper (II) acetate), Co (cobalt (II) acetate) and Ni (Nickle (II) acetate). The treatment with Cu or Co salt, **MOF-sal** forms a complex where the metal is coordinated to nitrogen (from H_2bpdc-$(NH_2)_2$ linker) and oxygen (from hydroxyl group of salicylaldehyde), denoted as **MOF-sal-Cu** and **MOF-sal-Co**, respectively (Figure 14). However, on treatment with Pd salt, the imine bond cleaves and Pd binds to amine group resulting in a complex surrounded by nitrogen from H_2bpdc-$(NH_2)_2$ linker and chloride from the Pd salt, referred as **MOF-Pd-(via sal)** (Figure 14). Moreover, the isolated complexes were successfully synthesized and characterized with ^{1}H NMR and single crystal X-ray diffraction.

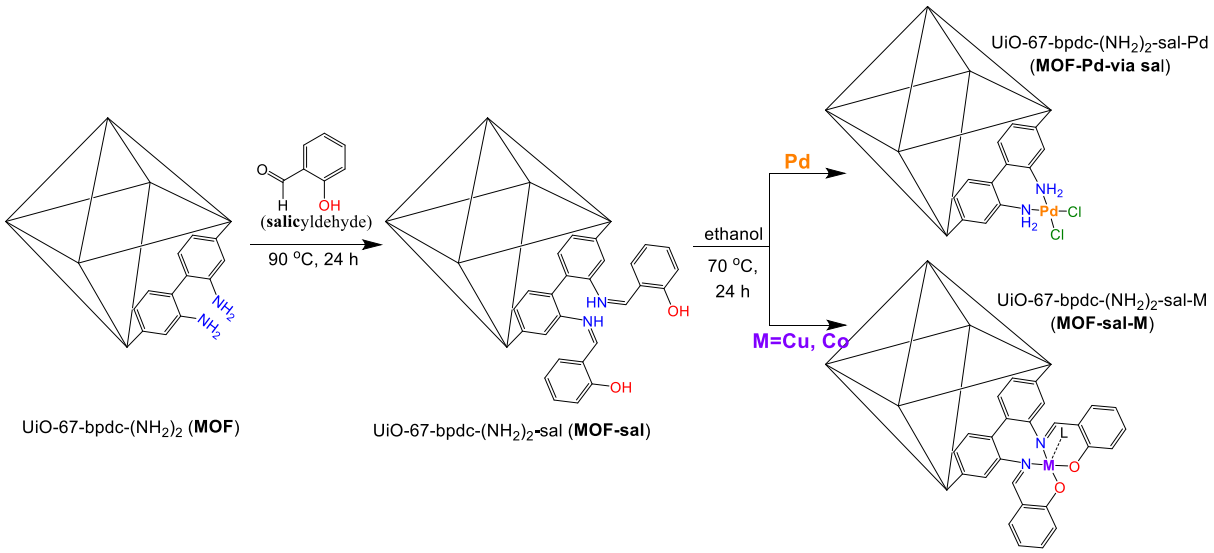

Figure 14. Schematic of synthesis of metal complexes in mixed linker UiO-67-(bpdc-$(NH_2)_2)_{0.1}$ MOF, where L may be acetate from the metal acetate salt.

MOF-sal forms a square planar complex upon treatment with copper(II) acetate or cobalt(II) acetate, where Cu or Co is coordinated to nitrogen (from H_2bpdc-$(NH_2)_2$) and oxygen (from the hydroxy group of salicylaldehyde), to form **MOF-sal-Cu or MOF-sal-Co** (Figure 14). Attempts to synthesize the analogous Pd(II) complex proved difficult, despite a nearly identical complexes being known from the literature.[127-129] While the synthesis of isolated Pd (II) complex, it was observed that Pd binds to the primary amine groups and retains two chloride resulting in a square planar complex. This indicates the most likely state of Pd in the pores of the MOFs as well (Scheme 1). Moreover, when **MOF-sal** was treated with nickel(II) acetate, the crystallinity of the MOF was destroyed, confirmed by its diffraction pattern. **MOF** and its derivatives were characterized by powder X-ray diffraction, TGA-DSC, 1H NMR, FT-IR and SEM-EDS analysis.

Control reactions were performed starting with the dimethyl-ester of the diamine linker. The intermediates and products of these reactions have been characterized by standard techniques, ensuring the efficiency of the reaction conditions. Spectroscopic features and single crystal X-ray diffraction of verified isolated complexes can then be used to indicate the formation of the desired complexes in the MOF.

2.5.2.1. Synthesis of MOF catalyst

i) Synthesis of UiO-67-(bpdc-$(NH_2)_2)_{0.1}$ (**MOF**): **MOF** was synthesized via a simple one-pot reaction in DMF at 130 °C, using benzoic acid and water as additives using the dilute synthesis procedure. 10.0 grams of $ZrCl_4$ (1 equiv) was added to the solution of 997 mL DMF

(300 equiv) and 2.32 mL distilled water (3 equiv) at room temperature on a stirring plate. This solution was heated and 47.16 grams of benzoic acid (9 equiv) was added, waited until completely dissolved and then 9.35 g H_2bpdc linker (0.9 equiv) and 1.17 g H_2bpdc-$(NH_2)_2$ linker (0.1 equiv) was added, together. The solution was transferred to a round bottom flask, fitted with condenser and heated at 130 °C overnight with stirring. A pale yellow colored powder was obtained, which was filtered and washed with hot DMF (50 mL*4) and acetone (50 mL*4). The **MOF** was further washed by suspending in 500 mL methanol and stirring it overnight at 60 °C, followed by drying of product at 150 °C overnight.

ii) Synthesis of UiO-67-(bpdc-$(NH_2)_2)_{0.1}$-sal (**MOF-sal**): 6 grams of dried **MOF** was weighed in a 50 ml round bottom flask and dispersed in neat salicylaldehyde was added so that the **MOF** was immersed in salicylaldehyde. A drop of formic acid was added to the flask and stirred at 90 °C overnight. The MOF was washed with ethanol (30 mL*3) and the product was dried at 100 °C overnight.

iii) Metal incorporation to form **MOF-Pd-(via sal), MOF-sal-Cu**, **MOF-sal-Co** and **MOF-sal-Ni**: 1.00 gram of dried product **MOF-sal** was suspended in 5.00 mL of ethanol and stirred at 70 °C for 15 min. Dissolved 35.0 mg of Bis(acetonitrile)dichloropalladium(II) ($PdCl_2(NCCH_3)_2$)/ copper (II) acetate/ cobalt (II) acetate/ Nickel (II) acetate (1 equiv) in 15 mL ethanol to get UiO-67-(bpdc-$(NH_2)_2)_{0.1}$-Pd via salicyaldehye (**MOF-Pd-(via sal)**), UiO-67-(bpdc-$(NH_2)_2)_{0.1}$-sal-Cu (**MOF-sal-Cu**), UiO-67-(bpdc-$(NH_2)_2)_{0.1}$-sal-Co (**MOF-sal-Co**) and UiO-67-(bpdc-$(NH_2)_2)_{0.1}$-sal-Ni (**MOF-sal-Ni**), respectively. This salt solution was added to the MOF solution and stirred at 70 °C overnight, under reflux at 250 rpm. The resultant material was washed with ethanol (2*50 mL) on filter followed by a prolonged washing for which the material was dispersed to ethanol in a centrifugation tube and put to a shaker for 1 hour. The ethanol solution was centrifuged and decanted, followed by drying of product at 80 °C overnight.

2.5.2.2. Synthesis of isolated Pd complex

The dimethyl-ester of the diamine linker (0.05 g, 1 mol) was treated with bis(acetonitrile)dichloropalladium(II) (0.026 g, 1 mol) in 5.0 mL of ethanol at 70 °C overnight. The precipitated product was isolated by filtration and washed with ethanol. The sample was recrystallized in a solution of THF and cyclohexane by vapor diffusion (and solvent evaporation) for single crystal X-ray diffraction measurements. The ^{1}H NMR spectra was

obtained by dissolving the sample in tetrahydrofuran-d_8. The sample was insoluble in most of the solvents except DMSO and THF.

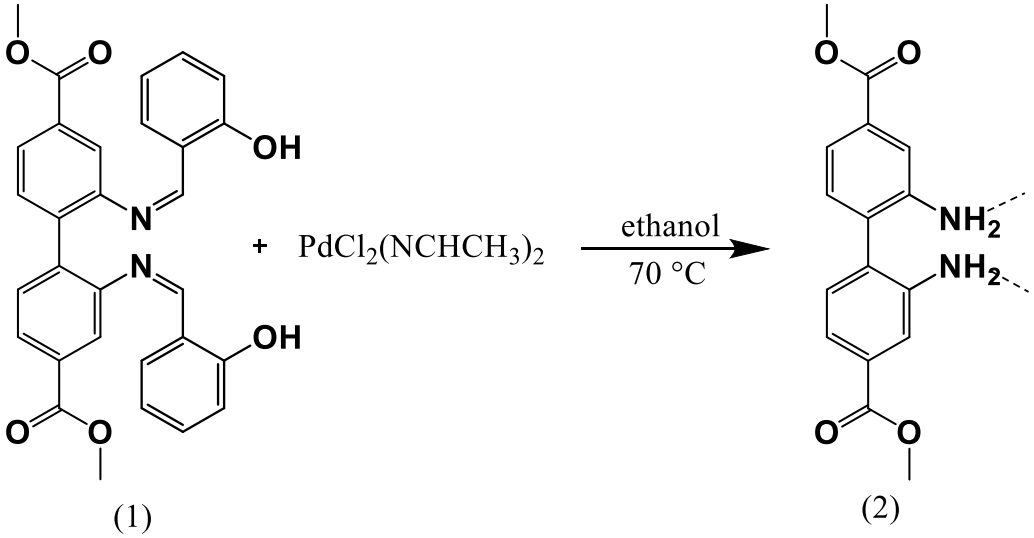

(1) (2)

Figure 15. Reaction of dimethyl-ester of the diamine linker (1) with bis(acetonitrile)dichloropalladium(II) in ethanol to give $PdCl_2$(diaminobiphenyl diester) (2).

3. Results and Discussion

3.1. UiO-67

3.1.1. Screening the reaction conditions

3.1.1.1. Preliminary high-throughput synthesis

In the first part of this study, high-throughput screening synthesis was performed in order to define proper starting conditions for the subsequent, detailed investigations. As described in section 2.3.1.1, two sets of 36 trial reactions to synthesize UiO-67 were obtained by varying, i) Aqueous additives (water or $HCl_{(aq)}$), ii) Modulator (Acetic acid-"Ac" or Benzoic acid-"BA"), iii) Reaction temperature (120 °C /130 °C /140 °C) and iv) Amount of modulator (0 to 18 molar equiv, in the interval of 3) (see Table 1).

PXRD pattern were recorded for set W (use of water as additive) and set H (use of $HCl_{(aq)}$ as additive), presented in Figure 16a and Figure 17a, respectively. Further, the effect of elevated temperature on all the samples were monitored by recording the PXRD pattern, before and after heating them for 2 hours in air at 450 °C (Figure 16b and Figure 17b). The crystallite size was estimated by refining the diffraction pattern by Pawley refinement using the software TOPAS against an ideal UiO-67 structure (Table A1 and Figure A1).

Firstly, diffraction pattern of set W shows sharp high intensity peaks as compared to set H, which correlates with the estimated particle size (Table A1). High intensity sharp peaks of diffraction patterns are attributed to larger particles with high crystallinity. Diffraction pattern of Set W has particles in the range of 10 to 370 nm whereas the particles in set H are up to 100 nm only. Set W and set H were heated for 2 hours at 450 °C and analyzed by the PXRD to check their thermal stability (Figure 16b and Figure 17b). The material has been critically affected by heating at high temperature and most of the sample lose crystallinity as seen by the loss of peaks in the respective diffraction patterns. PXRD pattern refinement was performed for the samples which sustained crystallinity and their crystal size regularity decreases (Table A1). The set W now have the crystal size in the range of 10 to 270 nm and set H has particles mostly up to 20 nm with the exception of two sample having 90 and 100 nm size.

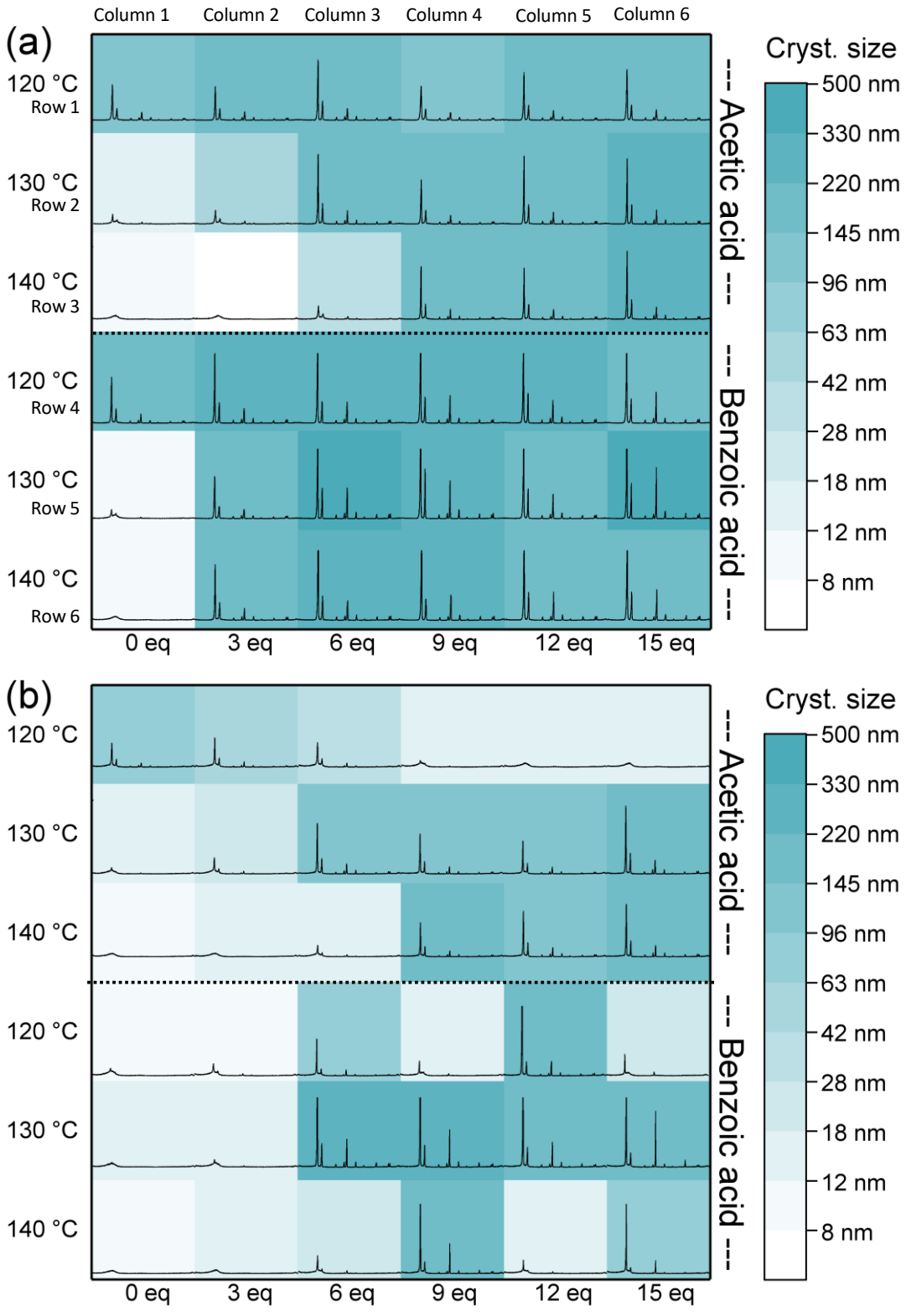

Figure 16. PXRD patterns of set W (using water as an additive) of a) as-synthesized samples and b) after thermal treatment. There are 36 samples, represented in six rows and six columns. Row 1 to 3 is synthesized with BA and row 4 to 6 with Ac as modulator at 120 °C, 130 °C and 140 °C, respectively. Each column has different amount of modulator (BA or Ac) from 0 to 15 equiv.

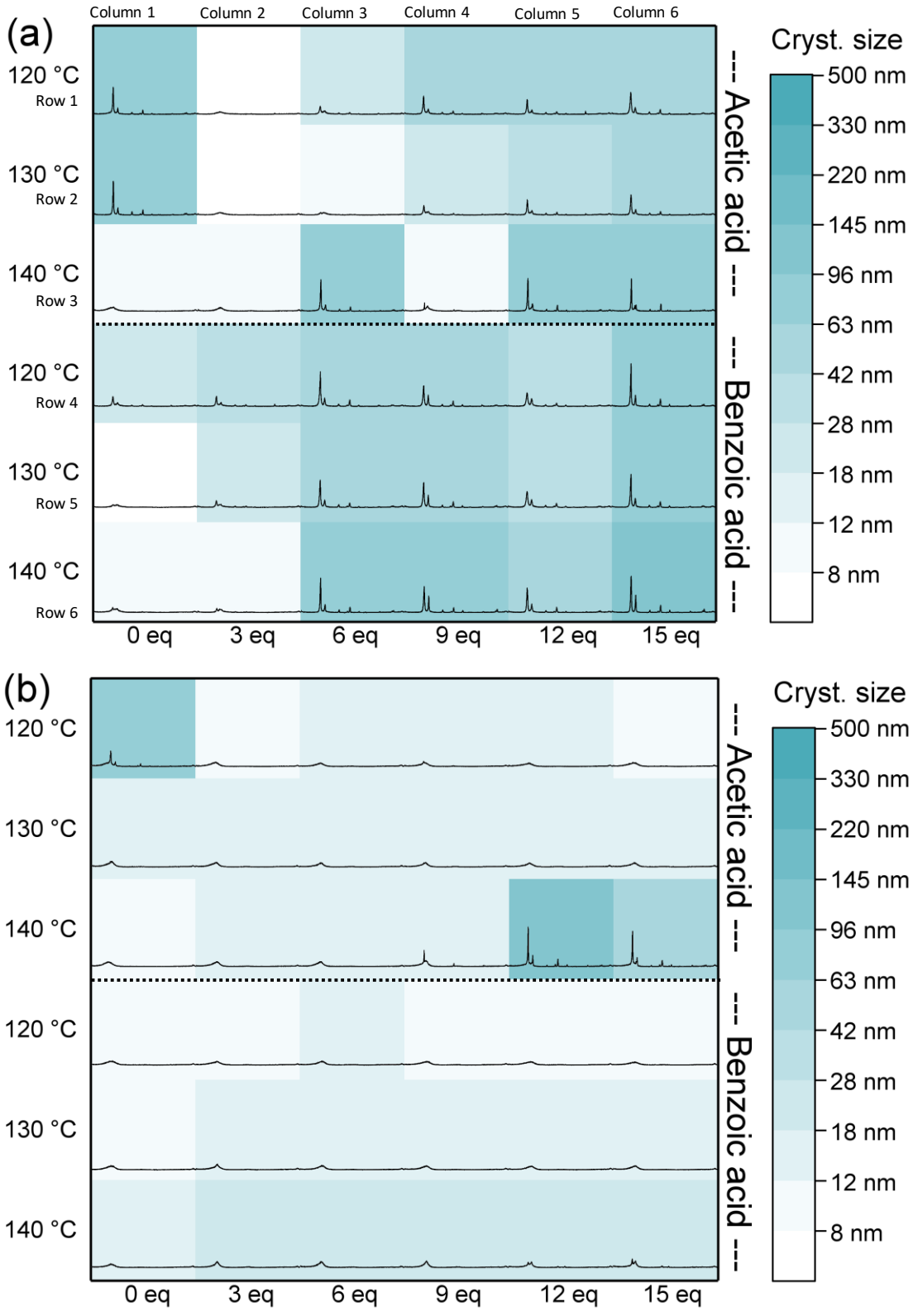

Figure 17. PXRD patterns of set H (using $HCl_{(aq)}$ as an additive) of a) as-synthesized samples and b) after thermal treatment. There are 36 samples, represented in six rows and six columns. Row 1 to 3 is synthesized with BA and row 4 to 6 with Ac as modulator at 120 °C, 130 °C and 140 °C, respectively. Each column has different amount of modulator (BA or Ac) from 0 to 15 equiv.

In 2013, Farha and coworkers extensively explored the use of ($HCl_{(aq)}$) in the synthesis of UiO-66, UiO-67 and UiO-type MOFs.[88] They demonstrated that concentrated HCl enhances the solubility of $ZrCl_4$ in DMF, and speed up the product formation. It was proposed that HCl neutralizes the basic impurities like amines which is formed in the hydrolysis of DMF and/or that HCl facilitates the formation of zirconium clusters before the linker is attached.[88] Based on the assessment shown in Figure 16 and Figure 17, UiO-67 synthesized with added HCl consistently shows inferior crystallinity to those synthesized with added water. Furthermore, the effect of the thermal treatment is more severe for the HCl samples, indicating lower thermal stability. Our screening also corroborates other literature reports that find a correlation between crystallite size and modulator concentration.[79, 84, 90]

Furthermore, diffraction pattern of the set W synthesized at 130 °C (row 2 and 5 of Figure 16b) showed to be most resistant to the thermal treatment suggesting that 130 °C is a suitable reaction temperature. It is interesting to note that samples synthesized without modulator are expected to be identical in both the sets (column 1 of Figure 16a and Figure 17a). But the diffraction pattern are not identical which highlights the fact that without the use of modulators, reproducibility of synthesis of UiO-67 MOF is challenging.[84]

To sum up, these preliminary results narrows the work and for simplicity, following parameters were chosen as the starting criteria, reagents in molar equivalents = Zr:H_2bpdc:H_2O:BA:DMF = 1:1:3:9:300. Reaction temperature was set to 130 °C.

3.1.1.2. Screening of amount of solvent

Previous work in our group suggests that the solubility of H_2bpdc in DMF is approximately 1:150-200 at synthesis temperature (120-130 °C), but a systematic study has not been carried out. The solubility is dependent on the temperature and the presence of modulator and water. In this screening, UiO-67 synthesis was performed using the following Zr:DMF molar ratios; 1:20, 1:35, 1:50, 1:100 and 1:300. A white solid was obtained in all syntheses, which was washed extensively with hot DMF and acetone, and dried overnight at 150 °C. Interestingly, diffraction patterns of the sample with molar ratio of 1:50 (and more dilute) resembles with the diffraction pattern of UiO-67 (Figure 18). This suggests that it is possible to synthesize UiO-67 with as low as 1:50 ratio of Zr to DMF, a reaction environment about 6 times concentrated as compared to usually published protocol where 1:300 ratio is used. At lower concentrations (1:35 and below), no MOF formation was observed and the diffraction patterns of the white solid obtained from the syntheses matches the pattern of pure H_2bpdc linker.

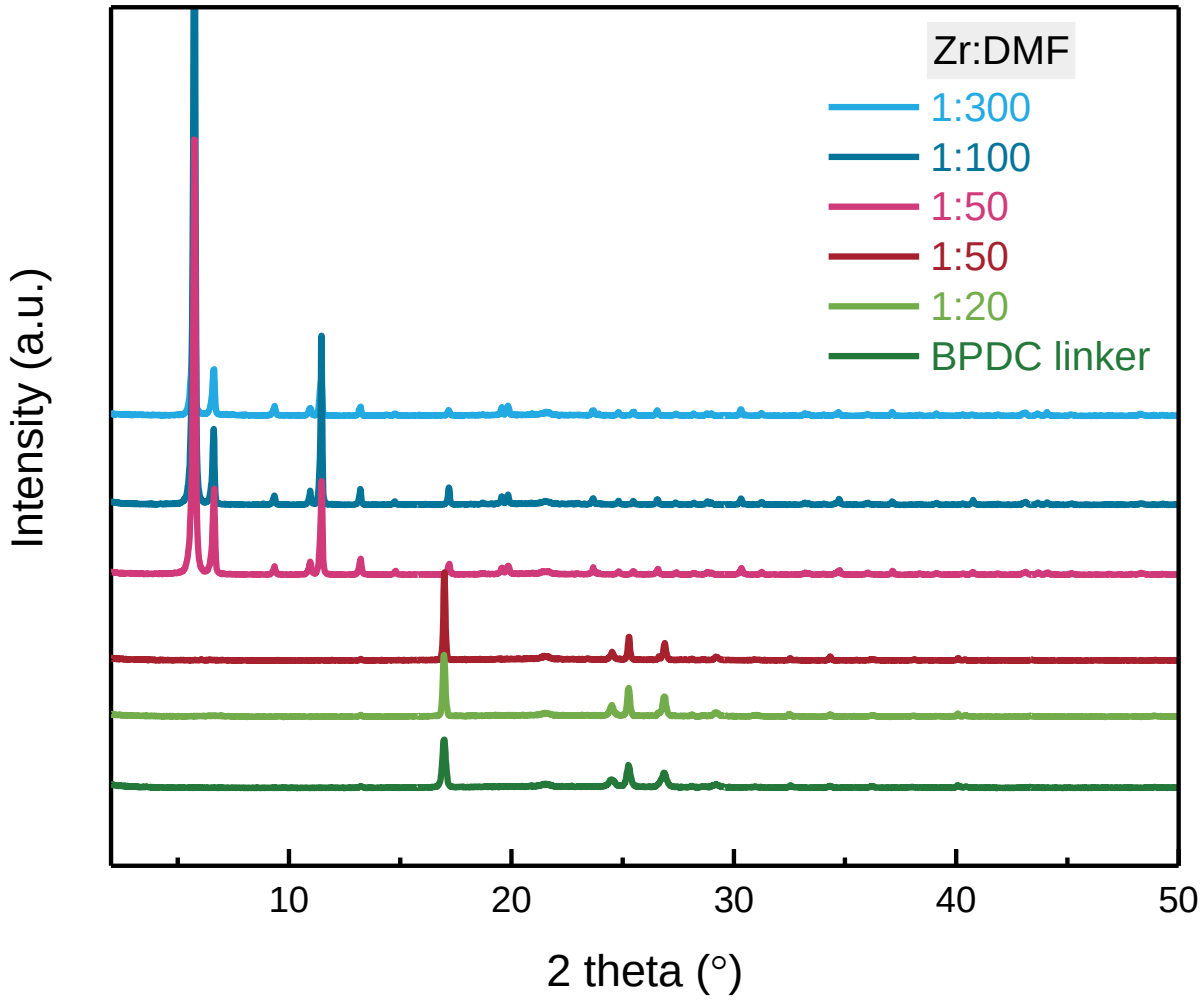

Figure 18. PXRD of the UiO-67 to be synthesized with different concentrations of DMF with Zr:DMF molar ratio as 1:20, 1:35, 1:50, 1:100 and 1:300.

3.1.1.3. Screening the amount of modulator for concentrated and dilute synthesis

The screening studies led to the selection of H_2O over $HCl_{(aq)}$ as aqueous additive, benzoic acid over acetic acid as modulator, a reaction temperature of 130 °C with the possibility to synthesize UiO-67 at Zr:DMF ratio as 1:50. Therefore, the amount of modulator was screened relative to Zr:DMF ratio as 1:50 (concentrated) or 1:300 (dilute). Under dilute synthesis conditions, a clear solution is obtained at the start of the synthesis whereas in concentrated synthesis conditions, however, $ZrCl_4$ and the modulator are fully soluble, while the linker is not. A series of samples was prepared with $ZrCl_4$:H_2bpdc:H_2O:DMF molar ratios of 1:1:3:50 (called concentrated synthesis-"**C-x$_{BA}$** series") or 1:1:3:300 (dilute synthesis-"**D-x$_{BA}$** series") as starting conditions. Different amounts of BA was then screened for **C-x$_{BA}$** series and the results were compared with that of the **D-x$_{BA}$** series where x is the amount of BA in molar equivalents.

PXRD pattern showed that pure UiO-67 is formed only in experiments **C-3$_{BA}$**, **C-6$_{BA}$** and **C-9$_{BA}$** (Figure 19a). **C-0$_{BA}$** contains UiO-67 as well as an unidentified crystalline phase indicated by the presence of extra peaks (for example at 2θ= 12.7°, 13.7°, and 14.3°). In **C-12$_{BA}$** and **C-15$_{BA}$**, mainly linker with smaller amounts of UiO-67 is observed in the diffraction pattern, presumably because the high concentration of benzoic acid lowers the solubility of H_2bpdc. For the conventional, dilute syntheses (**D-x$_{BA}$** series), the diffraction patterns revealed that an increase in BA concentration (x= 0 equiv to 18 equiv) leads to sharper and narrower diffraction peaks, indicating larger particle size and/or more ordered crystal structure (Figure 19b). This observation is in agreement with the findings of Behrens and coworkers.[130]

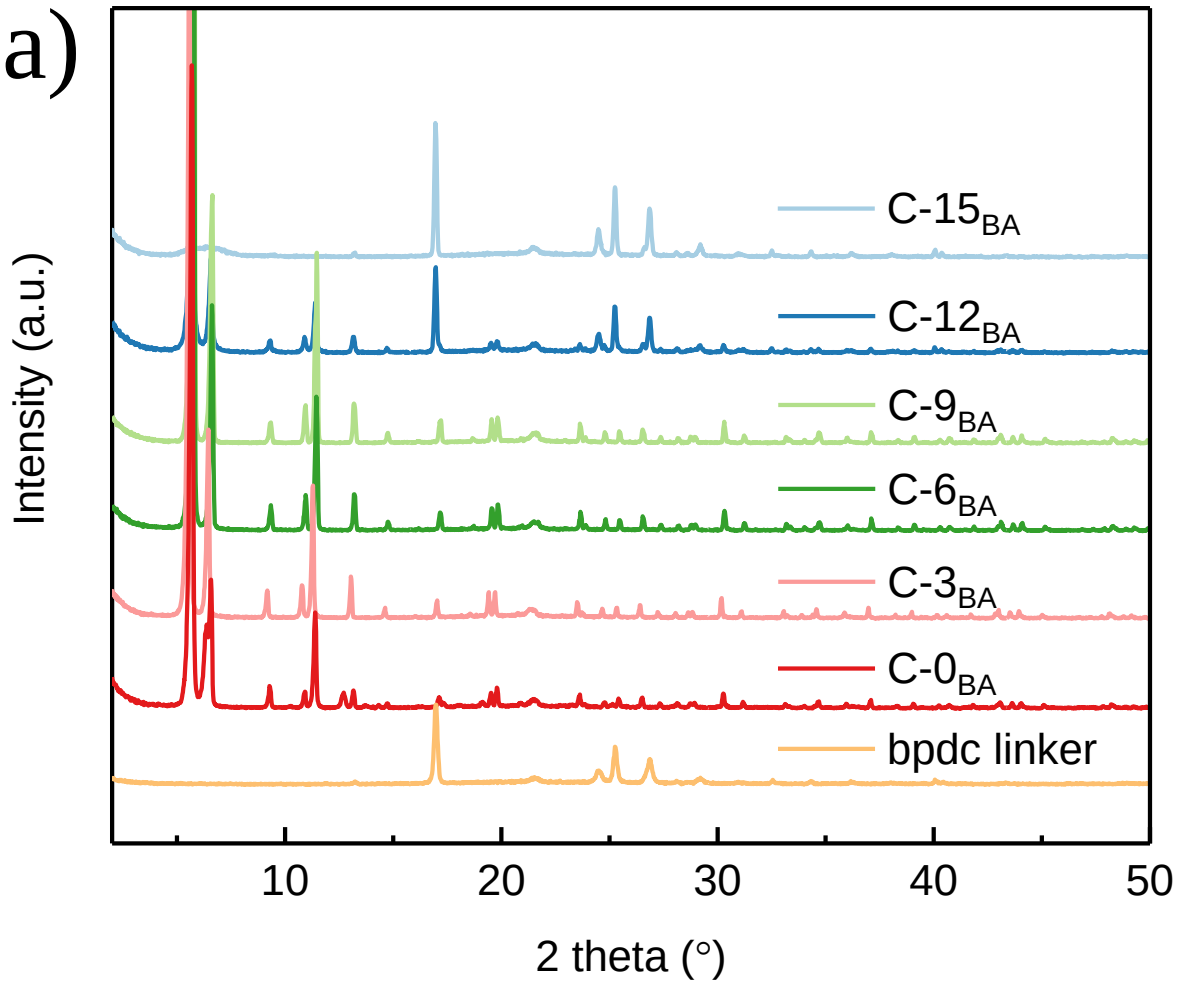

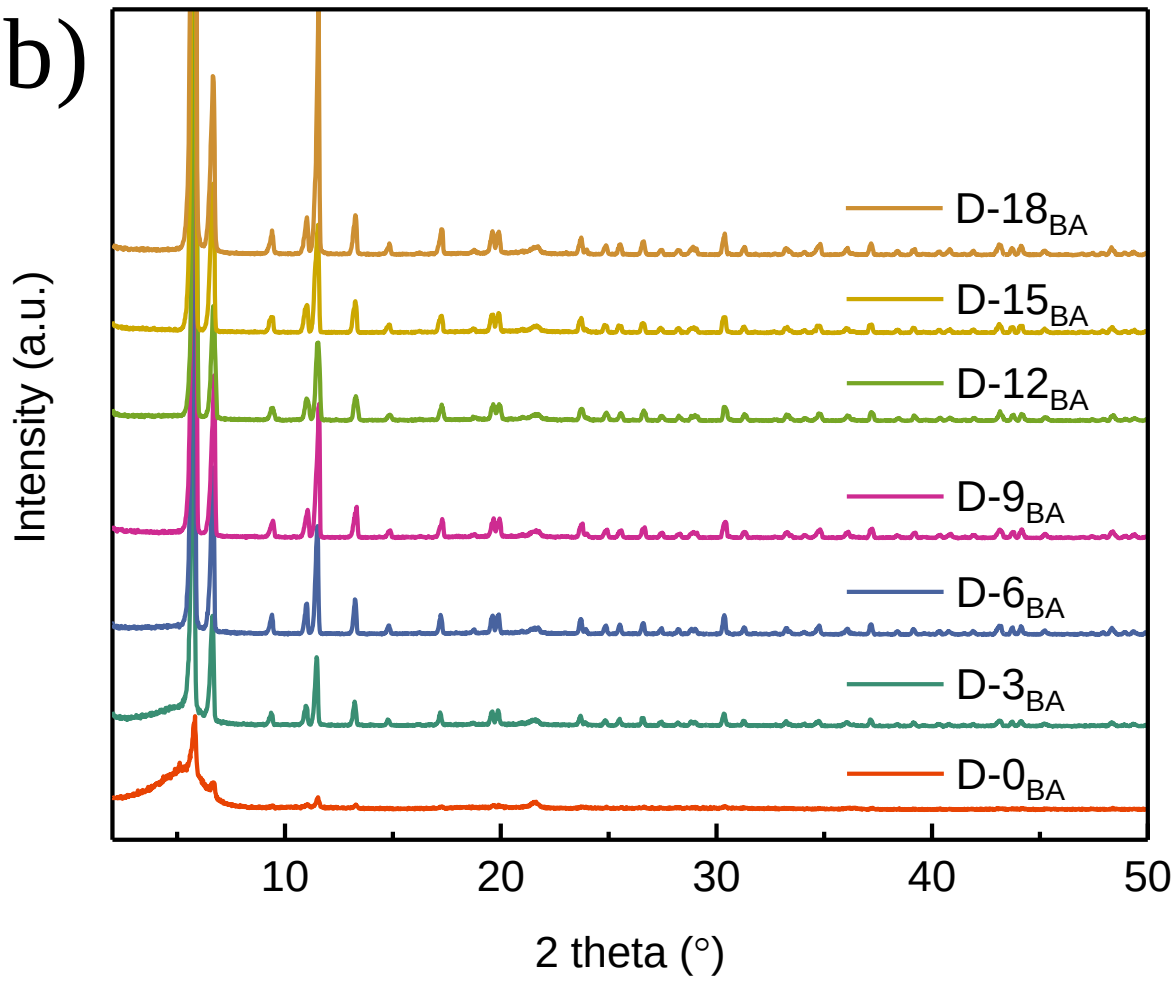

Figure 19. PXRD patterns of a) C-x_{BA} (Zr:DMF ratio 1:50) and b) D-x_{BA} (Zr:DMF ratio 1:300) series depicting the possibility to synthesize UiO-67 in the presence of various concentration of benzoic acid, x (x= 0 to 18 equiv).

SEM micrographs depict well-defined homogeneous octahedral shaped crystals with particle size around 1.5 µm for C-3_{BA} series (Figure 20). As the amount of benzoic acid increases to 6 equiv and 9 equiv in C-x_{BA}, irregular particles with new facets (particularly [1 0 0] in addition to [1 1 1]) are observed, as well as an increase in particle intergrowth and particle size dispersion (Figure 20 and Figure A2). Particle sizes for C-0_{BA}, C-12_{BA} and C-15_{BA} were not possible to determine (Figure A2). In spite of the well-crystalline UiO-67 phase indicated by the PXRD for C-0_{BA}, SEM did not reveal any particles with well-defined crystal morphology. C-12_{BA} and C-15_{BA} consist of irregular agglomerates without clear morphology, in line with XRD results. For D-x_{BA}, SEM micrographs confirmed the trend of increasing particle size with increasing amount of modulator. Furthermore, it revealed that samples D-0_{BA}, D-3_{BA} and D-6_{BA} also contains an unidentified phase of small particles.

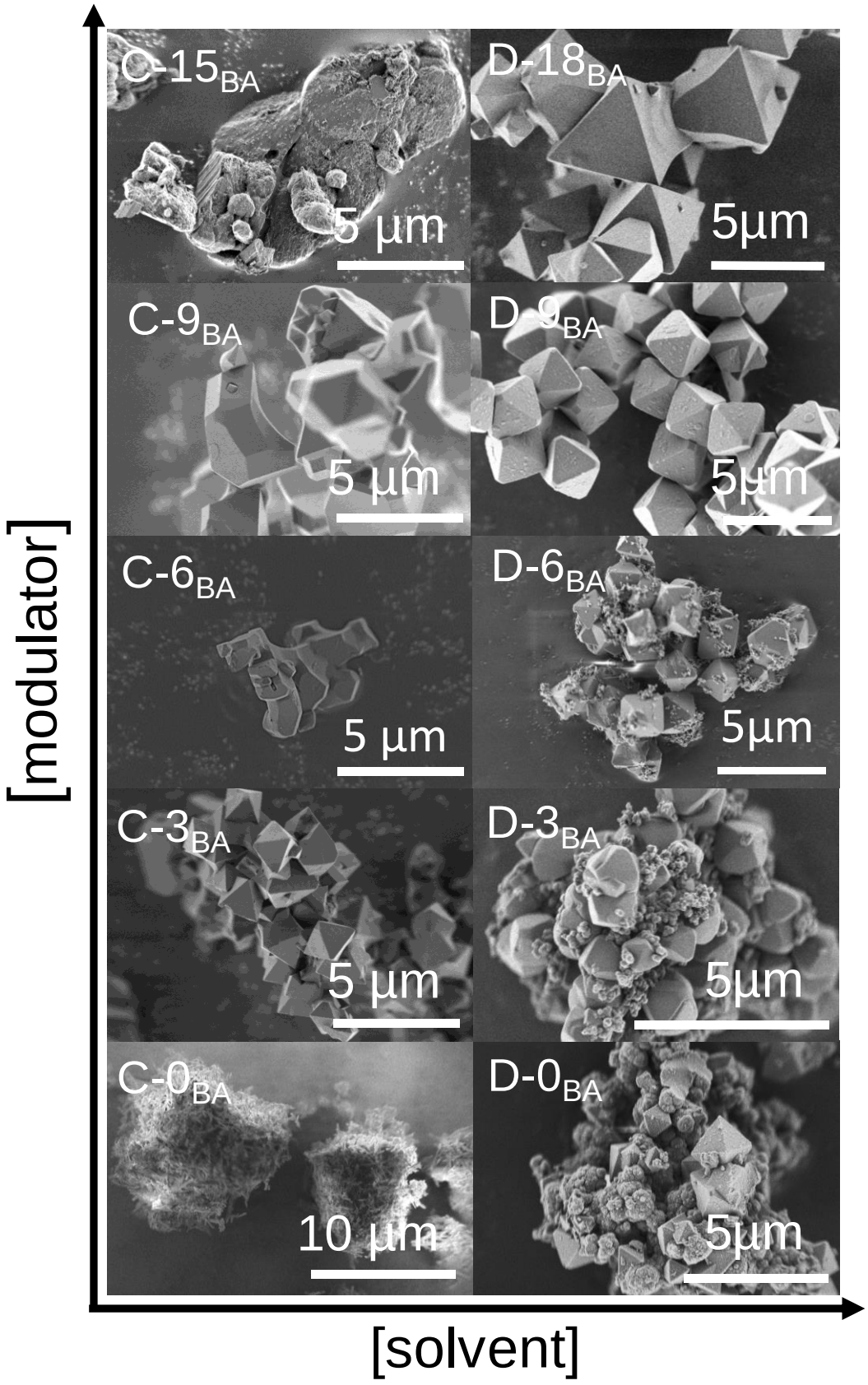

Figure 20. Representative SEM micrographs for the C-x_{BA} (where x = 0, 3, 6, 9 and 15) and D-x_{BA} (x = 0, 3, 6, 9 and 18) samples.

The porosity of the C-x_{BA} and D-x_{BA} series was determined by nitrogen adsorption at 77 K and the BET surface areas were calculated from the nitrogen isotherms using established consistency criteria.[131] The highest porosity is found for C-3_{BA}, with a slight decrease as the amount of BA increased (Figure 21). The BET surface area of C-3_{BA} (2734 m^2 g^{-1}) is close to the originally reported Langmuir surface area of 3000 m^2 g^{-1} (Figure A3 and Table A2).[11] In the case of the D-x_{BA} series, the porosity increases abruptly with the amount of BA up till D-6_{BA}, followed by a minor increase with further increase of BA.

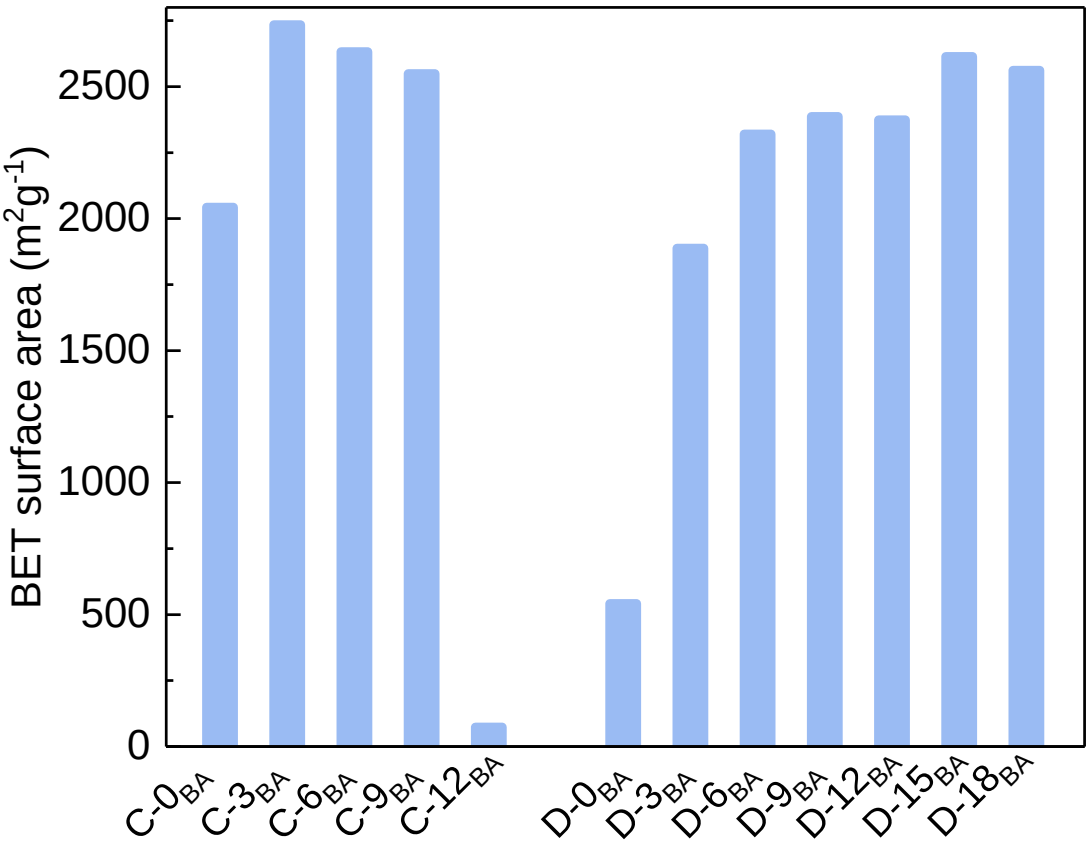

Figure 21. BET Surface area of C- x_{BA} and D-x_{BA} samples, calculated from N_2 adsorption isotherms at 77 K.

In full agreement with the high specific surface areas, Attenuated total reflectance (ATR) analysis made on the pristine materials confirmed the presence of only a small amount of unreacted benzoic acid or DMF (broad, complex, and very weak components around 1700−1730 cm^{-1}, assigned to the peculiar ν(C=O) mode, shown in Figure A5. The same analyses suggest that the syntheses performed in the absence of modulators (C-0_{BA} and D-0_{BA}) make materials with some impurities (Figure A5 shows the ATR spectra that are characterized by some extra peaks).

DRIFT analysis was further performed after samples were activated in helium at 300 °C, followed by cooling to 70 °C. The samples were monitored by DRIFT before and after CD_3CN dosing. The results, illustrated in Figure A6 and Figure A7, show that all the residual traces of unreacted modulator or DMF have been removed (absence of any band around 1700-1730 cm^{-1}) and all the samples are characterized by fully hydroxylated clusters (intense band at 3676 cm^{-1}). Upon interaction with CD_3CN, the bands associated with the OH groups were eroded and shifted to lower frequencies. As counterpart, in the ν(CN) region (see the insets of Figure A6 and Figure A7) new components around 2276 $cm^{-1}$are observed, while the absence of relevant bands around 2300 cm^{-1} exclude the abundance of accessible Lewis sites (e.g., uncoordinated Zr sites).

TGA-DSC analysis (30 to 800 °C) was performed to determine the total organic content in the synthesized materials. At 800 °C in an oxygen atmosphere we assume that only ZrO_2 remains, and thus all the TGA curves were normalized to this value (100%). Two main weight losses were observed in the samples (Figure 22); near 200 °C, corresponding to the removal of physisorbed solvent and modulator, and near 490 °C with the combustion of the organic components of the material. The weight of the samples before dehydroxylation of the $Zr_6O_4(OH)_4^{12+}$ cluster (at 200 °C) and before linker combustion (at 400 °C) were compared with the expected weight of the hydroxylated (287 %) and dehydroxylated (282 %) UiO-67, respectively, as calculated from the ideal structure (Section 2.3.2).

At 400 °C, sample C-3_{BA} shows close to ideal relative mass of 282 %, whereas C-0_{BA}, C-6_{BA} and C-9_{BA} show 284 %, 283 % and 286 %, respectively (Figure 22a). The corresponding figures of the D-x_{BA} samples were all in the range of 233-274 %, indicating a lower relative content of linker (Figure 22b). The method relies on the assumption that the modulator content is negligible at 400 °C. In case this assumption is incorrect (thus overestimating the linker content), the method was further developed to determine the identity of the organic components.

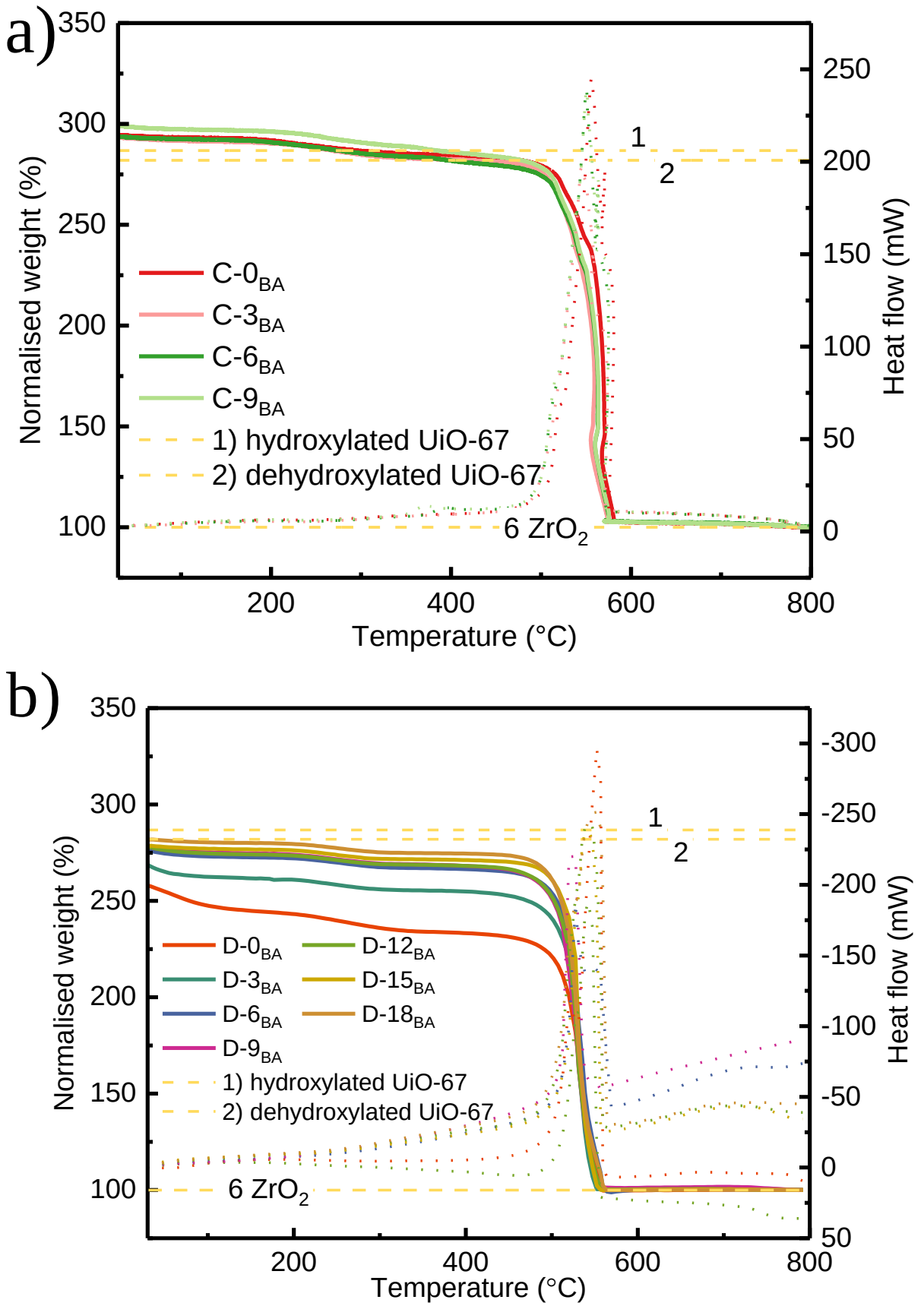

Figure 22. TGA-DSC and DSC signals of a) C-x_{BA} (x= 0 to 9) and b) D-x_{BA} (x= 0 to 18).

^{1}H NMR spectroscopy of the dissolved/ digested MOF samples can be used to estimate the relative molar ratios of the organic species ($bpdc^{2-}$, benzoate, formate) in the MOF samples. ^{1}H NMR spectra of this solution is depicted in Figure 24 and Figure A3 for C-x_{BA} series and D-x_{BA} series. Strikingly, the D-x_{BA} series has a much lower $bpdc^{2-}$ content, with high contents of benzoate (15-20% with respect to $bpdc^{2-}$) and formate (as high as 10% with respect to $bpdc^{2-}$) throughout the series (Figure 23). The presence of BA in the thoroughly washed MOF implies that this BA is coordinated to the MOF framework which indicated that BA could be present as capping agents at the missing-linkers sites.

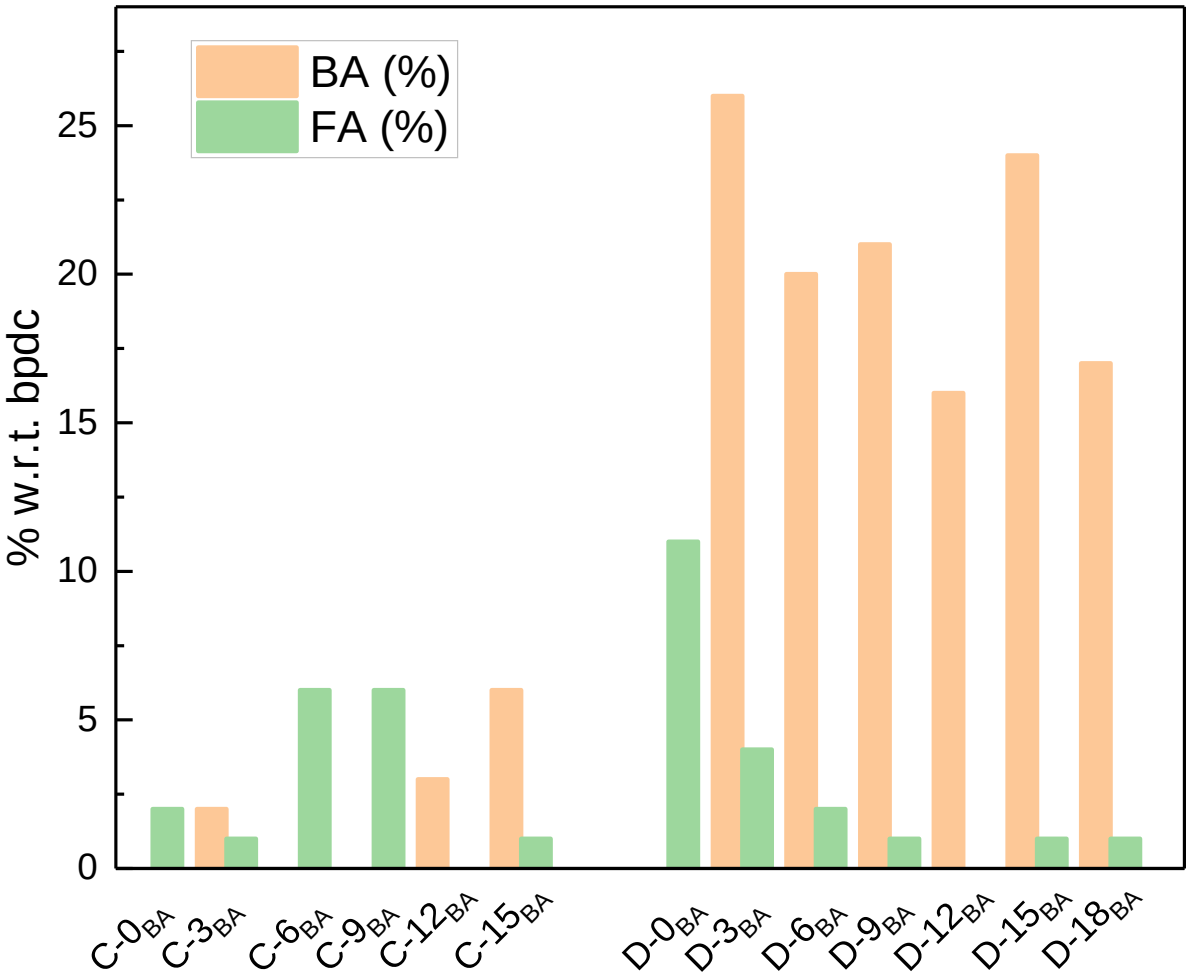

Figure 23. Relative molar ratio of BA and FA in the sample of concentrated and dilute synthesis in percentage with respect to H_2bpdc linker (calculated from ^{1}H NMR).

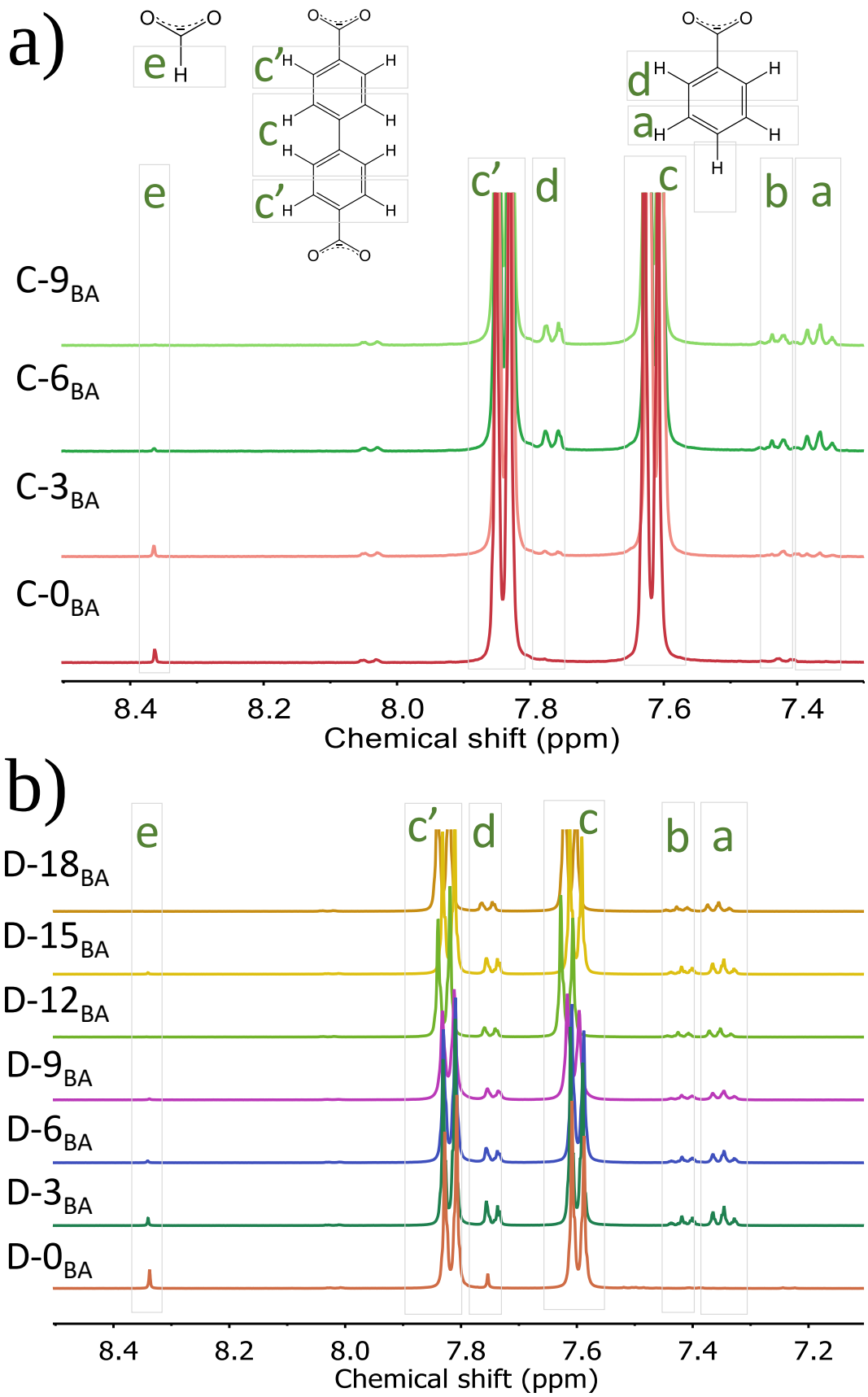

Figure 24. ^{1}H NMR spectra for a) C-x_{BA} series and b) D-x_{BA} series.

The results from ^{1}H NMR spectroscopy and TGA-DSC were combined to estimate the total organic content in the samples (Section 2.3.2), which estimates the amount of total relative organics. In the **C-x$_{BA}$** series, a near ideal bpdc^{2-} to Zr ratio is observed in all samples (x = 0 to 9), Figure 25. A small increase of the benzoate content is observed when its concentration in the reaction mixture is increased, yielding a total molar organic content that surpasses the Zr content. DRIFT studies suggest the absence of physisorbed modulator (Figure A6 and Figure A7) and EDX spectroscopy did not show the presence of chlorine in any of the samples, so the amount is assumed to be negligible.

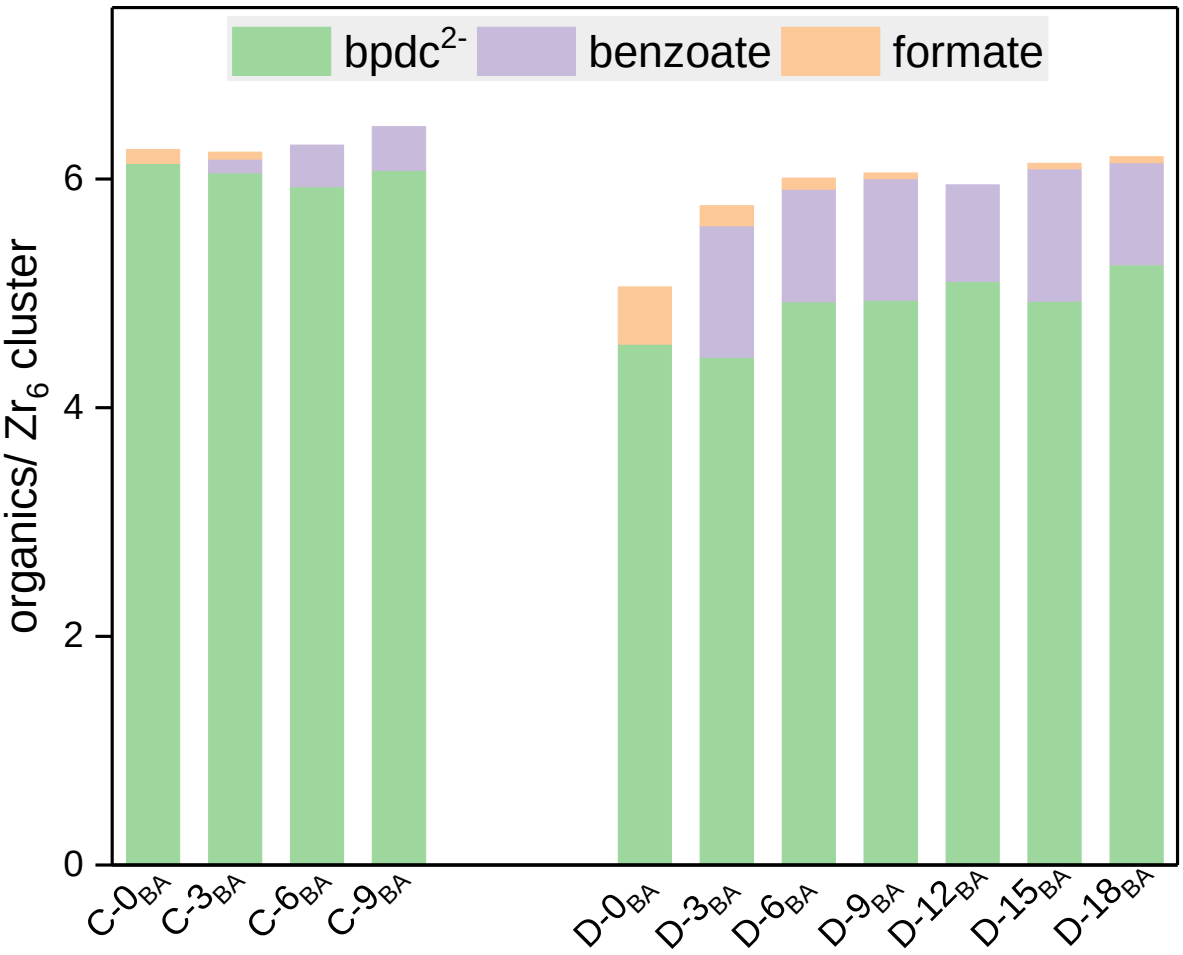

Figure 25. Composition of the organic constituents in each sample, determined by ^{1}H NMR and scaled to the organic:Zr$_6$ ratio found by TGA (at 200 °C) in the C-x$_{BA}$ and D-x$_{BA}$ series. The total organic content in an ideal UiO-67 (Zr$_6$O$_6$(bpdc)$_6$) is 6.

In the highly crystalline **D-x$_{BA}$** (x = 6 to 15) samples with high BET surface area, the benzoate to linker ratio is rather high and constant, while for low modulator x = 0 and 3, other constituents such as formic acid, Cl^{-}, and OH^{-} seem to compete favorably with both benzoate and bpdc^{2-} for the Zr sites. In **D-x$_{BA}$** samples there is a consistent disagreement and contain a lot of

benzoate coordinated to Zr sites, and our results suggest that it cannot be readily assumed that all of this benzoate is removed once the sample is heated to 400 °C.

Therefore, this study demonstrates that the amount of missing-linker defects in UiO-67 can be controlled by tuning the ratios of reagents, modulator, and solvent. Conventional approaches to UiO-67 synthesis yield materials with high concentration of linker vacancy defects, which may be desirable for catalytic purposes or as starting material for post-synthetic linker insertion. Near defect-free UiO-67 (i.e., negligible amount of missing linker defects, low amount of residual species, highly porous and well-defined particle morphology) can be produced by using a minimal amount of DMF, in combination with an optimal linker-to-modulator ratio, due to thorough balancing of the multiple reversible interactions taking place between the components of the synthesis liquor during UiO-67 formation. An added benefit of the concentrated solution method is the lowering of toxic waste to a fraction of previously reported methods.

3.1.2. Time course studies

Throughout MOF synthesis, the deprotonated analogues of linker $bpdc^{2-}$, benzoate and formate participate in reversible interactions with the growing MOF crystallites, and therefore their concentration and affinity for the Zr_x sites control the rate of nucleation, the rate of growth, and the fraction of defects in the final material (Figure 9). While modulator and solvent are present in excess, implying that their concentration changes little during MOF crystal growth, the linker is optimally present in stoichiometric ratio to Zr (especially in case of dilute synthesis). Hence, its concentration will decrease with MOF crystal growth, thereby increasing the probability of modulator or decomposed linker-covered defect formation with time. Ultimately, the linker concentration becomes too low to compete with modulator and hydrolyzed solvent (formate) for the Zr_x sites, and crystal growth stops. This is addressed in time-resolved experiments performed by extracting the samples on intervals from the formation of UiO-67 and obtaining their composition with ^{1}H NMR. Therefore, a guiding hypothesis is that maintenance of a stable linker concentration in the mother liquor until the Zr source is consumed is key to the formation of defect-free UiO-67, and may be achieved by tuning the initial Zr:linker:modulator:solvent ratios.

In order to verify the hypothesis that linker concentration in the synthesis liquor is kept constant by the presence of its corresponding solid throughout MOF crystal formation, synthesis using the C-3_{BA} protocol was performed by sampling the suspension 25 times during the first 12 h of

the synthesis (Figure 26). The solid fraction of each sample was isolated by filtration and PXRD patterns were acquired. We observed a gradual decrease in the diffraction pattern of H_2bpdc(s), until it disappeared after around 11 h. It can be assumed that the solution is saturated by H_2bpdc in this period, due to the continuous agitation of the mixture. Simultaneously, the most intense diffraction peaks from UiO-67 ((1 1 1) and (2 0 0)) appeared as well-resolved peaks already after 45 min of reaction, and the reaction was mainly complete after 12 h.

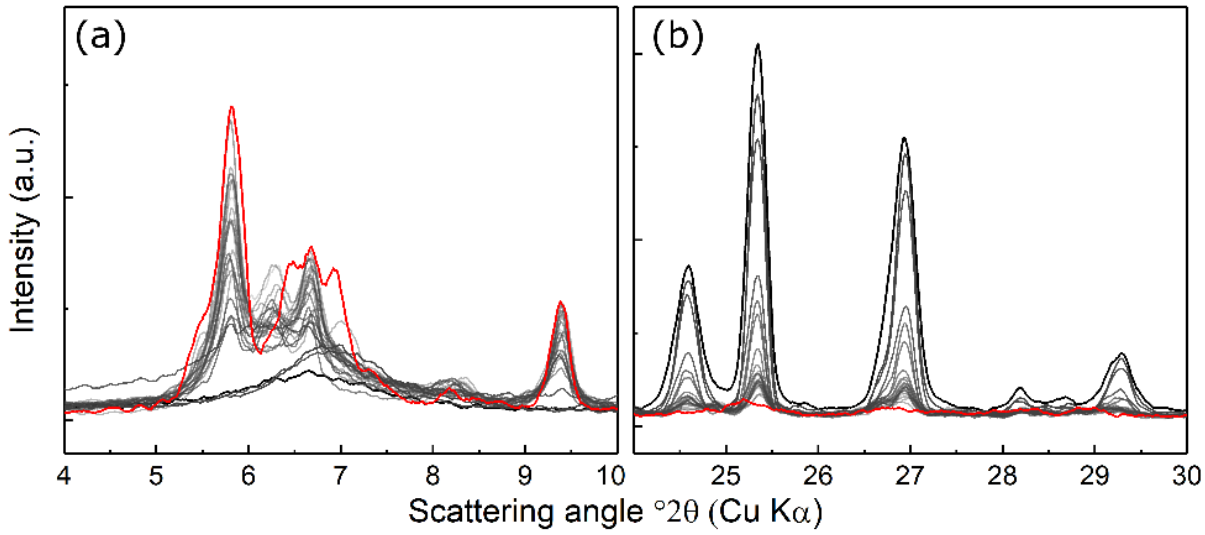

Figure 26. Superimposed PXRD patterns (regions of interest) of samples taken at ~20 minute intervals from a synthesis of C-3_{BA}. The black line is at the start of the reaction, whereas the red line is the final (unwashed) product. Intermediate stages are shown in grey notes (gradually lighter as time progresses). (a) shows the growth of the (1 1 1), (2 0 0), (2 2 0) and merged (3 1 1) and (2 2 2) peaks of UiO-67. (b) shows the gradual disappearance of the most intense peaks of the linker in its solid, crystalline phase.

Moreover, another time course study was carried out to monitor the composition of D-9_{BA} over the period of 24 hours using three identical reaction sets (called reaction 1, 2 and 3). The samples were collected after 0.5 h of onset of the precipitation in the reaction and continued every 4 hours. The yield of the reaction at various intervals are presented in Figure 27a. The formation of UiO-67 is favored as the time proceeds and 70 % of the product is formed in 8.5 hours (Figure 27a). After 8.5 h, probably the exchange of modulator and linker takes place with the slight increase in the yield. After 24 hours, the reaction reaches maximum with almost 100 % yield. Discrepancies in this study could result from the errors caused by 1) the uncertainty of collection of homogeneous sample from the reaction slurry and 2) these results are obtained from three different parallel reactions prepared identically.

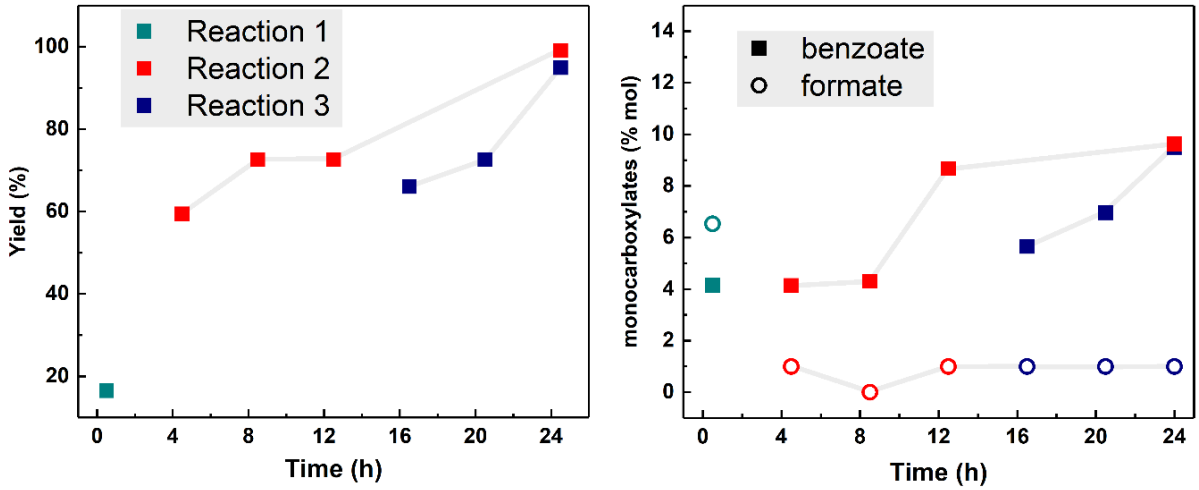

Figure 27. a) Yield for the samples extracted at various intervals and b) their composition, determined by ^{1}H NMR.

Furthermore, the composition of the samples were observed by digesting the samples and collecting 1H NMR spectra. It reveals that the benzoate concentration increases as the reaction time proceeds (Figure 27b and Figure A8). This indicates that linker incorporation in the MOF follows the waning concentration of linker in the mother liquor. The amount of formate in the beginning of the reaction is about 7 % but as the reaction proceeds, formic acid decreases and remains constant for about 1 %. Moreover, the SEM images shows the formation of octahedral crystals at 4.5 hour and not much change in the topology of the material after 4.5 hour (Figure 28). Interestingly the TGA-DSC data for these samples do not show major differences (Figure A9). At 0.5 hour the MOF is highly defective and as the time proceeds, the mass of the MOF is closer to the theoretically expected mass of UiO-67. This supports that while modulator and solvent are present in excess (implying that their concentration changes little during MOF crystal growth), the linker is optimally present in stoichiometric ratio to Zr. Hence, its concentration decreases with MOF crystal growth, leading to increase of modulator-covered defect formation with time.

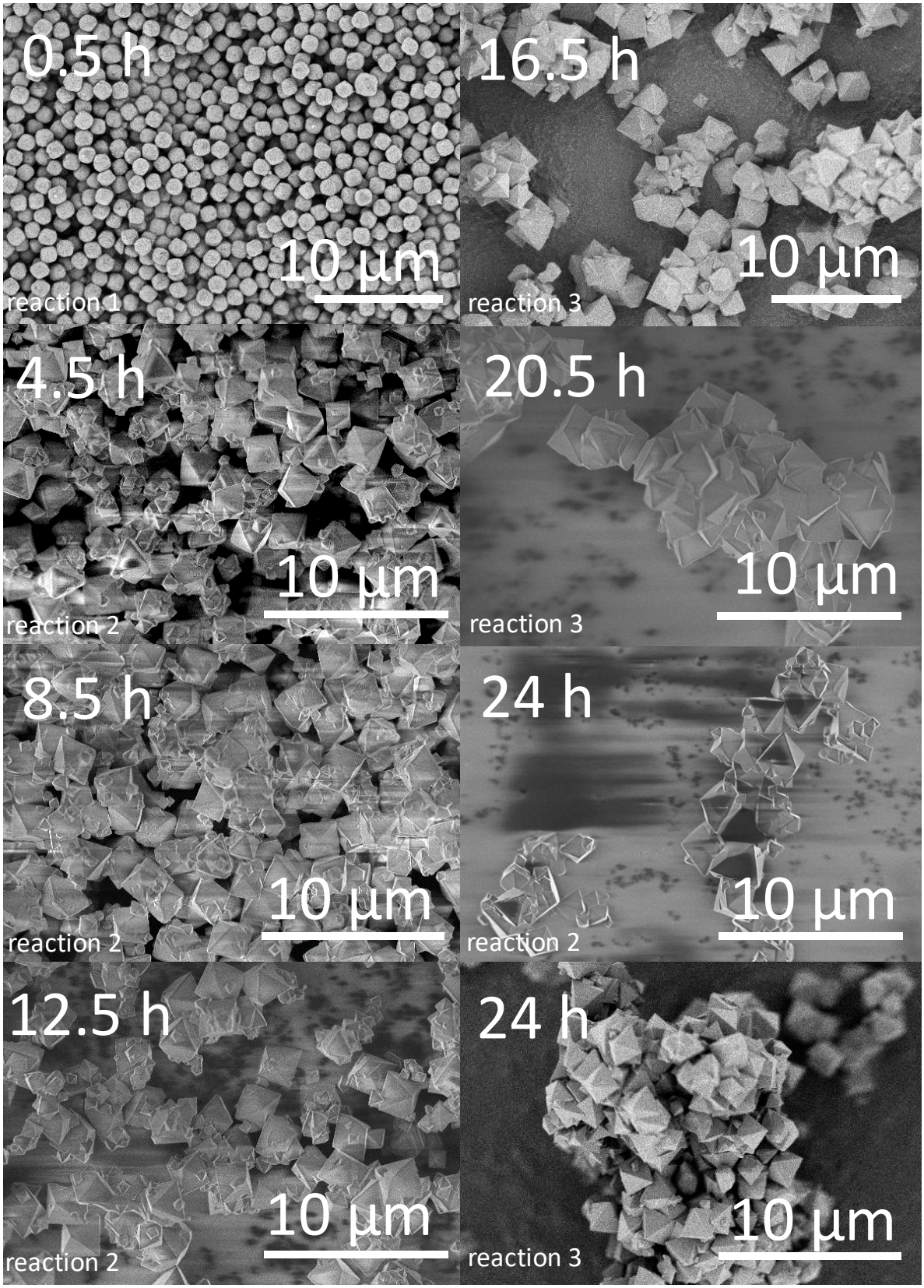

Figure 28. SEM images of the samples of D-9_{BA}, collected at various time intervals. The noted time is after the addition of linkers to the reaction solution (which is considered time zero).

After the insights about the MOF formation with dilute synthesis condition, similar study was performed on concentrated synthesis to study composition of C-3_{BA} at various interval during its formation. Within 24 hours the yield increases gradually and reaches about 92 % in 24 hours (Figure 29).

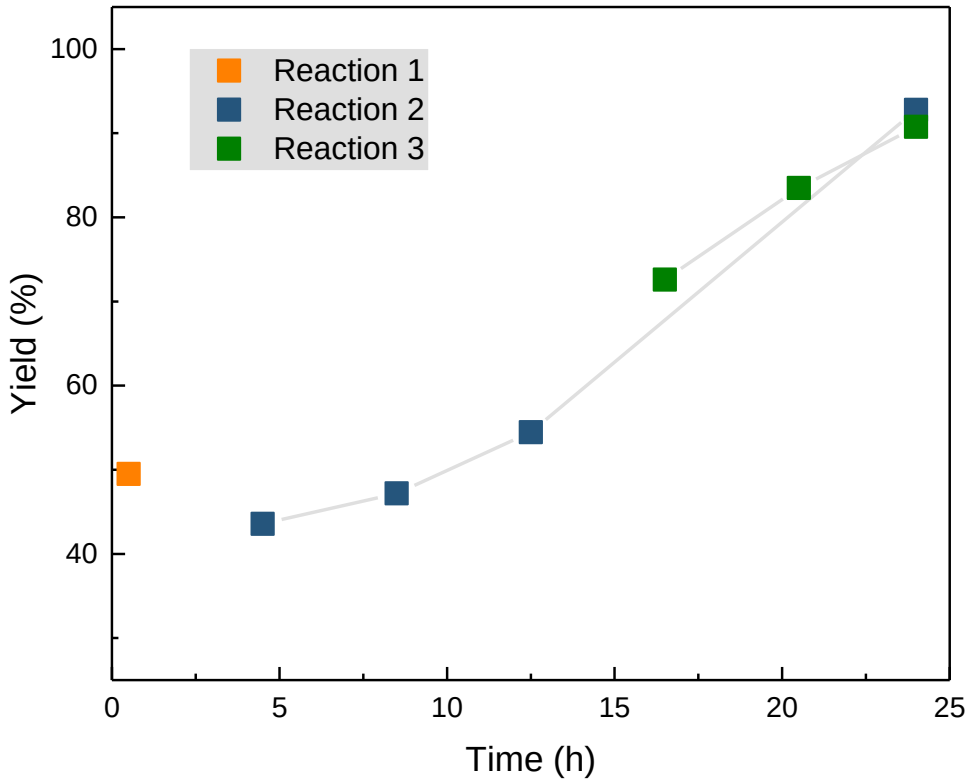

Figure 29. Yield for the samples of C-3_{BA} extracted at various intervals.

SEM images shows the formation of typical UiO-67 octahedral crystals at 0.5 hour (Figure 30). The crystals looks homogenously monodispersed and similar in size at 4.5 to 12.5 h. Surprisingly, after 16.5 h, SEM shows the formation of elongated plate-like crystals together with the octahedral crystals in both the reactions (reaction 2 and reaction 3). Further, the PXRD for the samples at 24 h shows that there is a presence of forbidden peaks in the diffraction pattern suggesting the formation of other type of phases (Figure 31). This behavior can be attributed to a small amount of loss of water during the extraction of samples during the course of the experiment, knowing the literature report where water plays an important role in determining phase of MOF material.[77, 121] In combination, these results led to a systematic screening of amount of water for the synthesis of UiO-67 under concentrated synthesis conditions.

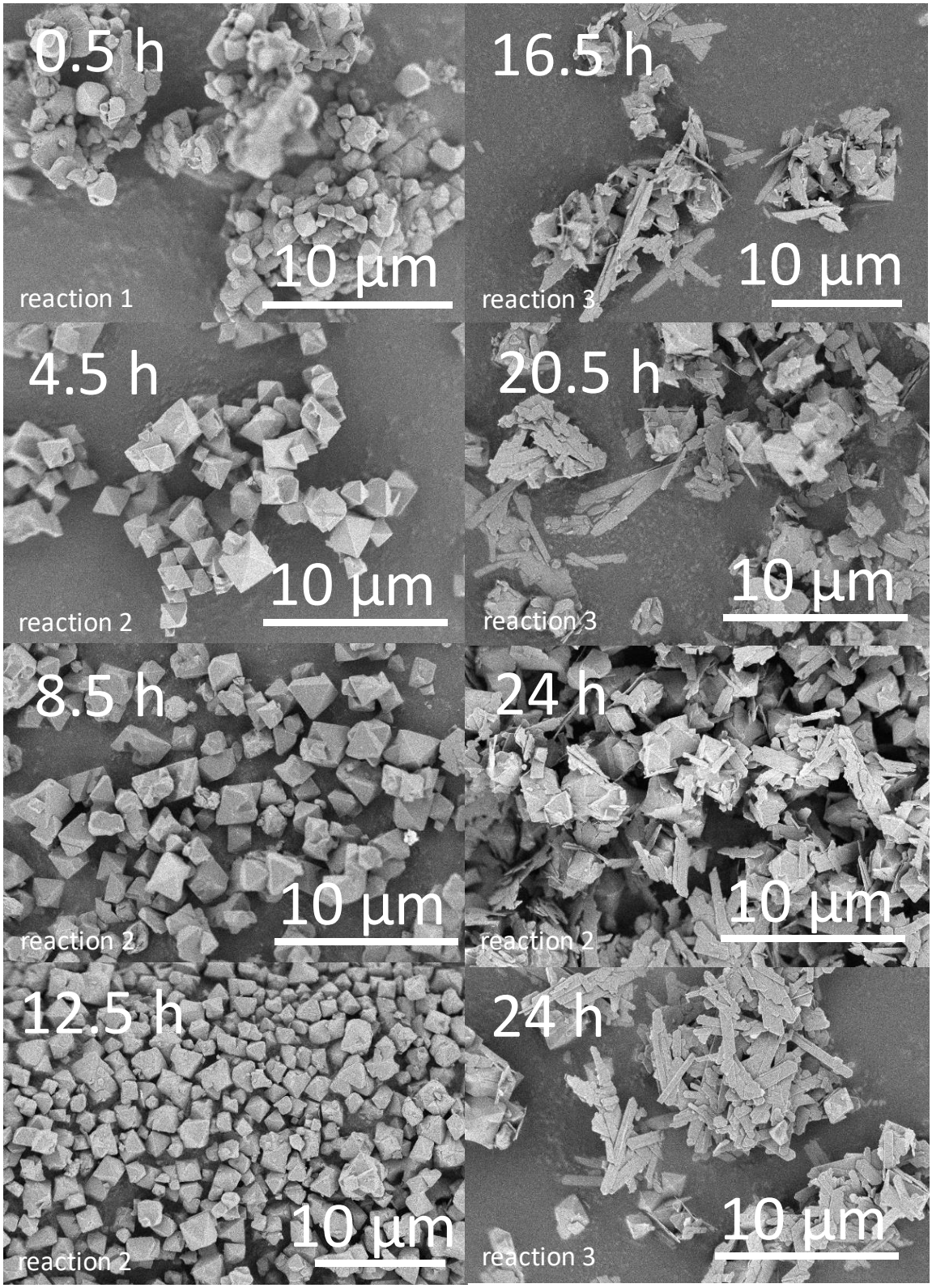

Figure 30. SEM images of the samples of C-3_{BA}, collected at various time intervals. The noted time is after the addition of linkers to the reaction solution (which is considered time zero).

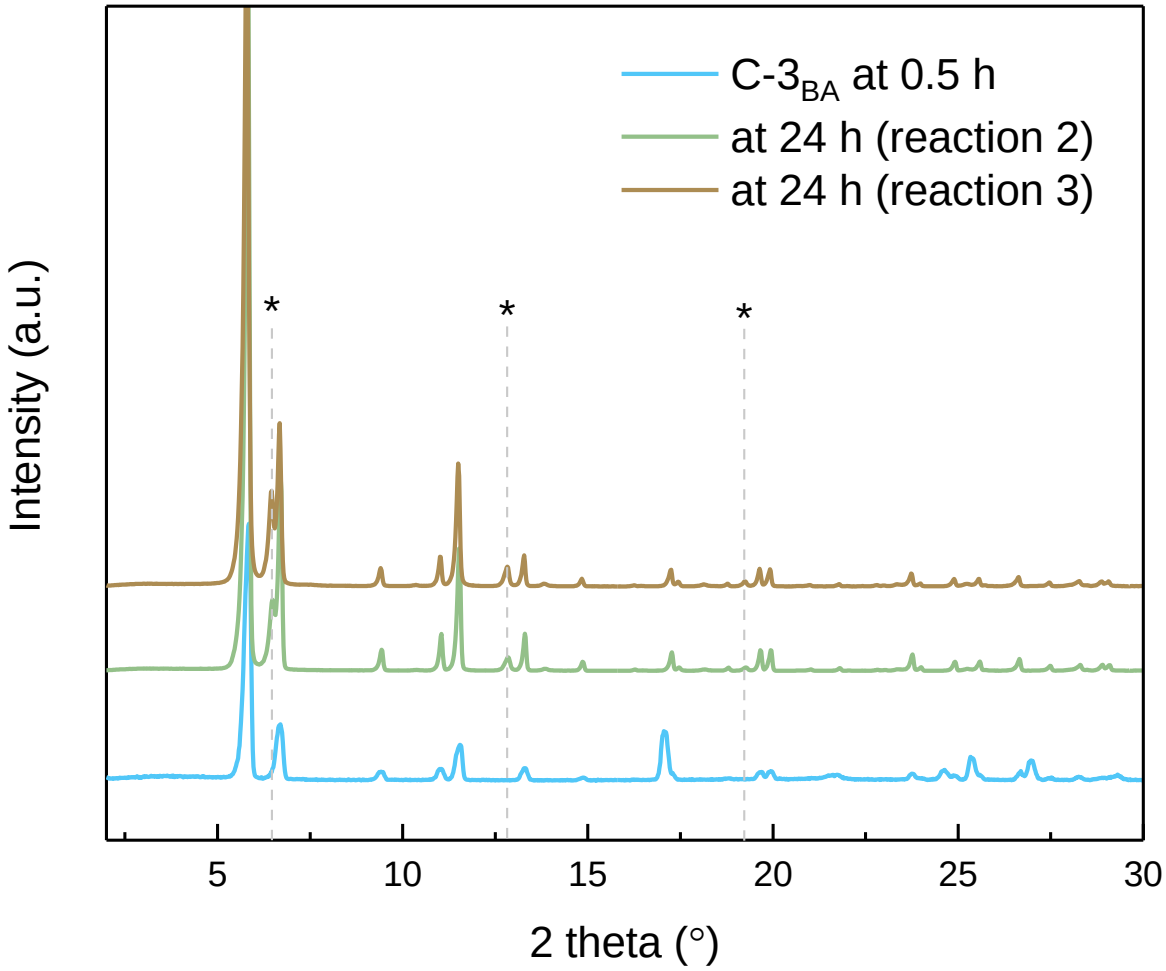

Figure 31. PXRD patterns for the samples collected at 0.5 h and 24 h from reaction 1, 2 and 3 for the synthesis of C-3_{BA}.

3.1.3. Screening of water

The effect of varying amount of water in the synthesis of UiO-67-bpydc$_{(0.1)}$ was studied by six samples, synthesized using 0.3, 3, 4, 5, 6 and 9 molar equiv of water. UiO-67-bpydc$_{(0.1)}$ is composed of 0.1 equiv of H_2bpydc linker ([2,2'-bipyridine]-5,5'-dicarboxylic acid) and 0.9 equiv of H_2bpdc linker. Therefore the samples were labelled as UiO-67-bpydc$_{(0.1)}$-y_{H_2O} where y is the molar equiv of water. Figure 32 shows the diffraction patterns of all the samples where the presence of extra peaks are observed (marked by star), in UiO-67-bpydc$_{(0.1)}$-$0.3_{H_2O,}$ UiO-67-bpydc$_{(0.1)}$-3_{H_2O}, UiO-67-bpydc$_{(0.1)}$-4_{H_2O} and UiO-67-bpydc$_{(0.1)}$-5_{H_2O}. Pawley refinement of these diffractograms revealed that the extra peaks are forbidden in the ideal UiO-67 structure (Figure A10). This indicates that the MOFs made with 0.3, 3, 4 and 5 equiv are phase impure

whereas samples with no extra peaks (6 and 9 equiv) are mostly **fcu** UiO-67. In addition, the intensity of the forbidden peaks decreases with increasing amount of water in the synthesis.

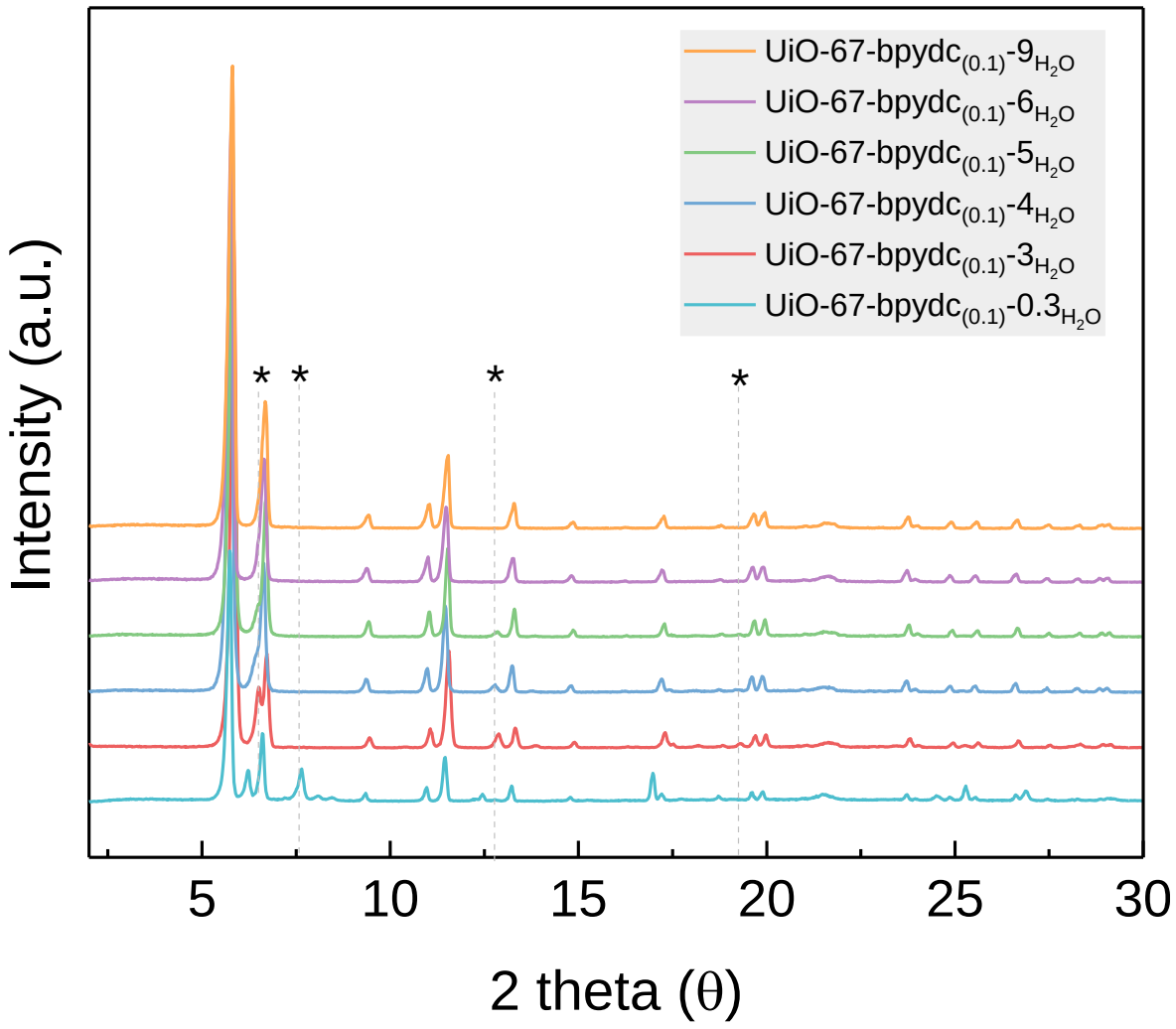

Figure 32. PXRD patterns of UiO-67-bpydc$_{0.1}$ synthesized with different amount of water; 0.3 3, 4, 5, 6, 9 equiv.

A Pawley refinement of the four known Zr-bpdc MOF phases (UiO-67, MIL-140C, **hxl**-Zr-bpdc and hcp-Zr-bpdc) was performed on the diffraction pattern of UiO-67-bpydc$_{(0.1)}$-3$_{H_2O}$ to determine the identity of the unknown phase(s).[121] MIL-140C (ZrO($O_2C_{12}H_8$-CO_2)) has an inorganic subunits of complex zirconium oxide chains of ZrO_7. The main chain is connected to six other chains though dicarboxylate (from H_2bpdc linker). Each zirconium atom exhibit seven coordination modes with μ_3-O oxygen atoms and four oxygen atoms from H_2bpdc linker (Figure 11).[132-134] Almost all of the observed peaks can be assigned to a combination of UiO-67 and MIL-140C (with the exception of two peaks) shown in Figure 33.[132-134] These two peaks do not belong to the linker or benzoic acid as well. The relative amount of MIL-140C with

respect to UiO-67 was also estimated. The presence of MIL-140C phase decreases as the water increases in the synthesis conditions. The presence of MIL-140 was 23 %, 11 %, 8 %, 6 %, 2 % and 1.4 % in samples synthesized with 0.3, 3, 4, 5, 6 and 9 equiv.

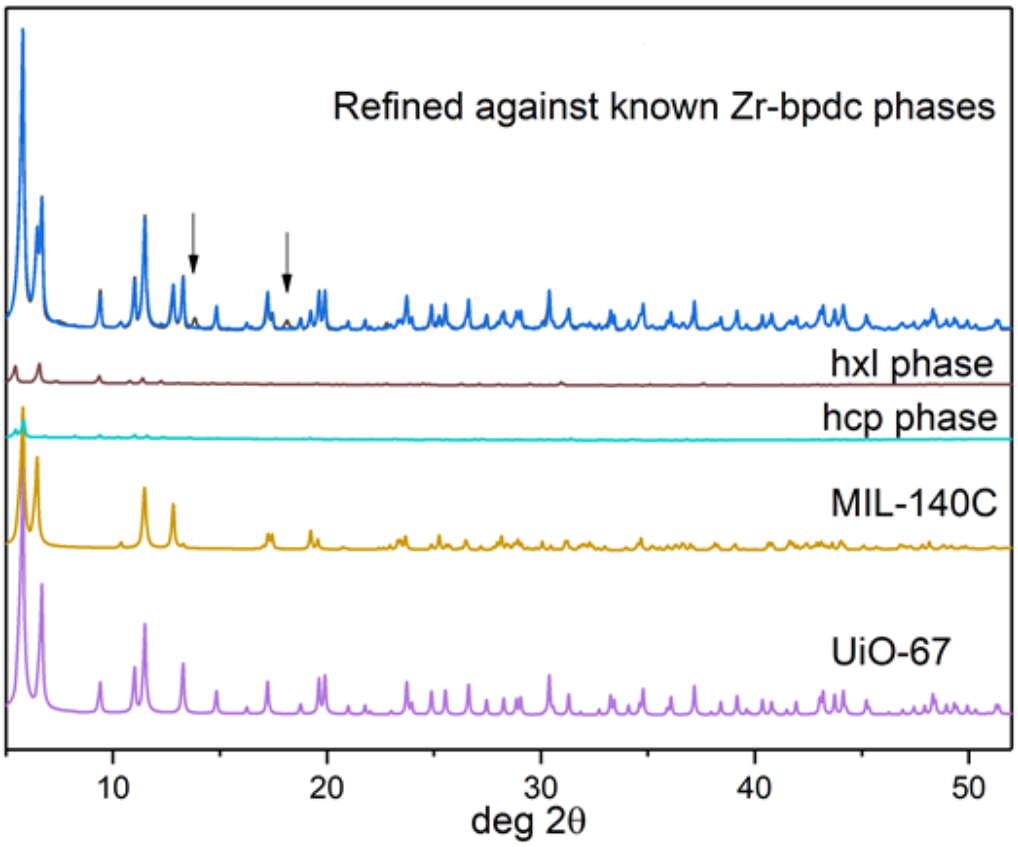

Figure 33. PXRD pattern of UiO-67-bpydc$_{0.1}$-3$_{H_2O}$ refined against MIL-140C, hcp phase and hexagonal nanosheets phase of Zr based MOFs with H_2bpdc linker.

The balance between isolated $Zr_6O_4(OH)_4$ nodes in UiO-66 and ZrO_2-chains in MIL-140A was recently investigated by Soldatov and coworkers.[77] Water was seen to interact with $ZrCl_4$ with the formation of tetragonal ZrO_2 nanoparticles which exhibits Zr_6O_8 clusters and act as a seed for the UiO-66 growth. They also observe a shift from UiO-66 to MIL-140A when water was added to the crystallization mixture, but only when the synthesis was performed at 220 °C but not when the synthesis was performed at 120 °C. Moreover, the original report on the synthesis of MIL-140 was performed at 220 °C which applies to both MIL-140A and C, the UiO-66 and 67 analogs.[132] It was therefore surprising that we observe this water induced transformation at such low temperature as 130 °C for UiO-67 to MIL-140C. UiO-67-bpydc$_{0.1}$-3$_{H_2O}$ and UiO-67-bpydc$_{0.1}$-4$_{H_2O}$ was also sent to our collaborators at the Stockholm University, to perform

rotation electron diffraction and their results are correlated to our refinement results. Formation of MIL-140C is observed. This manuscript is under preparation.

Furthermore, SEM micrographs reveals two different morphology in UiO-67-bpydc$_{(0.1)}$-0.3_{H_2O}, UiO-67-bpydc$_{(0.1)}$-3_{H_2O}, UiO-67-bpydc$_{(0.1)}$-4_{H_2O} and UiO-67-bpydc$_{(0.1)}$-5_{H_2O} which is in agreement with the presence of extra peaks in diffraction pattern (Figure 34). These samples has the usual octahedral crystals together with the long hexagonal plate-like crystals until 5 equiv of water is added in the synthesis. After 6 equiv of water is added in the synthesis, the MOF appears to be have only octahedral crystals.

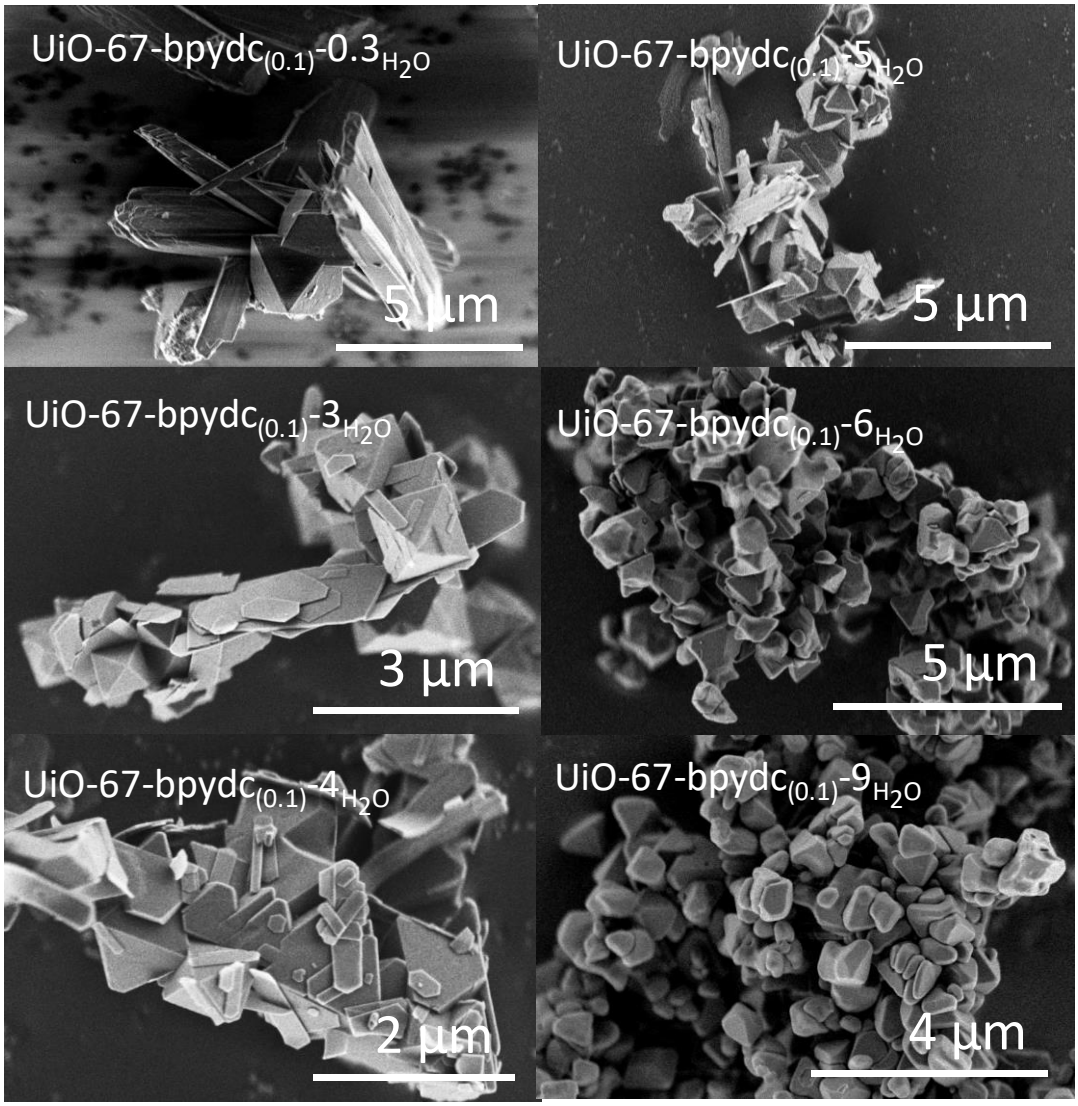

Figure 34. SEM micrographs of UiO-67-bpydc$_{0.1}$ with different amount of water; 0.3, 3, 4, 5, 6 and 9 equiv.

Furthermore, TGA-DSC shows a usual two-step thermal decomposition: near 200 °C, corresponding to the removal of physisorbed solvent and modulator, and near 490 °C with the

combustion of the organic components of the material, presented in Figure A11. UiO-67-bpydc$_{(0.1)}$-0.3_{H_2O} shows an abnormal large excess of starting mass of the sample (Figure A11). The stability of all the samples are quite similar but the normalized weight of the samples slightly decreases with the increase of water in the synthesis.

The relative molar ratio of organic species was calculated by ^{1}H NMR which was performed on the dissolved MOF samples (Figure A12 and Figure A13). It shows the presence of bpydc^{2-} and formate consistently in the range of 10-13 % and 2-4 % (relative to bpdc^{2-}) respectively. Interestingly, the amount of benzoate clearly increases with the increasing amount of water in the synthesis. The amount of benzoate increases from 3 to 15 % with respect to bpdc^{2-} in UiO-67-bpydc$_{0.1}$-3_{H_2O} to UiO-67-bpydc$_{0.1}$-9_{H_2O}, which implies that amount of water in the MOF synthesis affects the total amount of benzoic acid incorporated in the MOF (Figure A13).

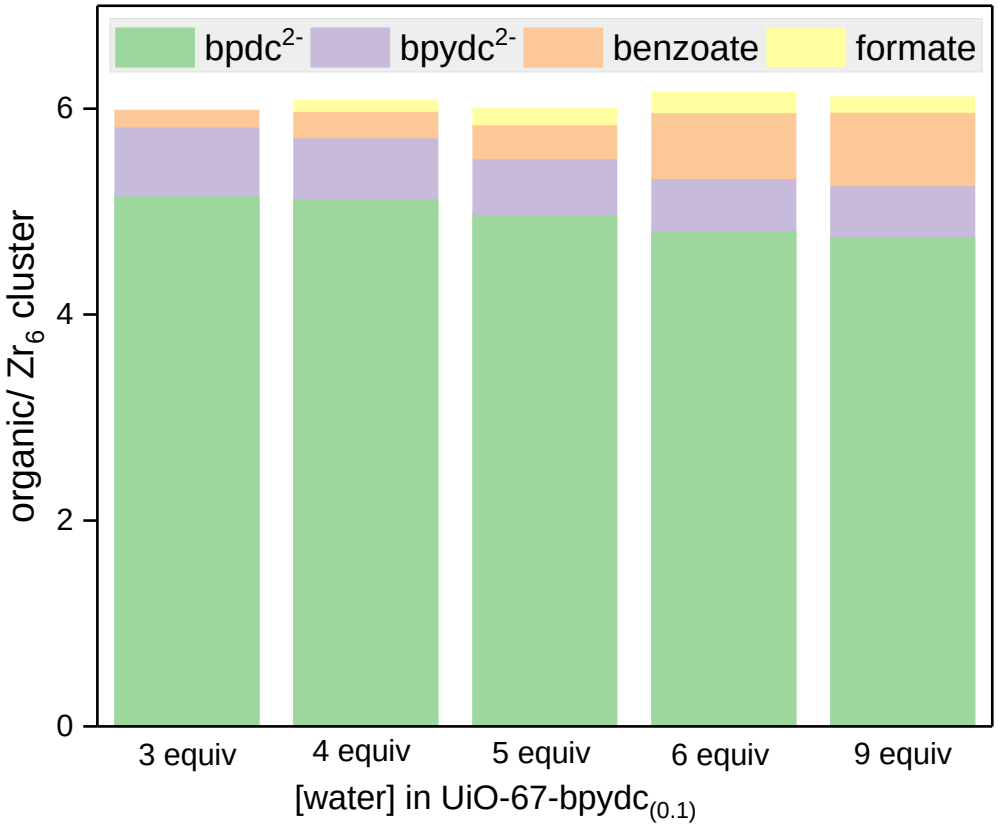

Figure 35. Composition of the organic constituents in each sample, determined by 1H NMR and scaled to the organic:Zr ratio found by TGA (at 200 °C) in the UiO-67-bpydc$_{0.1}$-y_{H_2O} where y is amount of water in the synthesis (3, 4, 5, 6, 9 equiv) The total organic content in an ideal UiO-67-bpydc$_{0.1}$ (Zr_6O_6(bpdc+bpydc)$_6$) is 6.

The TGA and ^{1}H NMR results were together used to calculate the relative amount of organics in order to estimate missing-linker defects in the samples (as discussed above). Strikingly, UiO-

67-BPY-9_{H_2O} has much lower $bpdc^{2-}$ content, with high contents of benzoate (13 % with respect to $bpdc^{2-}$), and this trend reverse as the amount of water in the synthesis is decreased (Figure 35). This shows that water not only affects the crystallization and controls the phases from MIL-140C to UiO-67 but also affects the defectivity.

In conclusion, this study shows that water concentration in the synthesis of UiO-67 plays an important role where it controls the structure of the MOF. At low concentration of the water, MIL-140C is observed, together with UiO-67 whereas pure phase UiO-67 is obtained on increasing the water concentration in the synthesis. Moreover, water is also seen to control the missing linker defects in the synthesized material where these defects increase with increase in the water concentrations in the syntheses.

Moreover, we were also interested in exploring the effect of large access of water in the synthesis of UiO-67, since it has been reported that excessive amounts of water impedes crystallization in the case of UiO-66.[135] Grey and coworkers have reported a study showing the formation of new defective phases of Zr and H_2bpdc linker with varying amounts of water.[121] This study was performed on the Hafnium (Hf) analogues of UiO-66 and UiO-67 where the different phases of the material are observed depending on the amount of water in the synthesis. A molar ration of $HfCl_4$:H_2bpdc:formic acid:water:DMF as 1:1:90:10:175 for **hcp** phase and 1:1:90:38:175 for hexagonal nanosheets were used. These conditions were used as a starting point for our own investigation using $ZrCl_4$ instead of $HfCl_4$ as Zr displays similar chemical properties to Hf. Also, Hf MOFs are isostructural with their Zr analogues where direct substitution of the Zr_6 nodes by Hf_6 is observed.[90, 136]

Figure 36a presents the PXRD pattern of the samples synthesized with $ZrCl_4$ and shows that the results are in agreement with the reported work.[121] The diffraction pattern for hexagonal nanosheets phase is identical with that of the reported diffraction pattern for hexagonal nanosheets phase. However, the obtained diffraction pattern of hcp phase has few forbidden peaks (Figure 36b). Furthermore, TGA-DSC analysis of the samples are in shown in Figure 37, which shows that these phases are slightly lower in thermal stable than usual Zr-MOF **fcu** phase but nevertheless stable up to 400 °C. But the thermal decay in case of hexagonal nanosheets phase is rapid without any clear plateau, unlike **fcu** phase. The **hcp** phase shows a two-step weight loss where major weight loss is observed from 200 to 300 °C.

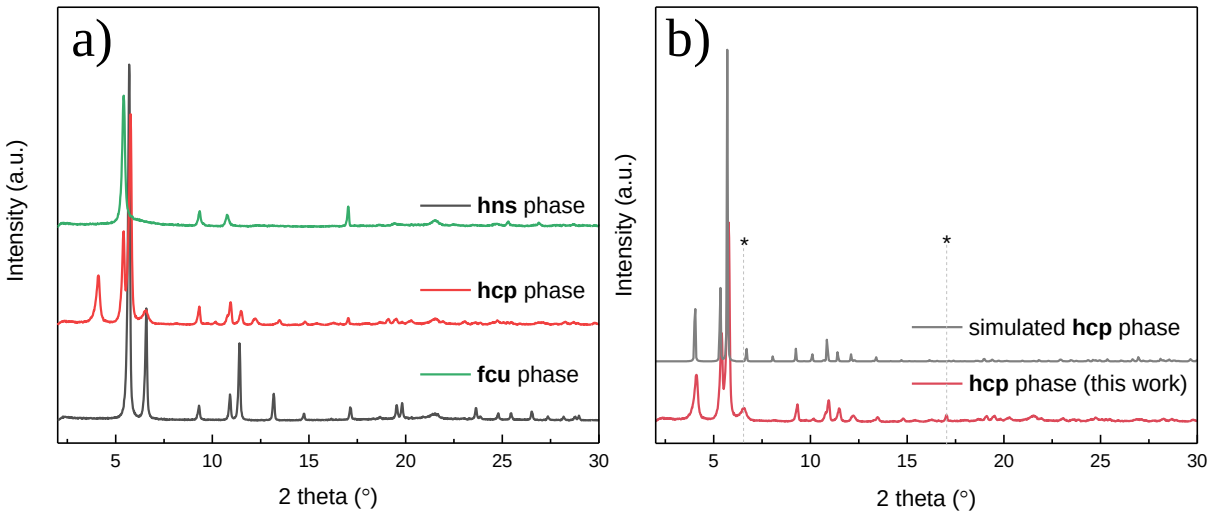

Figure 36. XRD pattern of a) **hcp** and **hexagonal nanosheets** phases (called **hns**) of Zr based MOFs in this work, fcu phase (C-3_{BA}) is showed for reference purpose and b) compared to the XRD pattern of simulated **hcp** phase pattern.

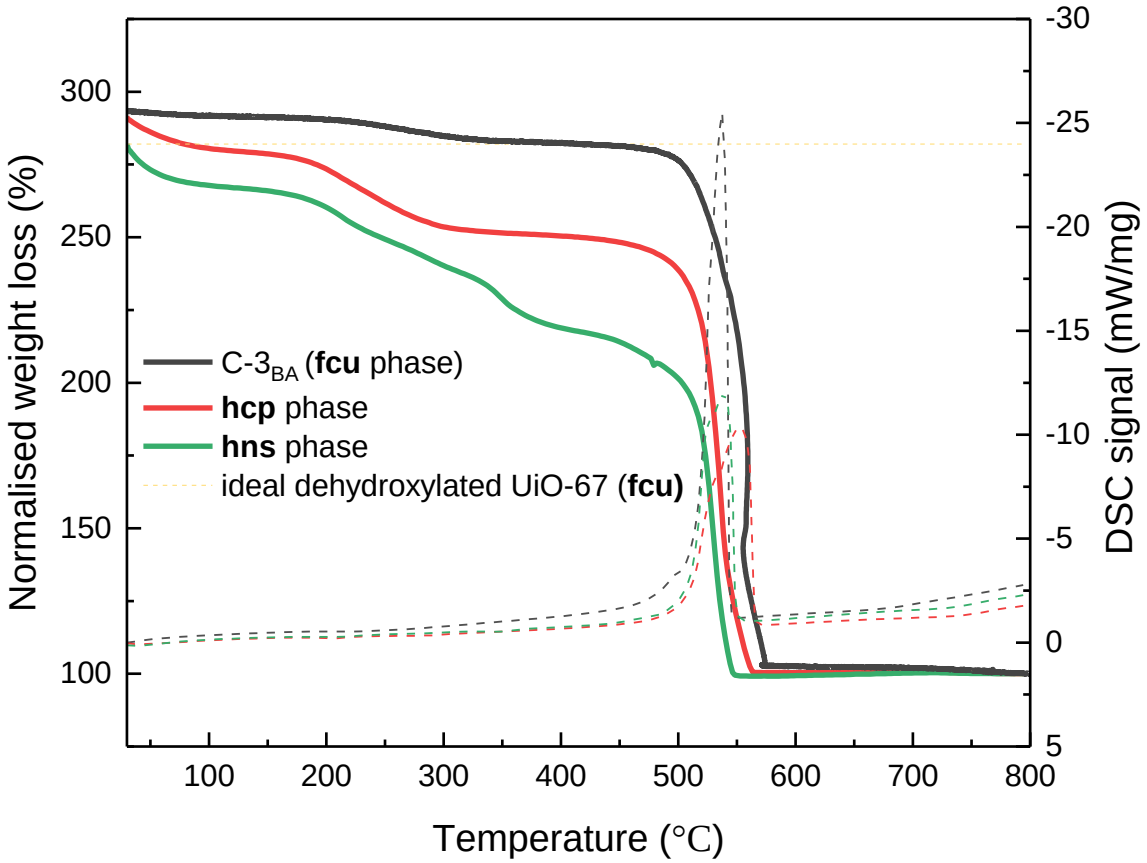

Figure 37. TGA-DSC analysis of **hcp** and **hexagonal nanosheets** phases (called **hns**) of Zr based MOFs in this work, **fcu** phase (C-3_{BA}) is put for reference purpose.

SEM images of the samples were collected and are presented in Figure 38, where image 1 to 5 is for the synthesis of **hcp** phase and image 6 is for **hexagonal nanosheets** phase. The crystals obtained for the synthesis of **hcp** phase are inhomogeneous and are of three different kinds;

hexagonal shaped (image 1 and 2), octahedral shaped with decorated edges (images 3) and mixtures of hexagonal, octahedral and spherically shaped crystals (image 4 and 5). Moreover, the hexagonal shaped crystals obtained in our experiments are not single layers, but rather crystals consisting of stacked layers. However, the spherical shaped crystal of image 5 resembles the SEM image of **fcu** phase Hf-MOF, reported by Grey and coworker. This shows that there are more than one phase of Zr-MOF in this sample which explains the forbidden peaks in the PXRD pattern as well. Despite this, the SEM image obtained for the **hexagonal nanosheets** phase synthesized in this work (image 6) resembles that of the reported **hexagonal nanosheets** phase.

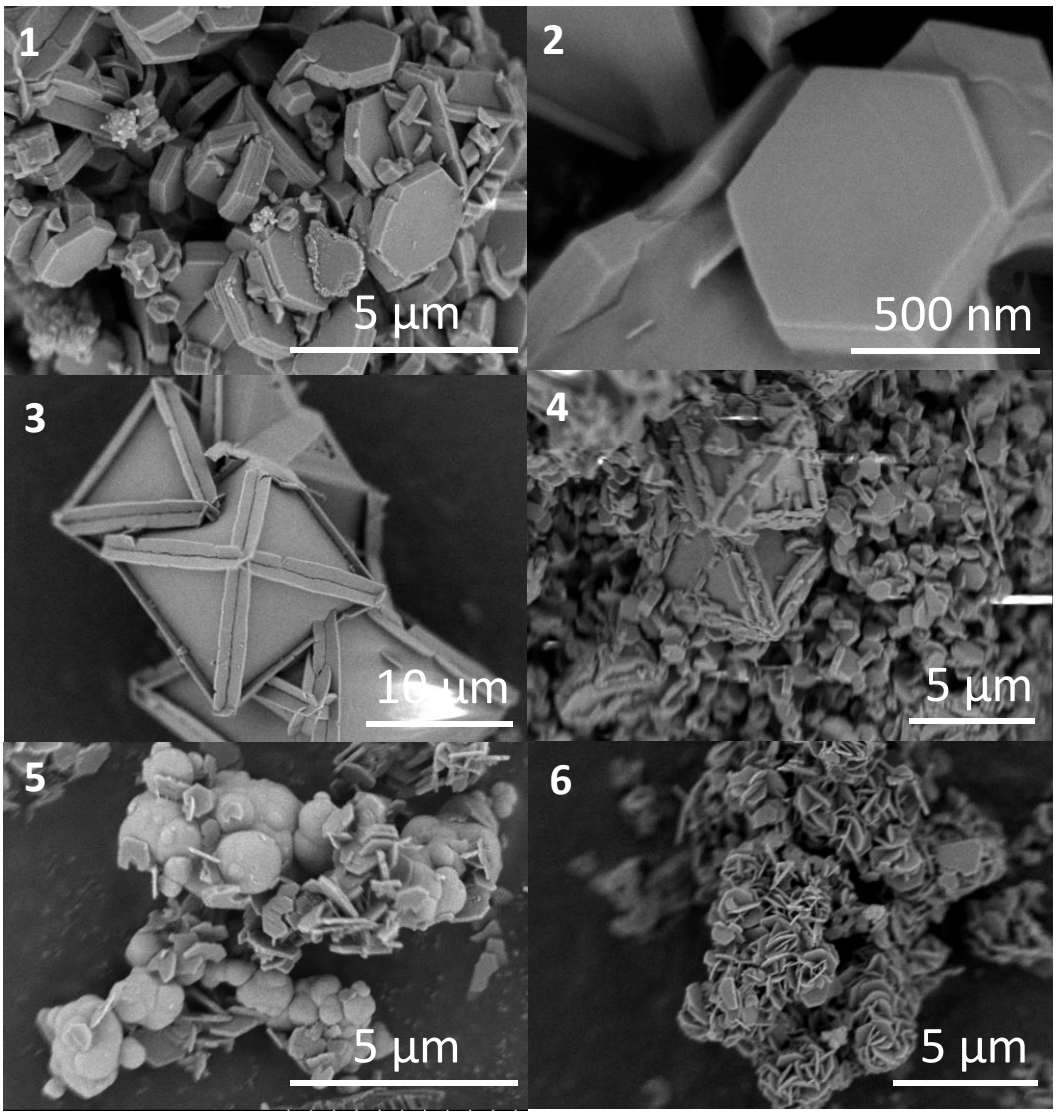

Figure 38. SEM images of the synthesized Zr-based hcp (1 to 5) and hexagonal nanosheets phase (6).

This study shows that variations within synthesis conditions that preserve the organic linker may alter both the linker connectivity and even alter the inorganic building unit. Different

phases associated with Zr-H_2bpdc is possible to make by tuning the synthetic conditions carefully. Moreover, the diffraction pattern of these phases are closely related which should be paid special attention to in order to determine the final outcome of the synthesized MOF.

To connect the results from studies done with low amount of water (3 to 9 equiv) and excess amount of water (10 and 38 equiv), there is a need for further experimental work where the synthesis conditions are kept same and only the amount of water is changed. Presently, for the synthesis of hcp and hexagonal nanosheets, formic acid is used as a modulator, unlike benzoic acid (used as a modulator in rest of the work). This is discussed further in the Suggestion for further work.

3.1.4. Thermal stability of C-3_{BA}

To examine the thermal stability of the optimal material, C-3_{BA}, in more detail, the sample was put-through static temperature treatment in air in the TGA instrument for 24 h, followed by pXRD analysis. PXRD patterns and nitrogen adsorption isotherms were acquired for the calcined samples (Figure 39). The PXRD patterns show that the MOF structure is intact in all the calcined samples, but C-3_{BA}@400 °C displays less intense peaks (Figure 39). The nitrogen adsorption isotherms shows that samples C-3_{BA}@300 °C and C-3_{BA}@350 °C have identical porosity with a BET surface area of 2459 m^2 g^{-1} and 2458 m^2 g^{-1} respectively (Figure 39 and Table 15). It is interesting to see that these samples shows only a 10 % decrease in surface area with respect to C-3_{BA}. However, C-3_{BA}@375 °C shows a 14 % decrease in the surface area, showing that heating C-3_{BA} at 375 °C affects the MOF to a greater magnitude. On the other hand, C-3_{BA}@400 °C is affected to the substantial magnitude and the surface area is seen to be decreased by 51 %, which reveals that the MOF is highly damaged. Together, the measurements reveal that the sample is stable at 350 °C, but slowly decomposes at temperatures above 350 °C.

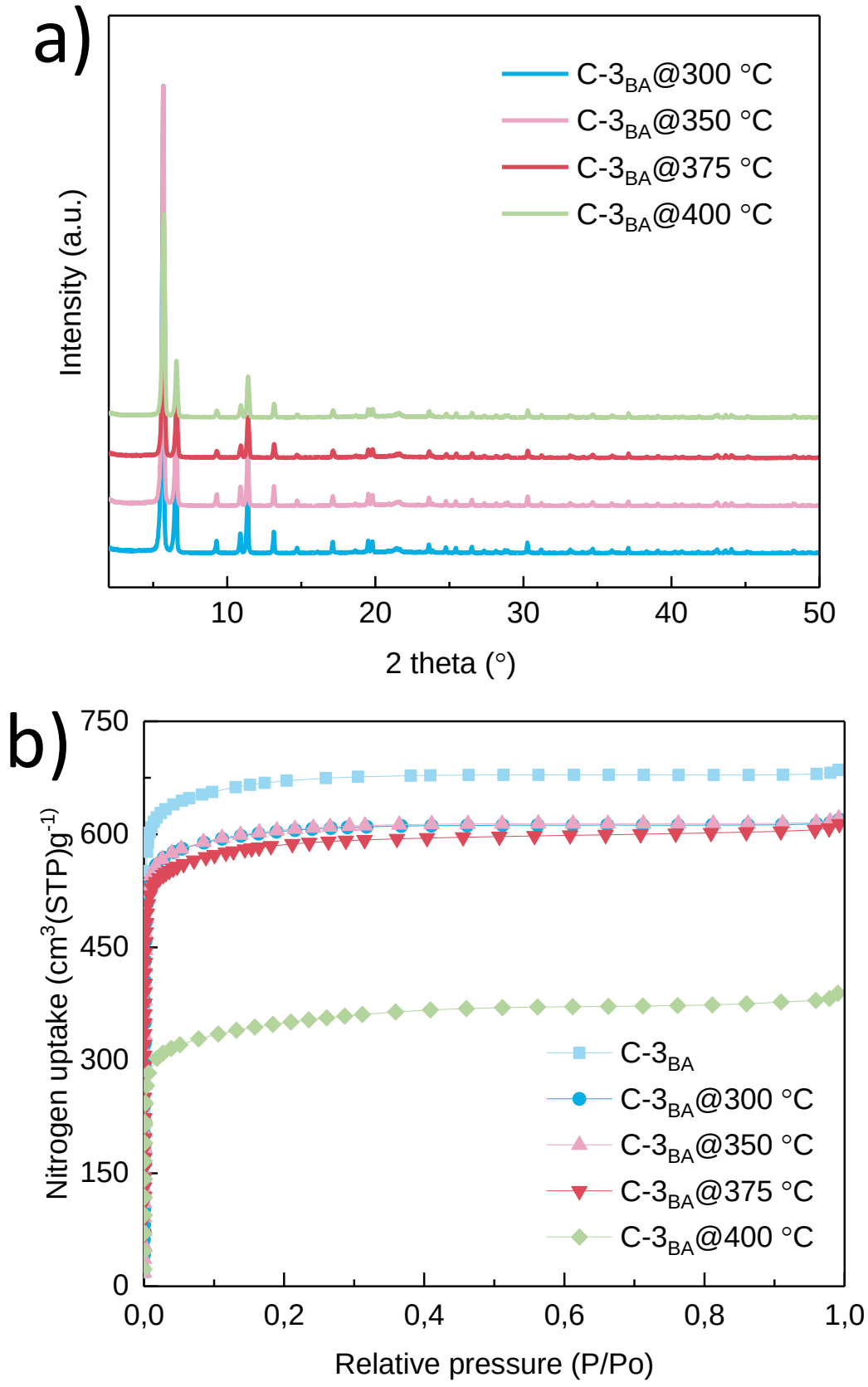

Figure 39. a) PXRD pattern and b) N_2 adsorption isotherm at 77 K of C-3_{BA} after calcination at 300 °C, 350 °C, 375 °C and 400 °C for 24 hours in air.

Table 15. Surface area and pore volume of C-3_{BA} after heating at 300 °C, 350 °C, 375 °C and 400 °C for 24 hours in air.

Entry	MOF (after 24 h)	Surface area [m^2 g^{-1}]	Pore volume [cm^3(STP) g^{-1}]
1	C-3_{BA} @300 °C	2459	565
2	C-3_{BA} @350 °C	2458	565
3	C-3_{BA} @375 °C	2351	540
4	C-3_{BA} @400 °C	1341	308

To further investigate the thermal stability, static TGA-DSC measurements for 12 h were performed at the respective temperatures (Figure 40). The TGA-DSC curve for C-3_{BA}@300 °C and C-3_{BA}@350 °C overlaps with the TGA-DSC curve for parent C-3_{BA} which shows that C-3_{BA} can withstand a temperature up to 350 °C without losing any species from the framework by the effect of heat. As we move to higher temperatures we see a weight loss during calcinations, indicating damage to the framework. The TGA-DSC results are in good agreement with the PXRD and nitrogen adsorption isotherm results which suggested that calcination of C-3_{BA} at 375 °C, affects it to some extent and at 400 °C, affects largely by diminishing its porosity to half. These thermal tests show that C-3_{BA} is stable at 350 °C, but slowly decomposes at temperatures above 350 °C.

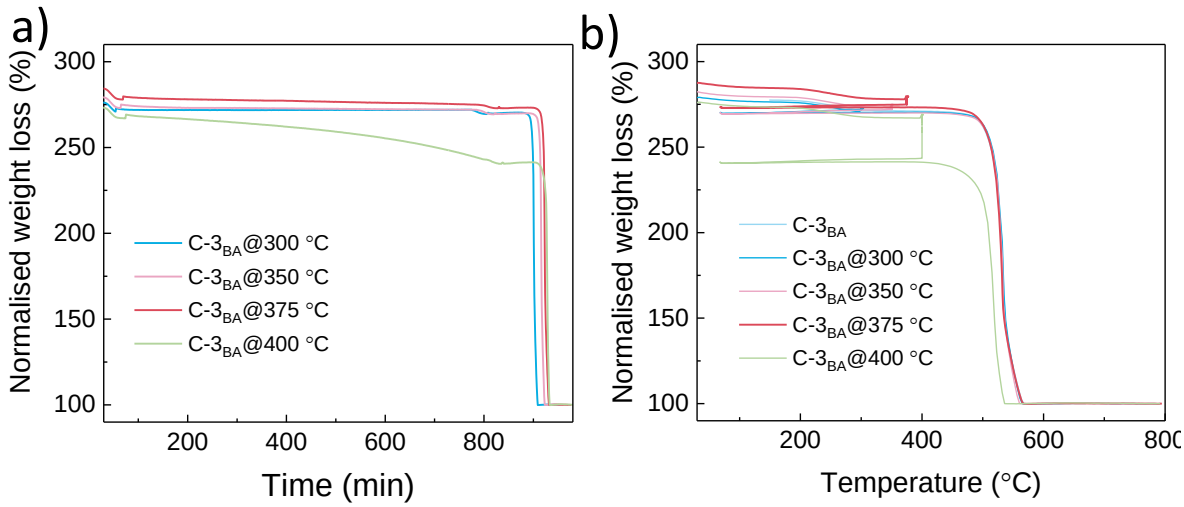

Figure 40. TGA-DSC curves for the thermally heated C-3_{BA} where a) is normalised weight loss vs time and b) normalised weight loss vs temperature. The samples were brought down to room temperature between the static treatment and a standard TGA ramp.

3.2. UiO-67-bndc (bndc = [1,1'-binaphthalene]-4,4'-dicarboxylate)

3.2.1. Screening the reaction conditions

After concluding the study on UiO-67, the experimental protocol were tested for various other UiO-67-type MOF where UiO-67-bndc is an evident choice (section 1.9). UiO-67-bndc is composed of $Zr_6O_4(OH)_4(COO)_{12}$ cluster, identical to that of UiO-67 where H_2bndc ([1,1'-binaphthalene]-4,4'-dicarboxylic acid) linker is used instead of H_2bpdc. Therefore, the results from the screening of UiO-67 were utilized for the tuning and optimization of UiO-67-bndc.

3.2.1.1. Preliminary screening

A similar preliminary screening was performed as it was performed for UiO-67 and based on the results from the screening in UiO-67, some of the selected parameters were studied for UiO-67-bndc. They were mainly the study of the effect of varying amount of benzoic acid ranging from 0 to 15 molar equiv in the presence of water and DMF (Table 9). PXRD was recorded for all the dried samples synthesized using varying amount of BA and H_2bndc linker using 150 molar equiv DMF. All the PXRD patterns corresponds to that of reflections from typical UiO-67 patterns, Figure 41. This confirms the possibility for the formation of UiO-67-bndc at the selected synthesis condition, i.e. BA= 1 to 15 and different synthesis temperature of 120, 130 and 140 °C.

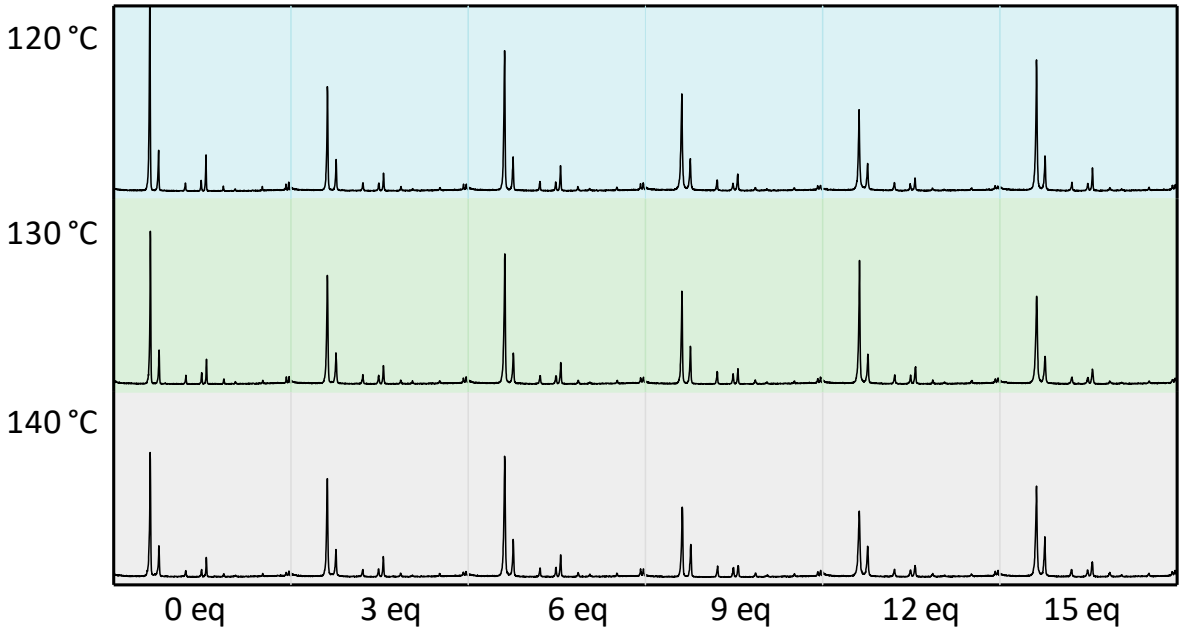

Figure 41. PXRD patterns of MOF produced by screening benzoic acid (from 0 to 15 equiv) and different temperatures (120 °C, 130 °C and 140 °C) for UiO-67-bndc.

Furthermore, all the prepared samples were tested for thermal stability by calcining them at 400 °C for 2 hours and repeating the PXRD (Figure 42). Surprisingly, the samples without the use of benzoic acid maintains high crystallinity unlike other samples in the series. This implies that presence of benzoic acid in the synthesis of UiO-67-bndc decreases its thermal stability. PXRD patterns of these samples are recorded and shown in Figure 43. The PXRD indicates the crystallinity is maintained with all the samples suggesting their high tolerance towards water, in agreement with literature.[65]

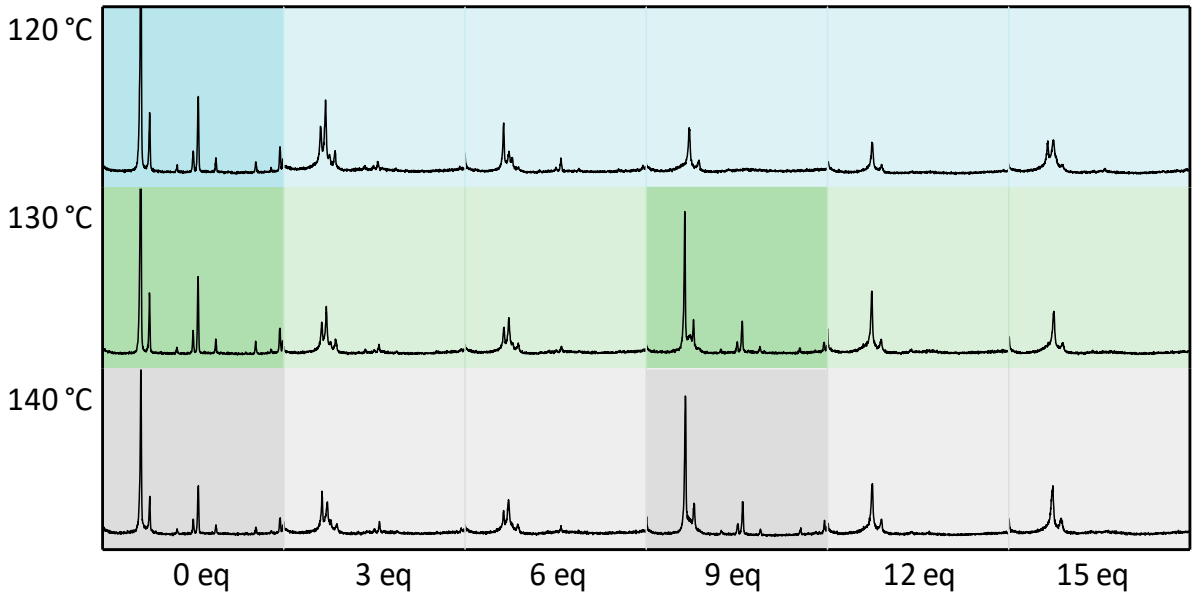

Figure 42. PXRD of the samples of UiO-67-bndc after thermal stability test at 400 °C for 2 h.

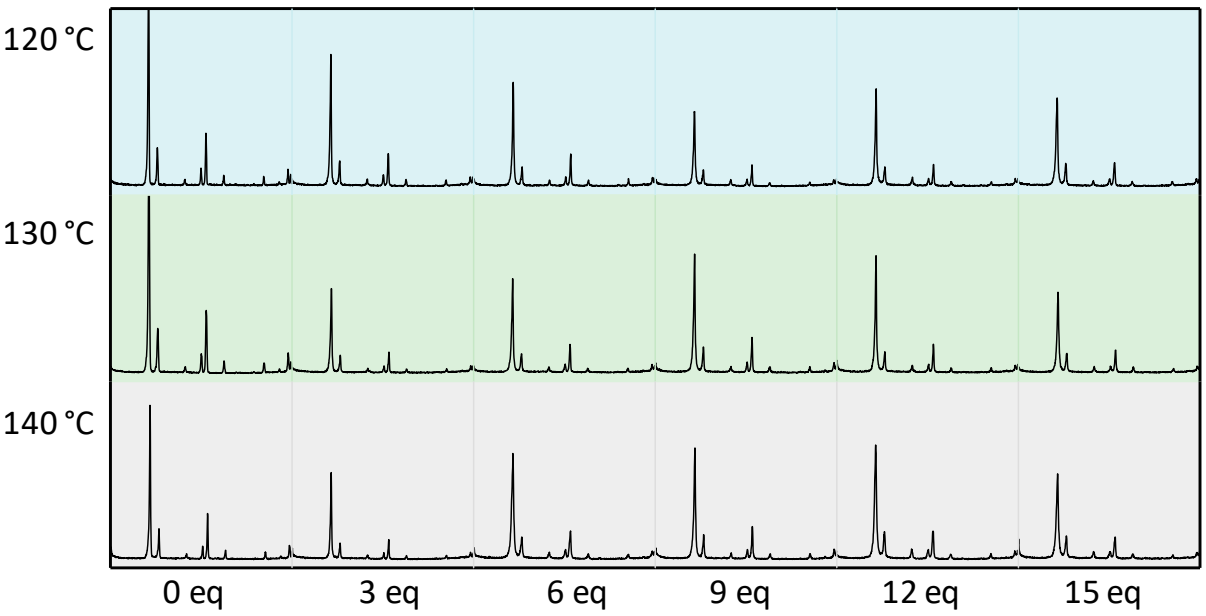

Figure 43. PXRD of the samples of UiO-67-bndc after water stability test for 24 h.

Figure 44 shows the SEM images of UiO-67-bndc (no modulator) synthesized at 130 °C, which shows octahedral crystals, where they maintain the octahedral crystal shape after undergoing thermal treatment and water treatment, suggesting the robust nature of this material.

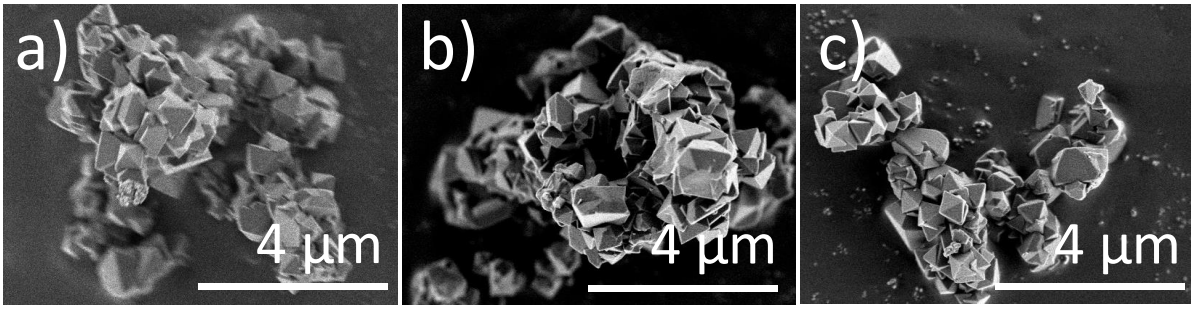

Figure 44. SEM images of a) UiO-67-bndc-0_{BA} synthesized at 130 °C, b) after heated at 200 °C for 2 h and c) after soaked in water for 24 h.

Therefore, synthesis of UiO-67-bndc is possible with and without the use of benzoic acid as modulator with the temperature range of 120-140 °C with Zr:DMF ratio as 1:150. The samples without the use benzoic acid is seen to have better thermal stability as compared to others. For further use, UiO-67-bndc was prepared with no modulator at 130 °C.

3.2.1.2. Screening of amount of solvent

Synthesis of UiO-67-bndc was attempted with Zr:DMF rations of (1:50; concentrated (C), 1:150; dilute (D) and 1:300; very dilute (VD)). The XRD patterns in Figure 45 suggests the possibility to synthesize of UiO-67-bndc with various amounts of DMF. Furthermore, the quality of all these samples were checked by further characterization. TGA-DSC shows that all the samples are stable up to 400 °C before the framework collapses. The BET surface area for C-0_{BA}-bndc, D-0_{BA}-bndc and VD-0_{BA}-bndc is 1528 m^2 g^{-1}, 1521 m^2 g^{-1} and 1463 m^2 g^{-1}, and pore volume is 351 cm^3 g^{-1}, 349 cm^3 g^{-1}, and 336 cm^3 g^{-1} respectively. The TGA-DSC and nitrogen uptake do not show much variation in these samples, suggesting negligible effect of varying DMF concentration for the synthesis of UiO-67-bndc (Figure 46). Similarly, the ^{1}H NMR shows very clean spectra with the peaks corresponding to [1,1'-binaphthalene]-4,4'-dicarboxylate (Figure 47). The VD-0_{BA}-H_2bndc shows a small peak of formate suggesting the incorporation of formate on the capping sites of the MOF.

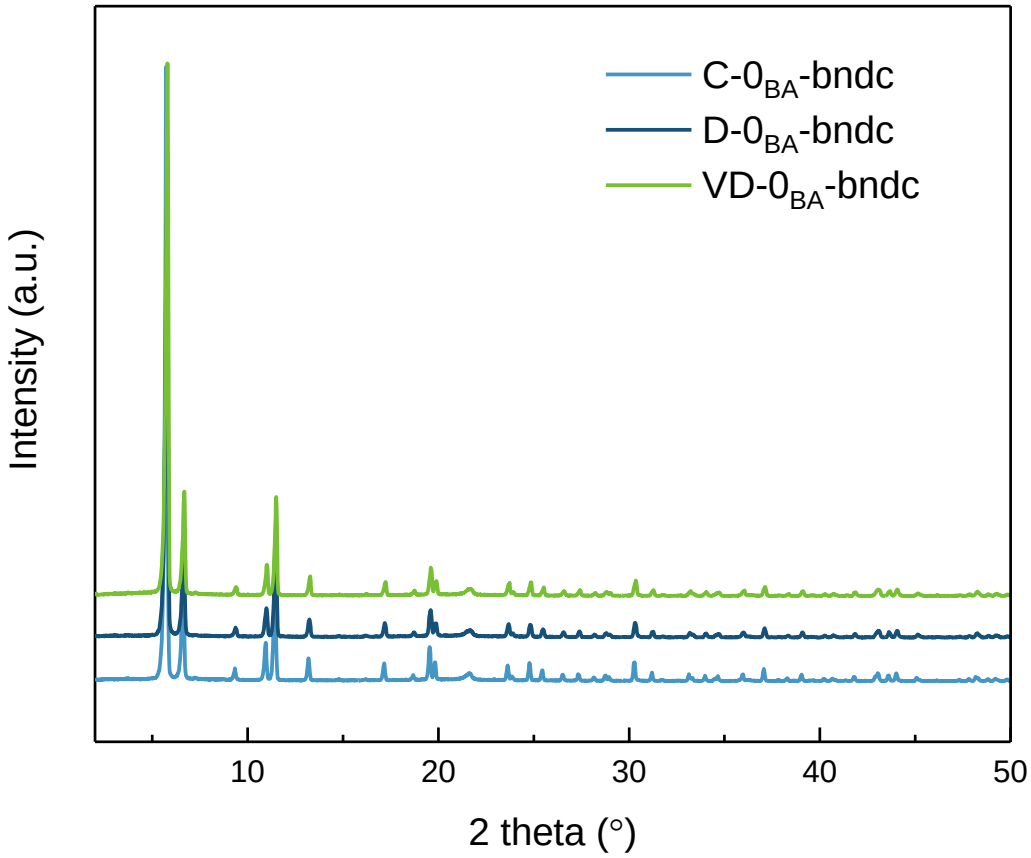

Figure 45. PXRD of the C-0_{BA}-bndc, D-0_{BA}-bndc and VD-0_{BA}-bndc.

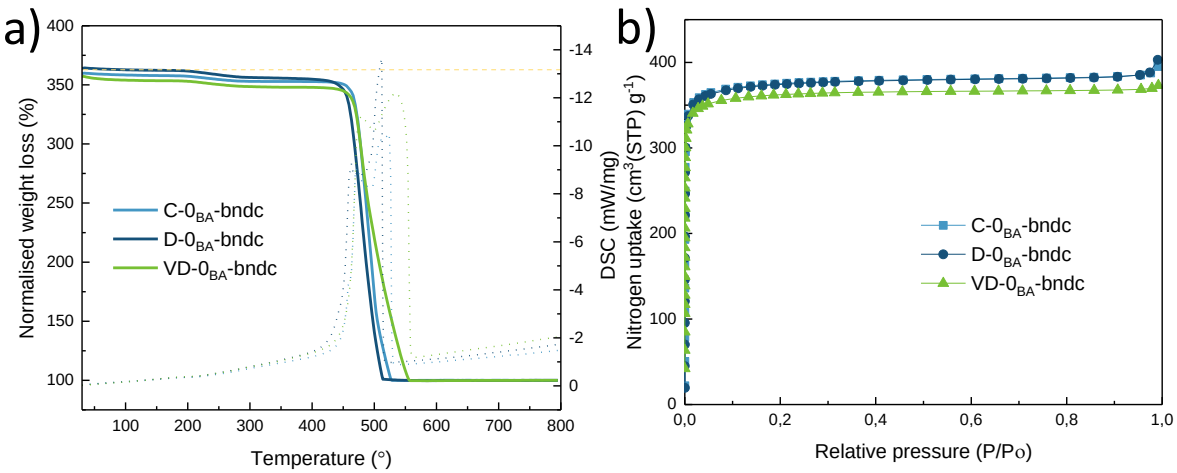

Figure 46. a) TG-DSC signals and b) nitrogen isotherm of C-0_{BA}-bndc, D-0_{BA}-bndc and VD-0_{BA}-bndc.

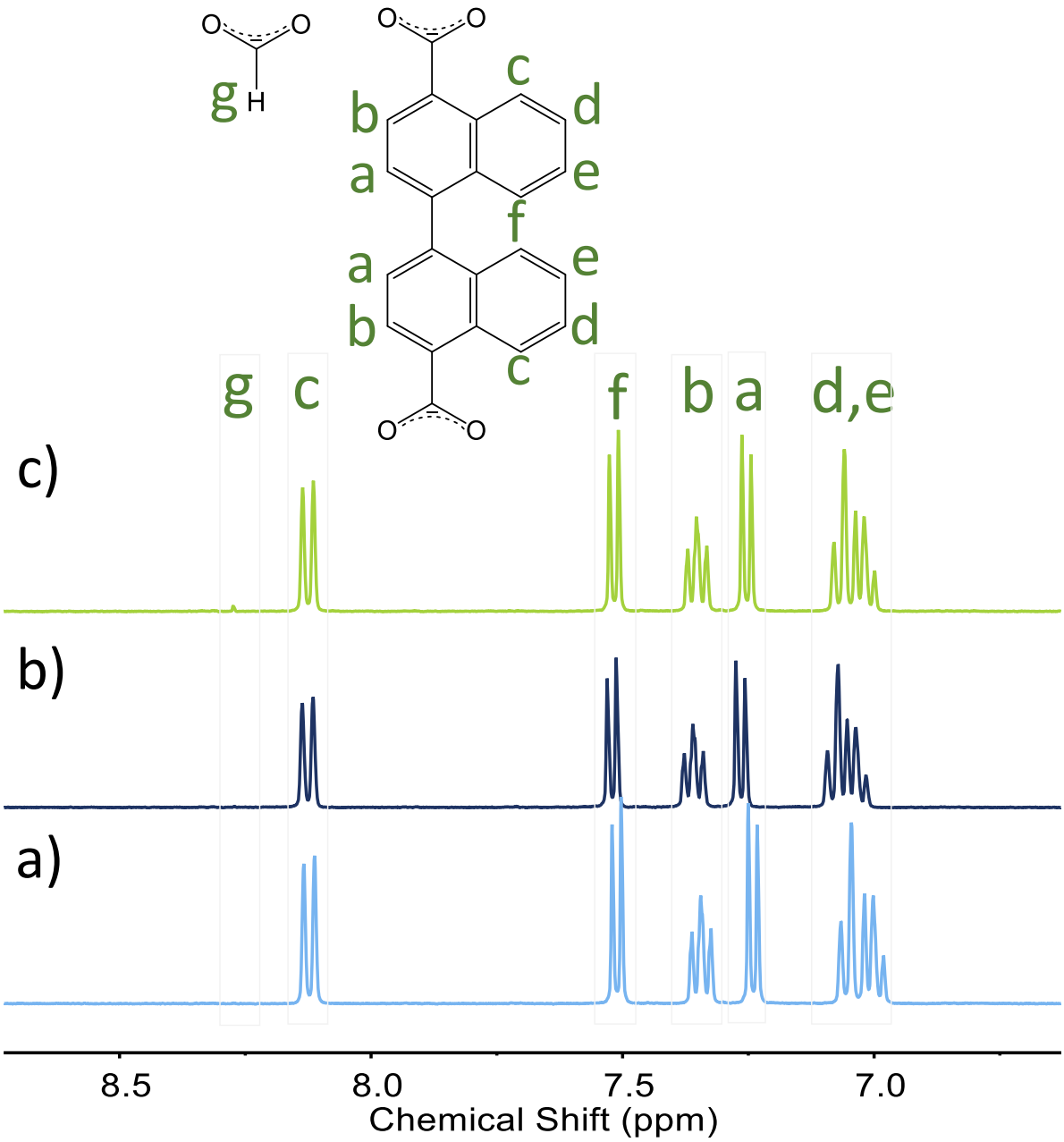

Figure 47. 1H NMR spectra of a) C-0_{BA}-bndc, b) D-0_{BA}-bndc and c) VD-0_{BA}-bndc.

Therefore, synthesis of UiO-67-bndc is possible various concentration of DMF from 50 to 300 equiv. The data suggest that there is not a large effect of varying the DMF concentration on the quality if UiO-67-bndc.

3.2.1.3. Screening of amount of modulator

PXRD and TGA-DSC data of C-3_{BA}-bndc suggests that with concentrated synthesis, it is possible to synthesize UiO-67-bndc and the use of 3 equiv does not affect the synthesis of the framework drastically **(**Figure 48 and Figure 49a). But the nitrogen adsorption isotherm shows 1107 m^2 g^{-1} as BET surface area, which is 10 % lower than C-0_{BA}-bndc (Figure 49b). This

suggests that some modulator is cooperated in the framework, which attributes to the lower surface area. The true composition of C-3_{BA}-bndc was observed by obtaining a ^{1}H NMR spectrum of the digested MOF, presented in Figure 50. It shows that thoroughly washed C-3_{BA}-bndc has about 10 % of benzoic acid (relative to $bndc^{2-}$) in the MOF framework. This is in accordance with the lower surface area of C-3_{BA}-bndc. Lastly, SEM images of C-0_{BA}-bndc and C-3_{BA}-bndc was taken to compare their morphology (Figure 51). Surprisingly, C-3_{BA}-bndc appears to be with very small crystal size with no specific morphology. On the other hand, C-0_{BA}-bndc shows octahedral crystals which are generally the case with UiO MOFs.

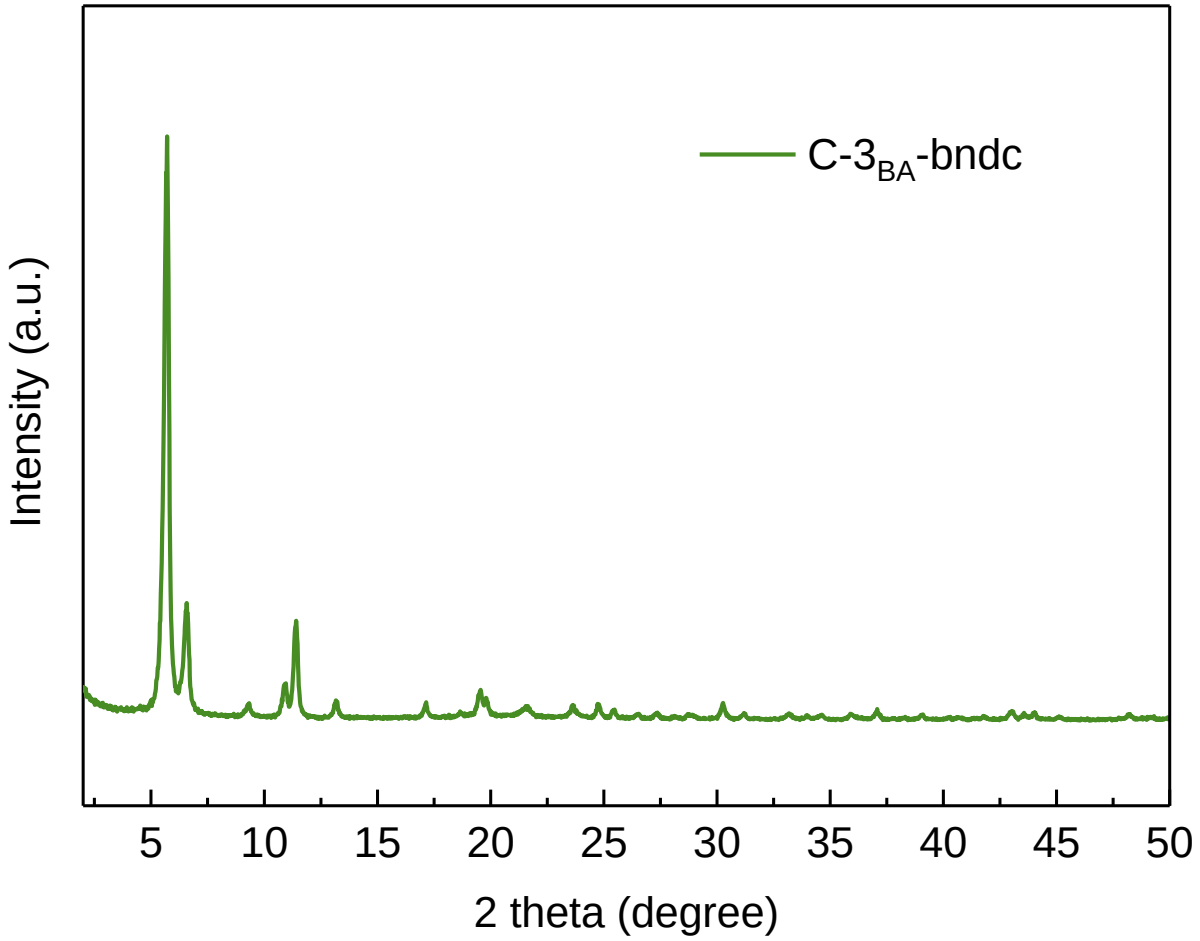

Figure 48. PXRD for C-3_{BA}-bndc.

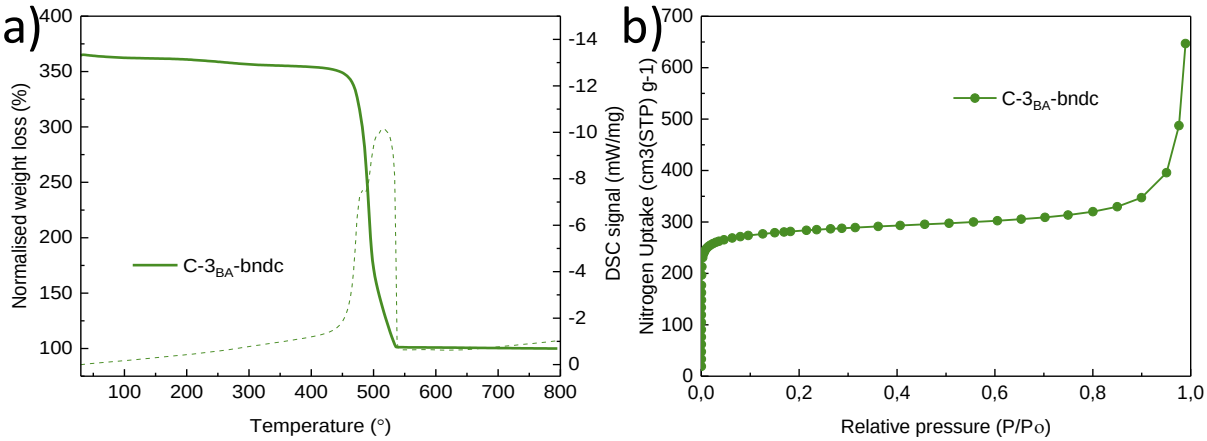

Figure 49. a) TGA-DSC signal and b) nitrogen isotherm for C-3_{BA}-bndc.

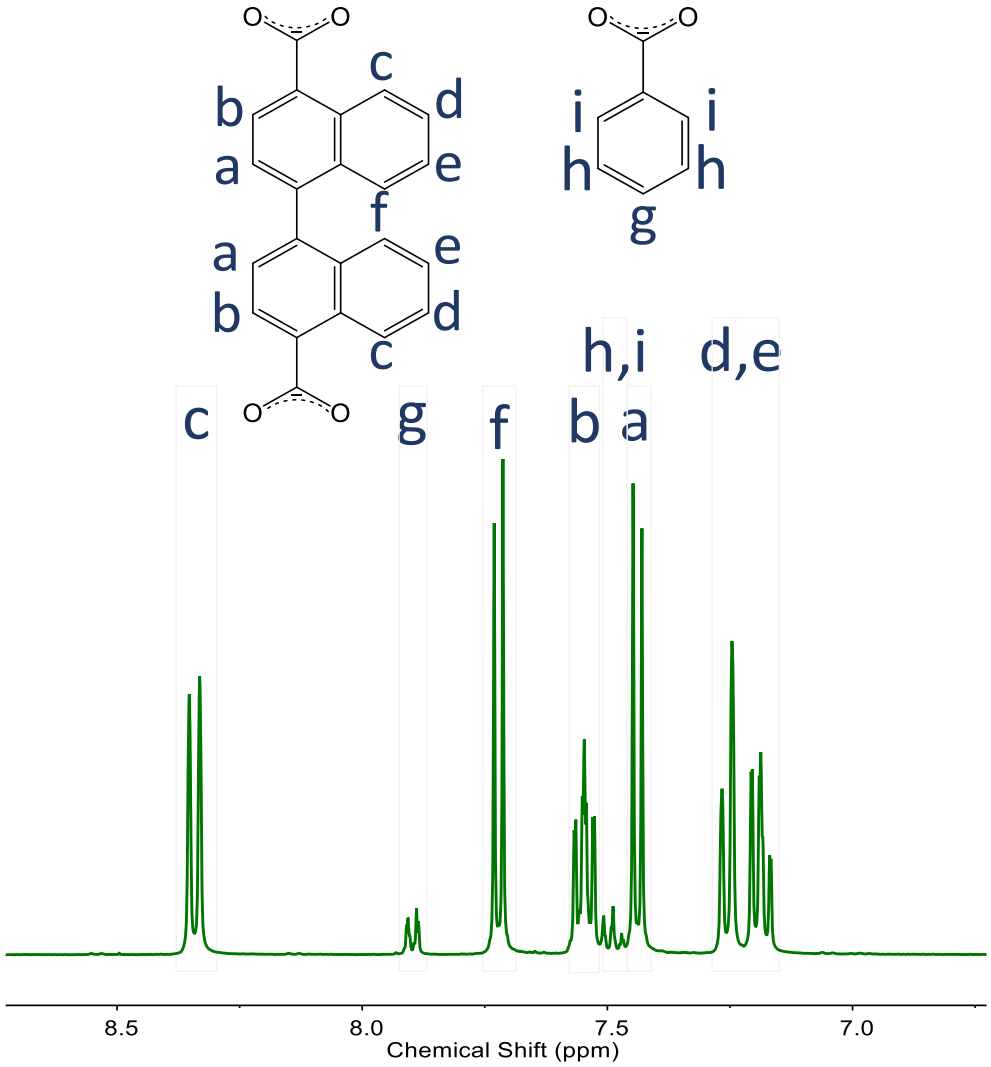

Figure 50. ^{1}H NMR of C-3_{BA}-bndc.

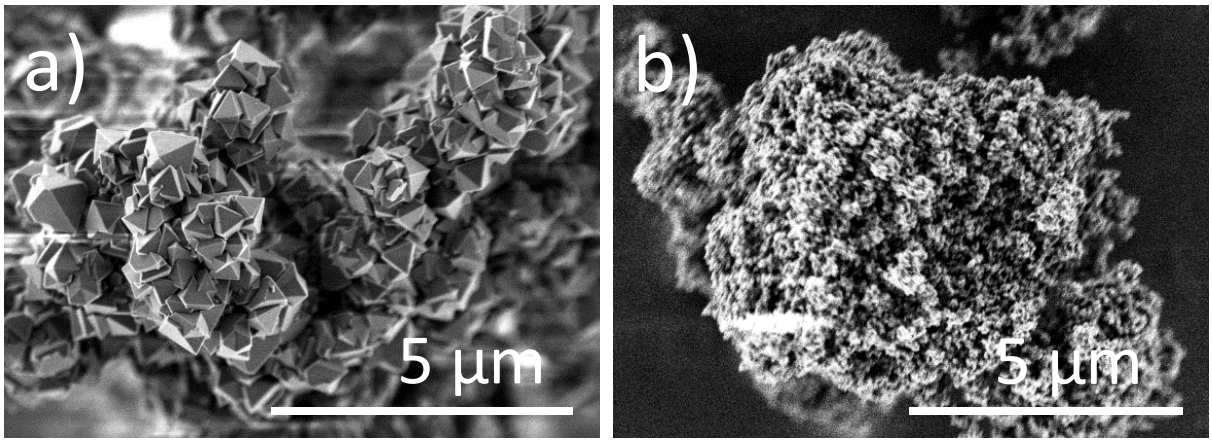

Figure 51. SEM images of a) C-0_{BA}-bndc and b) C-3_{BA}-bndc.

To sum up, the use of benzoic acid in the synthesis of UiO-67-bndc made under concentrated synthesis shows negative effect as the resultant material is with lower surface area and incorporation of 10 % benzoic acid. The crystal size is also very small and with undefined shape. This section also shows the importance of all characterization tools in order to avoid making false conclusions.

3.2.1.4. Screening of amount of water

The amount of water was screened for the synthesis of UiO-67-bndc, with Zr:water molar ratio as 1:3, 1:10, 1:40 and 1:80. As the amount of water increased, the resulting product appeared to be like a gel, which was difficult to filter. Moreover, the PXRD patterns shows that as the amount of water is increased in the synthesis, the material is seen to be amorphous with no sharp reflections. This implies that increasing amount of water does not have a positive effect of the synthesis of UiO-67-bndc (Figure 52).

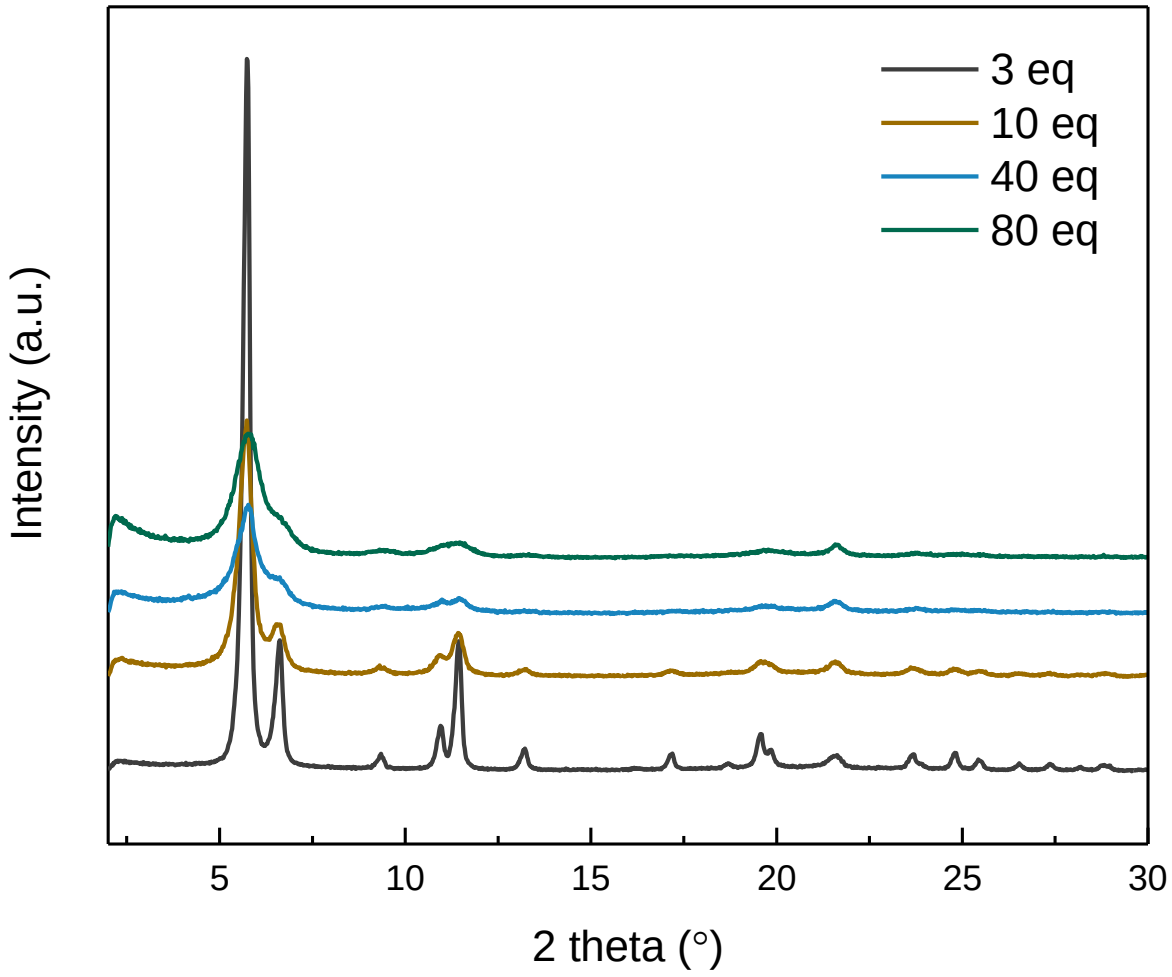

Figure 52. PXRD of screening of water for UiO-67-bndc.

Thus, the use of 3 equiv of water gives most promising material and high amount of water impedes the formation of UiO-67-bndc.

3.3. Mixed linker UiO-67

3.3.1. Synthesis of mixed linker UiO-67

The most commonly used variant of UiO-67 in heterogeneous catalysis is the one in which a fraction of the H_2bpdc linker is replaced by 2,2′-bipyridine-5,5′-dicarboxylic acid (H_2bpydc). Therefore, the applicability of concentrated protocol was tested by synthesizing such mixed-linker MOF which are useful for catalysis. The concentrated synthesis protocol was applied to UiO-67 with 10% H_2bpydc. Furthermore, with the same principle, MOFs with 10 % of other linkers like 2,2'-diamino-[1,1'-biphenyl]-4,4'-dicarboxylic acid (H_2bpdc-$(NH_2)_2$), 2-amino-

[1,1'-biphenyl]-4,4'-dicarboxylic acid (H_2bpdc-(NH_2)) and 2,2'-dihydroxy-[1,1'-biphenyl]-4,4'-dicarboxylic acid (H_2bpdc-$(OH)_2$).

The diffraction pattern of all the mixed-linker MOFs are displayed in Figure 53 and they resemble the diffraction pattern of UiO-67. This shows that substitution of 10 % of H_2bpdc with the new linker does not show any changes in the crystal structure of UiO-67. Figure 54a) displays TGA-DSC, which shows that the mixed-linker UiO-67 type MOF are as stable as the UiO-67 which is synthesized with 100 % of H_2bpdc linker. UiO-67 type mixed- linker MOFs UiO-67-bpydc$_{0.1}$, UiO-67-(bpdc-(NH_2)$_2$)$_{0.1}$, UiO-67-(bpdc-(NH_2))$_{0.1}$ and UiO-67-(bpdc-$(OH)_2$)$_{0.1}$ are stable up to 450 °C and UiO-67-bndc type (UiO-67-bndc$_{0.9}$-bpydc$_{0.1}$) is stable up to 400 °C, before the framework collapses. This implies that 10 % substitution of linker does not show major thermal stability changes in these MOFs. The nitrogen isotherms of all the mixed linker MOFs is shown in Figure 54b), which is used to calculate their surface area, reported in Table 16. The surface area of mixed linker UiO-67 type MOF is in the range of 2300-2500 m^2g^{-1} and that of UiO-67-bndc type is around 1500 m^2g^{-1}. These surface area are very close to their parent MOF which not only shows that these materials are very porous but also that they behave similar to their parent MOF.

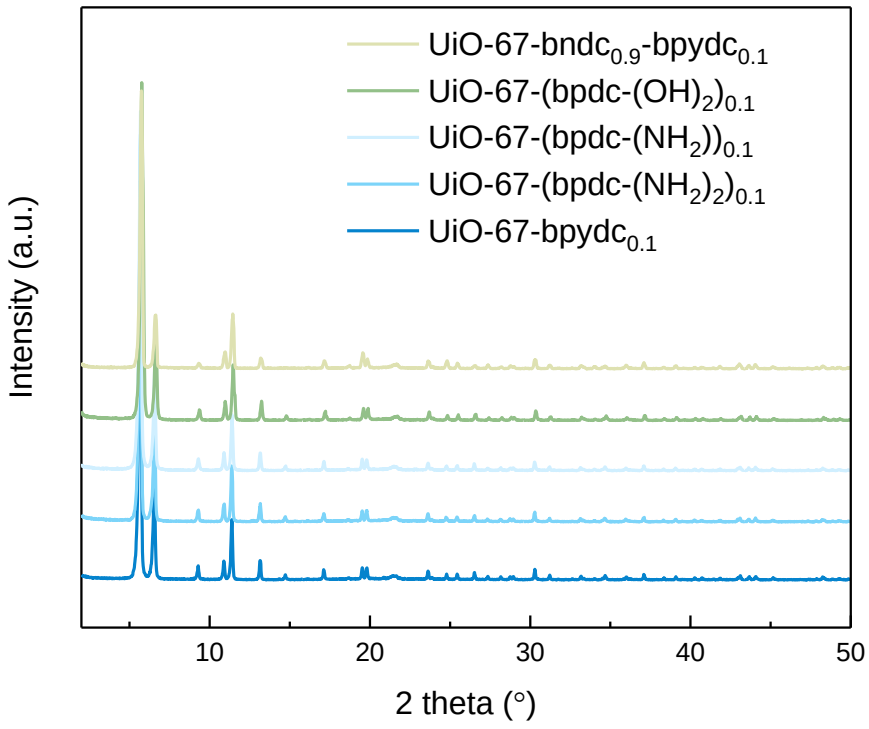

Figure 53. XRD diffraction pattern for mixed-linker MOFs.

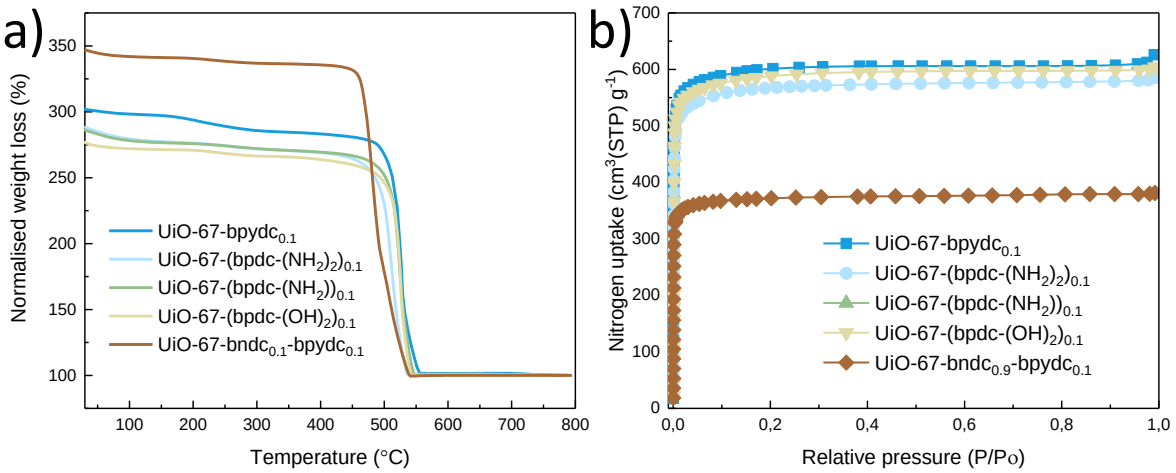

Figure 54. a) TGA-DSC and b) nitrogen isotherms at 77 K for mixed-linker MOFs.

Table 16. BET surface area and ^{1}H NMR results for mixed-linker MOFs (molar percentage given with respect to total linkers (x linker and y linker)).

#	MOF sample	Surface area [m^2 g^{-1}]	Pore volume [cm^3g^{-1}]	y-linker (%)	benzoate (%)	formate (%)
1	UiO-67-bpydc$_{0.1}$	2454	564	7.0	1.7	2.0
2	UiO-67-(bpdc(NH$_2$)$_2$)$_{0.1}$	2305	529	6.9	2.7	10
3	UiO-67-(bpdc(NH$_2$))$_{0.1}$	-	-	5.7	1.3	6.0
4	UiO-67-(bpdc(OH)$_2$)$_{0.1}$	2405	552	5.1	6.7*	3
5	UiO-67-bndc$_{0.9}$-bpydc$_{0.1}$	1501	345	5.6	NA	0

*This synthesis was performed at a 10 gram scale, so the discrepancies may have occur due to scale up.

To gain knowledge about the true composition of these mixed-linker MOFs, they were digested in 1M NaOH-D_2O solution. This solution was used to record the ^{1}H NMR which is shown in Figure 55. The ^{1}H NMR spectra was used to calculate the composition of the materials, reported in Table 16. The aim was to incorporate 10 % of functionalized linkers in the MOF, and ^{1}H NMR shows that they are in the range of 5 to 8 %, which is acceptable. ^{1}H NMR also shows the presence of small percentages of benzoic acid and formic acid, which might be the capping sites of missing-linker defects. The SEM images of the mixed-linker MOFs shows octahedral crystals supporting the successful synthesis of these materials (Figure 56).

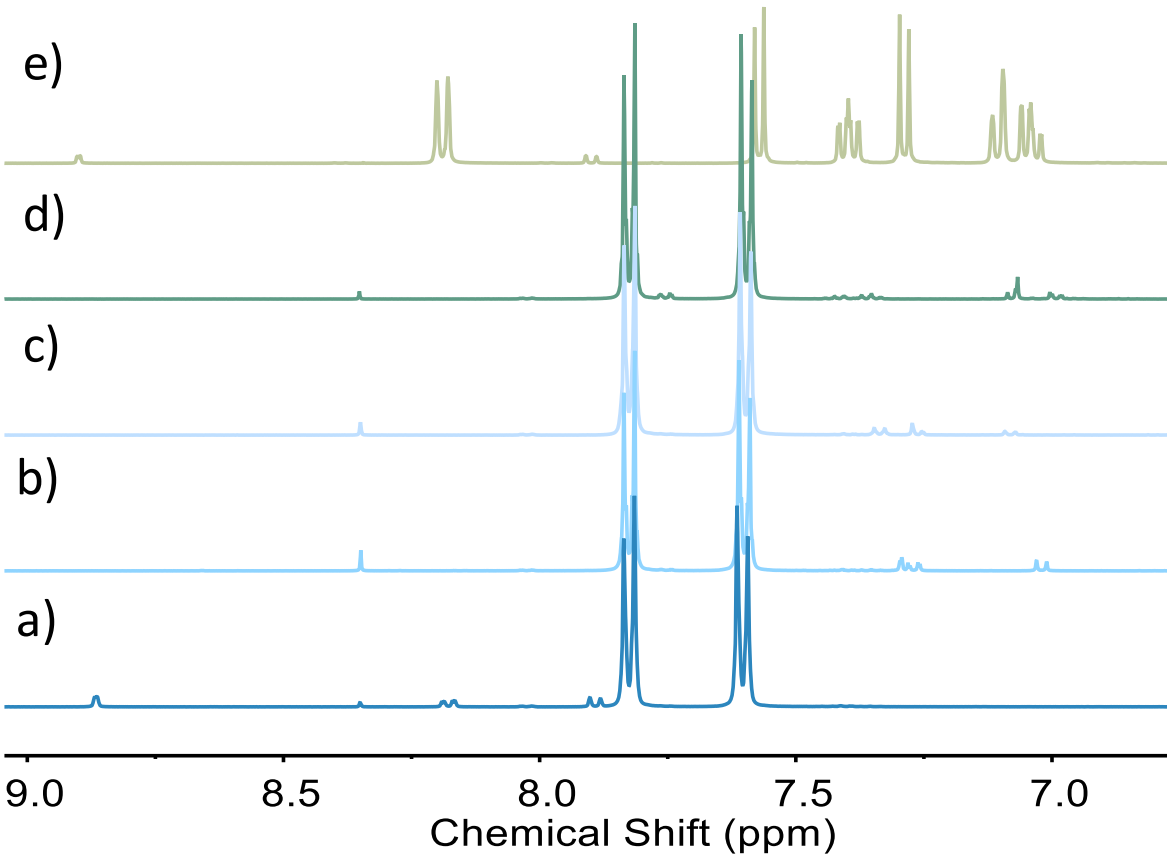

Figure 55. ^{1}H NMR of mixed-linker MOFs where a) UiO-67-bpydc$_{0.1}$, b) UiO-67-(bpdc-(NH$_2$)$_2$)$_{0.1}$, c) UiO-67-(bpdc-(NH$_2$))$_{0.1}$, d) UiO-67-(bpdc-(OH)$_2$)$_{0.1}$ and e) UiO-67-bndc$_{0.9}$-bpydc$_{0.1}$.

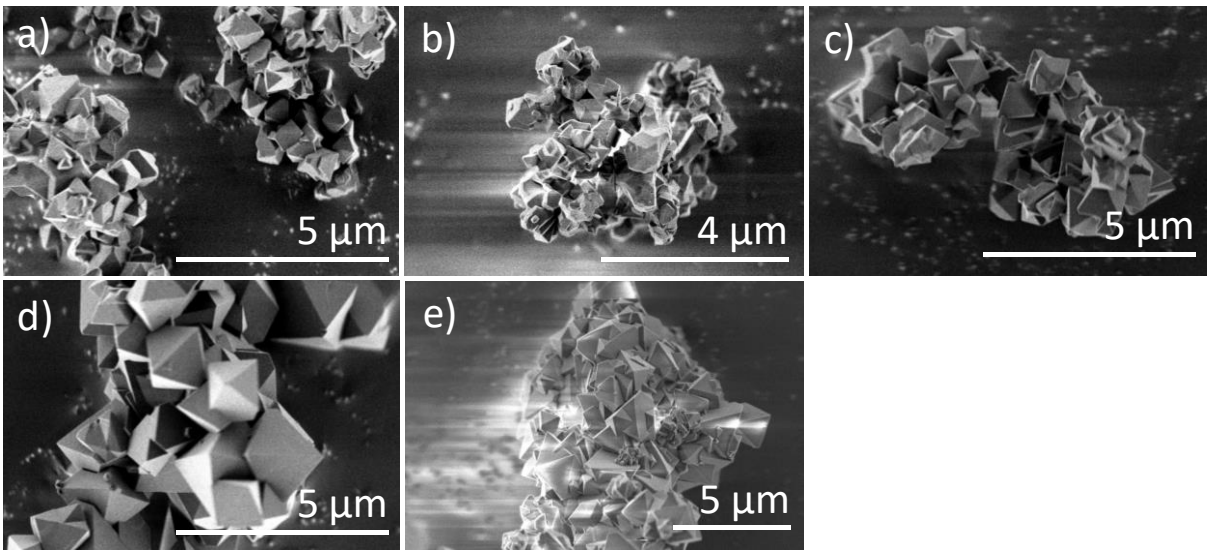

Figure 56. SEM images of mixed-linker MOFs where a) UiO-67-bpydc$_{0.1}$, b) UiO-67-(bpdc-(NH$_2$)$_2$)$_{0.1}$, c) UiO-67-(bpdc-(NH$_2$))$_{0.1}$, d) UiO-67-(bpdc-(OH)$_2$)$_{0.1}$ and e) UiO-67-bndc$_{0.9}$-bpydc$_{0.1}$.

Therefore, various mixed-linker UiO-67 type MOFs were- successfully synthesized with 10 % of functionalized biphenyl linkers. All the MOFs were characterized well and the data shows that these MOFs are as stable and porous as the parent MOF. True composition of the MOFs was determined by

1H NMR that shows presence of 5 to 8 % of these linkers with small percentage of benzoic acid and formic acid.

3.3.2. Metal incorporation in UiO-67 type MOFs

Two frequently reported methods of single site inclusion on linkers are 1) involving a linker that also contains a coordination site, e.g. 2,2'-bipyridine dicarboxylate[66, 112, 137] and 2) postsynthetical construction of such a site, e.g. condensation of an aldehyde onto free primary amine groups in the MOF.[124, 138-139] For the former approach, UiO-67 is commonly used, whereas for the latter, UiO-66 and MIL-101 are common starting points. The biphenyl moiety of UiO-67 provides an anchoring point for functional groups, for example allowing the construction of a tetradentate analogue of the frequently reported imine coordination sites. Its higher porosity also allows reactants and products of a catalyzed reaction to diffuse more freely, with less steric limitations.

To construct the tetradentate Schiff-base complex inside the MOF, a stepwise post-synthetic approach was used. Characterizing mixed-linker MOFs is very challenging due to the physical immobilization of the complex of interest which prevents the use of NMR and MS, and the dilution and disorder of the incorporated complexes which introduces uncertainty in diffraction-based methods. Stepwise reactions are useful for the synthesis of such complexes incorporated in MOFs because it allows the characterization of the intermediate stages. The size of the Schiff-base complex prohibits the use of linker exchange methods, and the imine moiety would not remain intact through the harsh conditions of MOF synthesis.[75]

UiO-67-bpdc-$(NH_2)_2$ (referred as **MOF**) was synthesized using 10 % of 2,2'-diaminobiphenyl-4,4'-dicarboxylic acid (H_2bpdc-$(NH_2)_2$) and 90 % of biphenyl-4,4'-dicarboxylic acid (H_2bpdc). This **MOF** was further treated with salicylaldehyde (2-hydroxybenzaldehyde) to form a Schiff base (imine) complex (**MOF-sal**). The MOF was further exposed to solutions of Co, Ni, Cu and Pd salts (Figure 14).

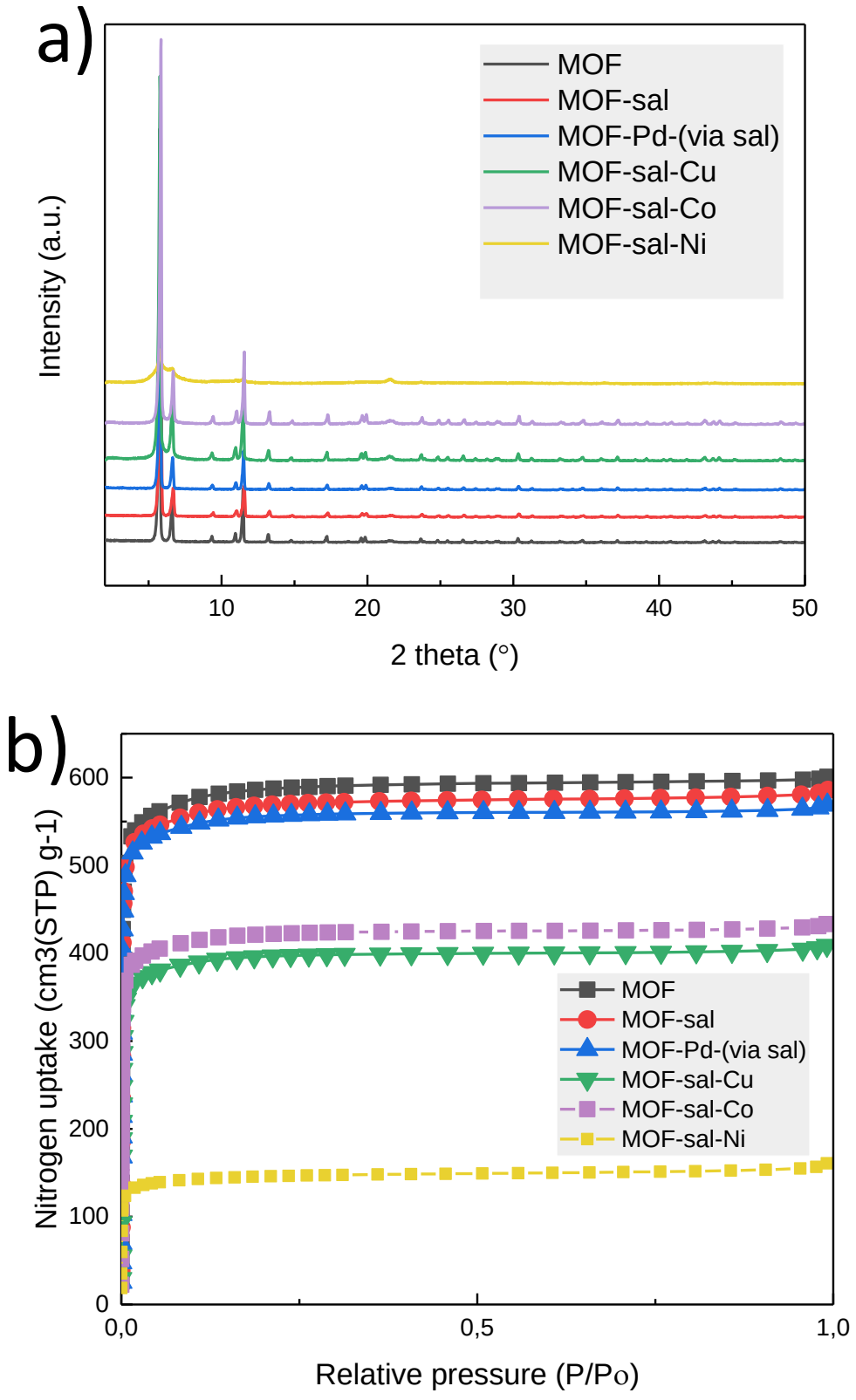

Figure 57. a) PXRD pattern and b) nitrogen adsorption isotherm of MOF (UiO-67-(bpdc-$(NH_2)_2)_{0.1}$), MOF-sal (UiO-67-(bpdc-$(NH_2)_2)_{0.1}$) with salicylaldehyde), MOF-Pd-(via sal), MOF-sal-Cu, MOF-sal-Co and MOF-sal-Ni.

The PXRD pattern of **MOF** and its derivatives (except MOF-sal-Ni) shows that the crystallinity of the MOF framework is intact throughout the modification treatment (Figure 57). MOF-sal-Ni clearly shows the loss of crystallinity indicating the collapse of MOF framework. The BET surface area was calculated from nitrogen adsorption isotherms is presented in Table 17 and Figure 57. The surface area of **MOF** (2372 m^2g^{-1}), slightly decreases after its modification with salicylaldehyde and bis(acetonitrile)dichloropalladium(II) (**MOF-sal** and **MOF-Pd-(via sal)**) indicating the partial occupancy of the pores of the MOF. Surprisingly, the surface area of **MOF-sal** treated with acetate salts of Cu, Co and Ni were slightly different. **MOF-sal-Cu** (1620 m^2g^{-1}) and **MOF-sal-Co** (1714 m^2g^{-1}) has significantly decreased, which is 27-32 % decrease with respect to the **MOF**. This suggests that the pores of the **MOF** are partially blocked by a larger complex/other species. The surface area of MOF-sal-Ni (579 m^2g^{-1}) has drastically decreased confirming the collapse of framework as suggested by PXRD pattern.

Table 17. Surface area and pore volume of MOF and its derivative, calculated from nitrogen adsorption isotherm.

Entry	Sample	Surface area [m^2/g]	Pore volume [cm^3/g]
1	**MOF**	2372	545
2	**MOF-sal**	2294	527
3	**MOF-Pd-(via sal)**	2276	523
4	**MOF-sal-Cu**	1616	371
5	**MOF-sal-Co**	1714	394
6	**MOF-sal-Ni**	579	133

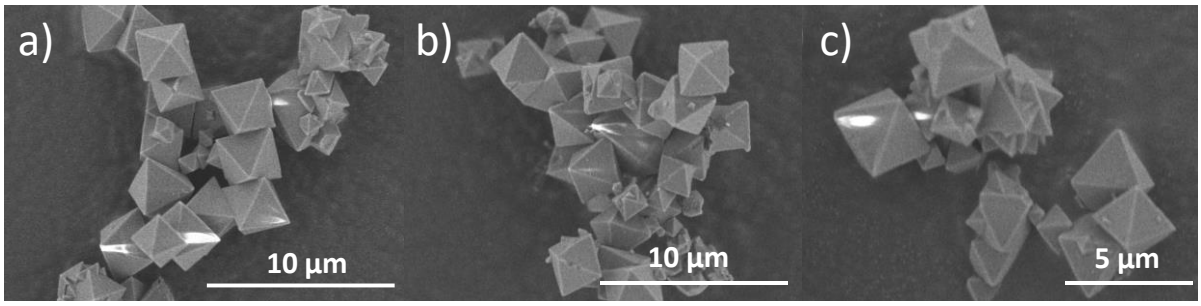

Figure 58. SEM images of a) MOF, b) MOF-sal and c) MOF-Pd-(via sal).

Furthermore, SEM images of **MOF** and its derivatives depict octahedral crystals with well-defined edges, indicating that the crystals are intact throughout the modification treatment (Figure 58). These results are also in agreement with the PXRD results.

The NMR calculation shows the presence of 6 % of diamino linker, 5 % of salicylaldehyde and 4-5 % formate in all the samples, with respect to $bpdc^{2-}$ linker (Figure 59, Table A5). The MOF

contains large amounts of benzoate (around 12 %) which decreases (to 6 %) after modifying it with salicylaldehyde, probably due to extensive washing and activation at 200 °C prior to sample preparation.

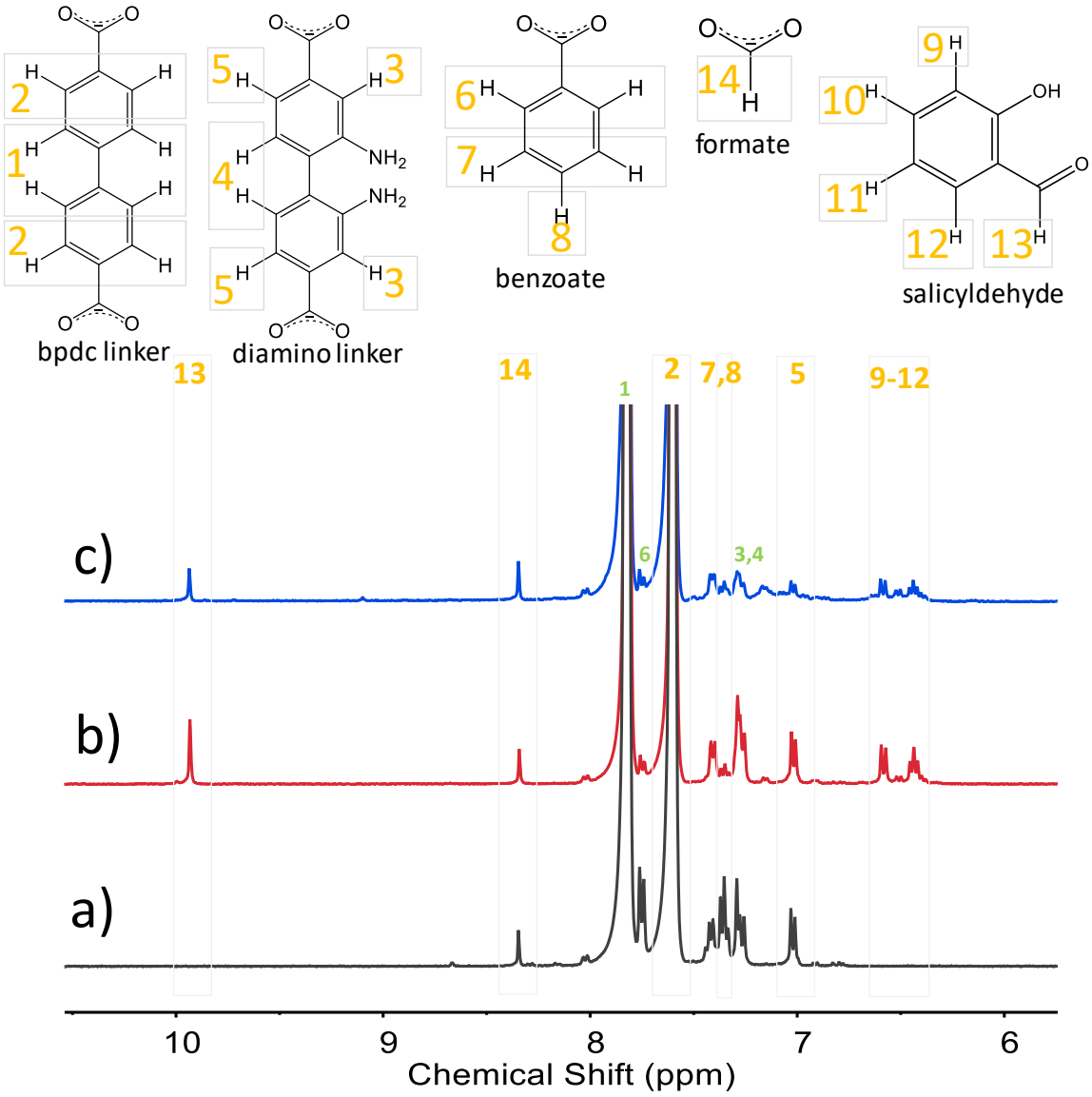

Figure 59. NMR spectra of a) MOF, b) MOF-sal and c) MOF-Pd-(via sal). The peaks marked in the grey box with yellow labels are used for the calculation of relative organic content. The peaks marked with green labels are merging with other peak, not suitable for calculations.

Figure 60 presents the FT-IR spectra of all the samples. UiO-67(bpdc-$(NH_2)_2)_{0.1}$ shows a double peak arising at 3480 and 3380 cm^{-1} (black curve, Figure 60), due to the symmetric and antisymmetric vibration of the NH_2 groups attached to the aromatic linkers, hence confirming the incorporation of H_2bpdc-$(NH_2)_2$ linker. These ν(NH) peaks disappear to a great extent in **MOF-sal** (red curve, Figure 60). This strongly suggests the successful condensation reaction of amine functional group of H_2bpdc-$(NH_2)_2$ linker of the **MOF** with the salicylaldehyde.

Interestingly the peak at 3480 cm^{-1} for **MOF-Pd-(via sal)** does not disappear suggesting the presence of $–NH_2$ groups in the MOF. Furthermore, the peaks arising from imine functional group are expected at 1630 cm^{-1} but unfortunately that region is covered by the peaks form the MOF framework (Figure A14).

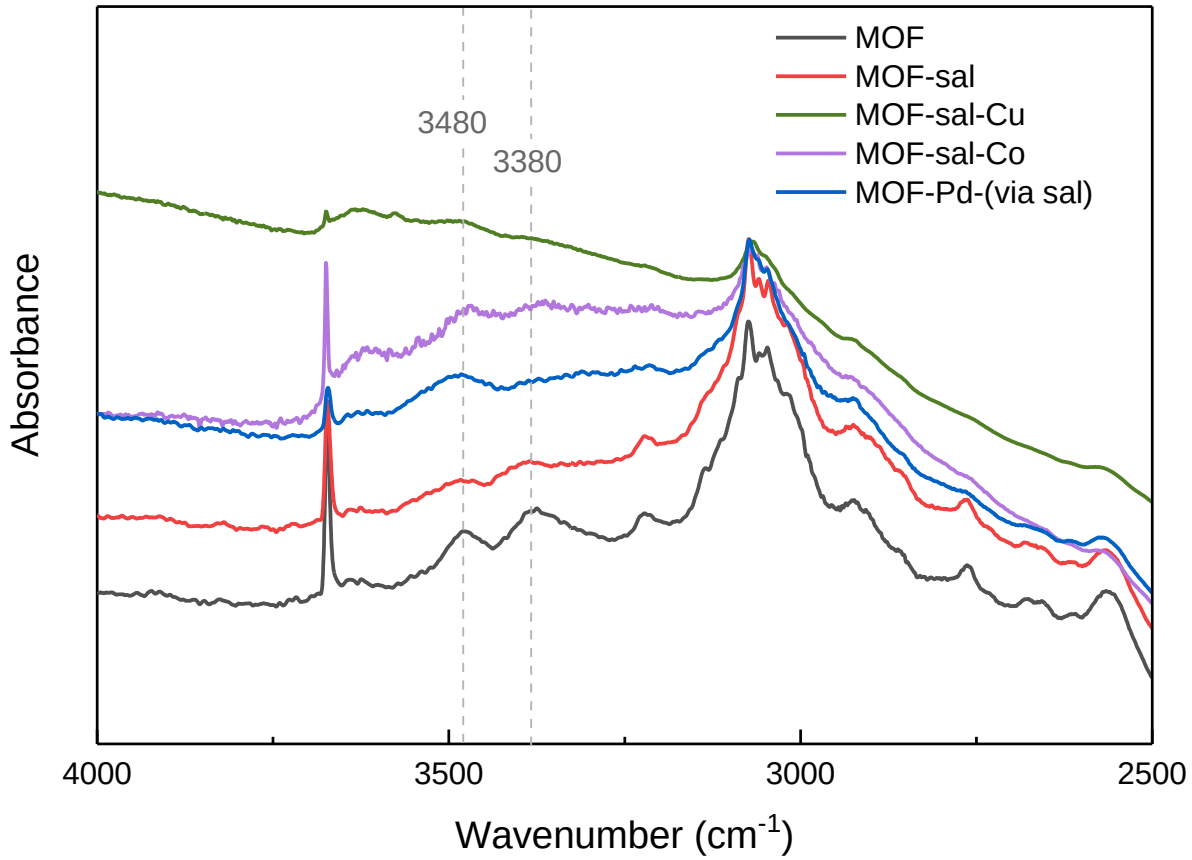

Figure 60. FT-IR spectra of MOF (black) and its derivatives, MOF-sal (red), MOF-sal-Cu (green), MOF-sal-Co (violet) and MOF-Pd-(via sal) (blue).

The metal to Zr molar ratios were estimated using Energy-dispersive X-ray spectroscopy and the results are shown in Table 18. The average Pd/Zr ratio was estimated 0.047 and Cu/Zr as 0.080 atomic percent in MOF-sal-Pd and MOF-sal-Cu, respectively whereas in case of MOF-sal-Co the Co/Zr ratio is very low, at 0.013. Interestingly, **MOF-Pd-(via sal)** contains a significant amount of chloride which indicates the presence of a chloride based complex in the MOFs. Furthermore, **MOF-Pd** was synthesized as a control reaction by treating **MOF** directly with bis(acetonitrile)dichloropalladium(II), Figure A15 .The peak for 3480 cm^{-1} in the FT-IR does not disappears and the Pd/Zr ratio was also estimated as 0.047 (Figure 61 and Figure A 16). The experiments shows similar results as in the case of **MOF-Pd-(via sal),** indicating the presence of $PdCl_2$-bpdc$(NH_2)_2$ system in both the cases.

Table 18. Composition of MOF-Pd-(via sal), MOF-sal-Cu and MOF-sal-Co, determined using EDS, all the values are given in atomic percentage.

Catalyst	Zr	C	O	N	M	Cl	M/Zr
MOF-Pd-(via sal)	4.39	66.36	26.90	2.26	0.21	0.30	0.047
MOF-Pd	5.49	64.64	26.95	2.12	0.25	0.50	0.046
MOF-sal-Cu	5.61	64.75	27.11	2.06	0.44	0.01	0.080
MOF-sal-Co	4.81	65.73	27.58	1.78	0.07	0.02	0.013

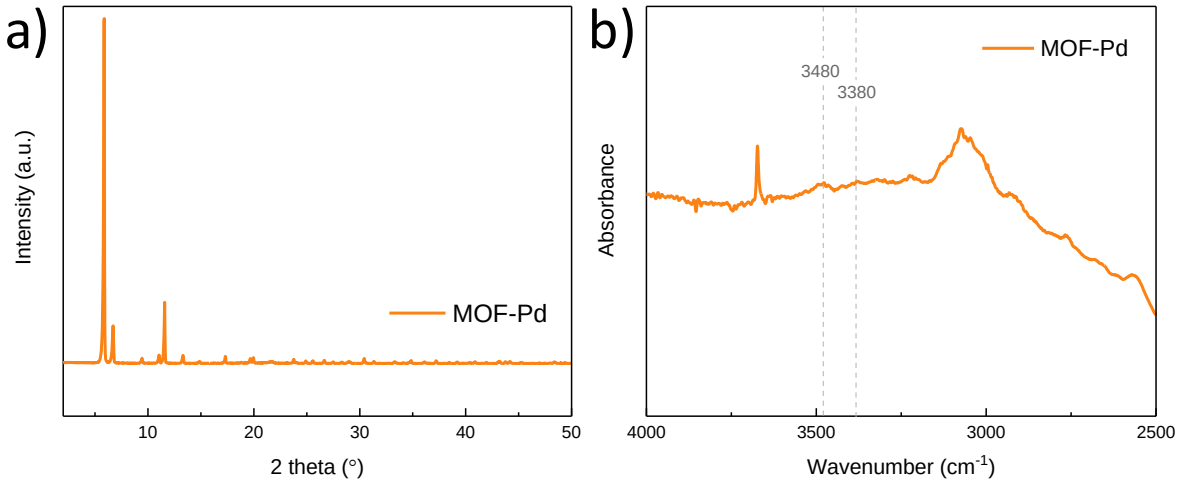

Figure 61. a) PXRD and a) FT-IR pattern of MOF-sal.

Moreover, control reactions were performed by making the isolated complexes with the dimethyl-ester of the diamine linker (Figure 15). In the case of Pd, when the linker was reacted with bis(acetonitrile)dichloropalladium(II), the imine bond was cleaved, clearly indicated by the two broad peaks by hydrogens of $–NH_2$ groups in the 1H NMR spectrum (Figure 62). The 1H NMR spectra of the starting linker is also presented for comparison. The single crystal analysis of the thus obtained crystals confirmed the synthesis of $PdCl_2$(diaminobiphenyl diester) (Figure A17). The reaction for the synthesis of the Pd-isolated complex was done under same condition as for the synthesis of the metal incorporation MOF-sal.

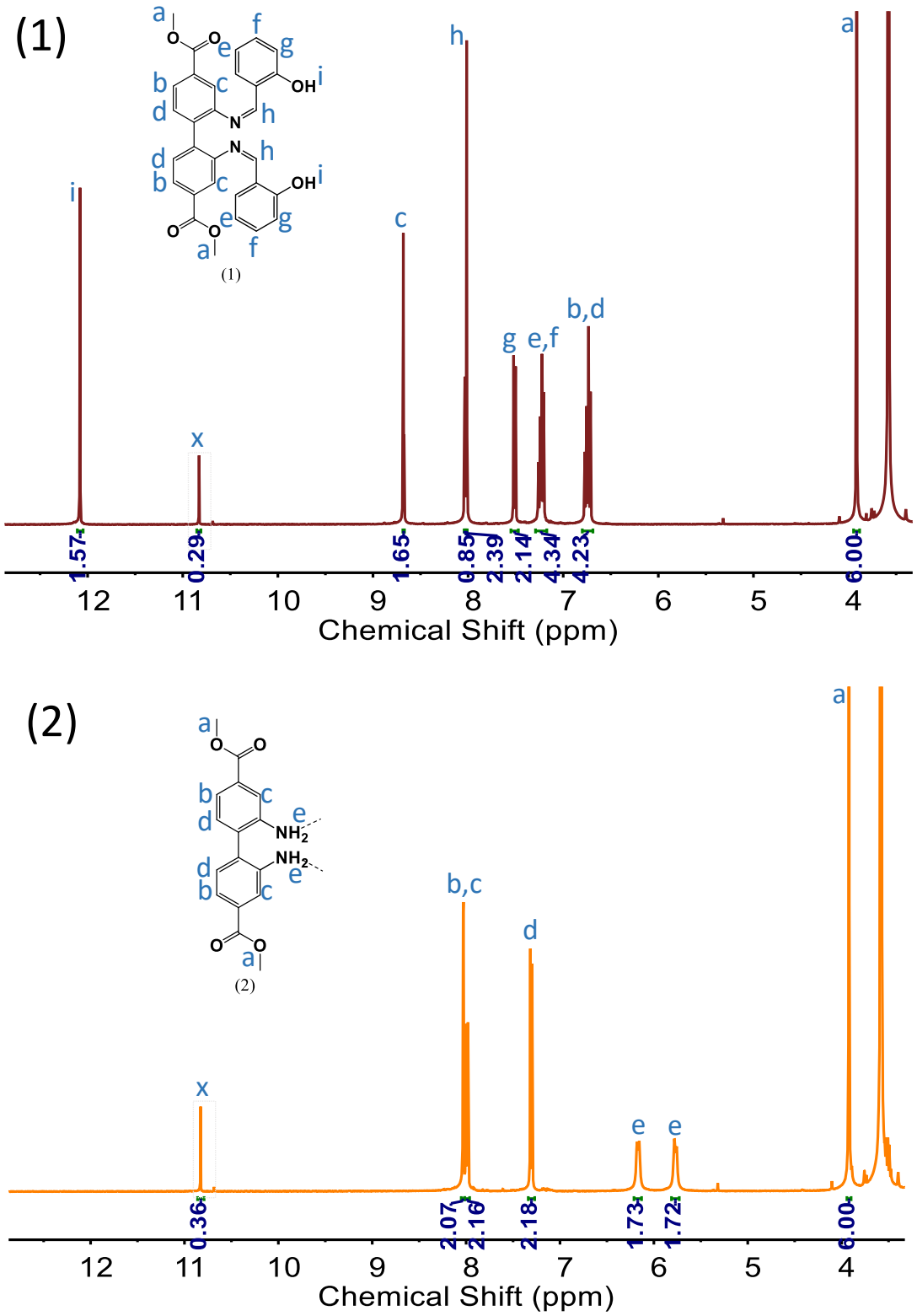

Figure 62. NMR spectra of the (1) dimethyl-ester of the diamine linker and (2) $PdCl_2$(diaminobiphenyl diester) complex in tetrahydrofuran-d_8 (Figure 15), where x is the impurity from the contaminated solvent.

Therefore, a tetradentate catalyst has been designed and incorporated into a MOF by stepwise post-synthetic modification. In general, this example of metal incorporation shows the versatility of UiO-67 MOFs. This ligand provides numerous opportunities for exploration of new catalysts, since its steric and electronic properties are easily tuned by changing the aldehyde reagent, and it can incorporate multiple metals.

4. Conclusions

4.1. Results

An extensive work on UiO-67 has been performed which gives a deep understanding of the material.

- The amount of missing-linkers defects in UiO-67 can be controlled.
  - A near-defect free UiO-67 can be obtained with the use of Zr:H_2bpdc:H_2O:BA:DMF = 1:1:3:3:50 (concentrated synthesis) at 130 °C.
  - If desired, UiO-67 with missing-linker defects can be obtained with the use of Zr:H_2bpdc:H_2O:BA:DMF = 1:1:3:9:300 (dilute synthesis) at 130 °C.

- The concentration for benzoate in the product increases along with the yield as the reaction progressed, indicating that linker incorporation in the MOF follows the waning concentration of linker in the mother liquor.

- Concentrated synthesis method is further tuned and the effect of amount of water is defined
  - If critically dry conditions, less than 5 equiv of water in the synthesis lead to a combination of two phase i.e. UiO-67 and MIL-140C MOF.
  - The presence of MIL-140C decrease with the increase of water concentration in the synthesis of the material, hence showing that water plays a role as a structural directing agent.
  - Missing-linker defects are increased with the increase in water as an additive in the synthesis, at given condition Zr:H_2bpdc:BA:DMF = 1:1:3:50 and water (3 to 9 molar equiv)
- Under right conditions, where water is present in large excess, different phases such as **hcp** and hexagonal nanosheets can be observed where the inorganic nodes are different than the usual **fcu** phase, therefore potential catalytic site.

- The UiO-67 material obtained with concentrated synthesis is thermally stable up to 350 °C for 24 hours in air and gradually starts to collapse above 350 °C.

- The synthesis of UiO-67-bndc is studied in detail (where [1,1'-binaphthalene]-4,4'-dicarboxylic acid linker is used instead of H_2bpdc).
    - The concentrated synthesis protocol suits the synthesis of UiO-67-bndc with tuning it slightly further, therefore, Zr:H_2bpdc:H_2O:BA:DMF = 1:1:3:0:50.
    - The best material is obtained in the absence of modulator and the use of low amount of benzoic acid (3 equiv) yield very poor quality material.
    - Moreover, it is best to use 3 equiv of water and increased amount of water shows no MOF formation.
    - Unlike UiO-67, no changes in the phase of the material was observed at the given conditions.

- Concentrated synthesis was employed in the synthesis of mixed-linker UiO-67 type MOFs where 10 % of the H_2bpdc were partially replaced by functionalized biphenyl linker
    - It shows similar results as for UiO-67 and the samples show the presence of very low missing-linker defects
    - The functionalized biphenyl linker is present 6-7 % in the synthesized mixed linker MOF

- This deep understanding of UiO-67-type MOFs is used for the synthesis of metal-based MOF catalysts.

4.2. Suggestion for further work

The reaction conditions for the synthesis of UiO-67 has been studied in detail where the effect of concentrations of the reagents are shown to display important role in the outcome of the material. The effect of different concentration of DMF, benzoic acid and water has been investigated. These results were employed for the synthesis of various UiO-67 type MOF and later used for the synthesis of metal based MOF catalysts. Here are few suggestions for further work related to this thesis:

- The concentrated synthesis provides high yield with low amounts of reagents which makes it suitable for upscaling. Some of the preliminary upscaling of the concentrated protocol is done but the synthesized material does not always resemble the small-scale synthesis results. Therefore, to increase the applicability of the suggested protocol, its application for scaling up could be investigated in detail.
- The effect of amount of water is studied in two ways, 1) effect of low amount of water (3 to 9 equiv) on UiO-67-bpydc$_{0.1}$ and 2) large excess amount of water (38 equiv) on UiO-67. In order to see the effect of amount of water in the synthesis, one series of UiO-67 samples with varying amount of water (0 to 60 equiv or so) should be carefully done for the concentrated synthesis. The author envisions the synthesis of hcp and other phases by increasing large excess of water in the established concentrated protocol.
- The μ_2-OH and μ_3-OH sites in the hcp phase Zr-H_2bpdc MOF are fascinating for exploring them for metal insertions. The author anticipates a great potential of this MOF for catalysis.
- A lot of work has been done for the development of synthesis of UiO-67-bndc where the results shows that the reproducible, highly stable material is obtained without the use of modulator. This is a great achievement in author's opinion as UiO-67-bndc has smaller pore than UiO-67 and has no modulator, which can act as capping agent of the open Zr sites, therefore is an interesting candidate to see confinement effects for testing it as a catalyst.
- Preliminary investigation of the effect of water in the synthesis of UiO-67-bndc was done but further work is needed to tune the synthesis condition and hopefully synthesize hcp and hexagonal phase of UiO-67-bndc.
- Thermal stability of UiO-67 was studied in detail but a lot of work could be done for improving the water stability of UiO-67. The application of UiO-67 are sometimes limited due to its lack of stability in water, thus alternative MOFs are preferred over UiO-67.
- The development of metal based catalysts has always been interesting but the study related to synthesis of Schiff base in UiO-67 MOFs needs more work. It is difficult to comment in detail about the local environment of the metals incorporated in **MOF-sal**. Therefore, further study is needed to develop such complex materials in the MOFs and characterize them well.

References

1. Batten, S.; Champness, N.; Chen, X.-M.; García-Martínez, J.; Kitagawa, S.; Öhrström, L.; Keeffe, M.; Suh, M.; Reedijk, J., Terminology of metal–organic frameworks and coordination polymers (IUPAC Recommendations 2013)*. *Pure and Applied Chemistry* **2013,** *85*, 1715-1724.
2. Furukawa, H.; Cordova, K. E.; O'Keeffe, M.; Yaghi, O. M., The Chemistry and Applications of Metal-Organic Frameworks. *Science* **2013,** *341* (6149), 1230444.
3. O'Keeffe, M., Design of MOFs and intellectual content in reticular chemistry: a personal view. *Chemical Society Reviews* **2009,** *38* (5), 1215-1217.
4. Eddaoudi, M.; Li, H.; Yaghi, O. M., Highly Porous and Stable Metal−Organic Frameworks: Structure Design and Sorption Properties. *Journal of the American Chemical Society* **2000,** *122* (7), 1391-1397.
5. Li, H.; Eddaoudi, M.; Groy, T. L.; Yaghi, O. M., Establishing Microporosity in Open Metal−Organic Frameworks: Gas Sorption Isotherms for Zn(BDC) (BDC = 1,4-Benzenedicarboxylate). *Journal of the American Chemical Society* **1998,** *120* (33), 8571-8572.
6. Eddaoudi, M.; Kim, J.; Rosi, N.; Vodak, D.; Wachter, J.; Keeffe, M.; Yaghi, O. M., Systematic Design of Pore Size and Functionality in Isoreticular MOFs and Their Application in Methane Storage. *Science* **2002,** *295* (5554), 469.
7. Li, H.; Eddaoudi, M.; O'Keeffe, M.; Yaghi, O. M., Design and synthesis of an exceptionally stable and highly porous metal-organic framework. *Nature* **1999,** *402* (6759), 276-279.
8. Rowsell, J. L. C.; Yaghi, O. M., Effects of Functionalization, Catenation, and Variation of the Metal Oxide and Organic Linking Units on the Low-Pressure Hydrogen Adsorption Properties of Metal−Organic Frameworks. *Journal of the American Chemical Society* **2006,** *128* (4), 1304-1315.
9. Horcajada, P.; Serre, C.; Vallet-Regí, M.; Sebban, M.; Taulelle, F.; Férey, G., Metal–Organic Frameworks as Efficient Materials for Drug Delivery. *Angewandte Chemie International Edition* **2006,** *45* (36), 5974-5978.
10. Rosi, N. L.; Kim, J.; Eddaoudi, M.; Chen, B.; O'Keeffe, M.; Yaghi, O. M., Rod Packings and Metal−Organic Frameworks Constructed from Rod-Shaped Secondary Building Units. *Journal of the American Chemical Society* **2005,** *127* (5), 1504-1518.
11. Cavka, J. H.; Jakobsen, S.; Olsbye, U.; Guillou, N.; Lamberti, C.; Bordiga, S.; Lillerud, K. P., A New Zirconium Inorganic Building Brick Forming Metal Organic Frameworks with Exceptional Stability. *Journal of the American Chemical Society* **2008,** *130* (42), 13850-13851.
12. Puchberger, M.; Kogler, F. R.; Jupa, M.; Gross, S.; Fric, H.; Kickelbick, G.; Schubert, U., Can the Clusters Zr6O4(OH)4(OOCR)12 and [Zr6O4(OH)4(OOCR)12]2 Be Converted into Each Other? *European Journal of Inorganic Chemistry* **2006,** *2006* (16), 3283-3293.
13. Furukawa, H.; Cordova, K. E.; O'Keeffe, M.; Yaghi, O. M., The Chemistry and Applications of Metal-Organic Frameworks. *Science* **2013,** *341* (6149).
14. Eddaoudi, M.; Kim, J.; Rosi, N.; Vodak, D.; Wachter, J.; O'Keeffe, M.; Yaghi, O. M., Systematic Design of Pore Size and Functionality in Isoreticular MOFs and Their Application in Methane Storage. *Science* **2002,** *295* (5554), 469-472.
15. Yaghi, O. M.; O'Keeffe, M.; Ockwig, N. W.; Chae, H. K.; Eddaoudi, M.; Kim, J., Reticular synthesis and the design of new materials. *Nature* **2003,** *423* (6941), 705-714.
16. Ma, S.; Zhou, H.-C., Gas storage in porous metal–organic frameworks for clean energy applications. *Chemical Communications* **2010,** *46* (1), 44-53.
17. Mason, J. A.; Veenstra, M.; Long, J. R., Evaluating metal–organic frameworks for natural gas storage. *Chemical Science* **2014,** *5* (1), 32-51.
18. Van de Voorde, B.; Bueken, B.; Denayer, J.; De Vos, D., Adsorptive separation on metal–organic frameworks in the liquid phase. *Chemical Society Reviews* **2014,** *43* (16), 5766-5788.

19. Li, J.-R.; Kuppler, R. J.; Zhou, H.-C., Selective gas adsorption and separation in metal–organic frameworks. *Chemical Society Reviews* **2009,** *38* (5), 1477-1504.
20. Lee, J.; Farha, O. K.; Roberts, J.; Scheidt, K. A.; Nguyen, S. T.; Hupp, J. T., Metal–organic framework materials as catalysts. *Chemical Society Reviews* **2009,** *38* (5), 1450-1459.
21. Furukawa, H.; Gándara, F.; Zhang, Y.-B.; Jiang, J.; Queen, W. L.; Hudson, M. R.; Yaghi, O. M., Water Adsorption in Porous Metal–Organic Frameworks and Related Materials. *Journal of the American Chemical Society* **2014,** *136* (11), 4369-4381.
22. Li, Z.-Q.; Yang, J.-C.; Sui, K.-W.; Yin, N., Facile synthesis of metal-organic framework MOF-808 for arsenic removal. *Materials Letters* **2015,** *160*, 412-414.
23. Trickett, C. A.; Helal, A.; Al-Maythalony, B. A.; Yamani, Z. H.; Cordova, K. E.; Yaghi, O. M., The chemistry of metal–organic frameworks for CO2 capture, regeneration and conversion. *Nature Reviews Materials* **2017,** *2* (8), 17045.
24. Murray, L. J.; Dincă, M.; Long, J. R., Hydrogen storage in metal–organic frameworks. *Chemical Society Reviews* **2009,** *38* (5), 1294-1314.
25. Frameworks for commercial success. *Nature Chemistry* **2016,** *8* (11), 987-987.
26. Opelt, S.; Türk, S.; Dietzsch, E.; Henschel, A.; Kaskel, S.; Klemm, E., Preparation of palladium supported on MOF-5 and its use as hydrogenation catalyst. *Catalysis Communications* **2008,** *9* (6), 1286-1290.
27. Phan, N. T. S.; Le, K. K. A.; Phan, T. D., MOF-5 as an efficient heterogeneous catalyst for Friedel–Crafts alkylation reactions. *Applied Catalysis A: General* **2010,** *382* (2), 246-253.
28. Vermoortele, F.; Bueken, B.; Le Bars, G.; Van de Voorde, B.; Vandichel, M.; Houthoofd, K.; Vimont, A.; Daturi, M.; Waroquier, M.; Van Speybroeck, V.; Kirschhock, C.; De Vos, D. E., Synthesis Modulation as a Tool To Increase the Catalytic Activity of Metal–Organic Frameworks: The Unique Case of UiO-66(Zr). *Journal of the American Chemical Society* **2013,** *135* (31), 11465-11468.
29. Mondloch, J. E.; Bury, W.; Fairen-Jimenez, D.; Kwon, S.; DeMarco, E. J.; Weston, M. H.; Sarjeant, A. A.; Nguyen, S. T.; Stair, P. C.; Snurr, R. Q.; Farha, O. K.; Hupp, J. T., Vapor-Phase Metalation by Atomic Layer Deposition in a Metal–Organic Framework. *Journal of the American Chemical Society* **2013,** *135* (28), 10294-10297.
30. Wang, R.; Wang, Z.; Xu, Y.; Dai, F.; Zhang, L.; Sun, D., Porous Zirconium Metal–Organic Framework Constructed from 2D → 3D Interpenetration Based on a 3,6-Connected kgd Net. *Inorganic Chemistry* **2014,** *53* (14), 7086-7088.
31. Kim, M.; Cahill, J. F.; Fei, H.; Prather, K. A.; Cohen, S. M., Postsynthetic Ligand and Cation Exchange in Robust Metal–Organic Frameworks. *Journal of the American Chemical Society* **2012,** *134* (43), 18082-18088.
32. Deng, H.; Doonan, C. J.; Furukawa, H.; Ferreira, R. B.; Towne, J.; Knobler, C. B.; Wang, B.; Yaghi, O. M., Multiple Functional Groups of Varying Ratios in Metal-Organic Frameworks. *Science* **2010,** *327* (5967), 846-850.
33. Dhakshinamoorthy, A.; Asiri, A. M.; Garcia, H., Mixed-metal or mixed-linker metal organic frameworks as heterogeneous catalysts. *Catalysis Science & Technology* **2016,** *6* (14), 5238-5261.
34. Shi, D.; Cui, C.-J.; Hu, M.; Ren, A. H.; Song, L.-B.; Liu, C.-S.; Du, M., A microporous mixed-metal (Na/Cu) mixed-ligand (flexible/rigid) metal–organic framework for photocatalytic H2 generation. *Journal of Materials Chemistry C* **2019,** *7* (33), 10211-10217.
35. Canivet, J.; Aguado, S.; Schuurman, Y.; Farrusseng, D., MOF-Supported Selective Ethylene Dimerization Single-Site Catalysts through One-Pot Postsynthetic Modification. *Journal of the American Chemical Society* **2013,** *135* (11), 4195-4198.
36. Cancino, P.; Paredes-García, V.; Aguirre, P.; Spodine, E., A reusable CuII based metal–organic framework as a catalyst for the oxidation of olefins. *Catalysis Science & Technology* **2014,** *4* (8), 2599-2607.
37. Llabrés i Xamena, F. X.; Abad, A.; Corma, A.; Garcia, H., MOFs as catalysts: Activity, reusability and shape-selectivity of a Pd-containing MOF. *Journal of Catalysis* **2007,** *250* (2), 294-298.

38. https://www.ccdc.cam.ac.uk/, The Cambridge Crystallographic Data Centre. How Many MOFs are there in the CSD? **2019**.
39. Ding, M.; Cai, X.; Jiang, H.-L., Improving MOF stability: approaches and applications. *Chemical Science* **2019,** *10* (44), 10209-10230.
40. McHugh, L. N.; McPherson, M. J.; McCormick, L. J.; Morris, S. A.; Wheatley, P. S.; Teat, S. J.; McKay, D.; Dawson, D. M.; Sansome, C. E. F.; Ashbrook, S. E.; Stone, C. A.; Smith, M. W.; Morris, R. E., Hydrolytic stability in hemilabile metal–organic frameworks. *Nature Chemistry* **2018,** *10* (11), 1096-1102.
41. Zhuang, J.; Ceglarek, D.; Pethuraj, S.; Terfort, A., Rapid Room-Temperature Synthesis of Metal-Organic Framework HKUST-1 Crystals in Bulk and as Oriented and Patterned Thin Films. *Adv. Funct. Mater.* **2011,** *21* (8), 1442-1447.
42. Li, Y.; Yang, R., Hydrogen storage in metal-organic and covalent-organic frameworks by spillover. *AlChE J.* **2008,** *54* (1), 269-279.
43. Wang, X.; Li, P.; Chen, Y.; Zhang, Q.; Zhang, H.; Chan, X.; Ganguly, R.; Li, Y.; Jiang, J.; Zhao, Y., A Rationally Designed Nitrogen-Rich Metal-Organic Framework and Its Exceptionally High CO2 and H-2 Uptake Capability. *Scientific Reports* **2013,** *3*.
44. Wu, H.; Yildirim, T.; Zhou, W., Exceptional Mechanical Stability of Highly Porous Zirconium Metal-Organic Framework UiO-66 and Its Important Implications. *Journal of Physical Chemistry Letters* **2013,** *4* (6), 925-930.
45. Tan, J.; Cheetham, A., Mechanical properties of hybrid inorganic-organic framework materials: establishing fundamental structure-property relationships. *Chem. Soc. Rev.* **2011,** *40* (2), 1059-1080.
46. Chapman, K.; Halder, G.; Chupas, P., Pressure-Induced Amorphization and Porosity Modification in a Metal-Organic Framework. *J. Am. Chem. Soc.* **2009,** *131* (48), 17546-17547.
47. Hu, Y.; Zhang, L., Amorphization of metal-organic framework MOF-5 at unusually low applied pressure. *Physical Review B* **2010,** *81* (17).
48. Peng, Y.; Krungleviciute, V.; Eryazici, I.; Hupp, J.; Farha, O.; Yildirim, T., Methane Storage in Metal-Organic Frameworks: Current Records, Surprise Findings, and Challenges. *J. Am. Chem. Soc.* **2013,** *135* (32), 11887-11894.
49. Casco, M.; Martinez-Escandell, M.; Gadea-Ramos, E.; Kaneko, K.; Silvestre-Albero, J.; Rodriguez-Reinoso, F., High-Pressure Methane Storage in Porous Materials: Are Carbon Materials in the Pole Position? *Chem. Mater.* **2015,** *27* (3), 959-964.
50. Hu, Y. H.; Zhang, L., Amorphization of metal-organic framework MOF-5 at unusually low applied pressure. *Physical Review B* **2010,** *81* (17), 174103.
51. Waitschat, S.; Reinsch, H.; Stock, N., Water-based synthesis and characterisation of a new Zr-MOF with a unique inorganic building unit. *Chemical Communications* **2016,** *52* (86), 12698-12701.
52. Bai, Y.; Dou, Y.; Xie, L.-H.; Rutledge, W.; Li, J.-R.; Zhou, H.-C., Zr-based metal–organic frameworks: design, synthesis, structure, and applications. *Chemical Society Reviews* **2016,** *45* (8), 2327-2367.
53. Bon, V.; Senkovska, I.; Baburin, I. A.; Kaskel, S., Zr- and Hf-Based Metal–Organic Frameworks: Tracking Down the Polymorphism. *Crystal Growth & Design* **2013,** *13* (3), 1231-1237.
54. Wang, T. C.; Vermeulen, N. A.; Kim, I. S.; Martinson, A. B. F.; Stoddart, J. F.; Hupp, J. T.; Farha, O. K., Scalable synthesis and post-modification of a mesoporous metal-organic framework called NU-1000. *Nature Protocols* **2016,** *11* (1), 149-162.
55. Valenzano, L.; Civalleri, B.; Chavan, S.; Bordiga, S.; Nilsen, M. H.; Jakobsen, S.; Lillerud, K. P.; Lamberti, C., Disclosing the Complex Structure of UiO-66 Metal Organic Framework: A Synergic Combination of Experiment and Theory. *Chemistry of Materials* **2011,** *23* (7), 1700-1718.
56. Shearer, G. C.; Chavan, S.; Bordiga, S.; Svelle, S.; Olsbye, U.; Lillerud, K. P., Defect Engineering: Tuning the Porosity and Composition of the Metal–Organic Framework UiO-66 via Modulated Synthesis. *Chemistry of Materials* **2016,** *28* (11), 3749-3761.

57. Shearer, G. C.; Chavan, S.; Ethiraj, J.; Vitillo, J. G.; Svelle, S.; Olsbye, U.; Lamberti, C.; Bordiga, S.; Lillerud, K. P., Tuned to Perfection: Ironing Out the Defects in Metal–Organic Framework UiO-66. *Chemistry of Materials* **2014,** *26* (14), 4068-4071.
58. Øien, S.; Wragg, D.; Reinsch, H.; Svelle, S.; Bordiga, S.; Lamberti, C.; Lillerud, K. P., Detailed Structure Analysis of Atomic Positions and Defects in Zirconium Metal–Organic Frameworks. *Crystal Growth & Design* **2014,** *14* (11), 5370-5372.
59. Shearer, G. C.; Vitillo, J. G.; Bordiga, S.; Svelle, S.; Olsbye, U.; Lillerud, K. P., Functionalizing the Defects: Postsynthetic Ligand Exchange in the Metal Organic Framework UiO-66. *Chemistry of Materials* **2016,** *28* (20), 7190-7193.
60. Fei, H.; Pullen, S.; Wagner, A.; Ott, S.; Cohen, S. M., Functionalization of robust Zr(IV)-based metal-organic framework films via a postsynthetic ligand exchange. *Chem. Commun.* **2014**, Ahead of Print.
61. Kim, M.; Cahill, J. F.; Su, Y.; Prather, K. A.; Cohen, S. M., Postsynthetic ligand exchange as a route to functionalization of 'inert' metal–organic frameworks. *Chem. Sci.* **2012,** *3* (1), 126.
62. Garibay, S.; Cohen, S., Isoreticular synthesis and modification of frameworks with the UiO-66 topology. *Chem. Commun.* **2010,** *46* (41), 7700-7702.
63. Cavka, J. H.; Jakobsen, S.; Olsbye, U.; Guillou, N.; Lamberti, C.; Bordiga, S.; Lillerud, K. P., A New Zirconium Inorganic Building Brick Forming Metal Organic Frameworks with Exceptional Stability. *J. Am. Chem. Soc.* **2008,** *130*, 13850-13851.
64. Wang, C.; Xie, Z.; deKrafft, K. E.; Lin, W., Doping Metal-Organic Frameworks for Water Oxidation, Carbon Dioxide Reduction, and Organic Photocatalysis. *J. Am. Chem. Soc.* **2011,** *133* (34), 13445-13454.
65. Øien-Ødegaard, S.; Bouchevreau, B.; Hylland, K.; Wu, L.; Blom, R.; Grande, C.; Olsbye, U.; Tilset, M.; Lillerud, K. P., UiO-67-type Metal–Organic Frameworks with Enhanced Water Stability and Methane Adsorption Capacity. *Inorganic Chemistry* **2016,** *55* (5), 1986-1991.
66. Øien, S.; Agostini, G.; Svelle, S.; Borfecchia, E.; Lomachenko, K. A.; Mino, L.; Gallo, E.; Bordiga, S.; Olsbye, U.; Lillerud, K. P.; Lamberti, C., Probing Reactive Platinum Sites in UiO-67 Zirconium Metal–Organic Frameworks. *Chemistry of Materials* **2015,** *27* (3), 1042-1056.
67. Das, A.; Biswas, S., A multi-responsive carbazole-functionalized Zr(IV)-based metal-organic framework for selective sensing of Fe(III), cyanide and p-nitrophenol. *Sensors and Actuators B: Chemical* **2017,** *250*, 121-131.
68. Li, Y.-A.; Zhao, C.-W.; Zhu, N.-X.; Liu, Q.-K.; Chen, G.-J.; Liu, J.-B.; Zhao, X.-D.; Ma, J.-P.; Zhang, S.; Dong, Y.-B., Nanoscale UiO-MOF-based luminescent sensors for highly selective detection of cysteine and glutathione and their application in bioimaging. *Chemical Communications* **2015,** *51* (100), 17672-17675.
69. McGuirk, C. M.; Katz, M. J.; Stern, C. L.; Sarjeant, A. A.; Hupp, J. T.; Farha, O. K.; Mirkin, C. A., Turning On Catalysis: Incorporation of a Hydrogen-Bond-Donating Squaramide Moiety into a Zr Metal–Organic Framework. *Journal of the American Chemical Society* **2015,** *137* (2), 919-925.
70. Meyer, K.; Ranocchiari, M.; van Bokhoven, J. A., Metal organic frameworks for photo-catalytic water splitting. *Energy & Environmental Science* **2015,** *8* (7), 1923-1937.
71. Toyao, T.; Miyahara, K.; Fujiwaki, M.; Kim, T.-H.; Dohshi, S.; Horiuchi, Y.; Matsuoka, M., Immobilization of Cu Complex into Zr-Based MOF with Bipyridine Units for Heterogeneous Selective Oxidation. *The Journal of Physical Chemistry C* **2015,** *119* (15), 8131-8137.
72. Wang, C.; Xie, Z.; deKrafft, K. E.; Lin, W., Doping Metal–Organic Frameworks for Water Oxidation, Carbon Dioxide Reduction, and Organic Photocatalysis. *Journal of the American Chemical Society* **2011,** *133* (34), 13445-13454.
73. Wei, Y.-L.; Li, Y.; Chen, Y.-Q.; Dong, Y.; Yao, J.-J.; Han, X.-Y.; Dong, Y.-B., Pd(II)-NHDC-Functionalized UiO-67 Type MOF for Catalyzing Heck Cross-Coupling and Intermolecular Benzyne–Benzyne–Alkene Insertion Reactions. *Inorganic Chemistry* **2018,** *57* (8), 4379-4386.

74. Xin, S.; Ying, Y.; Yi, J.; Yi, L.; Daniele, R., Direct synthesis of Fe(III) immobilized Zr‐based metal–organic framework for aerobic oxidation reaction. *Applied Organometallic Chemistry* **2017,** *31* (12), e3862.
75. Yu, X.; Cohen, S. M., Photocatalytic metal-organic frameworks for the aerobic oxidation of arylboronic acids. *Chemical Communications* **2015,** *51* (48), 9880-9883.
76. Zwoliński, K. M.; Chmielewski, M. J., TEMPO-Appended Metal–Organic Frameworks as Highly Active, Selective, and Reusable Catalysts for Mild Aerobic Oxidation of Alcohols. *ACS Applied Materials & Interfaces* **2017,** *9* (39), 33956-33967.
77. Butova, V. V.; Budnyk, A. P.; Charykov, K. M.; Vetlitsyna-Novikova, K. S.; Lamberti, C.; Soldatov, A. V., Water as a structure-driving agent between the UiO-66 and MIL-140A metal–organic frameworks. *Chemical Communications* **2019,** *55* (7), 901-904.
78. Siu, P. W.; Brown, Z. J.; Farha, O. K.; Hupp, J. T.; Scheidt, K. A., A mixed dicarboxylate strut approach to enhancing catalytic activity of a de novo urea derivative of metal–organic framework UiO-67. *Chemical Communications* **2013,** *49* (93), 10920-10922.
79. Gutov, O. V.; Hevia, M. G.; Escudero-Adán, E. C.; Shafir, A., Metal–Organic Framework (MOF) Defects under Control: Insights into the Missing Linker Sites and Their Implication in the Reactivity of Zirconium-Based Frameworks. *Inorganic Chemistry* **2015,** *54* (17), 8396-8400.
80. Ko, N.; Hong, J.; Sung, S.; Cordova, K. E.; Park, H. J.; Yang, J. K.; Kim, J., A significant enhancement of water vapour uptake at low pressure by amine-functionalization of UiO-67. *Dalton Transactions* **2015,** *44* (5), 2047-2051.
81. Trickett, C.; Gagnon, K.; Lee, S.; Gandara, F.; Burgi, H.; Yaghi, O., Definitive Molecular Level Characterization of Defects in UiO-66 Crystals. *Angewandte Chemie-International Edition* **2015,** *54* (38), 11162-11167.
82. Tulig, K.; Walton, K., An alternative UiO-66 synthesis for HCl-sensitive nanoparticle encapsulation. *Rsc Advances* **2014,** *4* (93), 51080-51083.
83. Biswas, S.; Van der Voort, P., A General Strategy for the Synthesis of Functionalised UiO-66 Frameworks: Characterisation, Stability and CO2 Adsorption Properties. *Eur. J. Inorg. Chem.* **2013,** (12), 2154-2160.
84. Schaate, A.; Roy, P.; Godt, A.; Lippke, J.; Waltz, F.; Wiebcke, M.; Behrens, P., Modulated Synthesis of Zr‐Based Metal‐Organic Frameworks: From Nano to Single Crystals. *Chemistry – A European Journal* **2011,** *17* (24), 6643-6651.
85. Zahn, G.; Zerner, P.; Lippke, J.; Kempf, F. L.; Lilienthal, S.; Schröder, C. A.; Schneider, A. M.; Behrens, P., Insight into the mechanism of modulated syntheses: in situ synchrotron diffraction studies on the formation of Zr-fumarate MOF. *CrystEngComm* **2014,** *16* (39), 9198-9207.
86. Tsuruoka, T.; Furukawa, S.; Takashima, Y.; Yoshida, K.; Isoda, S.; Kitagawa, S., Nanoporous Nanorods Fabricated by Coordination Modulation and Oriented Attachment Growth. *Angew. Chem. Int. Edit.* **2009,** *48* (26), 4739-4743.
87. Gokpinar, S.; Diment, T.; Janiak, C., Environmentally benign dry-gel conversions of Zr-based UiO metal-organic frameworks with high yield and the possibility of solvent re-use. *Dalton Transactions* **2017,** *46* (30), 9895-9900.
88. Katz, M. J.; Brown, Z. J.; Colon, Y. J.; Siu, P. W.; Scheidt, K. A.; Snurr, R. Q.; Hupp, J. T.; Farha, O. K., A facile synthesis of UiO-66, UiO-67 and their derivatives. *Chemical Communications* **2013,** *49* (82), 9449-9451.
89. Ragon, F.; Horcajada, P.; Chevreau, H.; Hwang, Y. K.; Lee, U. H.; Miller, S. R.; Devic, T.; Chang, J.-S.; Serre, C., In Situ Energy-Dispersive X-ray Diffraction for the Synthesis Optimization and Scale-up of the Porous Zirconium Terephthalate UiO-66. *Inorganic Chemistry* **2014,** *53* (5), 2491-2500.
90. Marshall, R. J.; Hobday, C. L.; Murphie, C. F.; Griffin, S. L.; Morrison, C. A.; Moggach, S. A.; Forgan, R. S., Amino acids as highly efficient modulators for single crystals of zirconium and hafnium metal-organic frameworks. *Journal of Materials Chemistry A* **2016,** *4* (18), 6955-6963.

91. Chavan, S.; Vitillo, J. G.; Gianolio, D.; Zavorotynska, O.; Civalleri, B.; Jakobsen, S.; Nilsen, M. H.; Valenzano, L.; Lamberti, C.; Lillerud, K. P.; Bordiga, S., H2storage in isostructural UiO-67 and UiO-66 MOFs. *Physical Chemistry Chemical Physics* **2012,** *14* (5), 1614-1626.
92. Larabi, C.; Quadrelli, E. A., Titration of Zr3(μ‐OH) Hydroxy Groups at the Cornerstones of Bulk MOF UiO‐67, [Zr6O4(OH)4(biphenyldicarboxylate)6], and Their Reaction with [AuMe(PMe3)]. *European Journal of Inorganic Chemistry* **2012,** *2012* (18), 3014-3022.
93. Nunes, P.; Gomes, A. C.; Pillinger, M.; Gonçalves, I. S.; Abrantes, M., Promotion of phosphoester hydrolysis by the ZrIV-based metal-organic framework UiO-67. *Microporous and Mesoporous Materials* **2015,** *208*, 21-29.
94. V., G. O.; Sonia, M.; C., E.-A. E.; Alexandr, S., Modulation by Amino Acids: Toward Superior Control in the Synthesis of Zirconium Metal–Organic Frameworks. *Chemistry – A European Journal* **2016,** *22* (38), 13582-13587.
95. Howarth, A. J.; Peters, A. W.; Vermeulen, N. A.; Wang, T. C.; Hupp, J. T.; Farha, O. K., Best Practices for the Synthesis, Activation, and Characterization of Metal–Organic Frameworks. *Chemistry of Materials* **2017,** *29* (1), 26-39.
96. Mondloch, J. E.; Katz, M. J.; Planas, N.; Semrouni, D.; Gagliardi, L.; Hupp, J. T.; Farha, O. K., Are Zr6-based MOFs water stable? Linker hydrolysis vs. capillary-force-driven channel collapse. *Chemical Communications* **2014,** *50* (64), 8944-8946.
97. Kaskel, S., *The Chemistry of Metal–Organic Frameworks-Synthesis, Characterization, and Applications*. Wiley-VCH 2016.
98. Atzori, C.; Shearer, G. C.; Maschio, L.; Civalleri, B.; Bonino, F.; Lamberti, C.; Svelle, S.; Lillerud, K. P.; Bordiga, S., Effect of Benzoic Acid as a Modulator in the Structure of UiO-66: An Experimental and Computational Study. *The Journal of Physical Chemistry C* **2017,** *121* (17), 9312-9324.
99. Gutterød, E. S.; Øien-Ødegaard, S.; Bossers, K.; Nieuwelink, A.-E.; Manzoli, M.; Braglia, L.; Lazzarini, A.; Borfecchia, E.; Ahmadigoltapeh, S.; Bouchevreau, B.; Lønstad-Bleken, B. T.; Henry, R.; Lamberti, C.; Bordiga, S.; Weckhuysen, B. M.; Lillerud, K. P.; Olsbye, U., CO2 Hydrogenation over Pt-Containing UiO-67 Zr-MOFs—The Base Case. *Industrial & Engineering Chemistry Research* **2017,** *56* (45), 13206-13218.
100. Trickett, C. A.; Gagnon, K. J.; Lee, S.; Gándara, F.; Bürgi, H.-B.; Yaghi, O. M., Definitive Molecular Level Characterization of Defects in UiO-66 Crystals. *Angewandte Chemie International Edition* **2015,** *54* (38), 11162-11167.
101. Choi, J.-S.; Son, W.-J.; Kim, J.; Ahn, W.-S., Metal–organic framework MOF-5 prepared by microwave heating: Factors to be considered. *Microporous and Mesoporous Materials* **2008,** *116* (1), 727-731.
102. Cubillas, P.; Anderson, M. W.; Attfield, M. P., Crystal Growth Mechanisms and Morphological Control of the Prototypical Metal–Organic Framework MOF-5 Revealed by Atomic Force Microscopy. *Chemistry – A European Journal* **2012,** *18* (48), 15406-15415.
103. Feng, Y.; Chen, Q.; Jiang, M.; Yao, J., Tailoring the Properties of UiO-66 through Defect Engineering: A Review. *Industrial & Engineering Chemistry Research* **2019,** *58* (38), 17646-17659.
104. Kleist, W.; Jutz, F.; Maciejewski, M.; Baiker, A., Mixed-Linker Metal-Organic Frameworks as Catalysts for the Synthesis of Propylene Carbonate from Propylene Oxide and CO2. *European Journal of Inorganic Chemistry* **2009,** *2009* (24), 3552-3561.
105. Marx, S.; Kleist, W.; Baiker, A., Synthesis, structural properties, and catalytic behavior of Cu-BTC and mixed-linker Cu-BTC-PyDC in the oxidation of benzene derivatives. *Journal of Catalysis* **2011,** *281* (1), 76-87.
106. Yang, X.-L.; Zou, C.; He, Y.; Zhao, M.; Chen, B.; Xiang, S.; O'Keeffe, M.; Wu, C.-D., A Stable Microporous Mixed-Metal Metal–Organic Framework with Highly Active Cu2+ Sites for Efficient Cross-Dehydrogenative Coupling Reactions. *Chemistry – A European Journal* **2014,** *20* (5), 1447-1452.

107. Salomon, W.; Roch-Marchal, C.; Mialane, P.; Rouschmeyer, P.; Serre, C.; Haouas, M.; Taulelle, F.; Yang, S.; Ruhlmann, L.; Dolbecq, A., Immobilization of polyoxometalates in the Zr-based metal organic framework UiO-67. *Chemical Communications* **2015,** *51* (14), 2972-2975.
108. Kleist, W.; Maciejewski, M.; Baiker, A., MOF-5 based mixed-linker metal–organic frameworks: Synthesis, thermal stability and catalytic application. *Thermochimica Acta* **2010,** *499* (1), 71-78.
109. Braglia, L.; Borfecchia, E.; Lomachenko, K. A.; Bugaev, A. L.; Guda, A. A.; Soldatov, A. V.; Bleken, B. T. L.; Oien-Odegaard, S.; Olsbye, U.; Lillerud, K. P.; Bordiga, S.; Agostini, G.; Manzoli, M.; Lamberti, C., Tuning Pt and Cu sites population inside functionalized UiO-67 MOF by controlling activation conditions. *Faraday Discussions* **2017,** *201* (0), 265-286.
110. Braglia, L.; Borfecchia, E.; Maddalena, L.; Øien, S.; Lomachenko, K. A.; Bugaev, A. L.; Bordiga, S.; Soldatov, A. V.; Lillerud, K. P.; Lamberti, C., Exploring structure and reactivity of Cu sites in functionalized UiO-67 MOFs. *Catalysis Today* **2017,** *283*, 89-103.
111. Yang, S.; Pattengale, B.; Lee, S.; Huang, J., Real-Time Visualization of Active Species in a Single-Site Metal–Organic Framework Photocatalyst. *ACS Energy Letters* **2018,** *3* (3), 532-539.
112. Zhang, T.; Manna, K.; Lin, W., Metal–Organic Frameworks Stabilize Solution-Inaccessible Cobalt Catalysts for Highly Efficient Broad-Scope Organic Transformations. *Journal of the American Chemical Society* **2016,** *138* (9), 3241-3249.
113. An, Y.; Liu, Y.; Bian, H.; Wang, Z.; Wang, P.; Zheng, Z.; Dai, Y.; Whangbo, M.-H.; Huang, B., Improving the photocatalytic hydrogen evolution of UiO-67 by incorporating Ce4+-coordinated bipyridinedicarboxylate ligands. *Science Bulletin* **2019,** *64* (20), 1502-1509.
114. Deming, D. A.; Hurlock, M. J.; Li, X.; Kriegsman, K. W.; Ding, G.; Guo, X.; Zhang, Q., A facile method to introduce iron secondary metal centers into metal–organic frameworks. *Journal of Organometallic Chemistry* **2019,** *897*, 114-119.
115. Aunan, E. S. Synthesis and characterization of new linkers for Zr-based MOFs. University of Oslo, University of Oslo, 2018.
116. Metzger, E. D.; Brozek, C. K.; Comito, R. J.; Dincă, M., Selective Dimerization of Ethylene to 1-Butene with a Porous Catalyst. *ACS Central Science* **2016,** *2* (3), 148-153.
117. Madrahimov, S. T.; Gallagher, J. R.; Zhang, G.; Meinhart, Z.; Garibay, S. J.; Delferro, M.; Miller, J. T.; Farha, O. K.; Hupp, J. T.; Nguyen, S. T., Gas-Phase Dimerization of Ethylene under Mild Conditions Catalyzed by MOF Materials Containing (bpy)NiII Complexes. *ACS Catalysis* **2015,** *5* (11), 6713-6718.
118. Kømurcu, M.; Lazzarini, A.; Kaur, G.; Borfecchia, E.; Øien-Ødegaard, S.; Gianolio, D.; Bordiga, S.; Lillerud, K. P.; Olsbye, U., Co-catalyst free ethene dimerization over Zr-based metal-organic framework (UiO-67) functionalized with Ni and bipyridine. *Catalysis Today* **2020**.
119. Reinsch, H.; Frohlich, D.; Waitschat, S.; Chavan, S.; Lillerud, K.-P.; Henninger, S.; Stock, N., Optimisation of synthesis conditions for UiO-66-CO2H towards scale-up and its vapour sorption properties. *Reaction Chemistry & Engineering* **2018**.
120. Taddei, M.; Dau, P. V.; Cohen, S. M.; Ranocchiari, M.; van Bokhoven, J. A.; Costantino, F.; Sabatini, S.; Vivani, R., Efficient microwave assisted synthesis of metal-organic framework UiO-66: optimization and scale up. *Dalton Transactions* **2015,** *44* (31), 14019-14026.
121. Firth, F. C. N.; Cliffe, M. J.; Vulpe, D.; Aragones-Anglada, M.; Moghadam, P. Z.; Fairen-Jimenez, D.; Slater, B.; Grey, C. P., Engineering new defective phases of UiO family metal–organic frameworks with water. *Journal of Materials Chemistry A* **2019**.
122. An, B.; Li, Z.; Song, Y.; Zhang, J.; Zeng, L.; Wang, C.; Lin, W., Cooperative copper centres in a metal–organic framework for selective conversion of CO2 to ethanol. *Nature Catalysis* **2019**.
123. Lili, L.; Xin, Z.; Jinsen, G.; Chunming, X., Engineering metal–organic frameworks immobilize gold catalysts for highly efficient one-pot synthesis of propargylamines. *Green Chemistry* **2012,** *14* (6), 1710-1720.
124. Hou, J.; Luan, Y.; Tang, J.; Wensley, A. M.; Yang, M.; Lu, Y., Synthesis of UiO-66-NH2 derived heterogeneous copper (II) catalyst and study of its application in the selective aerobic oxidation of alcohols. *Journal of Molecular Catalysis A: Chemical* **2015,** *407*, 53-59.

125. Marshall, R. J.; Forgan, R. S., Postsynthetic Modification of Zirconium Metal-Organic Frameworks. *European Journal of Inorganic Chemistry* **2016,** *2016* (27), 4310-4331.
126. Gutterød, E. S.; Lazzarini, A.; Fjermestad, T.; Kaur, G.; Manzoli, M.; Bordiga, S.; Svelle, S.; Lillerud, K. P.; Skúlason, E.; Øien-Ødegaard, S.; Nova, A.; Olsbye, U., Hydrogenation of CO2 to Methanol by Pt Nanoparticles Encapsulated in UiO-67: Deciphering the Role of the Metal–Organic Framework. *Journal of the American Chemical Society* **2019**.
127. Zianna, A.; Geromichalos, G. D.; Hatzidimitriou, A. G.; Coutouli-Argyropoulou, E.; Lalia-Kantouri, M.; Psomas, G., Palladium(II) complexes with salicylaldehyde ligands: Synthesis, characterization, structure, in vitro and in silico study of the interaction with calf-thymus DNA and albumins. *Journal of Inorganic Biochemistry* **2019,** *194*, 85-96.
128. Shahrul Nizam Ahmad, H. B., Amalina Mohd Tajuddin Tetradentate Palladium(II) Salophen Complexes: Synthesis, Characterization and Catalytic Activities in Copper-Free Sonogashira Coupling Reaction *International Journal of Engineering & Technology* **2018,** *7 (3.11)*, 15-19
129. <Synthesis, Characterization, and Reactivity of Palladium(II) Salen and Oxazoline Complexes.pdf>.
130. Schaate, A.; Roy, P.; Godt, A.; Lippke, J.; Waltz, F.; Wiebcke, M.; Behrens, P., Modulated synthesis of Zr-based metal-organic frameworks: from nano to single crystals. *Chem.-Eur. J.* **2011,** *17* (24), 6643-51.
131. Gómez-Gualdrón, D. A.; Moghadam, P. Z.; Hupp, J. T.; Farha, O. K.; Snurr, R. Q., Application of Consistency Criteria To Calculate BET Areas of Micro- And Mesoporous Metal–Organic Frameworks. *J. Am. Chem. Soc.* **2016,** *138* (1), 215-224.
132. Guillerm, V.; Ragon, F.; Dan-Hardi, M.; Devic, T.; Vishnuvarthan, M.; Campo, B.; Vimont, A.; Clet, G.; Yang, Q.; Maurin, G.; Férey, G.; Vittadini, A.; Gross, S.; Serre, C., A Series of Isoreticular, Highly Stable, Porous Zirconium Oxide Based Metal–Organic Frameworks. *Angewandte Chemie International Edition* **2012,** *51* (37), 9267-9271.
133. Liang, W.; Babarao, R.; Church, T. L.; D'Alessandro, D. M., Tuning the cavities of zirconium-based MIL-140 frameworks to modulate CO2 adsorption. *Chemical Communications* **2015,** *51* (56), 11286-11289.
134. Van de Voorde, B.; Damasceno Borges, D.; Vermoortele, F.; Wouters, R.; Bozbiyik, B.; Denayer, J.; Taulelle, F.; Martineau, C.; Serre, C.; Maurin, G.; De Vos, D., Isolation of Renewable Phenolics by Adsorption on Ultrastable Hydrophobic MIL-140 Metal–Organic Frameworks. *ChemSusChem* **2015,** *8* (18), 3159-3166.
135. Decker, G. E.; Stillman, Z.; Attia, L.; Fromen, C. A.; Bloch, E. D., Controlling Size, Defectiveness, and Fluorescence in Nanoparticle UiO-66 through Water and Ligand Modulation. *Chemistry of Materials* **2019,** *31* (13), 4831-4839.
136. Jakobsen, S.; Gianolio, D.; Wragg, D. S.; Nilsen, M. H.; Emerich, H.; Bordiga, S.; Lamberti, C.; Olsbye, U.; Tilset, M.; Lillerud, K. P., Structural determination of a highly stable metal-organic framework with possible application to interim radioactive waste scavenging: Hf-UiO-66. *Physical Review B* **2012,** *86* (12), 125429.
137. Platero-Prats, A. E.; Bermejo Gómez, A.; Chapman, K. W.; Martín-Matute, B.; Zou, X., Functionalising metal–organic frameworks with metal complexes: the role of structural dynamics. *CrystEngComm* **2015,** *17* (40), 7632-7635.
138. Bogaerts, T.; Van Yperen-De Deyne, A.; Liu, Y.-Y.; Lynen, F.; Van Speybroeck, V.; Van Der Voort, P., Mn-salen@MIL101(Al): a heterogeneous, enantioselective catalyst synthesized using a 'bottle around the ship' approach. *Chemical Communications* **2013,** *49* (73), 8021-8023.
139. Shultz, A. M.; Sarjeant, A. A.; Farha, O. K.; Hupp, J. T.; Nguyen, S. T., Post-Synthesis Modification of a Metal–Organic Framework To Form Metallosalen-Containing MOF Materials. *Journal of the American Chemical Society* **2011,** *133* (34), 13252-13255.

140. Atzori, C.; Shearer, G. C.; Maschio, L.; Civalleri, B.; Bonino, F.; Lamberti, C.; Svelle, S.; Lillerud, K. P.; Bordiga, S., Effect of Benzoic Acid as a Modulator in the Structure of UiO-66: An Experimental and Computational Study. *J. Phys. Chem. C* **2017,** *121* (17), 9312-9324.
141. Chavan, S.; Vitillo, J. G.; Gianolio, D.; Zavorotynska, O.; Civalleri, B.; Jakobsen, S.; Nilsen, M. H.; Valenzano, L.; Lamberti, C.; Lillerud, K. P.; Bordiga, S., H_2 storage in isostructural UiO-67 and UiO-66 MOFs. *Phys. Chem. Chem. Phys.* **2012,** *14* (5), 1614-1626.
142. Morterra, C.; Cerrato, G.; Novarino, E.; Mentruit, M. P., On the adsorption of acetonitrile on pure and sulfated tetragonal zirconia (t-ZrO2). *Langmuir* **2003,** *19* (14), 5708-5721.
143. Plessers, E.; Fu, G. X.; Tan, C. Y. X.; De Vos, D. E.; Roeffaers, M. B. J., Zr-Based MOF-808 as Meerwein-Ponndorf-Verley Reduction Catalyst for Challenging Carbonyl Compounds. *Catalysts* **2016,** *6* (7), 104.

Appendix

Additional data

1. Preliminary high-throughput synthesis

Table A1. Estimated particle size of UiO-67 synthesized with water (set W) and $HCl_{(aq)}$ (set H) as additives and thermally tested at 450 °C for 2 hours, see Figure 16 and Figure 17.

Entry	Set W (nm)	Set W@450°C (nm)	Set H (nm)	Set H@450°C (nm)
1	101	82	74	89
2	152	54	7	11
3	177	38	25	14
4	110	13	43	14
5	155	14	44	13
6	145	13	46	10
7	152	12	27	9
8	221	10	34	11
9	267	73	49	13
10	243	13	55	11
11	230	147	35	11
12	211	22	89	10
13	16	17	80	15
14	59	22	7	14
15	163	125	8	18
16	174	101	25	18
17	212	119	39	15
18	253	161	52	15
19	8	13	7	12
20	158	15	24	18
21	371	265	57	14
22	282	255	60	15
23	196	191	35	15
24	371	203	72	15
25	10	12	10	9
26	7	13	8	15
27	34	14	73	14
28	169	154	8	18
29	184	144	75	100
30	219	192	91	53
31	10	12	8	15
32	178	13	8	21
33	229	24	92	19
34	232	179	68	23
35	216	16	56	20
36	189	64	96	20

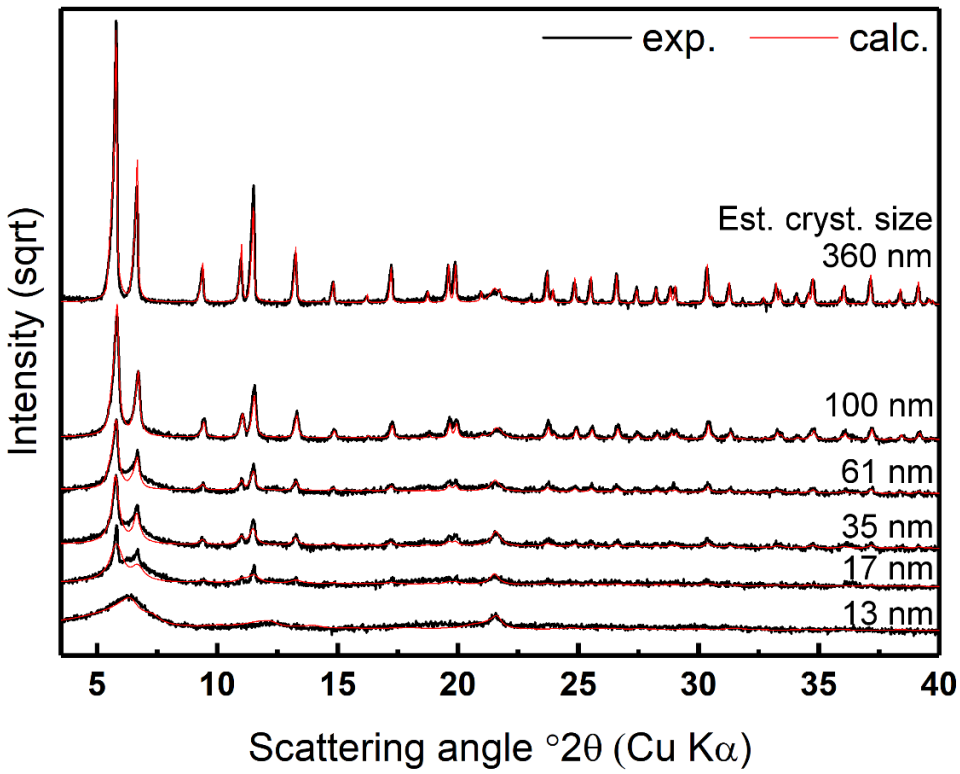

Figure A1. Examples of estimated sizes from the PXRD refinement. Note that the y-scale shows the square root of the diffraction signal to better accommodate the low and high intensity portions of the patterns in the same figure. Acquired patterns are shown in bold black lines, and the best fits are shown as thin red lines.

2. Screening of amount of modulator for UiO-67 (C-x_{BA} and D-x_{BA} series)

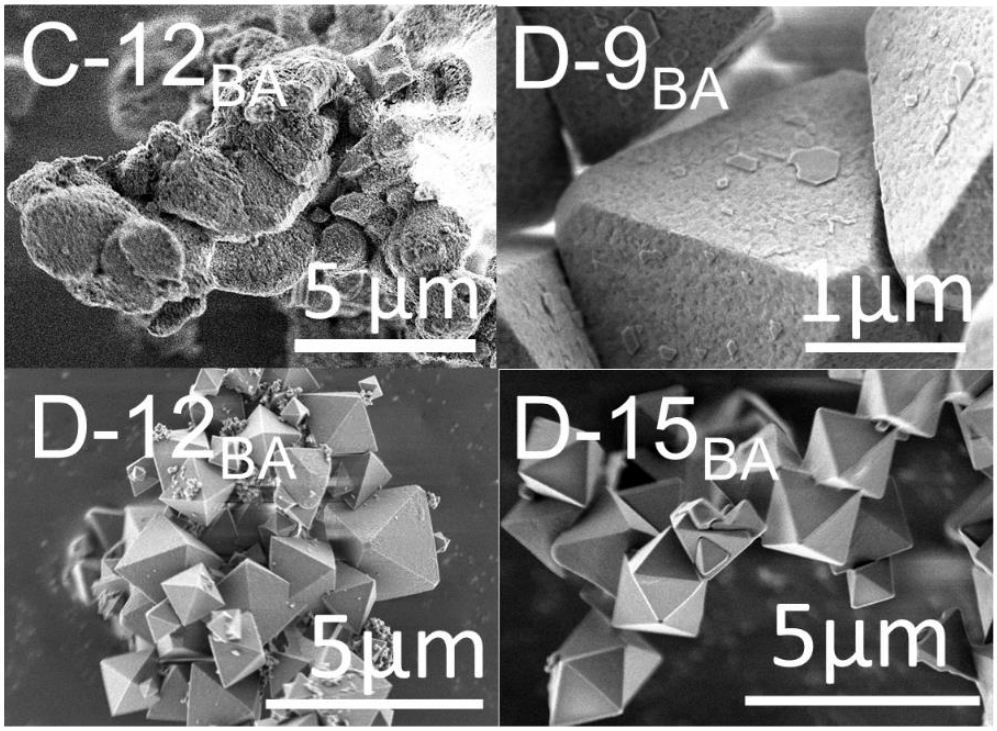

Figure A2. SEM micrograph for C-12_{BA}, D-9_{BA}, D-12_{BA} and C-15_{BA}.

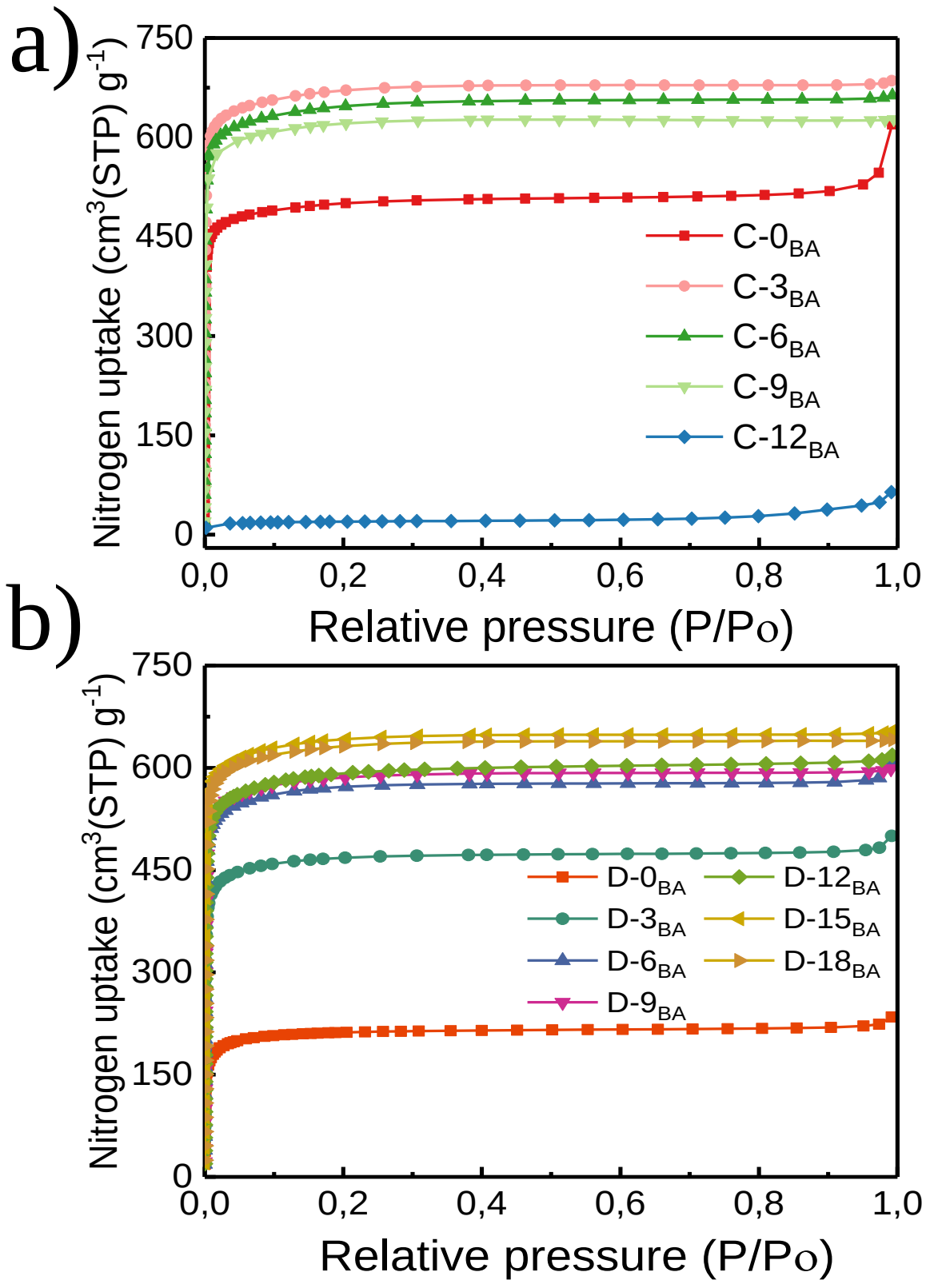

Figure A3. Nitrogen isotherms at 77 K for a) C-x_{BA} series and b) D-x_{BA} series.

Table A2. Surface area and pore volume data for C-x_{BA} and D-x_{BA} series (calculated from nitrogen adsorption isotherms)

Entry	BA concentration in synthesis (equiv)	C-x_{BA} series		D-x_{BA} series	
		Surface area [m^2 g^{-1}]	Pore volume [cm^3 g^{-1}]	Surface area [m^2 g^{-1}]	Pore volume [cm^3 g^{-1}]
1	0	2043	469	542	193
2	3	2734	628	1888	434
3	6	2632	605	2320	533
4	9	2549	585	2387	548
5	12	74	17	2474	545
6	15	-	-	2614	601
7	18	-	-	2562	589

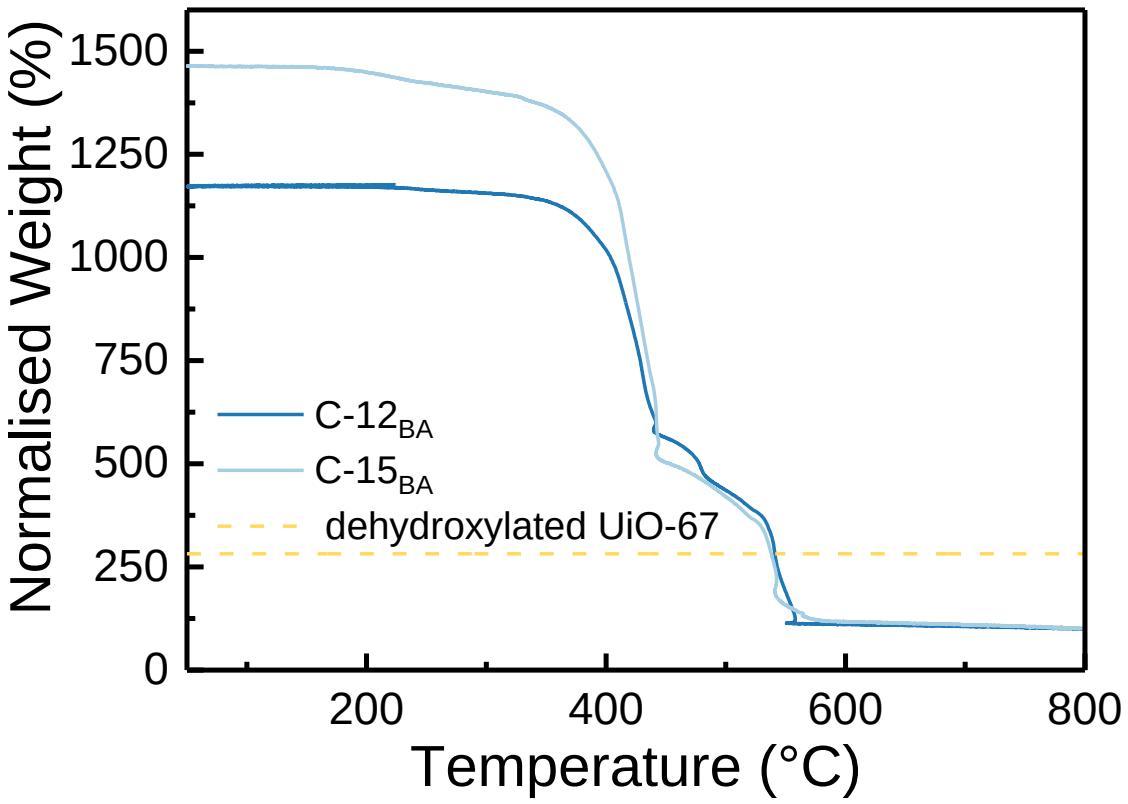

Figure A4. TGA and DSC signals of C-x_{BA} (x= 12 to 15).

Table A3. Relative organic mass in C-x_{BA} and D-x_{BA} series, calculated with NMR spectroscopy, the amount of benzoic acid (BA) and formic acid (FA) is given with respect to bpdc linker.

Entry	BA concentration in synthesis (equiv)	C-x_{BA} series		D-x_{BA} series	
		BA (%)	FA(%)	BA (%)	FA(%)
1	0	0	2	0	11
2	3	2	1	26	4
3	6	0	6	20	2
4	9	0	6	21	1
5	12	3	0	16	0
6	15	6	1	24	1
7	18	-	-	17	1

3. ATR and DRIFT spectroscopy (CD_3CN as probe molecule) on C-x_{BA} and D-x_{BA} series

Attenuated total reflectance spectra (ATR-IR) were collected with a Bruker Vertex 70 instrument, equipped with a liquid nitrogen-cooled MCT detector and a Bruker Platinum ATR accessory with diamond crystal. Before measurements, the samples were dried overnight at 200 °C in order to remove most of the solvent (DMF) and moisture. In-situ DRIFT-IR spectra, have been collected on the same instrument this time equipped with a Harrick Praying Mantis cell, monitoring the activation of the MOFs and interaction with CD3CN used as probe molecule. Samples activation was performed with 10 ml/min of He flow, from RT to 300 °C with a ramp rate of 5 °C/min and kept at 300 °C for 180 min. Successively the samples were cooled at 120 °C in inert and CD3CN vapors started to be dosed in a 10 ml/min He flow. This precaution was adopted in order to avoid samples re-hydration below 100 °C, which can interfere in the interaction between the samples and the probe molecule. Then the temperature was further lowered to 70 °C in the presence of CD3CN vapors till the spectra stopped changing upon the CD3CN flux. The relative stabilities of the adsorbed species were monitored during a 10 ml/min He flow overnight.

Figure A5 illustrates ATR-IR spectra for selected samples of **C-x_{BA}** and **D-x_{BA}** (Part a and Part b, respectively). The spectra collected on the samples prepared with concentrated synthesis (**C-3_{BA}**, **C-6_{BA}** and **C-9_{BA}**) and that with diluted synthesis (**D-3_{BA}**, **D-12_{BA}** and **D-18_{BA}**) are very similar. Major bands are:i) a sharp peak at 680 cm^{-1}, ascribed to Zr-μ_3-OH; ii) a very strong maximum at around 1400 cm^{-1}, due to the symmetric ν(O-C-O) stretching mode; iii) maxima around 1500−1550 cm^{-1}, due to the asymmetric ν(O-C-O) stretching mode of the carboxylates; iv) a complex band around 1600 cm^{-1}, due to ν(C-C) stretching modes in the aromatic rings; v)

broad, complex and weak components around 1700−1730 cm^{-1} due to ν(C=O) of benzoic acid (coordinated to Zr or entrapped in the pores after the synthesis) or that of amide of DMF.[55, 140-141] A weaker counterpart at 1240 cm^{-1}, due to ν(C-O) is also expected. Between the two series of spectra, we observe that the signals of both species (ν(C=O) and ν(C-O)) are more evident in the spectra reported in Figure A5b), especially in case of **D-18$_{BA}$**. The ATR spectra obtained for **C-0$_{BA}$** and **D-0$_{BA}$** shows some differences. Particularly, **C-0$_{BA}$** shows clearly some extra bands (highlighted with dotted lines) whereas **D-0$_{BA}$** mostly shows broader bands with a different intensity ratio.

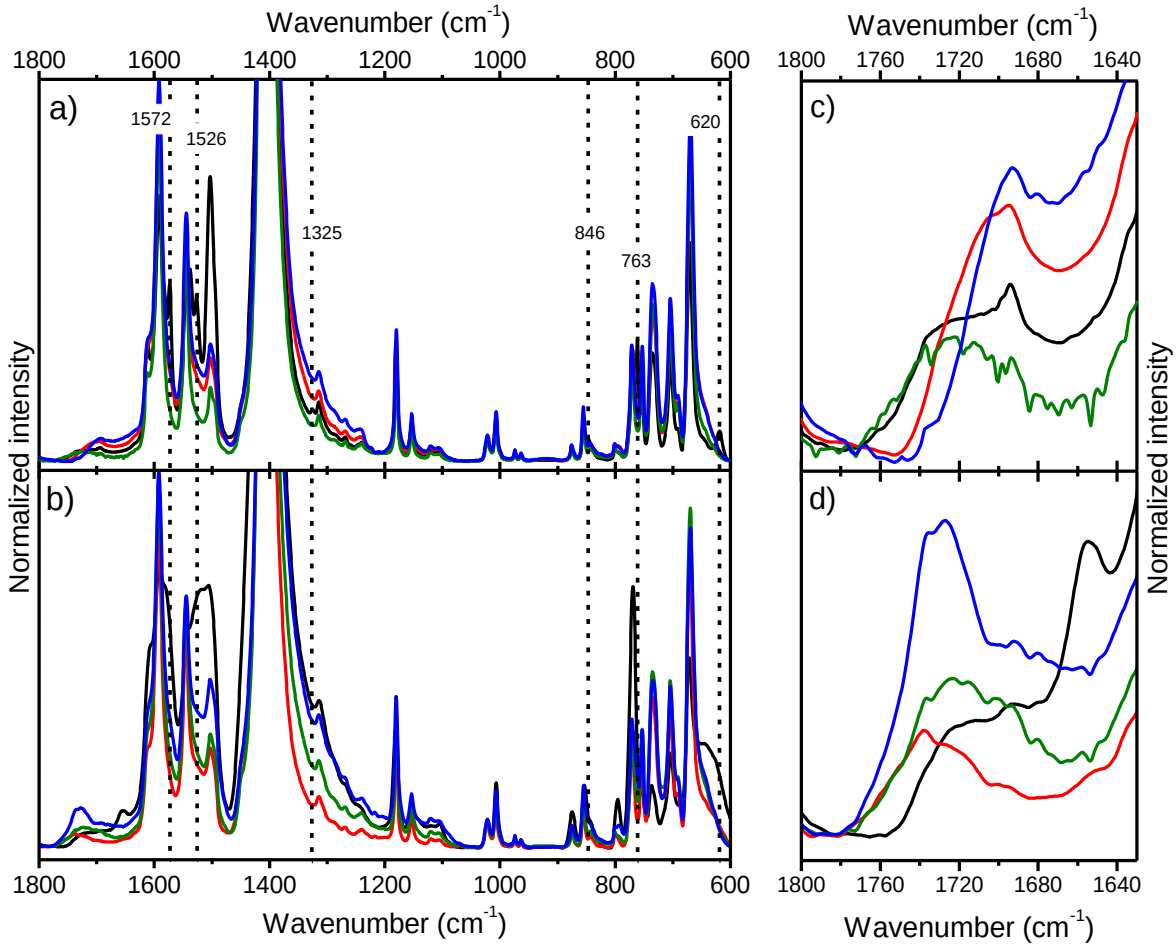

Figure A5. Part a) and c) ATR spectra of UiO-67 MOFs prepared with concentrated synthesis, using 0 equiv (black curve), 3 equiv (red curve), 6 equiv (green curve) and 9 equiv (blue curve) of benzoic acid as modulator. Dotted lines help in the identification of the extra signal for the sample synthesized without modulator. Part b) and d) ATR spectra of UiO-67 MOFs prepared with diluted synthesis, using 0 equiv (black curve), 3 equiv (red curve), 12 equiv (green curve) and 18 equiv (blue curve) of benzoic acid as modulator.

Figure A6 a), b) illustrates the spectra for samples **C-0$_{BA}$** and **C-3$_{BA}$**, while Figure A7 a), b) and c) reports the data for the samples **D-0$_{BA}$**, **D-3$_{BA}$** and **D-18$_{BA}$**. Main figures report the spectra collected after activation in the same color used in Figure A5 (black **C-0$_{BA}$** and **D-0$_{BA}$**; red **C-3$_{BA}$** and **D-3$_{BA}$**; blue **D-18$_{BA}$**); curves from dark to light gray, illustrate the effect of progressive desorption of CD_3CN from the samples. The activation procedure performed before the dosage of the probe (He flux from RT to 300 °C with a ramp rate of 5 °C/min and kept at 300 °C for 180 min) was able to completely remove the solvent but preserved the μ_3-OH groups formed at the Zr_6 clusters, as testified by the presence of the sharp band at 3676 cm^{-1}. Upon interaction with CD_3CN, the bands associated to the OH groups were eroded and shifted at lower frequencies (centered at 3350 cm^{-1}).[142] As counterpart, in the ν(CN) region (see the insets of Figure A6 and Figure A7), blue shifted, new components around 2276 cm^{-1}, are observed.[143] In the same spectral range, the absence of relevant bands around 2300 cm^{-1}, exclude the abundance of accessible Lewis sites (e.g. uncoordinated Zr sites). The only sample that shows a clear component at 2300 cm^{-1}, is the **D-0$_{BA}$** material (Figure A7a), inset). On the basis of what evaluated by TGA-DSC and by ^1H NMR, we know that also the sample **D-3$_{BA}$** should be highly defective. The fact that we do not appreciate a clear component at 2300 cm^{-1}, implies that the Zr species in that sample are not present as highly uncoordinated Lewis site, able to perturb the CN group, but are most probably capped by OH groups.

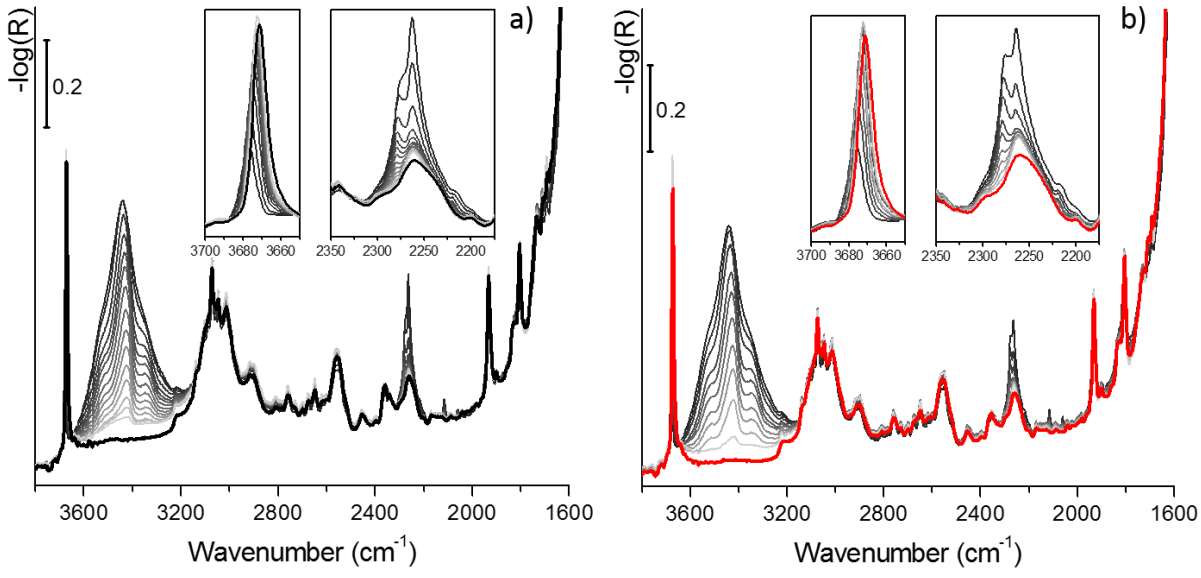

Figure A6. DRIFT spectra of samples C-0$_{BA}$ (part a) and C-3$_{BA}$ (part b). Black curve represent the sample C-0$_{BA}$ prior to CD_3CN dosing, the same for the sample C-3$_{BA}$ (red curve). Curves from dark to light grey represent the progressive desorption of CD_3CN from the adsorption sites on the samples.

Insets show a magnification of the ν(Zr-OH) region (3700-3650 cm^{-1}) and of the ν(C≡N) region (2350-2175 cm^{-1}).

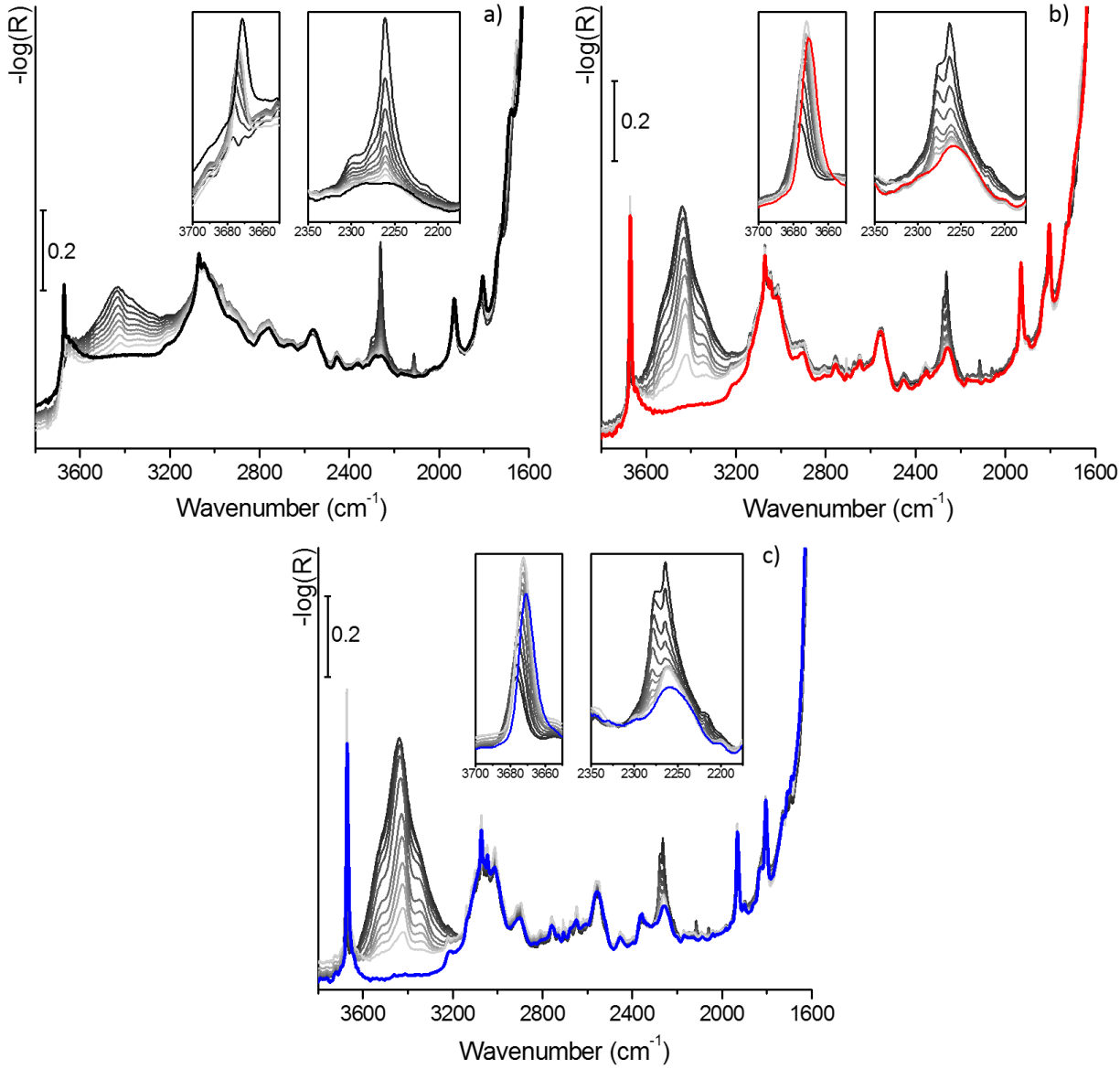

Figure A7. DRIFT spectra of samples a) D-0_{BA}, b) D-3_{BA} and c) D-18_{BA}. Black curve represent the sample D-0_{BA} prior to CD_3CN dosing, the same for the sample D-3_{BA} (red curve) and D-18_{BA} (blue curve). Curves from dark to light grey represent the progressive desorption of CD_3CN from the adsorption sites on the samples. Insets show a magnification of the ν (Zr-OH) region (3700-3650 cm^{-1}) and of the ν(C≡N) region (2350-2175 cm^{-1}).

4. Yield

Table A4. Yield of C-x_{BA} and D-x_{BA} series.

Entry	Sample label	Yield (%)	Sample label	Yield (%)
1	C-0_{BA}	92	D-0_{BA}	73
2	C-3_{BA}	86	D-3_{BA}	89
3	C-6_{BA}	92	D-6_{BA}	92
4	C-9_{BA}	86	D-9_{BA}	96
5	C-12_{BA}	25	D-12_{BA}	86
6	C-15_{BA}	22	D-15_{BA}	92
7	-		D-18_{BA}	95

5. Time course study

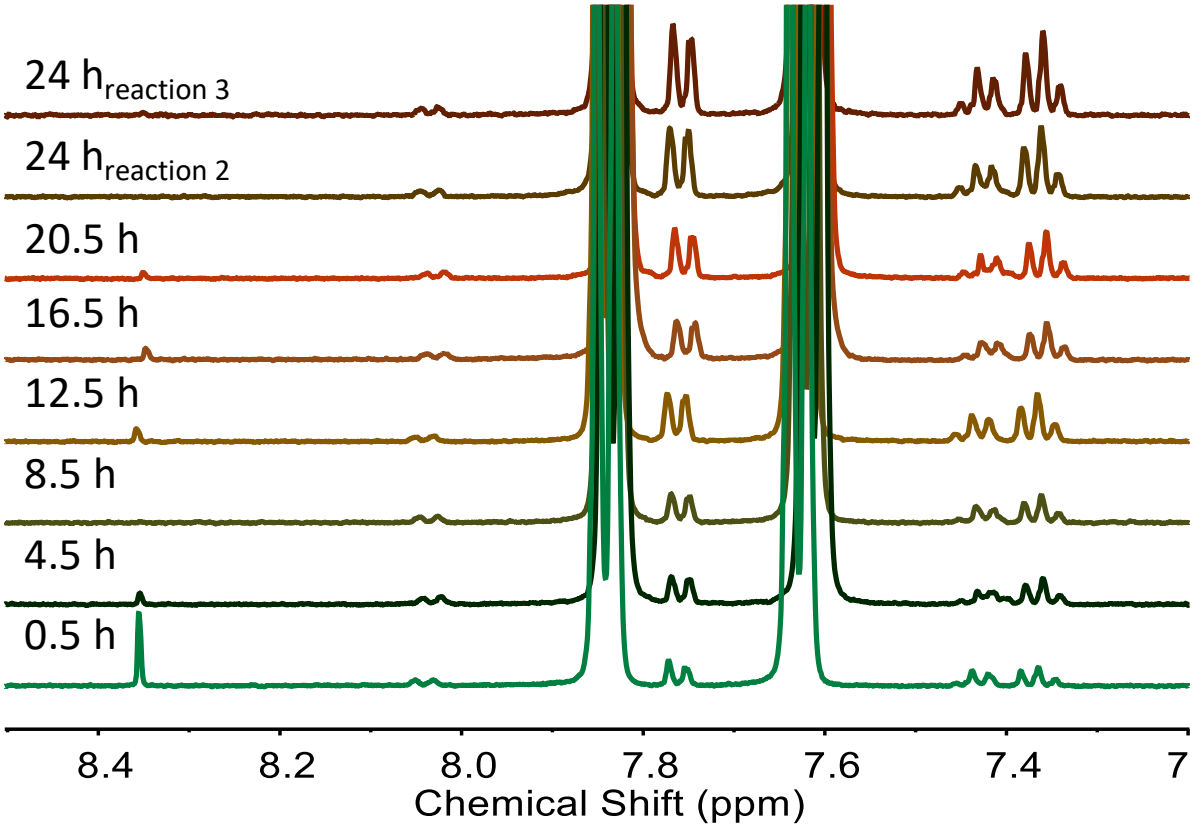

Figure A8. NMR spectra of the samples from time course study of D-9_{BA}.

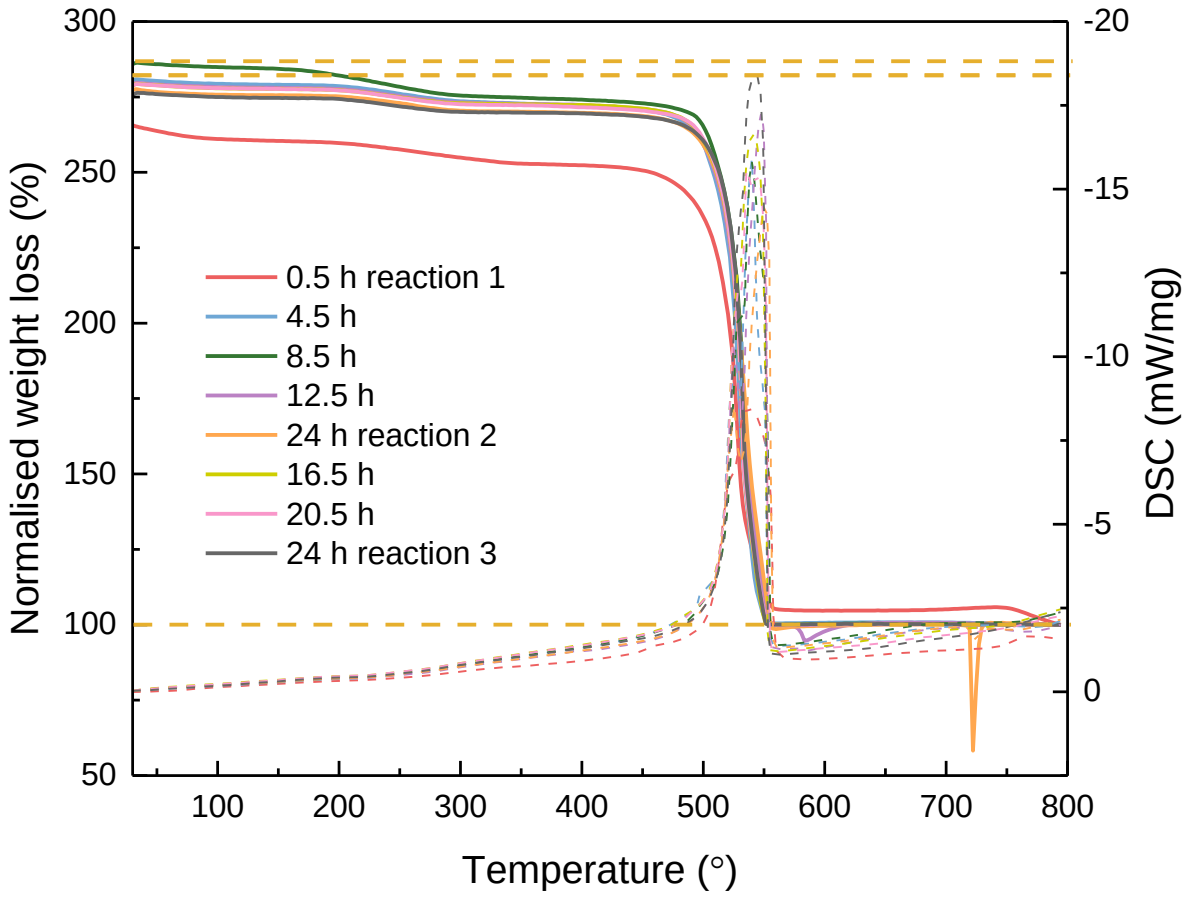

Figure A9. TGA-DSC curves on the samples from time course study.

6. Water screening

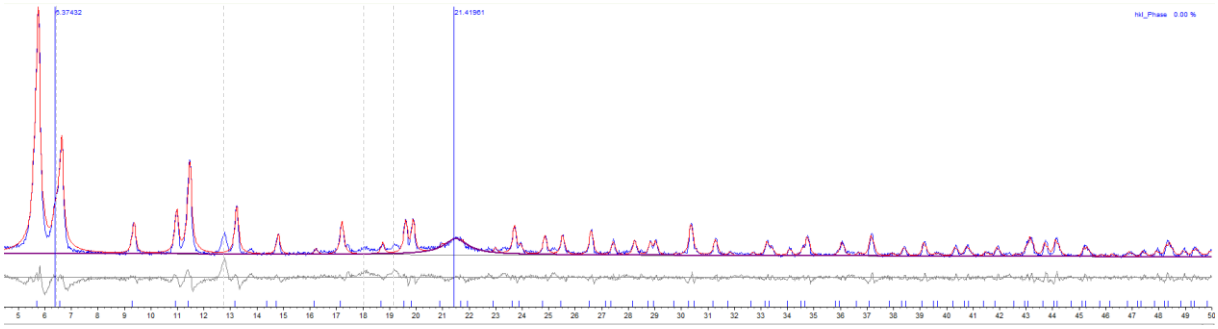

Figure A10. XRD pattern of UiO-67-bpydc$_{0.1}$-4$_{H_2O}$(blue) refined against ideal UiO-67 XRD pattern (red) where the extra peaks are marked by grey dotted lines.

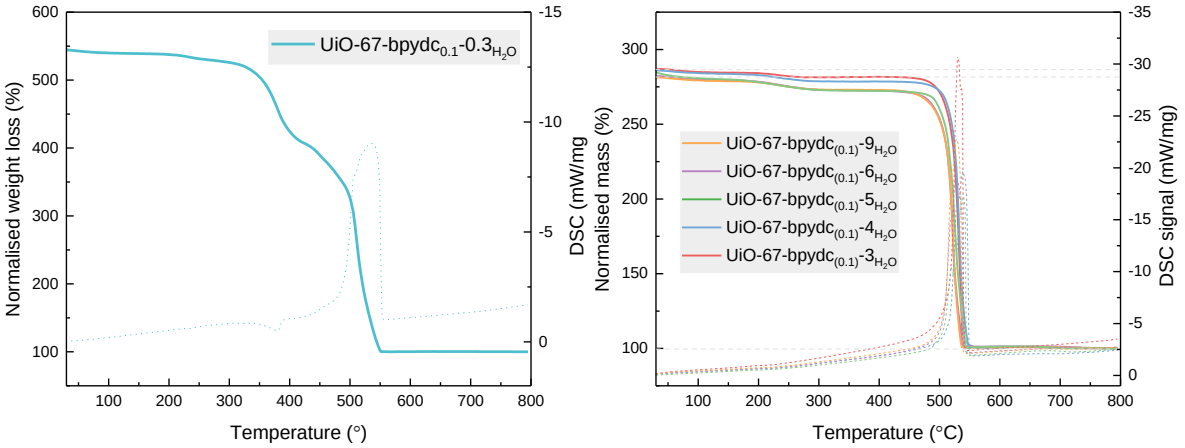

Figure A11. TGA-DSC of UiO-67-bpydc$_{0.1}$ with different amount of water; 0.3, 3, 4, 5, 6, 9 equiv.

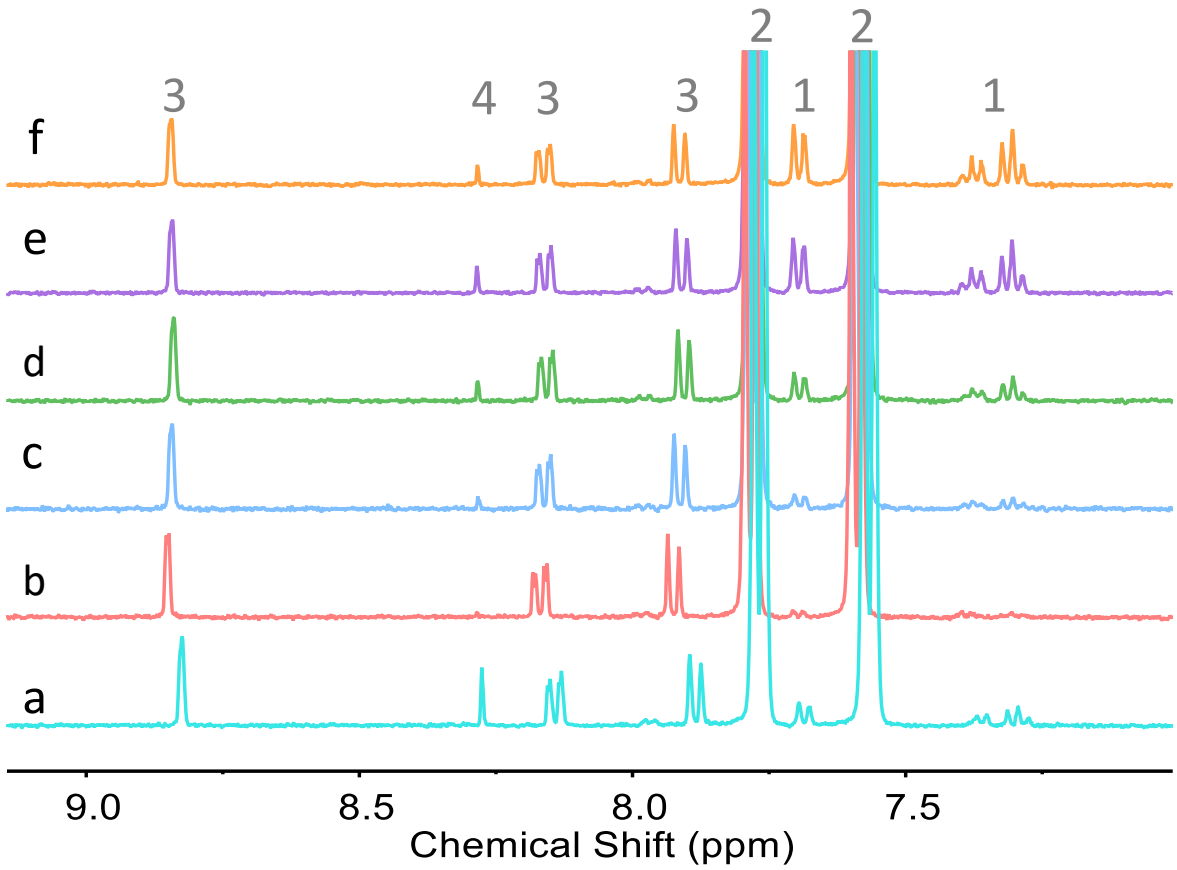

Figure A12. NMR of UiO-67-bpydc$_{0.1}$ with different amount of water; a) 0.3, b) 3, c) 4, d) 5, e) 6 and f) 9 equiv, where the peaks are from the protons of 1) benzoate, 2) bpdc^{2-}, 3) bpydc^{2-} and 4) formate.

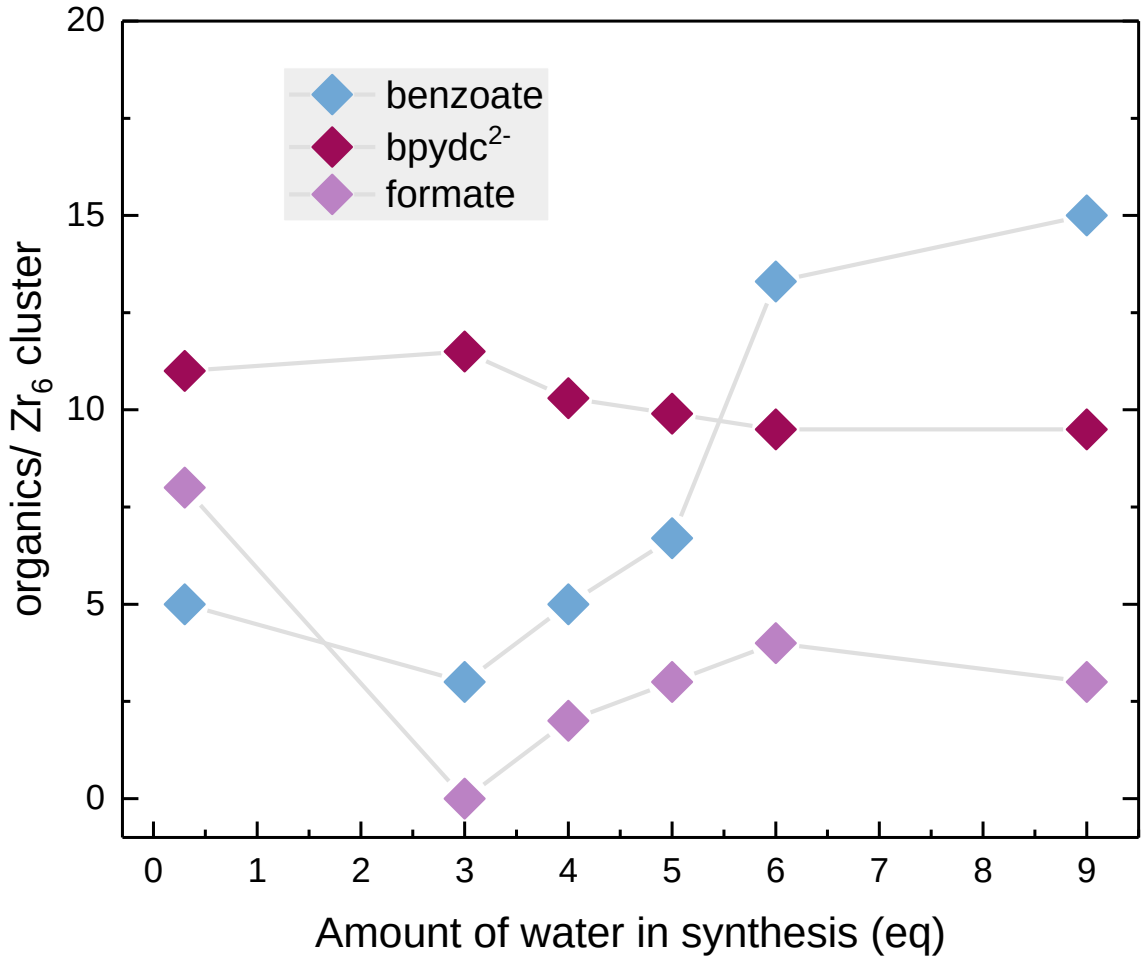

Figure A13. Composition of the organic constituents in each sample, determined by ^{1}H NMR and scaled to the organic:Zr_6 ratio found by TGA (at 200 °C) in the samples synthesized with varying amount of water. The total organic content in an ideal UiO-67 ($Zr_6O_6(bpdc)_6$) is 6.

7. Post synthetic modification and metal incorporation

Table A5. Relative organic content with respect to bpdc linker in the MOF and its derivative, calculated using ^{1}H NMR.

Entry	Sample	$bpdc(NH_2)_2^{2-}$ (%)	Salicylaldehyde (%)	Benzoate (%)	formate (%)
1	**MOF**	6	NA	12	4
2	**MOF-sal**	6	5	6	3
3	**MOF-Pd-(via sal)**	6	5	5	5

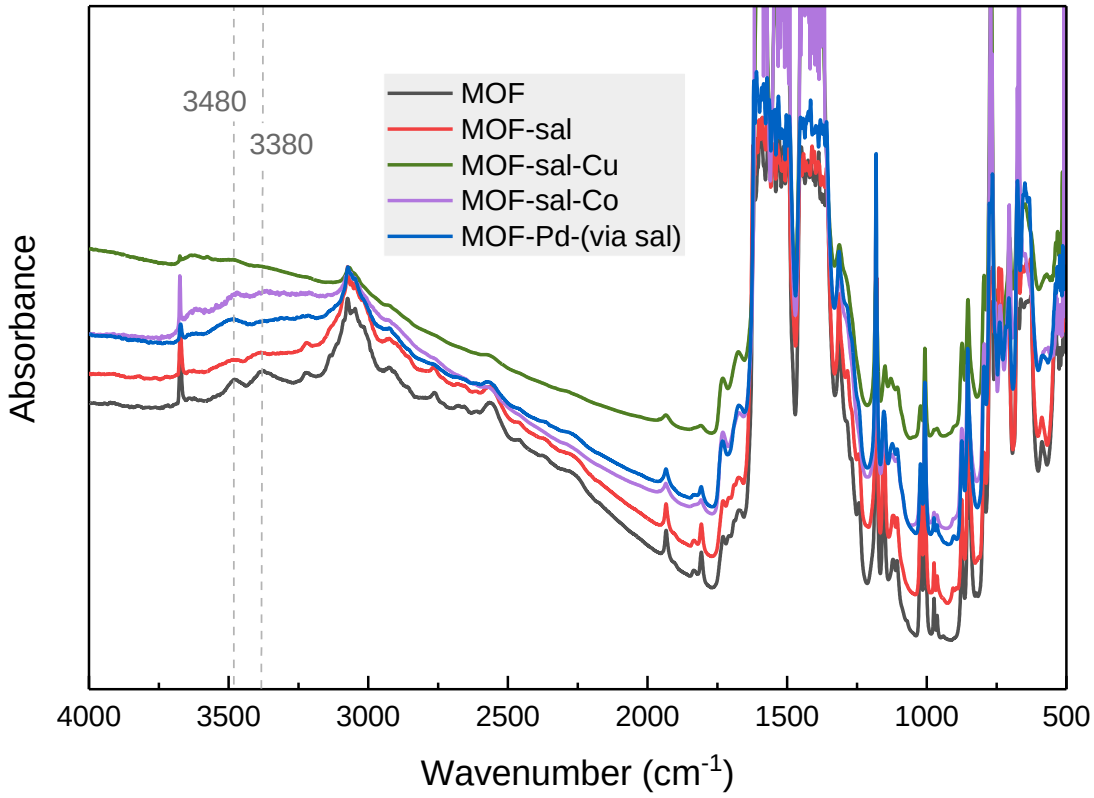

Figure A14. FT-IR spectra of MOF (black) and its derivatives, MOF-sal (red), MOF-sal-Cu (green), MOF-sal-Co (violet) and MOF-Pd-(via sal) (blue).

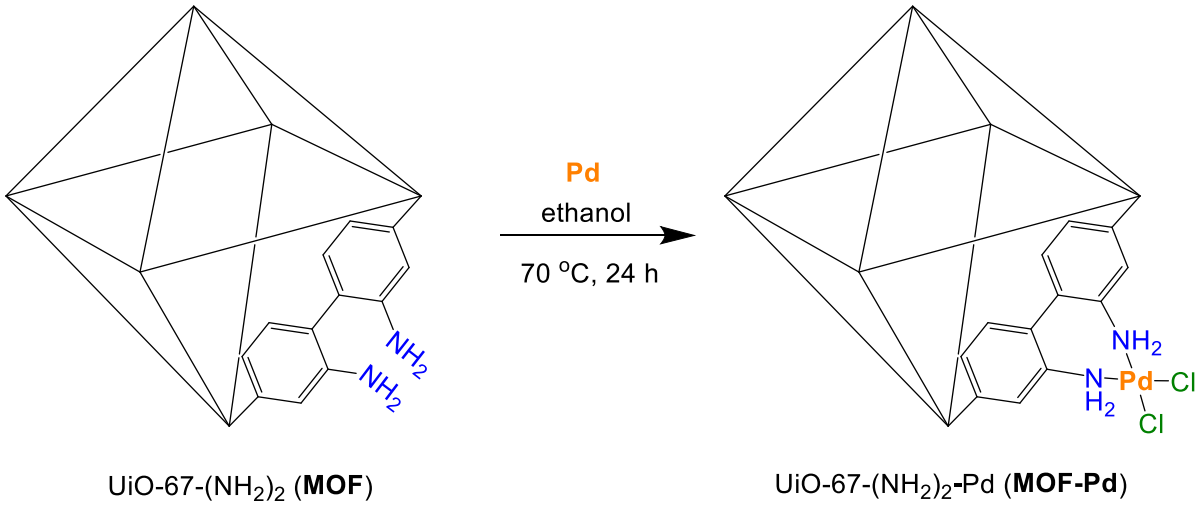

Figure A15. Synthesis of MOF-Pd where UiO-67-bpdc-$(NH_2)_2$ is reacted with Bis(acetonitrile)palladium dichloride, for comparison with MOF-Pd-(via sal).

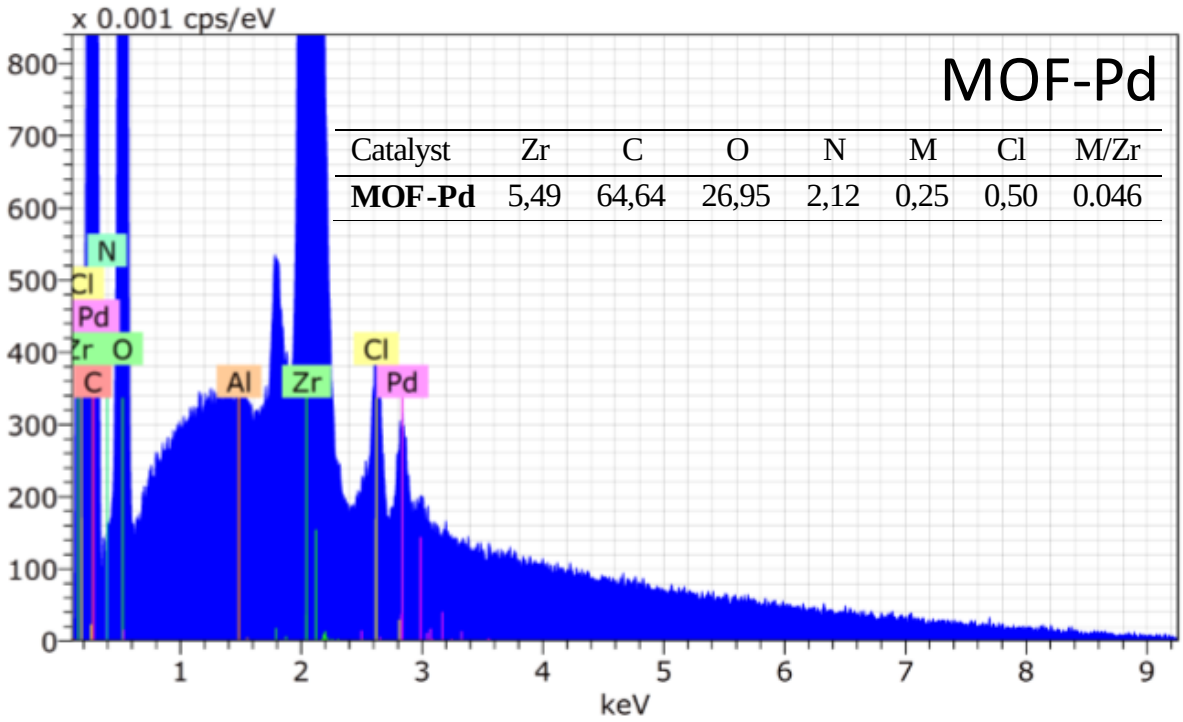

Figure A 16. EDX data for MOF-Pd.

Single crystal X-ray diffraction

Complete data sets for the reported single crystals were acquired on a Bruker D8 Venture diffractometer equipped with a Photon 100 detector and using Mo Kα radiation (λ = 0.71073 Å). Data reduction was performed with the Bruker Apex3 Suite, the structure was solved with ShelxT and refined with ShelxL.

Table A6. Data collection and refinement details of single crystal structure determinations.

Crystal data	Schiff-diester	Br-Schiff Cu(II)	Aminobiphenyl-PdCl2
Chemical formula	$C_{30}H_{24}N_2O_6 \cdot CO$	$2(C_{32}H_{24}Br_2CuN_2O_6) \cdot (C_2H_3N)$	$C_{16}H_{16}Cl_2N_2O_4Pd \cdot C_4H_8O$
M_r	432.42	1519.68	461.98
Crystal system, space group	Triclinic, $P\bar{1}$	Monoclinic, $P2_1/c$	Triclinic, $P\bar{1}$
Temperature (K)	100	100	100
a, *b*, *c* (Å)	9.7050 (7), 11.0878	20.1681 (12), 11.3946	8.5427 (12), 10.1799 (12),

	(8), 12.4021 (9)	(7), 26.6729 (16)	13.0547 (18)
□, □, □ (°)	85.344 (1), 72.774 (1), 89.658 (1)	90, 93.554 (2), 90	95.983 (3), 97.412 (4), 100.812 (3)
V (Å^3)	1270.26 (16)	6117.8 (6)	1096.2 (3)
Z	2	12	2
Radiation type	Mo K□	Mo K□	Mo K□
□ (mm^{-1})	0.08	1.28	1.11
Crystal size (mm)	0.208×0.175×0.078	0.338×0.093×0.077	0.260×0.134×0.098
Data collection			
Diffractometer	Bruker D8 Venture	Bruker D8 Venture	Bruker D8 Venture
Absorption correction	Multi-scan	Multi-scan	Multi-scan
No. of measured, independent and observed [I > 2□(I)] reflections	45807, 12264, 9430	45945, 11015, 7002	8384, 2382, 1902
R_{int}	0.037	0.092	0.064
□$_{max}$ (°)	36.4	25.4	21.1
(sin □/□)$_{max}$ (Å^{-1})	0.834	0.604	0.506
Refinement			
R[F^2 > 2□(F^2)], wR(F^2), S	0.058, 0.178, 1.06	0.072, 0.178, 1.07	0.036, 0.079, 1.04
No. of reflections	12264	11015	2382
No. of parameters	365	452	273
H-atom treatment	H-atom parameters constrained w = 1/[□^{2}(F_o^2) + (0.089P)^2 + 0.7777P] where P = (F_o^2 + 2F_c^2)/3	H-atom parameters constrained w = 1/[□^{2}(F_o^2) + (0.069P)^2 + 40.932P] where P = (F_o^2 + 2F_c^2)/3	H-atom parameters constrained w = 1/[□^{2}(F_o^2) + (0.0327P)^2 + 0.7758P] where P = (F_o^2 + 2F_c^2)/3
□ρ$_{max}$, □ρ$_{min}$ (e Å^{-3})	0.71, -1.28	1.38, -0.90	0.59, -0.44

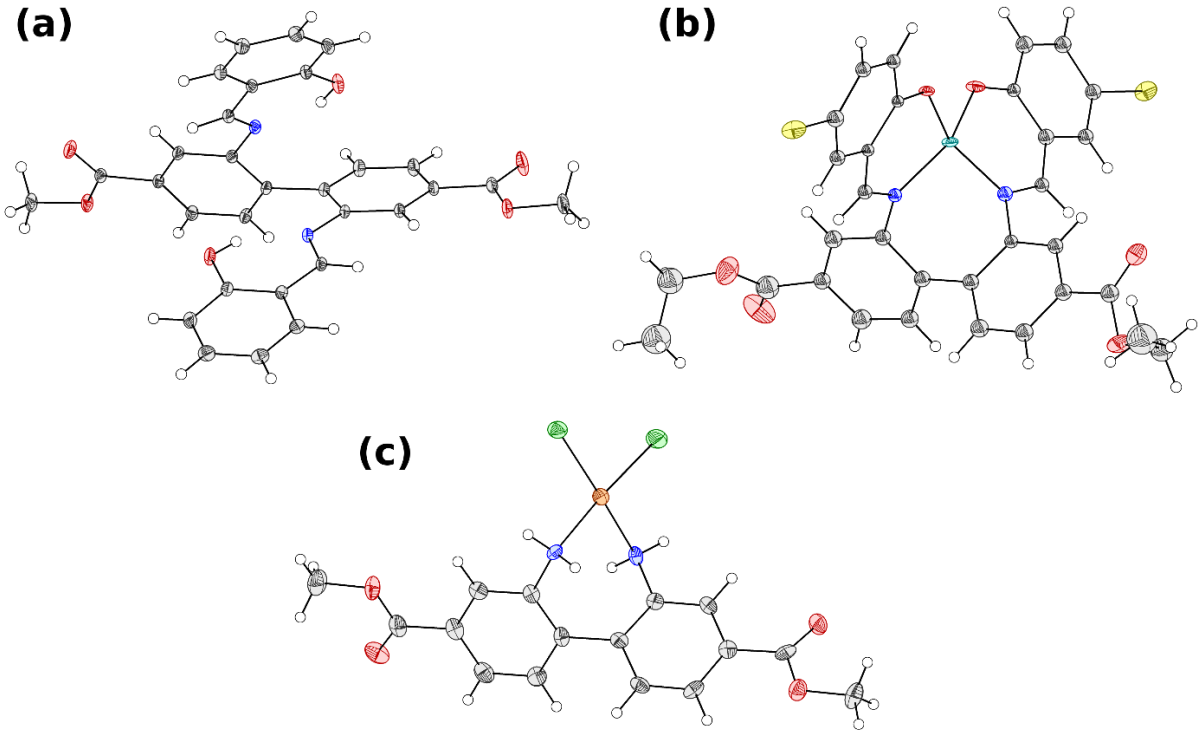

Figure A17. Molecular structures (from single crystal structure refinement) of (a) diester of the un-metalated complex, (b) Cu(II) functionalized bromosalicyl-complex and (c) $PdCl_2$(diaminobiphenyl diester).

Papers presented in this thesis